CHARLES UNIVERISTY

Faculty of Science

Department of Analytical Chemistry

Eva Harazim, M.Sc.

Lipidomic analysis of vernix caseosa

Lipidomická analýza novorozeneckého mázku

Ph.D. Thesis

Supervisor: doc. RNDr. Josef Cvačka, Ph.D.

Prague 2017

I hereby declare that this thesis is my own work and effort and that it has not been submitted anywhere with the intention to acquire any other academic degree.

I am aware that any use of the results obtained in this work, beyond the Charles University and the Institute of Organic Chemistry and Biochemistry of the Czech Academy of Sciences is possible only with a written consent of these institutions.

In Prague, 17. 7. 2017

…..……...

This work includes results obtained during my Ph.D. studies at the Department of Analytical Chemistry of the Faculty of Science, Charles University in 2013-2017. The work was carried out in the laboratories of the Mass Spectrometry Group at the Institute of Organic Chemistry and Biochemistry of the Czech Academy of Science, and at the Queensland University of Technology and the University of Wollongong, Australia.

This work was financially supported by the Grant Agency of the Czech Republic (Project no. P206/12/0750), Grant Agency of Charles University (Project no. 1182216), and the SVV project (Project no. SVV260440).

Supervisor: doc. RNDr. Josef Cvačka, Ph.D.
Mass Spectrometry Group
The Institute of Organic Chemistry and Biochemistry of the Czech Academy of Sciences

Supervisor-consultant: doc. RNDr. Zuzana Bosáková, CSc.
Department of Analytical Chemistry
Faculty of Science, Charles University

Preface & Acknowledgement

I had the opportunity to work out my Ph.D. project at the Institute of Organic Chemistry and Biochemistry of the Czech Academy of Sciences as a member of the Mass Spectrometry Group. I have spent great years there. This thesis sums up the results from the lipid analysis of vernix caseosa. My main goal was to develop the methods for identification and characterization of low abundant lipid classes or subclasses present in vernix caseosa. During my studies, I also had the opportunity to collaborate with laboratories abroad.

This thesis consists of a brief *Introduction* to the lipidomics and analytical techniques used in this field with detailed focus on the techniques used during Ph.D. studies. Here, an investigated material, vernix caseosa, is described as well. The introduction is followed by the summary of *Research aims* of this thesis. *Publications and Proceedings* and *Declaration of authorship* is followed, where my contribution to each publication is summed up. Unfortunately, not all the data have been published so far, but these publications are shortly before their finishing. The overview of used *Material and Instrumentations* is followed by *Summary of results and discussion,* where my experimental work is concluded. This chapter demonstrates the indispensable role of analytical chemistry, especially chromatography and mass spectrometry in lipid research. In addition to that, it is shown how I learned a lot of analytical techniques during my Ph.D. studies and improved my knowledge in analytical chemistry. The thesis is ended by *Summary and Conclusion* and *References* cited here.

At this point, I would like to thank my supervisor, Josef Cvačka, whose passion for science got me interested in lipidomics. He has shown me that the mass spectrometry and chromatography would be an amusement. He has been always very helpful and has encouraged me in my scientific goals. Especially, with arrangement of my research internship at the Queensland University of Technology (Stephen Blanksby's lab) and University of Wollongong (Todd Mitchell's lab). It was the best experience during my Ph.D. studies and I am very grateful to all of them for this opportunity because I have learned a lot in both labs. I would also like to thank for the financial support which made this research internship possible. My thanks belong to Stephen Blanksby, Todd Mitchell, Fond mobility UK, Institute of Organic Chemistry and Biochemistry of the Czech Academy of Science, Hlávkova nadace, and Literární fond.

I am very grateful to all my collaborators for many professional pieces of advice and help. They were mainly friends for me, not just colleagues.

I would never finish my Ph.D. studies without the great support of my family and friends, namely, Iveta Černá, who is my friend from my childhood and has supported me all the time in everything that I have done. I also thank to Alena Keprová, Marie Zábranská, and Jiří Schimer who have always time for my exhausting monolog about science and other troubles and joys in my life, and Eva Pyrihová, who always gives me a new creative impulse.

I cannot forget to thank Petr Harazim for his boundless support. He has been here for me and has tried to show me that everything has two sides.

Abstract

Methods of analytical chemistry are widely used in lipidomics. Separation techniques coupled to mass spectrometry or nuclear magnetic resonance are used very often. They make it possible to identify lipids present in the matrix in very small quantities.

This work summarizes the application of modern analytical methods and instrumentation for identifying and characterizing lipids in vernix caseosa. It is shown how I contributed during the Ph.D. studies to the elucidation of the structure and characterization of unknown lipid classes followed by more detailed description of those lipid classes already identified in vernix caseosa.

An integral part of my work was the application of the method enabling the localization of double bonds developed by our laboratory in triacylglycerols and 1,2-diol diesters in vernix caseosa. This analytical method is based on the formation of an acetonitrile adduct in an ionization source of a mass spectrometer enabling atmospheric pressure ionization. The complexity of the triacylglycerol class did not allow a complete characterization of the double bonds. However, the fragmentation mostly showed that double bonds up to *n*-12 position are present, but small peaks in some spectra also indicated double bonds at more distant positions from the chain termini. I have also collaborated on the characterization of chain branching and the position of double bonds of triacylglycerols. The analyzes showed branching in *iso*-, *anteiso*- and other positions and double bonds even in unusual positions. In collaboration on the characterization of 1,2-diol diesters, we were able to localize the double bonds in the *n*-7, *n*-9 and *n*-5 positions.

Another part of this work was the hydrolysis of whole vernix lipidome and analysis of methyl esters of fatty acids. The results showed 167 mostly saturated molecular species containing a large number of branching sites in their chains. These results were part of a study focused on the difference in lipid composition in the cohort of 20 newborn subjects.

1-*O*-acylceramides are a new lipid subclass that I identified and characterized in the investigated matrix. The results showed more than 2,000 molecular species with mainly saturated fatty acid chains. Another newly characterized lipid class that we identified was cholesterol esters of ω- (-(*O*-acyl)-hydroxy fatty acids.

The results of my work confirm the complexity of the lipid composition of vernix caseosa and contribute to understanding the importance of this unique biofilm.

Abstrakt

Metody analytické chemie jsou v lipidomice široce používané, a to zejména chromatografie ve spojení s hmotnostní spektrometrií či nukleární magnetická rezonance. Díky těmto technikám je možné identifikovat i lipidy vyskytující se v matrici ve velice malém množství.

Tato práce shrnuje využití moderních analytických metod a instrumentace při zjišťování identity a charakterizace lipidů obsažených v novorozeneckém mázku. Ukazuje také, jakým dílem jsem v průběhu studia přispěla k rozpoznání struktury a charakterizaci neznámých lipidových tříd a k detailnějšímu popisu již těch identifikovaných v novorozeneckém mázku.

Nedílnou součástí mé práce byla aplikace metody umožňující lokalizaci dvojných vazeb vyvinutou naší laboratoří u triacylglycerolů a 1,2-diesterů diolů novorozeneckého mázku. Tato analytická metoda je založena na tvorbě acetonitrilového aduktu v iontovém zdroji hmotnostního spektrometru s chemickou ionizací za atmosférického tlaku. Složitost třídy triacylglycerolů neumožnila kompletní charakterizaci dvojných vazeb. Fragmentace však ukázala přítomnost dvojných vazeb až do polohy *n*-12, ale byly rovněž identifikovány malé píky naznačující dvojné vazby ve vzdálených pozicích od koncových řetězců. Spolupracovala jsem také na charakterizaci větvení řetězců a polohy dvojných vazeb mastných kyselin triacylglycerolů. Analýzy ukázaly větvení v *iso*-, *anteiso*- i jiných pozicích a dvojných vazeb i v neobvyklých pozicích. Při spolupráci na charakterizaci 1,2-diesterů diolů jsme lokalizovali dvojné vazby zejména v polohách *n*-7, *n*-9 a *n*-5.

Součástí této práce byla hydrolýza celého lipidomu novorozeneckého mázku a analýza methylesterů mastných kyselin. Výsledky ukázaly 167 především nasycených mastných kyselin obsahujících na svém řetězci ve velké míře větvení. Tyto výsledky byly součástí studie, která byla zaměřená na rozdílnost lipidového složení u 20 novorozenců v závislosti na jejich pohlaví.

1-*O*-acylceramidy jsou lipidovou podtřídou, kterou jsem nově identifikovala a charakterizovala ve zkoumané matrici. Výsledky ukázaly více než 2000 molekulových druhů s především nasycenými řetězci mastných kyselin. Další nově charakterizovanou lipidovou třídou, kterou jsme v naší laboratoři identifikovali, byly cholesterylestery ω-(*O*-acyl) hydroxykyselin.

Výsledky mé práce potvrzují komplexnost lipidové složky novorozeneckého mázku a přispívají k pochopení významu tohoto unikátního biofilmu.

TABLE OF CONTENT

LIST OF ABBREVIATIONS

1,2-DDE	1,2-Diol diester
ACTH	Adrenocorticotropic hormone
Ag-LC	Argentation (silver ion) liquid chromatography
Ag-HPLC	Argentation (silver ion) high-performance liquid chromatography
AMPP	N-(4-aminomethlyphenyl)pyridinium
APCI	Atmospheric pressure chemical ionization
APPI	Atmospheric pressure photo ionization
β^-	Beta particle
BEH	Ethylene Bridged Hybrid
Cer	Ceramide
CID	Collision-induced ionization
CN	Carbon number
Chol	Cholesterol
CRF	Corticotropin-releasing factors
DB	Double bond
DESI	Desorption electrospray ionization
DHEA	Dihydroepiandrosteron
ECL	Equivalent chain length
ECN	Equivalent carbon number
EI	Electron ionization
ESI	Electrospray ionization
FA	Fatty acid
FAME	Fatty acid methyl ester
GC	Gas chromatography
HCD	Higher-energy collision dissociation
HILIC	Hydrophilic interaction liquid chromatography
HPLC	High-performance liquid chromatography
HPTLC	High-performance thin-layer chromatography
LC	Liquid chromatography
LIPID MAPS®	LIPID Metabolites and Pathways Strategy

m/z	Mass to charge ratio
MALDI	Matrix-assisted laser desorption/ionization
MTBE	Methyl *tert*-butyl ether
MS	Mass spectrometry
NMR	Nuclear magnetic resonance
NP	Normal phase
OzID	Ozone-induced dissociation
PL	Phospholipid
PQD	Pulsed Q collision-induced dissociation
RDBE	Ring plus double bond equivalent
RP	Reversed phase
SE	Sterol ester
SFC	Supercritical fluid chromatography
SPE	Solid phase extraction
SQ	Squalene
TG	Triacylglycerol
TLC	Thin-layer chromatography
WE	Wax ester

INTRODUCTION

1. Lipidomics

Lipidomics was first introduced by Han and Gross in 2003 as a part of metabolomics [1]. "Lipidomics is defined as an analytical chemistry-based research field studying lipidomes on a large scale and at the levels of intact molecular species. A lipid research aims the following:

- Precisely identifying the structures of cellular lipid species including the number of carbon atoms, the number and location of double bonds (DB), the core structures and head groups, individual fatty acyl chains, the regiospecificity of each isomer, etc.
- Accurately quantifying individual identified lipid species for pathway analysis, comparably profiling the lipid samples for biomarker discovery.
- Determining the interactions of individual lipid species with other lipids, proteins, and metabolites in vivo.
- Disclosing the nutritional or therapeutic status for prevention or therapeutic intervention of diseases" [2] (p. 13).

Advanced analytical techniques are very important for lipidomics research, namely chromatography, nuclear magnetic resonance (NMR), and mass spectrometry (MS) [2-4]. Two approaches were established during the MS development in lipidomics, (i) target lipidomics and (ii) global lipidomics. The target lipidomics aims to identify and quantify a single lipid or subset of lipids in a cellular tissue or extract. The global lipidomics is focused on the identification and quantification of all the lipids in the system [5-7].

1.1. Lipids

Lipids are perceived as a diverse and ubiquitous group of compounds with many key biological functions [8]. Historically, lipids are defined according to their physical properties, thus the solubility in nonpolar solvents [6]. Fishy et al. accepted other classification of lipids based on lipid biosynthesis [9, 10]. "Lipids are hydrophobic or amphipathic small molecules that may originate entirely or in part by carbanion-based condensations of thioesters (*e.g.*, fatty acyls) and/or by carbocation-based condensation of isoprene units (*e.g.*, sterols)" [7] (p. 840). Lipids have extremely diverse structures which

can be seen, for instance, in the most comprehensive lipid structure database (LIPID Metabolites and Pathways Strategy (LIPID MAPS)) with more than 40 thousand different lipids [7].

1.1.1. Classification of lipids

Several systems for lipid classification exist, and perhaps the most frequently used one, is the classification developed by Fahy et al. [9]. Lipids are divided into eight categories: fatty acyls, glycerolipids, glycerophospholipids, sphingolipids, sterol lipids, prenol lipids, saccharolipids, and polyketides. This classification is based on the distinct hydrophobic and hydrophilic elements that the lipid is composed of [9]. **Figure 1** shows the lipid categories with prominent representatives as an example. Lipid classes may be further divided into smaller groups, i.e. subclasses of the lipid class. The lipid classes and subclasses are composed of individual lipid molecular species with a unique molecular structure [2].

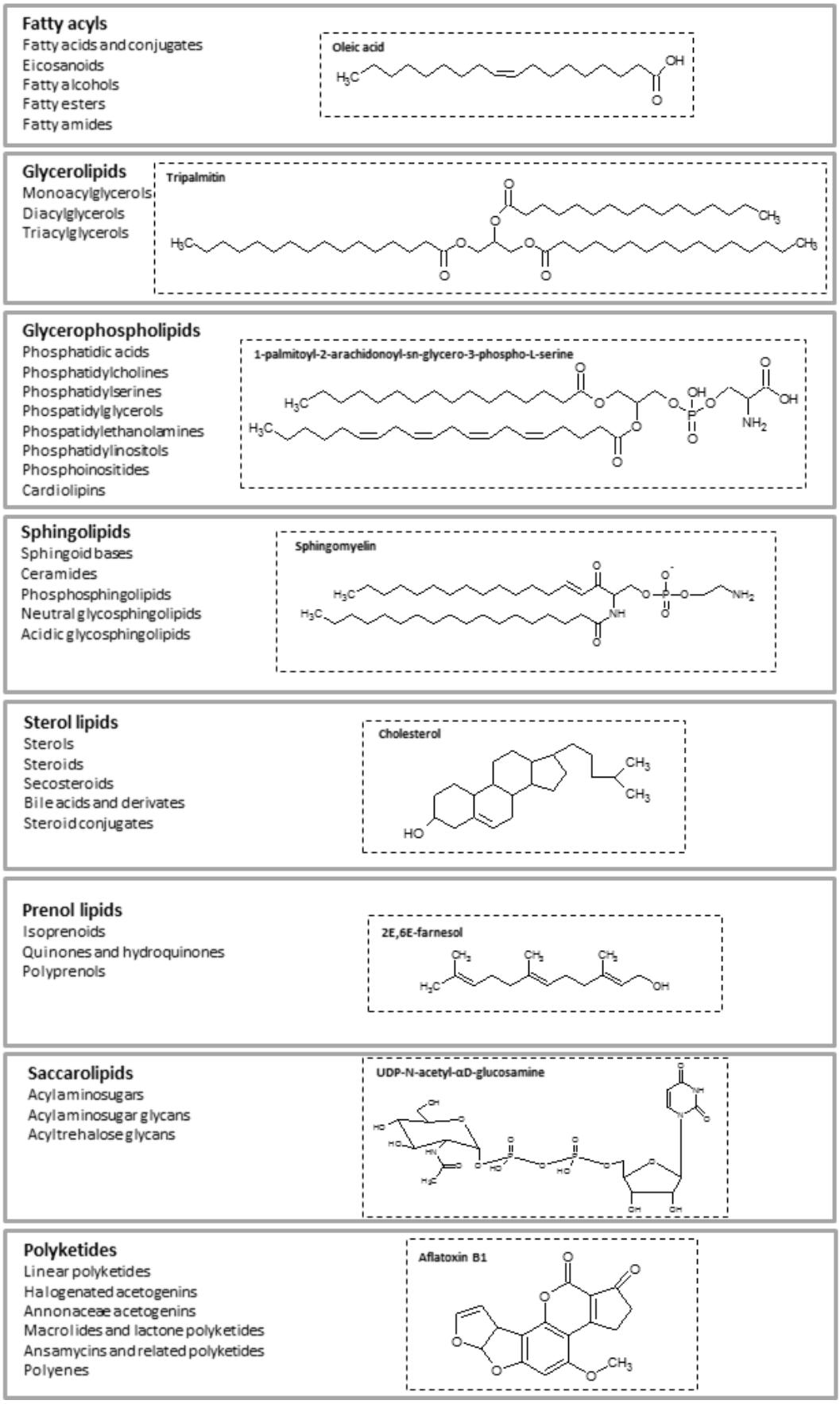

Figure 1. Lipid categories and prominent lipid classes (modified according to [6, 9]).

2. Analytical techniques in lipidomics

Identification and characterization of lipid structures are the key steps in lipidomic research. For this purpose, a number of common, but also very sophisticated analytical techniques have been developed recently.

2.1. Extraction

Lipid extraction is one of the most important step in the lipid analysis. A large number of methods has been developed for isolating lipids from biological materials. Solvent extraction being the most commonly employed in lipidomics. Lipids are frequently associated with other compounds in the original biological material, which makes the extraction rather difficult. Lipids often interact with nonpolar regions of proteins, namely with valine, leucine or isoleucine residues [11]. The majority of methods use mixtures of organic solvents, such as chloroform and methanol. The most commonly used extraction procedures are those developed by Folch et al. [12] and Bligh and Dyer [13]. The method according to Folch et al. is used for lipids from animal, plant and bacterial tissues [12]. The extraction described by Bligh and Dyer is suitable for water-rich systems, but the problem with the partial loss of nonpolar lipids, such as triacylglycerols (TG) exists [13]. Chloroform is known for its toxicity; therefore, it is being often replaced by an extraction employing methyl *tert*-butyl ether (MTBE) introduced by Matyash et al. [14]. The biggest advantage of this procedure is caused by the low density of MTBE, which makes the organic solvent to form the upper layer after the phase separation. Solid phase extraction (SPE) was introduced into lipidomics as well. This method is recommended for lipid fractionation or in-depth characterization of lipid classes [15].

2.2. Chromatographic techniques

Separation of analytes is an important step in lipidomics. There are more than one separation techniques for uncovering and analyzing investigated classes and species which must be used. Various separation modes, such as adsorption, liquid-liquid or gas-liquid partition, ion-exchange, gel-permeation and chiral-phase chromatography are widely used in lipid analysis [16].

2.2.1. Thin-layer chromatography

Thin-layer chromatography (TLC) belongs to one of the simplest chromatographic techniques. TLC is popular thanks to its low-cost and no need for instruments. It used for qualitative screening and preparative purposes [17]. Silica gel, alumina, and diatomaceous earth are the most common stationary phases for lipid separations. Nonpolar mobile phases (*e.g.*, hexane, diethyl ether, or chloroform) dominate in normal phase (NP) separation. NP chromatography enables separation based on the polarity differences, which translates onto the lipid classes. One of the biggest advantages of TLC separation is an easy visualization of separated fractions by binding to a dye. Nowadays, a number of reagents is available and they can be sorted according to their specificity or destructiveness. In the analytical mode, 50% sulfuric acid either in methanol or water is one of the most popular destructive and non-specific reagents. The plate is usually heated after being sprayed with these reagents. Lipids are completely reduced to carbon and the intensity of each spot on the plate can be quantified using densitometry. Solutions of rhodamine 6G, 2,7-dichlorofluorescein or primulin are widely used in the preparative or semi-preparative mode as non-destructive detection reagents. The plate is subsequently illuminated with UV light to visualize the spots [18, 19].

2.2.2. Liquid chromatography

Liquid chromatography (LC) and high-performance liquid chromatography (HPLC) is one of the most widely used tools in lipidomics. HPLC is suitable for the analysis of nonvolatile, high-molecular-weight lipids in several modes [20]. Lipidomics employs several LC systems, i.e. (i) normal-phase, (ii) reserved-phase, (iii) ion-exchange, (iv) hydrophilic interaction, (v) silver-ion/argentation and (vi) chiral chromatography [16].

2.2.2.1. Normal-phase liquid chromatography

NP-LC and NP-HPLC are based on the polar interactions between analytes and the stationary phase [21]. Lipids are separated according to their polarities, which are affected by number and nature of polar functional groups. Therefore, this mode is used for separation of lipid classes [16].

Unmodified silica gel is the most commonly used stationary phase in NP-LC or NP-HPLC due to its adsorptive properties. The polar interactions are mediated mostly by free silanol groups [16]. Properties of the stationary phase can be tuned by modification of the

silanol groups with a diol, nitrile, nitro, methyl cyano, or phenyl cyano, functionalities, bonded chemically via a short spacer to the surface. Lipid classes are often separated in a solvent system consisting of chloroform and methanol or hexane and propan-2-ol, sometimes with a small percentage of water [21]. However, water in the mobile phase causes worse reproducibility by creation of the layer on silanol groups [16].

A tendency for inferior reproducibility of the retention times, together with tailing of the peaks and longer equilibration times of a column in the case of gradient elution, are the biggest disadvantage of NP-HPLC. These complications may be minimized by using the bonded stationary phases [21].

2.2.2.2. Hydrophilic interaction liquid chromatography

Hydrophilic interaction liquid chromatography (HILIC) is a variant of NP-LC. HILIC employs hydrophilic stationary phases and reversed phase (RP) eluents, typically acetonitrile with a small amount of water. Aprotic solvents miscible with water, such as tetrahydrofuran or dioxane can be used as well.

The separation process is based on forming a liquid/liquid extraction system in a water-rich layer on the surface of the polar stationary phase, while the water-deficient mobile phase moves through the separation system. In this way, analytes are distributed between adsorbed water layer and a mobile phase. Polar analytes interact more strongly with the stationary aqueous phase than less polar molecules. The separation in this mode is therefore based on the polarity and degree of solvation of the molecule [21]. HILIC is mostly used for the separation of polar lipid classes or subclasses.

2.2.2.3. Reversed-phase liquid chromatography

RP-LC RP-HPLC mode are based on the interactions of analytes with a relatively nonpolar liquid stationary phase and polar liquid mobile phase. The retention of lipids is given by the hydrophobicity of the fatty acyl chains, such as the chain lengths, number of DBs, and number of headgroups in a molecule [21]. This separation mode is therefore suitable for separation of the molecular species of the same lipid class or subclass [22, 23]. Nevertheless, molecular species of different lipid classes can co-elute [24, 25]. The separation process itself is dependent on differences in the equilibrium distribution coefficients of molecules between two phases. Polar dipole-induced dipole, dipole-dipole, and proton acceptor-proton

donor are typical interactions affecting retention and separation of lipids. Moreover, lipids are attracted by London forces to the bonded hydrocarbon chain of the stationary phase [16].

Long hydrocarbons chains, such as octadecylsilyl groups covalently bonded to the surface of silica gel particles are widely used. Non-aqueous, as well as aqueous mobile phases containing acetonitrile, methanol or propan-2-ol are the most commonly used [15, 21]. Mobile phase additives (usually ammonium formate or acetate and formic or acetic acid) improve both LC separation and MS detection of lipids [15].

RP-LC is suitable for separation of lipid molecular species. Complex lipid material requires longer LC runs because the number of separated compounds can be high [15]. Retention behavior of lipid molecular species can be related to their structures using the equivalent carbon number (ECN). The concept of ECN is based on the observation that each DB decreases retention in the same way as shortening the chain by two carbon atoms [26]. Therefore, ECN values (Equation 2.1) are calculated as the actual number of carbons in the aliphatic residues (carbon number (CN)) minus twice the number of DBs in fatty acyl chains.

$$ECN = CN - 2DB \quad (2.1)$$

Two components with the same ECN value and close retention are called "critical pairs" [16].

2.2.2.4. Argentation chromatography

Argentation (silver ion) chromatography (Ag-LC) or its high-performance version (Ag-HPLC) are based on interactions of silver ions with π electrons of DBs. The unsaturated compound acts as an electron donor while the silver ion is an electron acceptor, which results in the formation of reversible complexes. The elution proceeds according to the number, configuration, and position of DBs in the hydrocarbon chains. A lipid with a higher number of DBs forms stronger complexes, which results in longer retention times.

Ag-LC can be used in TLC applications where silica gel impregnated with silver nitrate is usually employed. Commercial Ag-HPLC columns contain silver ions bonded to an ion exchange phase are also common [16].

2.2.3. Gas chromatography

The use of gas chromatography in connection with mass spectrometer has a long tradition in lipid analysis. GC/MS is a method of the choice for both qualitative and quantitative analysis of fatty acids (FA) derivatives and sterols [6].

Fatty acid methyl esters (FAME) are commonly analyzed on highly polar liquid phases, for instance, cyanopropyl siloxanes or polyethylene glycols (DB-WAX column). FAMEs are separated according to their chain length and degree of unsaturation. However, these columns have a low-temperature stability. Therefore, nonpolar stationary phases are used as well, such as (5% phenyl)-methyl polysiloxane (DB-5 column), which can be used at higher temperatures [20]. Kováts retention indexes are replaced by equivalent chain lengths (ECL) in the case of FAMEs analysis [27]. The calculation of ECL is performed by the reference to the straight chains FAMEs obtained by plotting the logarithms of the retention times of a homologous series of straight-chain saturated FAMEs against CN in the aliphatic chain of each acid. ECL values are useful for identifying unknown FAMEs using isothermal conditions or slow thermal gradients [16, 28-30].

2.2.3.1. Derivatization reactions for fatty acids

Lipids are derivatized before GC/MS measurement for several reasons: (i) increasing volatility, (ii) reducing polarity, (ii) improving chromatographic properties, (iii) improving the sensitivity and selectivity of the measurement, (iv) increasing of structural information, or (v) for chiral analysis [31].

The most commonly used derivatives are FAMEs. The preparation of FAMEs can be performed directly with no need for hydrolyze lipids before preparing esters. Care must be taken during the evaporation of solvents when short-chain esters (less than C14) are present. These esters can be lost by the use of stream of nitrogen or a vacuum evaporator. Generally, two types of transesterification exist, acid- or base-catalyzed reactions. During the reaction, fatty acids (FA) are esterified and *O*-acyl lipids are transesterified at higher temperature with a large excess of anhydrous methanol in the presence of an acidic or basic catalyst. The general scheme of the acid-catalyzed reactions is shown in **Figure 2**. The first step is protonation of the acid giving an oxonium ion. This ion can undergo an exchange reaction with an alcohol. The resulting intermediate can lose a proton to become an ester. The formation of the intermediate need not to run completely due to the presence of water, which is better electron donor than aliphatic alcohols [32].

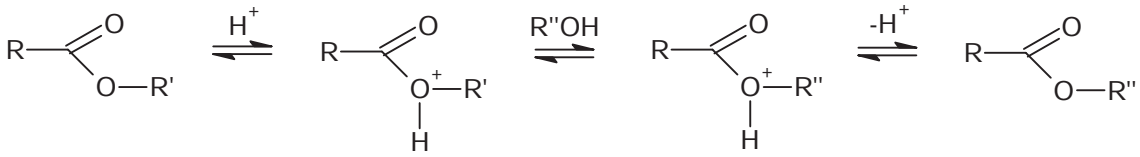

Figure 2. Acid catalyzed transesterification of lipids (modified according to [32]).

FAMEs can also be prepared from FAs using a reaction with diazomethane (**Figure 3**).

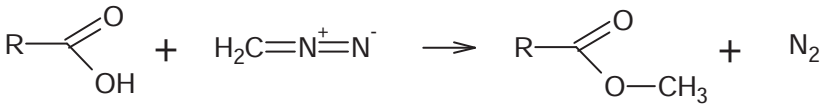

Figure 3. The reaction of diazomethane with FA [32].

Most of the transesterification reactions are time-consuming because of the repeated extraction into solvents, drying, concentration, evaporation and the sample re-dissolving before analysis. It results in decreased reproducibility and loss of the short chain FAs [16]. Therefore, Stránsky and Jursík [33] developed a transesterification procedure where the sample is dissolved in a mixture of chloroform and methanol, and acetyl chloride is added. The whole reaction takes place in a tightly sealed ampoule. After the reaction, hydrochloric acid is neutralized with silver carbonate. Another transesterification reaction introduced by Robb and Westbrook [34] uses pyrolysis of tetramethylammonium salts of unesterified FAs. FAMEs are released upon heating the salts between 330 and 365°C in the injection port of a GC. Trimethylsulfonium and trialkyl selenonium hydroxides appeared to be more advantageous than tetramethylammonium salts due to lower temperatures needed for the salt decomposition (approximately 200°C) [35, 36]. Nevertheless, El-Hamdy and Christie [37] claims that this method may cause a loss of polyunsaturated FAs. The reaction scheme of transesterification with trimethyl sulfonium hydroxide is shown in **Figure 4**.

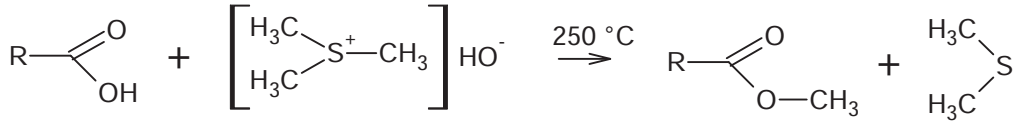

Figure 4. Methylation of FAs by pyrolysis of the salt formed from trimethyl sulfonium hydroxide [32].

Sphingolipids and other *N*-acyl lipids are transesterified by acid-catalyzed methanolysis. Nevertheless, amide-bonded FAs require harsher conditions for the transesterification reaction than ester-bonded FAs, most commonly solved by prolongation of reaction [16, 32].

Other esters of FAs are prepared for variety of reasons, such as to diminish the volatility of short-chain FAs. The most common derivatives of FAs are pyrrolidine, picolinyl ester, trimethylsilyl ether or dimethyl disulfide adducts. For example, picolinyl esters are used for the localization of DBs or trimethyl silyl ether is useful for recognizing of hydroxyl groups [16].

2.2.4. Supercritical fluid chromatography

Supercritical fluid chromatography (SFC) uses gas compressed above its critical temperature and pressure as an eluent. The supercritical fluid has an intermediate behavior between that of a liquid and gas. The viscosity of the supercritical fluid resembles a gas, but the density and solvation power are similar to a liquid.

Carbon dioxide is the most frequently used supercritical fluid due to its low critical temperature. However, the critical pressure and critical density are high enough for good solvation of many analytes. It is also possible to use a small amount of organic solvents which can help to overcome the problem with compatibility for polar molecules [16].

2.3. Mass spectrometry in lipid research

MS is an analytical discipline which uses the mass to charge ratio (*m/z*) of individual ions for structural elucidation and quantification. A mass spectrometer generally consists of an ion source, a mass analyzer, a detector, and a data processing system (**Figure 5**) [38].

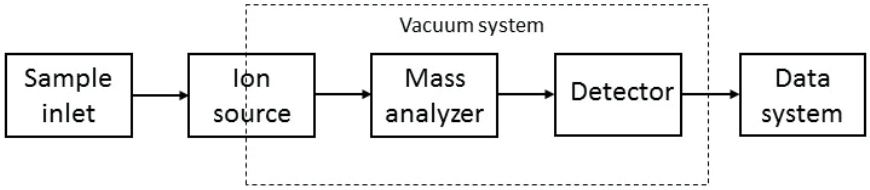

Figure 5. Schematic diagram of a mass spectrometer (modified according to [38]).

2.3.1. Ionization techniques

Lipidomics frequently employs these ionization techniques: (i) electron ionization (EI), (ii) electrospray ionization (ESI), (iii) matrix-assisted laser desorption/ionization (MALDI), (iv) atmospheric pressure chemical ionization (APCI), (v) atmospheric pressure photoionization (APPI), and ambient ionization techniques, such as (vi) desorption ESI (DESI) [39].

2.3.1.1. Electron ionization

EI is one of the oldest ionization techniques in mass spectrometry. It is widely used for the low- to medium-polarity lipids in the range of molecular weights up to $M_r \approx 1000$ [40]. EI is commonly coupled to GC.

During the ionization process, the radical cation is formed in gas phase according to the following reaction (Equation 2.2):

$$M + e^- \rightarrow M^{+\bullet} + 2e^-, \quad (2.2)$$

where M is the neutral molecule being ionized, e^- is the electron, and $M^{+\bullet}$ (radical cation) is the resulting molecular ion with an odd number of electrons. The electrons for ionization are created by a thermionic emission from a heated wire filament which has electric current running through it. The ionization energy of the molecules needs to be lower than the kinetic energy of the flying electrons. Commonly, molecules are ionized at 70 eV in the region between the filament and the entrance to the ion source block. A magnetic field increases the ionization efficiency by keeping the electrons on the spiral path. The analyte molecules are introduced into the ion source in a perpendicular orientation to the electron beam. The highly energetic electrons cause large fluctuations in the local electric field around the molecules, which results in ionization and fragmentation. The ions formed in the ion source are driven into the mass analyzer by the voltage applied on a repeller electrode (see in **Figure 6**) [40].

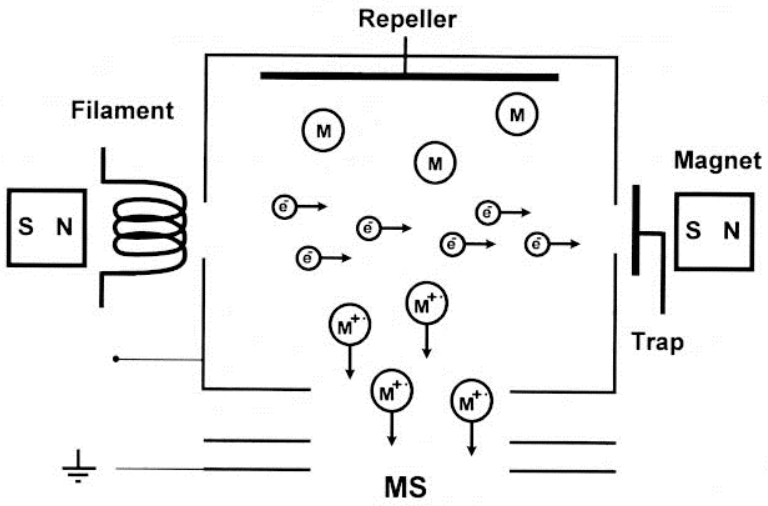

Figure 6. Schematic of EI (downloaded and modified according to *http://tera.chem.ut.ee/~jpenchuk/documents/kursused/Mass-spec/2.htm*).

2.3.1.2. Electrospray ionization

The ESI source contains a narrow tube called ESI needle, to which a high voltage is applied. The sample solution is sprayed by the ESI needle into a fine mist of droplets that are electrically charged at their surface [41]. The scheme of this ion source is shown in **Figure 7**.

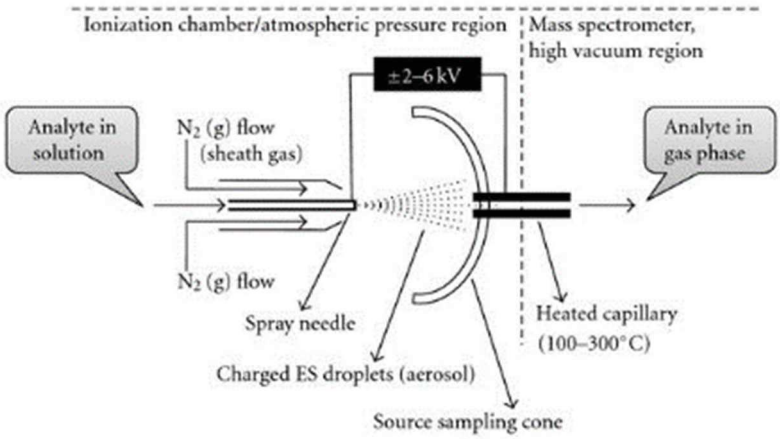

Figure 7. The scheme of ESI [42].

The ion formation proceeds in three steps: (i) creation of an electrically charged spray, (ii) dramatic reduction of the droplets size and (iii) liberation of fully desolvated ions. The continuous spraying is achieved at the end of an electrically conducting capillary which is held at an electric potential of 3-4 kV. Here, the liquid is exposed to an electric field. When the critical electric strength is reached, the Taylor cone is formed and starts ejecting a fine jet of liquid from its apex towards a counter electrode. After spraying, droplets are formed at the outlet of the capillary by means of nebulizing gas. The droplets bear on its surface a lot of charges. The liquid droplets start to form an ellipsoid under the influence of increasing field strength. Evaporation of the solvent results in an increase of charge density on the surface, which proceeds up to the critical point known as the Rayleigh stability limit. This is a state, when the electrostatic repulsion and the surface tension are balanced. After reaching the limit, Coulomb fission takes place and newly formed smaller droplets are driven away from each other by electrostatic repulsion [40]. This process ensures even distribution of charge and size of the droplets and is repeat continuously [41]. The mechanism is illustrated in **Figure 8**.

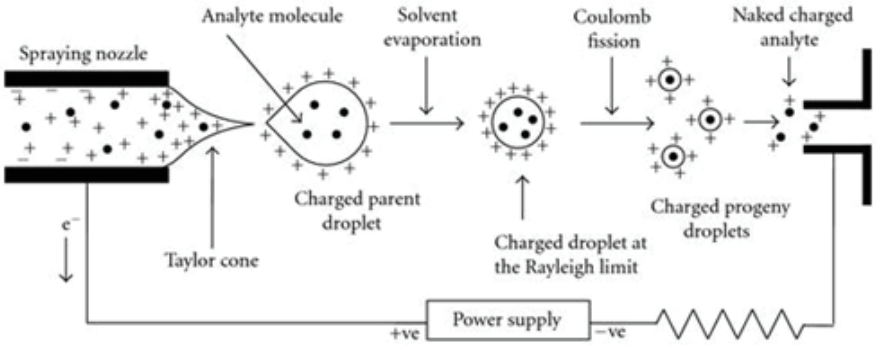

Figure 8. The mechanism of ESI [42].

2.3.1.3. Atmospheric pressure chemical ionization

APCI is a gas-phase ionization process initiated by electrons, which are generated either by a beta particle (β^-) emitting source or a corona discharge. The techniques based on ^{63}Ni foil as a source of electrons became obsolete. Today, corona discharge is used, with a needle kept at high negative potential placed near the inlet capillary or orifice [43]. APCI sources (**Figure 9**) consist of a heated vaporizer tube (300 – 500°C) placed concentrically around the LC capillary ended by a nozzle, a corona discharge needle, and an entrance into the mass spectrometer. For efficient desolvation of analytes, nebulizing gas and sometimes auxiliary gas are used [44].

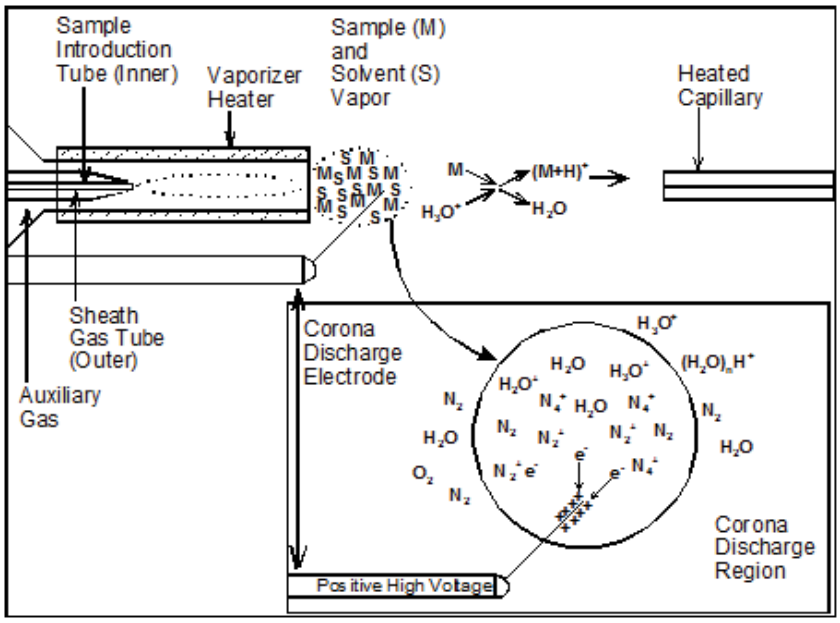

Figure 9. Ionization process occurring in the APCI source [44].

Ionization of analytes occurs in several steps. At the beginning, the EI ionization of gas (N_2) happens. After that, ion-molecule reactions provide secondary reactants which ionize analyte molecules [44, 45].

2.3.2. Mass analyzers

A mass analyzer is the part of the mass spectrometer which makes it possible to separate ions according to their *m/z*. The mass analyzers work on different principles: *m/z* range as well as resolution, and sensitivity also differ. It is also possible to connect two different analyzers into a hybrid mass analyzer.

2.3.2.1. Quadrupole

A linear quadrupole (**Figure 10**) is a mass analyzer consisting of four hyperbolically or cylindrically shaped rod electrodes. The opposing rod electrodes are connected together electrically. A radio frequency and direct current voltage are applied between both pairs of rod electrodes. Ions enter the quadrupole between the rod electrodes and those with a certain *m/z* proceed to the detector. The other ions follow unstable trajectories and they are directed towards the rod electrodes [40]. Quadrupole typically has a low (nominal) resolution [46].

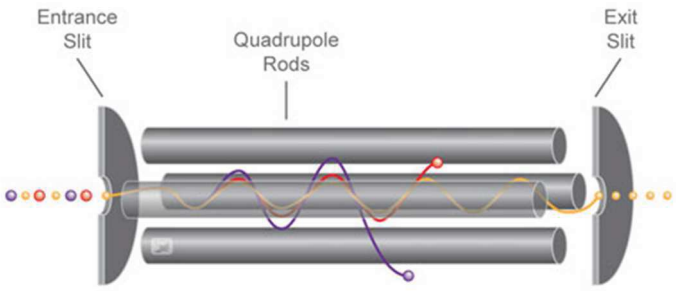

Figure 10. Quadrupole [47].

2.3.2.2. Ion trap

Ion trap is somewhat similar to quadrupole with some differences. Nowadays, two types of ion trap are used in mass spectrometry, namely linear [48] and spherical [49, 50] ion traps.

The linear ion trap is a quadrupole with electrodes on its both ends where the direct current voltage is applied. The alternating current voltage is put on the central quadrupole part of the ion trap. [51].

The spherical ion trap creates a three-dimensional radio-frequency quadrupole field. It consists of an entrance and an output hyperbolic electrode and a central ring electrode (**Figure 11**). The high-frequency voltages with changing amplitude are applied to the ring electrode and the end electrodes are joined electrically. The ion trajectory is stable for ions of a particular value or range of *m/z* and undesirable ions are ejected from the ion trap. For the detection, the ions are ejected towards the detector by rising of the alternating voltage on the ring electrode [40, 52]. Helium is used as a buffer gas to reduce the kinetic energy of ions, and thus to increase resolution and efficiency [53].

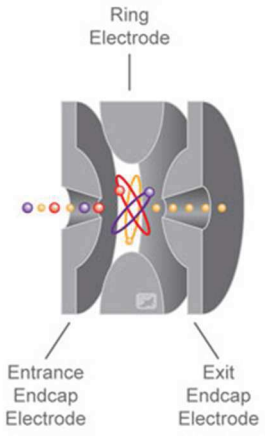

Figure 11. Quadrupole ion trap [47].

2.3.2.3. Orbitrap

An orbitrap consists of three electrodes, one axial central and two outer electrodes. The direct current and alternating current voltage are applied between the central and outer electrodes. The ions from the ion source are brought perpendicularly to the central electrode. The potential between the electrodes forces the ions to oscillate around the central electrode and also along it. The *m/z* value is proportional to the frequency of the ion oscillations along the central electrode. These oscillations are detected by the outer electrodes. The Fourier transformation of the measured signal provides ion frequencies, and thus *m/z* values. Scheme of orbitrap is in **Figure 12**.

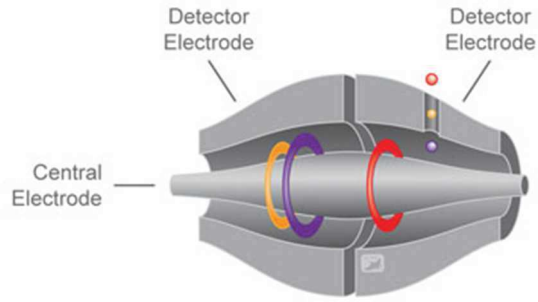

Figure 12. Orbitrap [47].

The orbitrap is also available in several hybrid mass spectrometers. Orbitrap is recognized for its high resolution (up to 450,000), high mass the accuracy (1-3 ppm), and range up to *m/z* 6,000 [54]. The disadvantage of orbitrap is its relatively slow scanning.

2.3.3. Structural characterization of lipids

Lipids represent a broad range of structurally diverse molecules and require relatively sophisticated approaches for their identification. The most commonly employed mass spectrometry techniques used in identification of lipids are high-resolution accurate mass measurement and fragmentation experiments.

High-resolution instruments offer high resolving power and mass accuracy typically better than 1-5 ppm. They make it possible to distinguish ions with the same nominal mass, but different elemental composition [15]. Based on accurately measured *m/z* values, the software is able to determine elemental composition, calculate ring plus double bond equivalents (RDBE) values and match isotope profiles with theoretically calculated patterns.

Ion fragmentation is a useful tool for deducing structures of unknown compounds. The precursor ions can be selected manually based on previous MS data acquisition, employing data-dependent acquisition or data-independent acquisition (non-selective tandem MS). In data-dependent acquisition, the precursor ion is selected in the MS step, it is activated in the next step, and the product ions are detected [15]. The ions can be fragmented by collision-induced dissociation (CID), which is the most frequently used ion activation method, or pulsed Q collision induced dissociation (PQD) in the case of the ion trap. The orbitrap employs a higher-energy collision dissociation (HCD).

2.3.3.1. Localization of double bonds

DBs in aliphatic chains have an immense effect on the physical properties and biological functions of lipids. Therefore, knowledge about their presence, position, number, and geometric isomerism of DBs in particular lipids is indispensable. The localization of DBs in lipids has been a domain of GC/MS or specialized techniques, such as silver ion chromatography for a long time [55]. GC/MS make it possible to analyze volatile and temperature stable lipids or their derivatives. Most of the hydrolyzed lipids fulfill these requirements, but the information about intact molecule is lost. Therefore, it is important to find the way how to localize DBs in intact lipids. Intact lipids are widely characterized by RP-HPLC/MS and there is a strong need to develop methods enabling identification of DBs in connection. Recently, several methods using HPLC and MS for localization of DBs in intact lipids have been developed.

Gas-phase acetonitrile-derived adducts have been employed for analysis of intact lipids, such as FAMEs [56-61], wax esters (WE) [62], TGs [63, 64] and 1,2-diol diesters (1,2-DDE) [65] using APCI-HPLC/MS. It has been observed that two different adducts, $[M + 54]^+$ and $[M + 55]^{+\bullet}$, are formed in APCI in the presence of acetonitrile. The formation of these adducts depends on the conditions in the APCI source. The first method is based on an ion/molecule reaction between $[C_2H_2N]^+$ and neutral acetonitrile, which yields (1-methyleneimino)-1-ethenylium ion ($CH_2 = C = N^+ = CH_2$, *m/z* 54). This ion forms a covalent adduct with DBs, and collisional activation of the adduct results in diagnostic fragments indicating the DB positions [57-61, 64]. The second approach is based on the formation of a radical cation $C_3H_5N^{+\bullet}$ (*m/z* 55). As in the previous case, the ion reacts with unsaturated lipid chains and subsequent fragmentation of the DBs. When applied for TGs, the fragmentation spectra make it possible to establish the total number of carbons and DBs in the molecule and acyls, the acyl in the *sn*-2 position on the glycerol backbone in TGs, and DB positions in acyls [56, 62, 63, 65].

The combination of CID with ozone-induced dissociation (OzID) has been used for the localization of DBs in TGs [66] and phosphatidylcholine [67] in natural samples. This technique uses sodium adducts $[M + Na]^+$ generated by ESI. Ozone is led into the ion trap, where the primary ozonide of the molecular adducts is formed. Its fragmentation results in two products which are characterized by neutral losses corresponding to an aldehyde and Criegee losses. DB positions in lipids are determined according to *m/z* values of these ions with depending on the degree of unsaturation [66-68]. This method allows not only

recognizing *sn*-position in glycerol backbone but also the DB geometry [69, 70]. Moreover, the combination of in-line ozonolysis with two dimensional HPLC enables the characterization of particular phospholipids in egg yolk. This type of ozonolysis does not require any instrumental modification because an ozonolysis device is placed in-line between the two dimensional HPLC and the mass spectrometer [71]. However, using the method employed in-line ozonolysis gives less sensitivity to DB isomers than OzID [72].

2.3.3.2. Localization of methyl branching in hydrocarbon chains

Branched-chain FAs are common across all kingdoms of life (bacteria, animals, and higher plants). Vernix caseosa lipids contain various branched chains both in bound lipids or free FAs [73-75]. The chains are usually branched with one or more methyl groups. It is hypothesized that branched lipids increase the fluidity of membranes similarly as in unsaturated lipids. The most common branching point is on the penultimate carbon and these chains are indicated by an *iso*- prefix. An *anteiso*-methyl-branched carbon chain has the branch point on the ante-penultimate carbon [16].

The most common way for addressing the structure branched FAs is EI-MS of their pyrrolidine [76] and picolinyl [77] ester derivatives. These derivatives provide characteristic fragmentations on both sides of the carbon atom linked to the methyl group. A diagnostic gap of 28 Da is seen in the spectra [16]. Charge remote fragmentation has been commonly used to the identification of methyl branching of the carbon chain. Recently, one-step derivatization with a charge-carrying reagent N-(4-aminomethylphenyl)pyridinium (AMPP) has been developed. ESI-HCD-MS/MS spectra clearly show the characteristic ions arising from cleavages of the CH(CH3)-CH2 bond together with CH2-CH(CH3) bond [78]. The derivatives can also be used as a tool for the localization of DBs position [79, 80].

3. Vernix caseosa

The term “vernix caseosa” appeared for the first time in 1846 in the Dunglison Dictionary of Medical Science [81]. It is described as human skin cheesy biofilm covering newborns (**Figure 13**), and it fascinates chemists, biochemists, and neonatologists even nowadays [82].

Figure 13. A newborn covered by vernix caseosa
(downloaded from *http://buildingthebaby.blogspot.cz/2013/01/week-19.html*).

3.1. Fetal skin development and formation of vernix caseosa

The first fetal skin starts to origins from the embryonic ectoderm during the embryogenesis in the 3rd week of gestation. At 21st week, the fetal skin is formed by two layers which are designed by the differentiation of ectoderm into the neuroderm and the epidermis. During the 4th week, the basal cell layer is developed and is covered with the periderm, which protects the epidermis from amniotic fluid and ensures glucose uptake [83, 84]. During 8th and 14th weeks, an epidermal intermediate layer is formed from the proliferation of keratinocytes from the spinous layer between the basal layer and periderm [85, 86]. By the end of the 4th month of gestation, stratum corneum is beginning to be formed by stratification and differentiation of the epidermis [87]. The periderm cells are replaced continuously by the stratum corneum until 23rd weeks [84]. The keratinization of the epidermis is finished by 26th weeks with one basal layer, 2-3 spinous layers, a granular layer and 5-6 stratum corneum layers [88]. The development of the skin shows **Figure 14**.

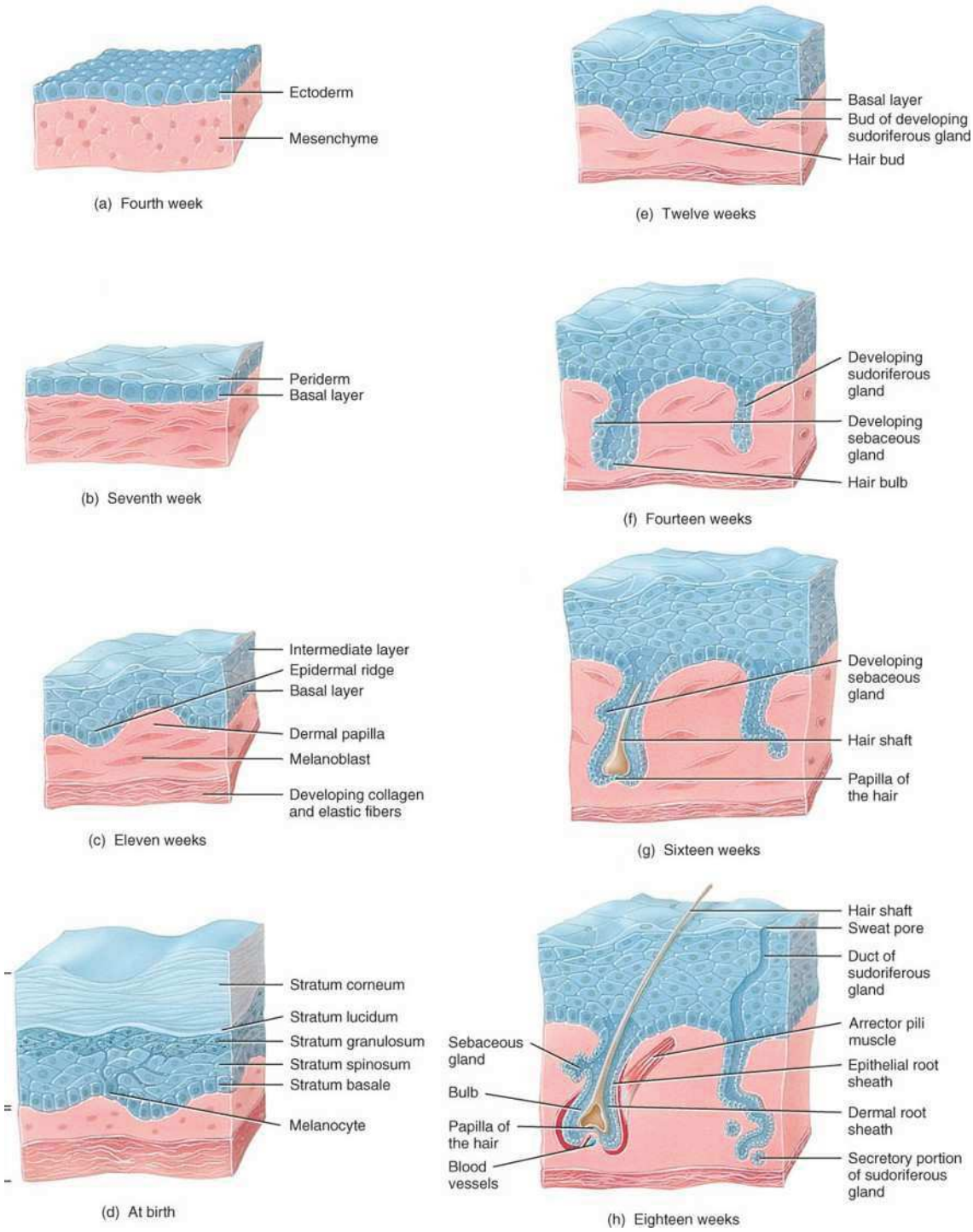

Figure 14. Development of the skin
(downloaded from *http://slideplayer.com/slide/10616090/*).

The fetal sebaceous glands have the peak of their activity in the 3rd trimester of gestation and their secretion together with desquamated maturing fetal corneocytes give the formation of vernix caseosa [82, 87]. Stratum corneum and vernix caseosa start to be formed

together during the last trimester of pregnancy [89]. Vernix caseosa helps stratum corneum to be formed in the wet uterine environment [90].

The production of lipids by the sebaceous gland is not fully understood yet. A study with rats showed that the activity of sebaceous glands is controlled by the sex hormones, androgens, and estrogens. Estrogens speed up the development of the skin and on the contrary, testosterone slows it up [91]. In the case of human sebaceous glands, the production of vernix caseosa is regulated by the endocrine system and assisted by steroids. Placenta and hypothalamus produce corticotropin-releasing factors (CRF), which initiate the release of adrenocorticotropic hormone (ACTH) from the pituitary gland. ACTH stimulates adrenal cortex that synthesizes androgenic steroids (*e.g.*, dihydroepiandrosteron (DHEA)). Subsequently, these steroids are enzymatically converted in the sebaceous gland to active androgens. The sebum (lipid film) is produced in the immediate vicinity of the hair follicle. Desquamate corneocytes finish the formation of vernix caseosa [82, 89]. The whole process is shown in **Figure 15**.

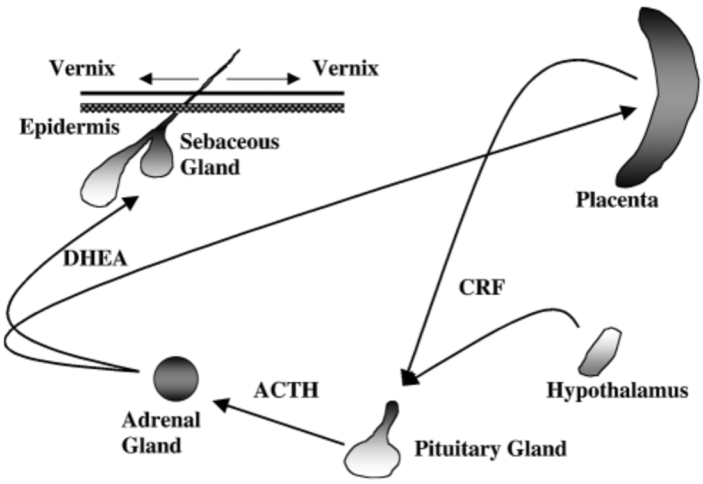

Figure 15. The hypothetical endocrine-based mechanism for vernix caseosa production [82].

3.2. Functions of vernix caseosa

Vernix caseosa and epidermal barrier lipids are essential for the fetal and neonatal skin because of their protective functions [92]. Vernix plays important role in the protection of the fetus from amniotic fluid maceration and loss of fluids and electrolytes. The neonatal skin is soft and smooth, and the exposition to the extrauterine environment is very stressful. Vernix caseosa helps to better adaptation to the extrauterine environment [93]. For this reason, vernix is recommended to leave on the newborn until spontaneous detachment [94].

Neonates born before the 28th week and less than 1,000 g do not have a protective layer of vernix. Their skin is characterized by the absence of stratum corneum and high transepidermal water loss [90].

3.2.1. Moisturizer function

Vernix caseosa is very important as a moisturizer for the stratum corneum [95]. It contains natural moisturizing factor which is described as a filament aggregating protein. This protein is placed in corneocytes, where water binding molecules contain in broken down forms are as well [96]. This protein is responsible for the maintaining of suppleness and elasticity of stratum corneum [97]. Hypothetically, the optimal high humidity microenvironment is arranged by the high water content in vernix caseosa [98].

3.2.2. Antimicrobial activity

Newborns often have to deal with bacterial infections of the skin. The critical point in newborns defense reactions is their immature adaptive immunity ensured by antimicrobial peptides and proteins [99-103]. Due to the presence of antimicrobial constituents, vernix may play important role in the protection of fetus from acute or subacute chorioamnionitis and facilitate colonization of the skin with microorganisms after the birth [90, 99-101]. Antimicrobial activity was also observed for lipids, namely for FAs [103].

3.2.3. Antioxidant properties

Newborns are exposed to high oxidative stress in the oxidative environment after a delivery. Vernix caseosa contains α-tocopherol (vitamin E) and melanin which are known for their antioxidant properties [90].

3.2.4. Influence on the development of the fetus organs

During the last trimester of the pregnancy, the development of lungs is finished, which is accompanied by an increase of pulmonary surfactant secretion into the amniotic fluid. As a result of this process, vernix caseosa is emulsified and detached which increases the amniotic fluid turbidity [104]. The benefit of detached vernix is a potential trophic effect on the developing foregut by the swallowing of the amniotic fluid by the fetus (see the mechanism in ***Figure 16***). The amniotic fluid is produced by the developing fetal kidneys that contain

high concentrations of the glutamine [82, 105, 106]. Glutamine is generally known as a trophic factor and is required for the proliferating cells (*e.g.*, intestinal epithelium and lymphocytes) [106].

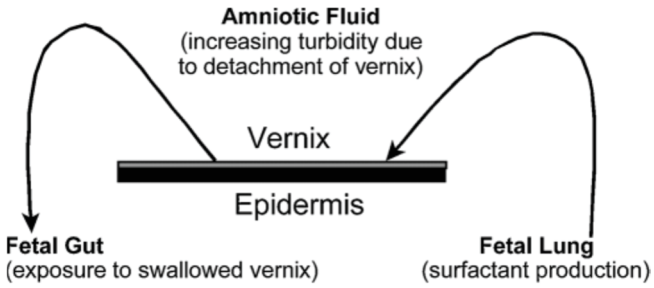

Figure 16. Proposed mechanism for surfactant-mediated vernix detachment [82].

3.2.5. Diagnostic and prognostic function and complications caused by vernix caseosa

Vernix caseosa can help to diagnose uterine rupture from the presence of vernix in urine (vernixuria) [107].

Vernix may bring rare complication during the cesarean section, such as vernix caseosa granuloma and vernix caseosa peritonitis, which are both caused by a big amount of vernix on the fetus and afterward insufficient cleaning of the abdominal cavity [108-110]. The presence of aspiration syndrome and granulomatous meningitis (vernicomyelia) could be caused by a big amount of vernix on the fetus skin [111, 112].

3.2.6. Potential application

Vernix substitutes have a potential to be used in medicine because of its excellent properties for the treatment of barrier-deficient skin of preterm infants [92, 113] or wounds healing of the adult skin [93]. The problem is, that the biological material itself cannot be used in treatment. Therefore, researchers have tried to generate the synthetic biofilms mimicking the unique composition and properties of natural vernix [114]. The biggest obstacle in this effort is the lack of knowledge of the vernix composition.

Another useful application may be in a cosmetic industry. Artificial vernix caseosa can function as an endogenous skin cleanser [113].

3.3. Structure and compositions of vernix caseosa

Vernix caseosa is composed from water (~80 %), proteins (~10%), and lipids (~10%) [92, 95]. The main part of vernix caseosa is water stored in corneocytes, which can be imagined as cellular sponges modulating water movement across the fetal skin [75, 96]. The stable water content in vernix caseosa is unclear from the perspective of the physiological meaning and relevance [98]. Vernix caseosa corneocytes have a significant influence on the osmotic regulation [98].

3.3.1. Lipids

Many earlier studies have been focused on characterizing the lipid composition in vernix [115-118]. The structure and organization of lipids in vernix caseosa and stratum corneum are different (**Figure 17**). Vernix caseosa is portrayed as a "pasta-and-cheese" because of its mobile architecture [82, 87]. A non-lamellar lipid matrix containing fetal corneocytes without intercorneocyte desmosomal connections exists in vernix caseosa [95]. On the contrary, mature stratum corneum has an organized framework with mature corneocytes (bricks) embedded in a lamellar matrix (mortar), portrayed as a "brick-and-mortar". Desmosomes are the special molecular complex which connects the corneocytes [119].

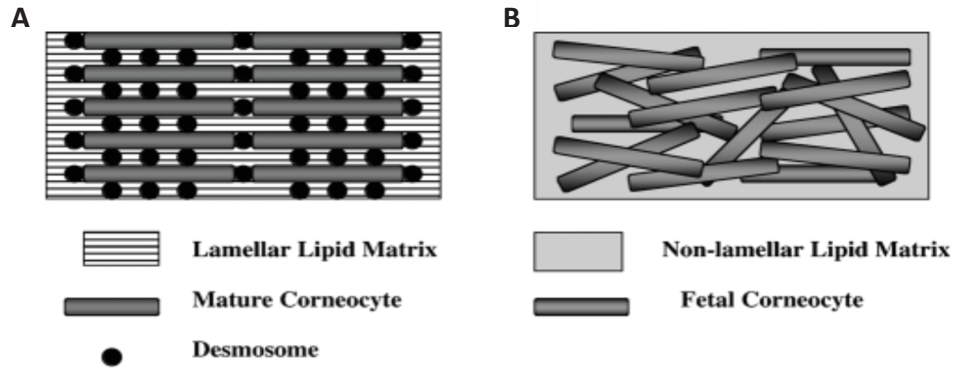

Figure 17. Comparison between stratum corneum (A) and vernix caseosa (B) architectures [119].

Vernix caseosa contains an extremely rich mixture of lipids. Despite significant analytical effort, lipids of vernix caseosa have not been comprehensively characterized yet. The most abundant lipid classes have been described just on the FA level, which means after hydrolysis of the lipid fractions.

The vernix caseosa lipidome have been shown to depend on the sex of fetus [120, 121]. The secretion of lipids comes from sebaceous glands and it is controlled hormonally. The

main role in hormonal regulation plays androgens, glucocorticoids, estrogens and thyroid hormones [122, 123].

Vernix caseosa is the unique skin barrier which is known only in humans. Nevertheless, periderm of rodents may hold a similar role in utero [124, 125].

3.3.1.1. Lipid classes in vernix caseosa

Lipids of vernix caseosa can be divided into two groups. (i) Barrier lipids are produced by developing epidermis and they are composed of cholesterol (Chol), FA, ceramides (Cer) and phospholipids (PL). They represent between 10% and 30% of the total vernix caseosa lipids [92, 115, 126-128]. (ii) Fetal sebaceous glands produce rather nonpolar lipids, such as WEs, sterol esters (SE), TGs, squalene (SQ) and 1,2-DDE [129, 130]. As evident from the **Figure 18**, vernix caseosa still contains unidentified lipid classes. Specifically, the fraction with polarities between 1,2-DDE and TG or Chol and FA [75]. It is also known that vernix contains polar lipids which are less polar than Cers, such as PL [104, 131]. Most of the lipid classes have been characterized a long time ago using analytical instruments available at that time. Therefore, our knowledge of even the most abundant lipid classes is limited.

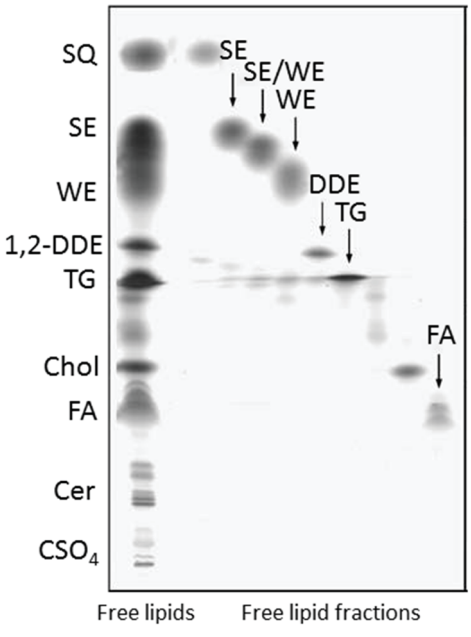

Figure 18. HPTLC separation of vernix caseosa lipids (modified according to [75]).

The least polar lipids in vernix caseosa are hydrocarbons represented almost exclusively by squalene [132]. WEs are relatively abundant lipid class (~15% of total vernix lipid) which contains straight, *iso*-, *anteiso*- or alternatively branched saturated and

monounsaturated FA chains; detailed information about the alcohol part of WEs is missing [116, 118]. SEs form ca 25% of total lipids. Their FAs are more frequently branched than in the case of WEs and they are less saturated. Chol is the most abundant sterol but other sterols, such as lathosterol or cholestanol have been found in the saponified samples as well [133]. 1,2-DDEs have been characterized well on FA level, but there is less information about aliphatic chains of diols [130]. TGs form more than 25% of total lipids and contain mostly saturated, *iso*- and *anteiso*-branched and unsaturated FA chains [75].

Polar lipids in vernix are less explored than the nonpolar lipids. Chol is the most abundant free sterol (ca 10%). Other sterols, like lathosterol, cholestanol, and desmosterol are much less abundant [75, 133]. Free FAs of vernix caseosa have mostly straight and saturated chains and they represent approximately 10 % of lipids. Cers are found in vernix roughly in the same amount as Chol and FAs [75]. Up to now, 8 structurally different Cer subclasses with ester- and amide- linked FAs have been identified in vernix caseosa [134]. The least known polar classes are PL which have an important role in the fetus development [131]. However, no publication about the detailed characterization of PL in vernix has been published so far.

The huge structural variability of vernix caseosa lipids can be illustrated also on FA level. The analysis of transesterified sample of vernix caseosa showed 133 FAME species, with saturated chains (46%), unsaturated branched chains (29%), unsaturated straight chains (22%), diunsaturated (2.3%) and triunsaturated (0.2%) carbon chain [74]. As regards branched FAs, *iso*-, *anteiso*-, middle chain monomethyl, dimethyl and trimethyl branched chains have been detected in vernix [73, 74]. Other study revealed FAs with 14 – 32 carbons in SEs, WEs, TGs and FAs [75]. Interestingly, vernix caseosa contains fatty acyls even and an odd number of carbons atom [73-75].

3.3.2. Proteins

Proteins in vernix originate from multiple sources. Some of them are dermal origin, but others come from amniotic fluid. There is a possible exchange of proteins between the fetal lungs and vernix caseosa through the amniotic fluid. Vernix caseosa found on newborns can also contain blood-related proteins like hemoglobin added during the vaginal delivery.

The most abundant protein is keratin which forms the scaffold of corneocytes. Quite a big portion of the proteins biosynthesized in the skin (ca 39%) are involved in innate immunity of a newborn, and ca 29% have direct antimicrobial properties [103]. The

antimicrobial activity has been proven in peptides, such as α-defensins (Human Neutrophil Peptide), or cathelicidins, and proteins, *e.g.*, psoriasin, secretory leukocyte protease inhibitor, calprotectin (calgranulin A and B), or lysozyme [99-103]. Further, the significant innate immunity was found attributes to cystatin A, calgranulin A and ubiquitin [102].

The most abundant free amino acids are asparagine and glutamine [105]. The importance of glutamine is described in the Chapter 3.2.4 .

RESEARCH AIMS

The general aim of this Theses is to contribute to our knowledge about the composition of vernix caseosa lipids. Specifically, new lipid classes have been identified in vernix caseosa. Newly identified lipids, as well as selected classes of already known lipids, have been comprehensively characterized using chromatography and mass spectrometry.

The work involves several tasks as follows:

- Optimization of lipid extraction from biological sample,
- development of separation method for lipid classes and subclasses,
- development of separation method for analysis of intact lipid subclass,
- transesterification and GC/MS.

LIST OF PUBLICATIONS AND PROCEEDINGS

This thesis is based on the following publications:

I. Míkova, R.; Vrkoslav, V.; Hanus, R.; Háková, E.; Hábová, Z.; Doležal, A.; Plavka, R.; Coufal, P.; Cvačka, J. *Newborn Boys and Girls Differ in the Lipid Composition of Vernix Caseosa.* Plos One, 2014. **9**(6).

II. Šubčíková, L.; Hoskovec, M.; Vrkoslav, V.; Čmelíková, T.; Háková, E.; Míková, R.; Coufal, P.; Doležal, A.; Plavka, R.; Cvačka, J. *Analysis of 1,2-Diol Diesters in Vernix Caseosa by High-Performance Liquid Chromatography - Atmospheric Pressure Chemical Ionization Mass Spectrometry.* Journal of Chromatography A, 2015. **1378**: p. 8-18.

III. Háková, E.; Vrkoslav, V.; Míková, R.; Schwarzová-Pecková, K.; Bosáková, Z.; Cvačka, J. *Localization of Double Bonds in Triacylglycerols Using High-Performance Liquid Chromatography/Atmospheric Pressure Chemical Ionization Ion-Trap Mass Spectrometry.* Analytical and Bioanalytical Chemistry, 2015. **407**(17): p. 5175-5188.

IV. Kalužíková, A.; Vrkoslav, V.; Harazim, E.; Hoskovec, Plavka, R.; Buděšínský, M; Bosáková, Z.; Cvačka, J. *Cholesteryl Esters of ω-(O-acyl)-hydroxy Fatty Acids in Vernix Caseosa*. Journal of Lipid Research, 2017 (accepted).

V. Harazim, E; Vrkoslav, V.; Buděšínský M.; Harazim, P.; Svoboda, M.; Plavka, R.; Bosáková, Z.; Cvačka. J. *1-O-acylceramides in Vernix Caseosa* (in preparation).

VI. Poad, B.L.J.; Marshall, D.L; Harazim, E.; Duchoslav, E.; Campbell, J.L.; Broadbent, J.A.; Mitchell, T.W.; Cvačka, J.; Blanksby, S.J. *Combining Charge-Switch Derivatization with Ozone-Induced Dissociation for Facile Fatty Acid Analysis* (in preparation).

This thesis is based on the following proceedings:

I. Háková, E.; Míková, R.; Vrkoslav, V.; Doležal, A.; Plavka, R.; Cvačka, J. *Separation of Nonpolar Lipids from Vernix Caseosa.* Cece 2014: 11th International Interdisciplinary Meeting on Bioanalysis, 2014: p. 216-219.

II. Háková, E.; Míková, R.; Vrkoslav, V.; Plavka, R.; Cvačka, J. *Analysis of Low Abundant Lipids in Vernix Caseosa Using Chromatographic Methods and Mass Spectrometry.* Proceedings of the 11th International Students Conference "Modern Analytical Chemistry", 2015: p. 23-28.

DECLARATION OF AUTHORSHIP

As a representative of the co-authors I declare that Eva Harazim, M.Sc. participated in the publications listed below:

I. I optimized the transesterification reaction for whole lipidome sample from vernix caseosa, carried out this reaction for 20 samples, help with optimization of GC/MS method, analyzed FAMEs in each 20 samples and interpreted all the data from this analysis.

(participation 20 %)

II. I cleaned the prepared unsaturated standards by Ag-TLC. I optimized HCD fragmentation analysis of the unsaturated standards of 1,2-DDE. I carried out the HCD fragmentation of HPLC/APCI-MS of the sample 1,2-DDE in vernix caseosa focused on the analysis of double bonds.

(participation 20 %)

III. A part of this publication was a component of my Diploma Thesis. I completed this work during the Ph.D. studies. I carried out a study of fragmentation of TGs regioisomers and interpreted HPLC/APCI-MS^2 data from olive oil and vernix caseosa.

(participation 80 %)

IV. I collaborate on the preliminary identification of newly isolated lipid class. I performed the extraction of the whole lipidom from vernix caseosa and isolated the lipid fraction of 1,2-DDE together with Cholesteryl esters of ω-(*O*-acyl)-hydroxy fatty acids.

(participation 20 %)

V. I carried out the extraction of the whole lipidome from vernix caseosa and isolated the lipid fraction of 1-*O*-acylceramides. I performed two types of transesterification and GC/MS measurement. After that, I did ESI-MS with an accurate mass of transesterified samples. I developed and optimized the RP-

HPLC/MS^3 method for characterization of molecular species and interpreted all data.

(participation 80 %)

VI. I did the extraction of the whole lipidome from vernix caseosa and isolated the lipid fraction of TGs. I carried out transesterification of TGs and GC/MS of FAMEs. I performed preliminary AMPP derivatization and its MS measurement.

(participation 20 %)

……..
doc. RNDr. Josef Cvačka, Ph.D.

As a representative of the co-authors I declare that Eva Harazim, M.Sc. participated in the proceedings listed below:

I. I developed and compare two NP-HPLC/MS^2 methods for separation of nonpolar lipids in vernix caseosa. I interpreted all found lipid classes.

(participation 90 %)

II. I developed an NP-HPLC/MS for identification and isolation of unknown particular lipids from vernix caseosa. I collected the sub-fraction of investigated lipids and carried out two different transesterification reactions, GC/MS measurement and ESI-MS analysis of transesterified samples. I did and investigated APCI-MS/MS spectra of intact lipids.

(participation 90 %)

……..
doc. RNDr. Josef Cvačka, Ph.D.

MATERIAL AND INSTRUMENTATIONS

Biological material

Samples of vernix caseosa were collected by staff of the 1st Faculty of Medicine, Charles University and General University Hospital in Prague.

Chemicals

Chemicals and synthetic standards were purchased from LachNer, Merck, Fluka, Lachema, Larodan, Nuc-Chek Prep and Avanti Polar Lipids.

Instrumentation

MS data at low resolution: LCQ Fleet with quadrupole ion trap (Thermo Fisher Scientific, San Jose, CA, USA)

MS data at high resolution: LTQ Orbitrap with linear ion trap (Thermo Fisher Scientific, San Jose, CA, USA)

Chip-based ESI: TriVersa NanoMate (Advion, Inhaca, USA)

Gas chromatography: gas chromatograph 7890N a 6890N coupled to quadrupole mass spectrometers 5975C or 5975 B, gas chromatograph Agilent 5975B MSD and mass spectrometer Shimadzu Triple Quadrupole 8040

SUMMARY OF RESULTS AND DISCUSSION

1. Lipid extraction

Several methods for lipid extraction have been accepted for routine analyses. Vernix caseosa contains ca 80% of water, and therefore the lipid extraction according to Bligh and Dyer [13] was chosen. The authors claim that the optimum lipid extraction should be done when the mixture of chloroform and methanol is mixed with the water in the tissue (sample) and yield a monophasic solution. A biphasic system is produced when water and/or chloroform is added. As a result, the chloroform layer should contain the lipids and methanol-water layer does not contain a significant amount of lipids.

The published procedure had to be slightly modified when extracting vernix caseosa, because a triphasic system was produced. The middle phase presumably consisted of corneocytes and dead cells from vernix caseosa. Therefore, re-extraction of organic phase and water layer was performed to minimize the middle layer in the chloroform layer (*Publication IV, V, VI*).

2. Characterization of lipids at the fatty acid level

2.1. Transesterification

Transesterification reaction is commonly used in lipid analysis. In this chapter two types of transesterification reactions are described. Both reactions have their pros and cons.

2.1.1. Transesterification of the whole lipidome

The whole lipidome was transesterified using a method described by Stránský and Jursík [33]. The study was focused on the differences in vernix caseosa from newborn boys and girls. 20 samples (10 female and 10 male samples) were compared. 167 distinct FAME species were detected. The representative chromatograms are shown in **Figure 19**. Both groups contained mostly saturated and branched chains with 11 to 31 carbons and containing up to 4 DBs. Principal component analysis visualization using the first two principal components clearly indicated that the samples can be divided into two groups according to

the sex. The sex differences were found at both qualitative and quantitative (relative abundances) levels. Interestingly, FAME 21:1 and FAME 22:1 were detected only in the girl and boy samples, respectively (*Publication I*).

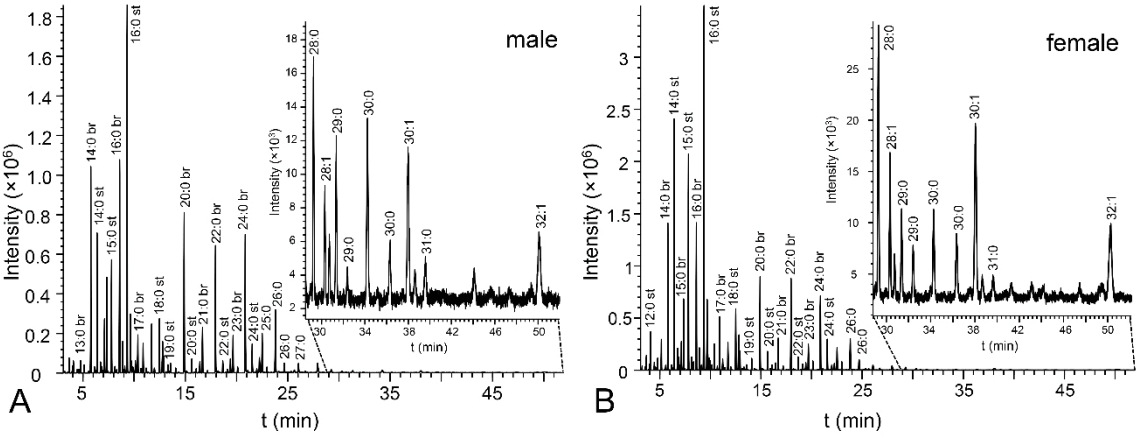

Figure 19. Reconstructed chromatograms (*m/z* 74) of the total lipid FAMEs [121].

2.1.2. Transesterification of triacylglycerols

The second type of transesterification was based on pyrolysis of tetramethyl sulfonium hydroxide [34] and was used in case of TGs. It made possible to detect FAMEs from 12 to 30 carbons, mainly saturated and branching chain. These results correspond to the FA composition found in vernix caseosa [74] and with previously recorded and so far unpublished data from our laboratory (*Publication VI*).

3. Separation of lipid classes

NP chromatography on TLC, LC or HPLC formats is widely used for separation of lipid classes.

3.1. Thin layer chromatography

The separation of nonpolar lipids using TLC with silica gel was used in *Publications IV, V* and *VI*. The procedure was modified from a method previously developed in our laboratory [121]. The original procedure was carried with the long glass plates (9 x 12 cm) and each plate was developed twice to focus the zone (in the first step to ¾ of the plate height and then, after air-drying, to the top). The procedure proved to be time consuming, and therefore,

the method was modified and shorter glass plates (6.5 x 7.5 cm) were used. TLC plates was developed only once without any loss of separation resolution of investigated lipid classes.

The polar lipids fraction was separated using TLC as well, however, the TLC plates used were bigger (9 x 12 cm) and composition of the mobile phase was changed. The best chromatographic resolution was achieved with a mobile phase composed of chloroform: methanol (85:15, by vol.) with 0.1% acetic acid and. A small percentage of acetic acid or in the mobile phase prevented the broadening of the zones corresponding to free FAs. This procedure was used for the isolation of a new lipid class from vernix caseosa. The reason is explained in the following chapter (*Publication V*).

3.2. Normal-phase high-performance liquid chromatography

A full characterization of all lipids in vernix caseosa has not been performed yet. The lipid material is extremely rich, and many lipid classes or subclasses are presented in very low quantities. Therefore, multistep separation scheme had to be developed. NP chromatography has been chosen for separation of lipid classes, where the lipids are separated according to the number and nature of polar functional groups. This type of separation can be used in low pressure or high-performance mode.

A scheme of the separation procedure used for identifying new lipid classes is in **Figure 20**. The total lipid extract was separated into 30 nonpolar lipid fractions by low-pressure column chromatography (the experiments were performed by Mgr. Radka Míková, Ph.D.). Most of the fractions contained several lipid classes, which required further separation step(s). Fractions F-12, 13 and 23 have been chosen for more detailed investigation. The second separation step was NP-HPLC because of its higher separation efficiency. Two different commercially available columns were compared: Acquity HILIC column (50 x 2.1 mm, particle size 1.7 μm) and Spherisorb column (250 + 250 x 4.6 mm, particle size 5 μm). Acquity HILIC column with Ethylene Bridged Hybrid (BEH) particles makes it possible to separate very polar analytes. However, in this case, the column was employed in NP separation mode. Using Acquity HILIC column a separation into four main chromatographic peaks (**Figure 21**) was achieved, whereas Spherisorb column separated the sample into nine chromatographic peaks (**Figure 22**). Therefore, Spherisorb column was chosen for further analysis (*Proceeding I*).

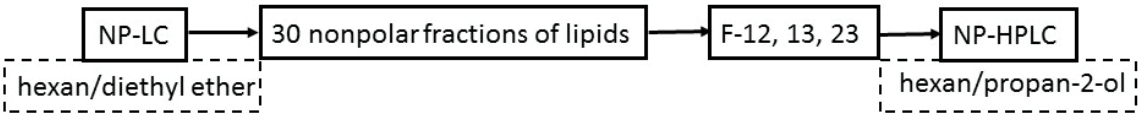

Figure 20. Scheme of the separation procedure of lipids from vernix caseosa.

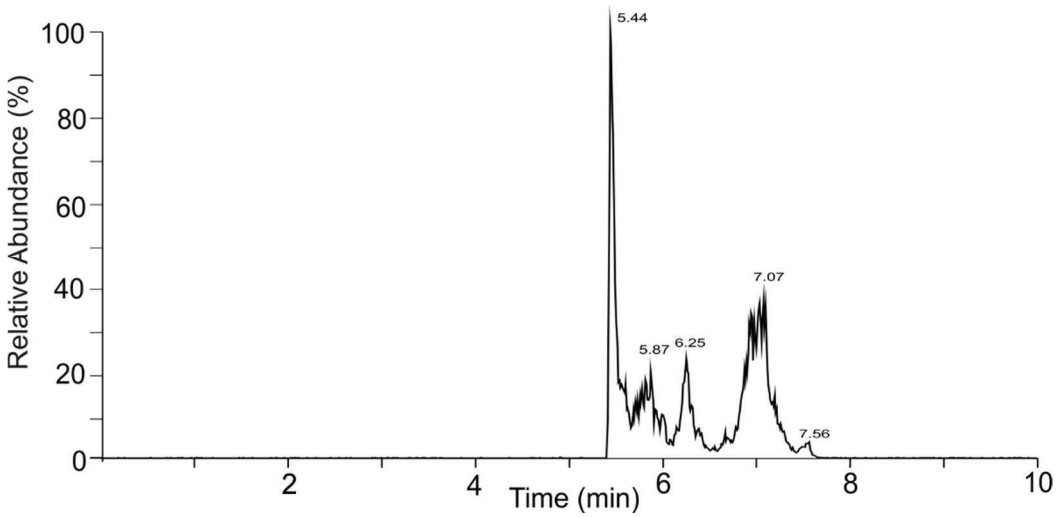

Figure 21. NP-HPLC/MS base peak chromatogram of F-12 obtained using Acquity HILIC column [135].

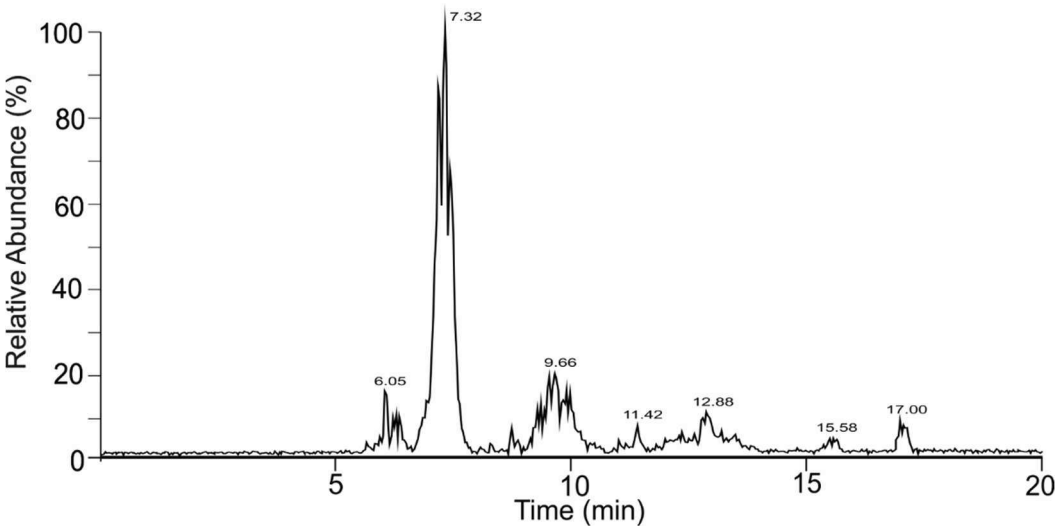

Figure 22. NP-HPLC/MS base peak chromatogram of F-12 obtained using two Spherisorb column [135].

Two Spherisorb columns connected in series were used for the separation of F-23 (**Figure 23**). In this way, six main chromatographic peaks were observed. The optimized method was also used as a semi-preparative isolation of individual lipid classes and sub-fractions for further investigation. As was mentioned above, the isolation of a new lipid class had to be repeated because of the more lipid classes in each fraction from the low pressure column chromatography. Moreover, each lipid class eluted in several fractions. Therefore,

a new approach of the isolation of the unknown lipid class was developed and is in **Figure 24** (*Publication V, Proceeding II*).

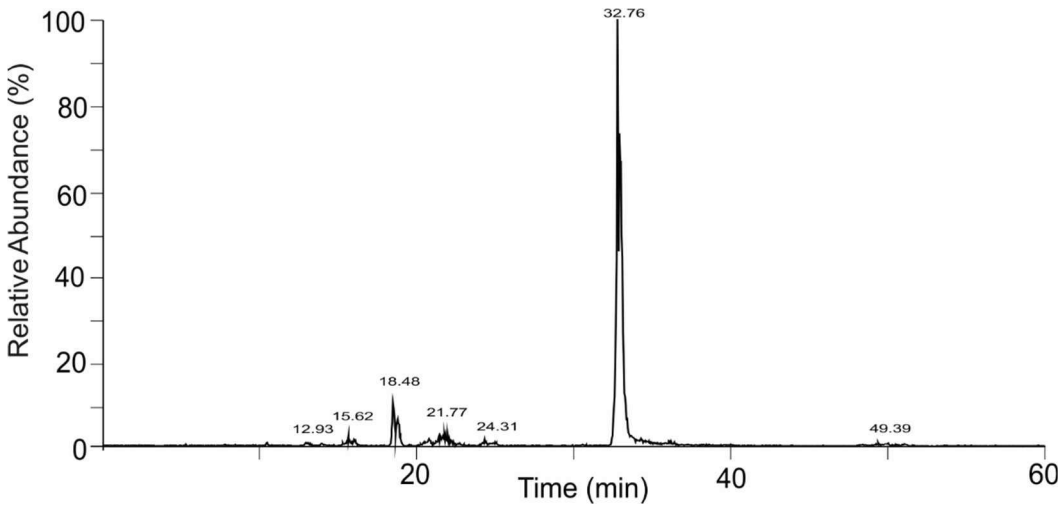

Figure 23. NP-HPLC/MS base peak chromatogram of F-23 [136].

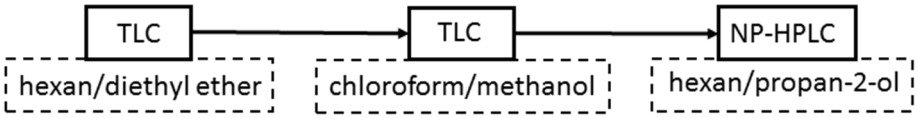

Figure 24. A new isolation scheme of unknown lipid class.

4. Identification of a new lipid subclass

The identification of unknown lipid classes in vernix caseosa is described below using acylceramides as an example (*Publication V, Proceeding II*).

4.1. Exact mass measurement

A mixture of isolated lipids corresponding to a single lipid class was measured by direct infusion into the mass spectrometer. APCI-MS of the unknown lipids provided protonated molecules accompanied by water loss fragments in the *m/z* 750 – 1200 range (**Figure 25**). The exact masses of protonated molecules were consistent with the elemental compositions $C_nH_{2n-x}O_4N$ (x = 0, 2, 4 or 6) and RDBEs of 1.5-4.5 showing species differing in degree of unsaturation. The presence of nitrogen pointed out to structures related to Cers. This hypothesis was also in agreement with the chromatographic behavior of the unknown lipids.

Thus, the elution on the column chromatography of investigated fraction F-23 was between TGs and more polar lipids.

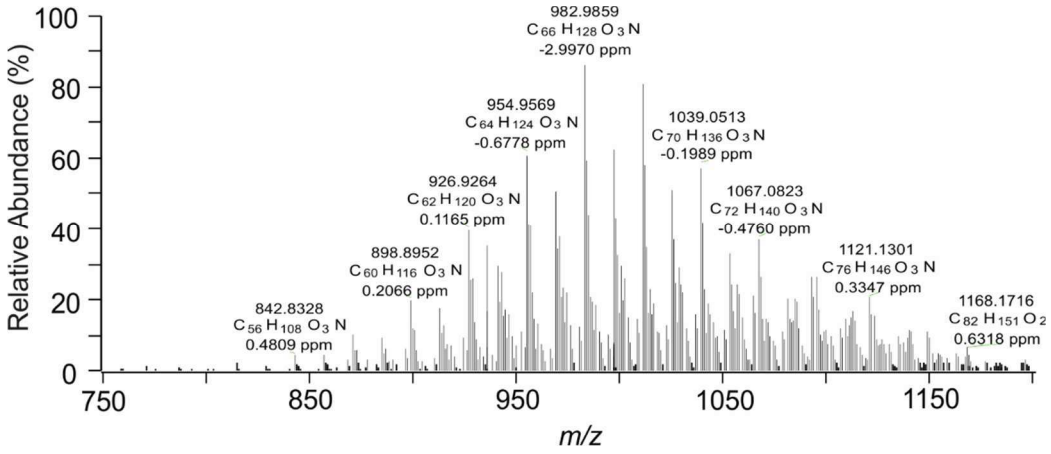

Figure 25. APCI-MS of the unknown lipids.

4.2. Transesterification

The next step of the structure elucidation was transesterification of the sample. From the measurement of the exact mass, it was obvious that these lipids contain nitrogen. Therefore, transesterification was carried out using conditions suitable for ester- and amide-linked FAs.

At the beginning, the transesterification according to Stranský and Jursík [33] was used. GC/MS analysis of transesterified sample showed mostly saturated and branched FAMEs with 12 to 32 carbons in the chain. A direct infusion of transesterified sample into Orbitrap mass spectrometer with APCI source mounted on revealed signals corresponding to the remaining part of the molecule after transesterification of ester-linked FAs (**Figure 26**). This measurement showed ions corresponding to $C_nH_{2n-x}O_2N^+$ (x = 0, 2, 4).

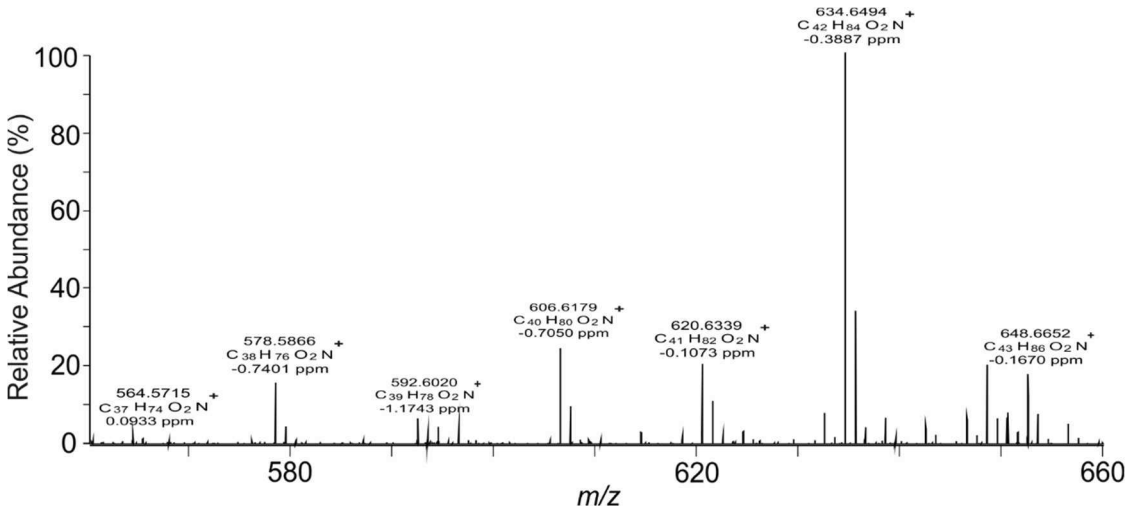

Figure 26. APCI-MS of the sample after transesterification.

After that, the next transesterification with stronger reaction conditions according to Oku et al. [134] was employed. This type of reaction is focused on both ester- and amide-linked FAs, because of harsher reaction conditions. The data showed mostly saturated and branching FAMEs with 12 to 34 carbons in the chain. Moreover, a direct infusion of the reaction mixture into the Orbitrap mass spectrometer with ESI source operated in the negative ion mode revealed signals consistent with sphingosine (*m/z* 336.3 as a chloride adduct) and dihydrosphingosine (*m/z* 334.3 as a chloride adduct), see **Figure 27**.

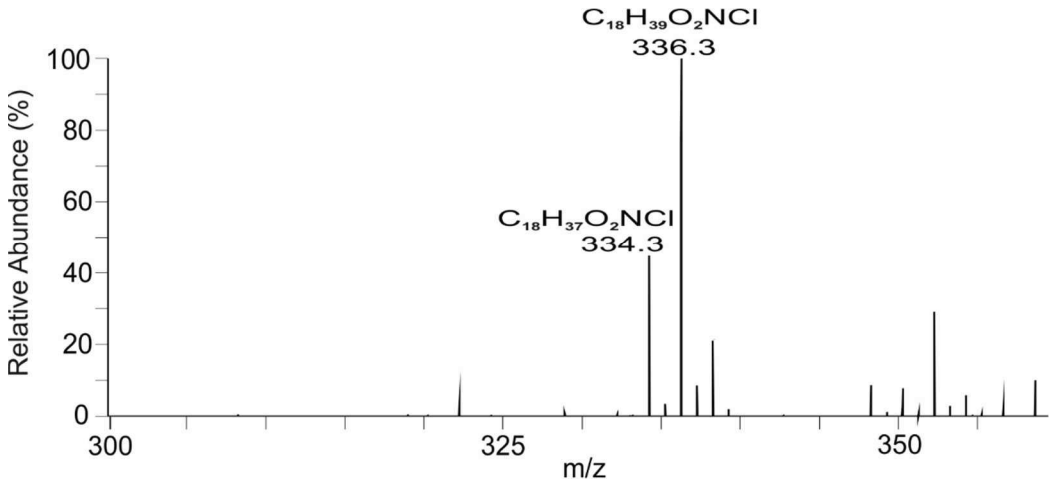

Figure 27. ESI-MS of the rest of the sample after transesterification reaction.

The investigated lipid subclass of Cers contained both ester- and amide-linked FAs. Such subclass of Cers have been described before for vernix caseosa.

4.3. Fragmentation experiments

The fragmentation of a commercial standard 17:0 Ceramide-1-*O*-18:1 (1-oleoyl-N-heptadecanoyl-*D*-erythro-sphingosine) was investigated in detail. The full scan APCI spectrum showed abundant dehydrated protonated molecule $[M + H - H_2O]^+$ (*m/z* 798.8) accompanied by protonated molecule at much lower intensity and was also used for deducing the total number of carbons and double bonds. Dehydrated protonated molecule was selected for CID in the ion trap. The MS^2 spectrum provided ion consistent with the neutral loss of ester-linked FA ($[M + H - H_2O - FA]^+$ at *m/z* 516.5) and a combined neutral loss of ester-linked fatty acid and alkadiene from the sphingoid base chain ($[M + H - H_2O - FA - C_nH_{2n-2}]^+$ at *m/z* 294.3). In addition, doubly dehydrated sphingoid base ion (*m/z* 264.3) was detected (**Figure 28a**). The MS^2 spectrum provided information on the ester-linked FA. Further fragmentation of the FA loss peak (MS^3 spectrum) led to the elimination of alkadiene ($[M + H - H_2O - FA - C_nH_{2n-2}]^+$ at *m/z* 294.3) and formation of doubly dehydrated sphingoid base ion (*m/z* 264.3). Fragment (at *m/z* 270.3) corresponding to protonated amide formed from the amide-linked FAs was detected at low intensities (**Figure 28b**). The MS^3 spectrum made it possible to identify amide-linked FA and sphingoid base.

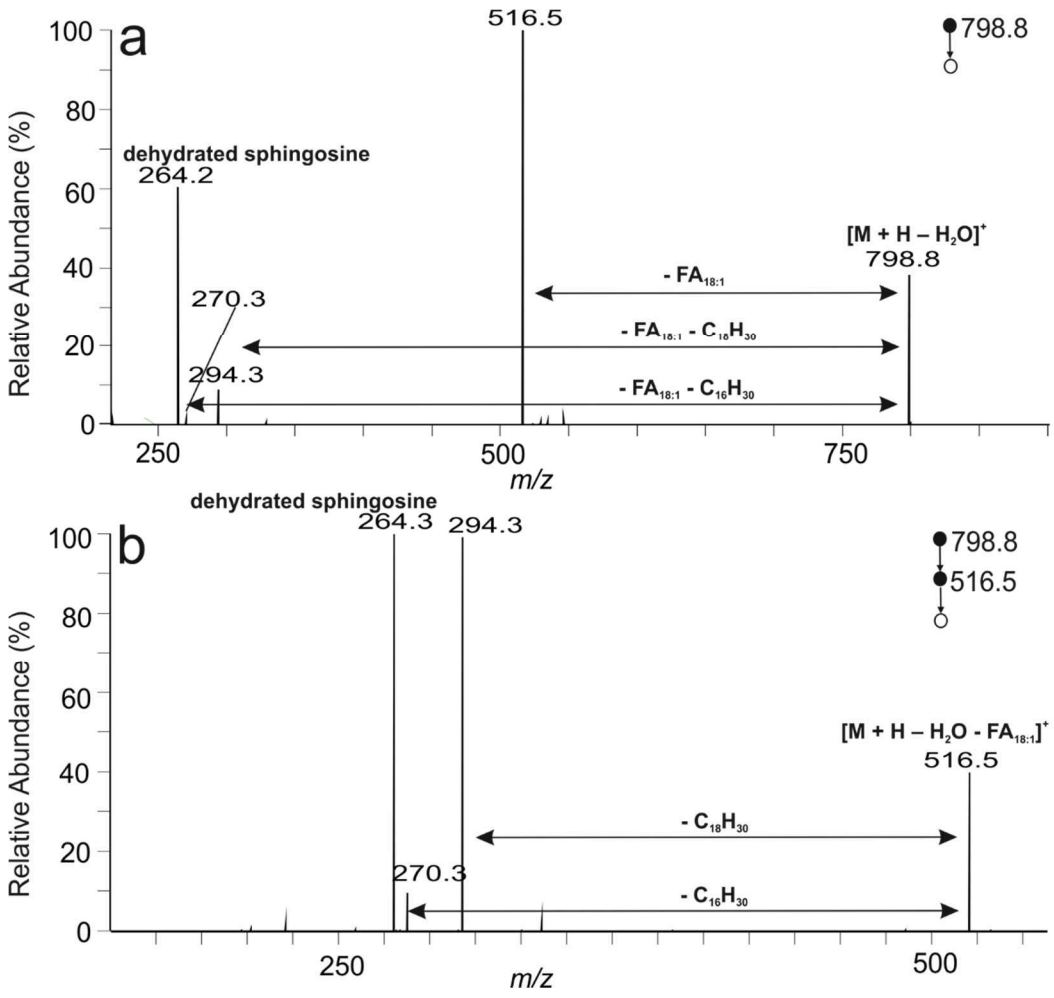

Figure 28. APCI-MS^2 of *m/z* 798.8 ([M + H - H_2O]$^+$) of 1-oleoyl-N-heptadecanoyl-*D*-erythro-sphingosine (**a**). APCI-MS^3 of *m/z* 516.5 ([M + H - H_2O - $FA_{18:1}$]$^+$) of 1-oleoyl-N-heptadecanoyl-*D*-erythro-sphingosine (**b**).

When compared with the investigated lipids of vernix caseosa with standard, the APCI-MS^2 spectrum is shown in **Figure 29a**. Thus, the ions at *m/z* 558.7, 572.7, 586.7, 600.7, 614.7, 628.7 and 642.7 were rationalized as products of neutral losses of FAs from the parent ion, thus marked as [M + H – H_2O – $FA_{24:0}$]$^+$, [M + H – H_2O – $FA_{23:0}$]$^+$, [M + H – H_2O – $FA_{22:0}$]$^+$, [M + H – H_2O – $FA_{21:0}$]$^+$, [M + H – H_2O – $FA_{20:0}$]$^+$, [M + H – H_2O – $FA_{19:0}$]$^+$ and [M + H – H_2O – $FA_{18:0}$]$^+$, respectively. The other important peak *m/z* 264.3 was identified as doubly dehydrated sphingosine. This fragmentation spectrum indicated the presence of multiple isobaric species. The APCI-MS^3 spectrum of investigated lipids showed ions formed in analogous way as in the standard (**Figure 29b**). The base peak at *m/z* 392.5 corresponded to the neutral loss of FA 24:0 and octadecadiene from the base. The less intense fragment at *m/z* 368.5 corresponds to the loss FA 24:0 and

alkatetraene from the precursor. The doubly dehydrated sphingosine is represented by the peak at *m/z* 264.3.

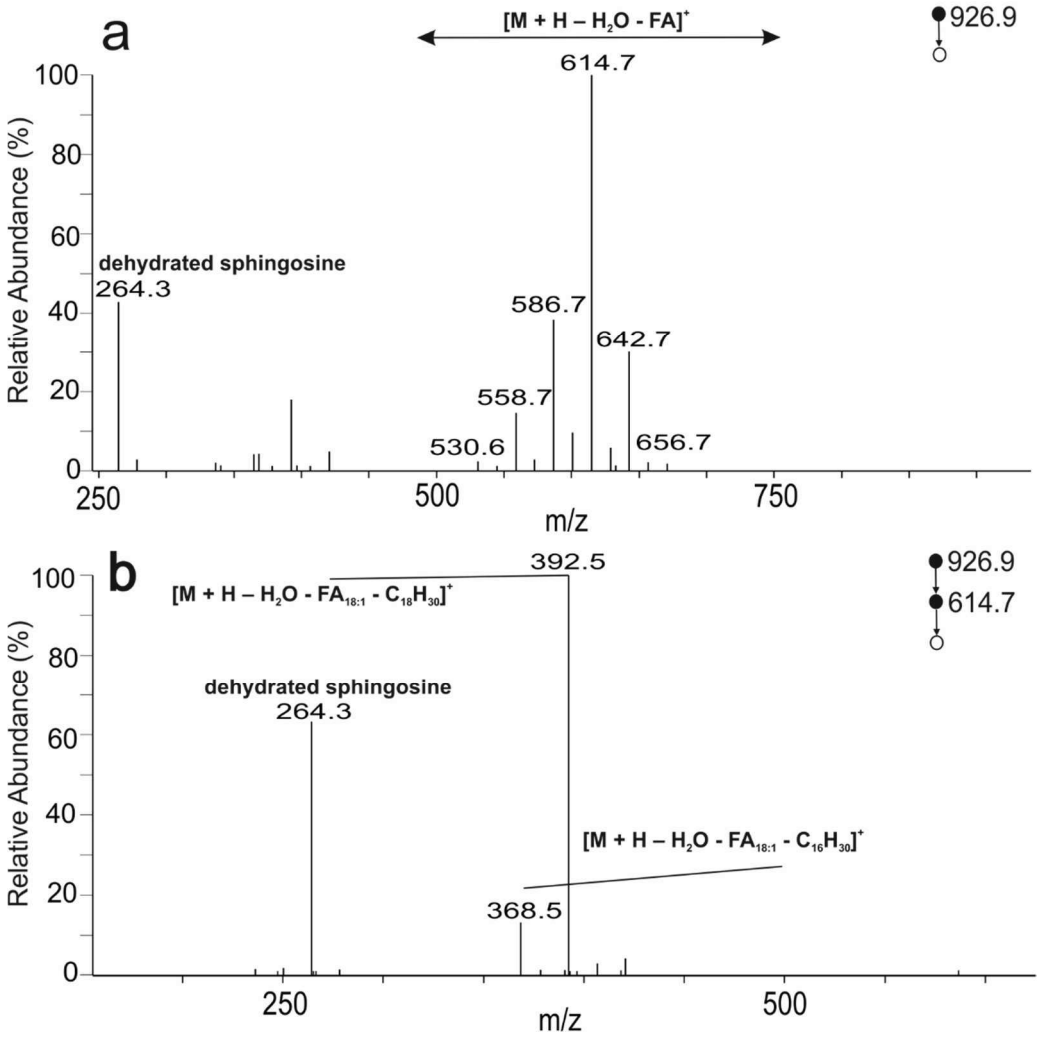

Figure 29. APCI-MS^2 of investigated lipids (**a**). APCI-MS^3 of investigated lipids (**b**).

These results showed that the fragmentation scheme of the commercial standard is the same as in the investigated lipids. Therefore, it was hypothesized that the isolated lipids were 1-*O*-acylceramides. This was also supported by the presence of this Cers in human stratum corneum [137].

4.4. Nuclear magnetic resonance

NMR measurement (the experiments were performed by RNDr. Miloš Buděšínský, CSc.) was chosen as a comparative experiment of the investigated sample and commercially available standard (17:0 Ceramide-1-*O*-18:1) for the confirmation of the hypothesis about the structure of the isolated lipids. NMR spectra were recorded for the isolated lipid class, i.e. for a rich mixture of molecular species. Although no conclusions could be made

regarding the side chains, the chemical shifts for the central part of the molecules observed in ^{1}H and ^{13}C NMR spectra were almost identical with data for the standard (**Figure 30**). Hence, the hypothesis was confirmed and the lipids isolated from vernix caseosa were identified as 1-*O*-acylceramides (**Figure 31**) (*Publication V, Proceeding II*).

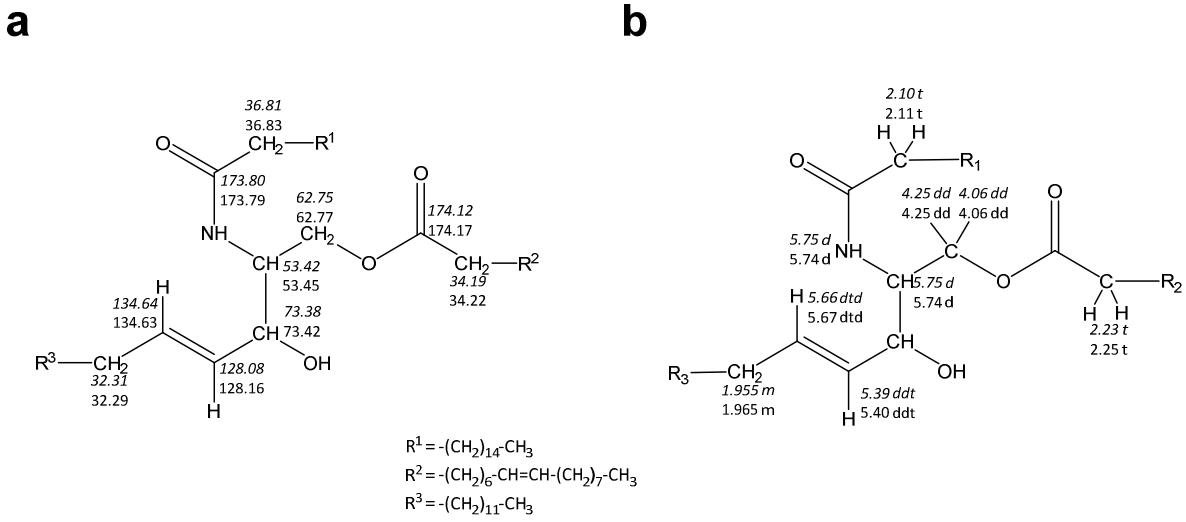

Figure 30. Carbon-13 (**a**) and proton (**b**) NMR chemical shifts of the investigated sample and authentic sample 17:0 Ceramide-1-*O*-18:1.

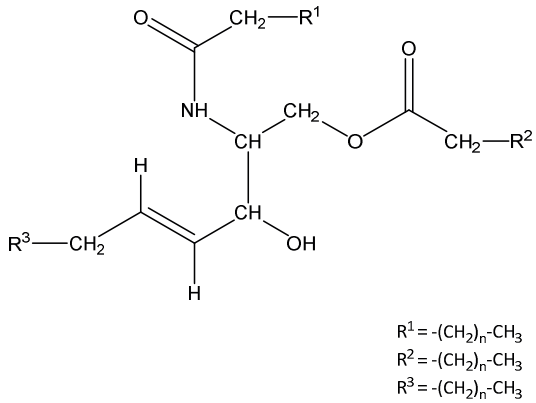

Figure 31. The general structure of 1-O-acylceramide.

5. Detailed characterization of lipid classes

Once the general structure of the lipid class is established and its fragmentation is known, molecular species within the class can be characterized in detail.

5.1. RP-HPLC/MS^3 of 1-*O*-acylceramides

To comprehensively characterize 1-*O*-acylceramides in vernix caseosa, an HPLC/MS method for separation and identification of the molecular species has been developed. The chromatographic conditions were optimized with the mixture of 1-*O*-acylceramides isolated from vernix caseosa. Excellent separation was achieved on NovaPak C18 column (column length of 30 cm), with a gradient elution of propan-2-ol in acetonitrile. The base peak chromatogram is seen in **Figure 32**. Data-dependent MS detection method consisted of three scanning events: (1) the full scan in the 400 – 2000 *m/z* range in orbitrap; (2) CID MS/MS of the first most intense ion from the parent mass list with a normalized collision energy between 26 and 29% and isolation width 2 Da for a 2-D ion trap; (3-8) CID MS^3 from the first to sixth most abundant fragments recorded in the previous event. The same sample was analyzed four times, each time with different inclusion list corresponding to 1-*O*-acylceramides with 0, 1, 2, and 3 double bonds.

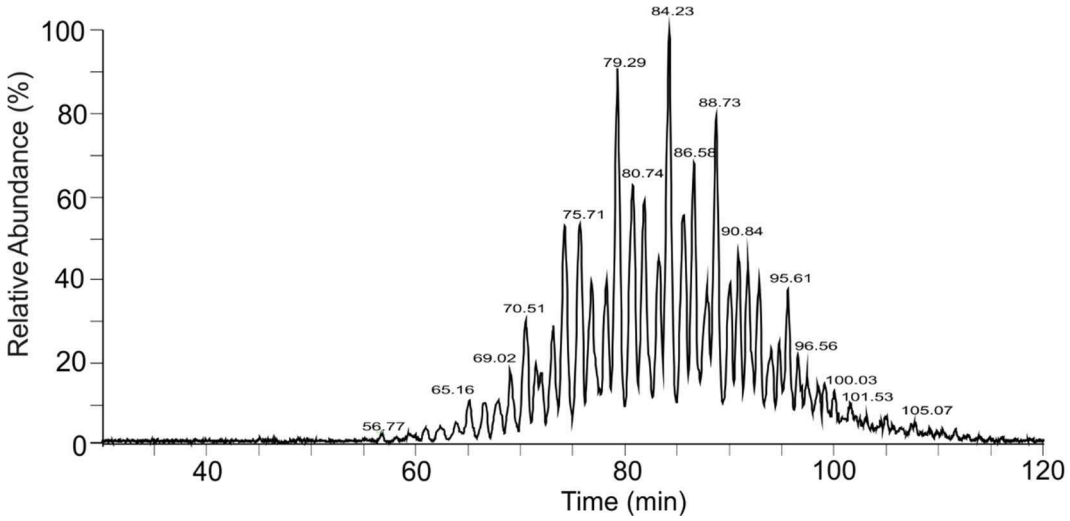

Figure 32. The base peak RP-HPLC/MS chromatogram of 1-*O*-acylceramides.

The data were manually interpreted using an in-house developed MS Excel macro. In this way, it was possible to characterize 2,343 molecular species of 1-*O*-acylceramides, out of which 970 molecular species were fully characterized. Unfortunately, it was not possible to fully identify all 1-*O*-acylceramides due to the low intensity of some of the MS^3 spectra. Therefore, the characterization was completed for some of these molecular species just from MS^2 data. The peak areas used for the calculation of relative intensities of 1-*O*-acylceramides were integrated in the full-scan chromatograms reconstructed for the sum of $[M + H]^+$ and $[M - H_2O + H]^+$ ions.

The results showed that 1-*O*-acylceramides contain saturated, monounsaturated, diunsaturated and trinusaturated species accounted for 17%, 54%, 31% and 5%, respectively. One DB was typically present in the sphingoid base. It corresponded well with the representation of the sphingoid bases in this lipid subclass in human stratum corneum, where sphingosine is the most abundant base [137].

The diversity of epidermal Cers reflects the huge number of FAs produced by human skin. The diverse carbon chain length is combined with the different degree of unsaturation, hydroxylation and methyl-branching in an *iso*- and an *anteiso*-positions [138]. From the wider perspective, C16 and C24 FAs are the major components of sphingolipids [139]. In human stratum corneum, Rabionet et al. [137] found 1-*O*-acylceramides containing ester-linked FAs from 14:0 to 26:0 with the most abundant 16:0 followed by 14:0 and 24:0. On the contrary, our study of 1-*O*-acylceramides from vernix caseosa showed 24:0 to be the most abundant FA followed by 22:0 and 26:0. In agreement with the stratum corneum [137], odd FA chains were found in 1-*O*-acylceramides. In stratum corneum, odd FA chain form approximately 30% of total Cers [140]. The difference in the composition of 1-*O*-acylceramides between fetal and adult skin is likely caused by changes in the Cer biosynthesis during skin ontogeny.

5.2. Localization of double bonds

A method for localization of DBs in TGs and 1,2-DDEs was developed. This technique employs CID and PQD of the $C_3H_5N^{+\bullet}$ adducts ($[M + 55]^{+\bullet}$) formed in the presence of acetonitrile in the APCI source. The $[M + 55]^{+\bullet}$ ions are cleaved at C-C bonds next to the DBs, and they are labeled "α" (ester moieties) or "ω" (terminal-carbon end which do not contain an ester group). To sum up, the fragmentation spectra of the adduct showed: (i) total number of carbons and DBs in the molecule (the mass of the $[M + 55]^{+\bullet}$ precursor), (ii) the number of carbons and DBs in acyls (masses of the $[M + 55 - FA]^{+\bullet}$ fragments), (iii) the acyl in the *sn*-2 position on the glycerol backbone in TGs (the intensity ratios of the $[M + 55 - FA]^{+\bullet}$ fragments), and (iv) the DBs positions in acyls (the masses of the α and ω ions) and diol chains in the case of 1,2-DDE.

5.2.1. Double bonds in triacylglycerols

HPLC-APCI-MS^2 was used for the comprehensive structural characterization of unsaturated TGs in olive oil and vernix caseosa. The separation was performed on Nova-Pak C18

columns with acetonitrile/propan-2-ol gradient [141-143]. The full-scan spectra gave information about the total number of carbons and DBs in TG acyls [144]. The CID spectra of $[M + 55]^{+\bullet}$ provided the same information as well. FA neutral loss ions ($[M + 55 - FA]^{+\bullet}$) were used for determination of the number of carbon atoms and DBs in acyls, *sn*-position of FAs on the glycerol backbone and the position of the DBs. The approach can be illustrated on two regioisomers 1-arachidin-olein-3-palmitin (TG 20:0/18:1(n-9)/16:0; AOP) and 1-palmitin-2-arachidin-3-olein (TG 16:0/20:0/18:1(n-9); PAO), see **Figure 33**. The oleyl chain was modified with $C_3H_5N^{+\bullet}$. Therefore, only the two saturated acyls were cleaved off as neutral FAs. **Figure 33a** shows that both fragments in AOP ($[M + 55 - FA_{20:0}]^{+\bullet}$ and $[M + 55 - FA_{16:0}]^{+\bullet}$) had comparable intensities, whereas in PAO (**Figure 33b**), the intensity of $[M + 55 - FA_{20:0}]^{+\bullet}$ was significantly lower. This way FA in *sn*-2 position was identified.

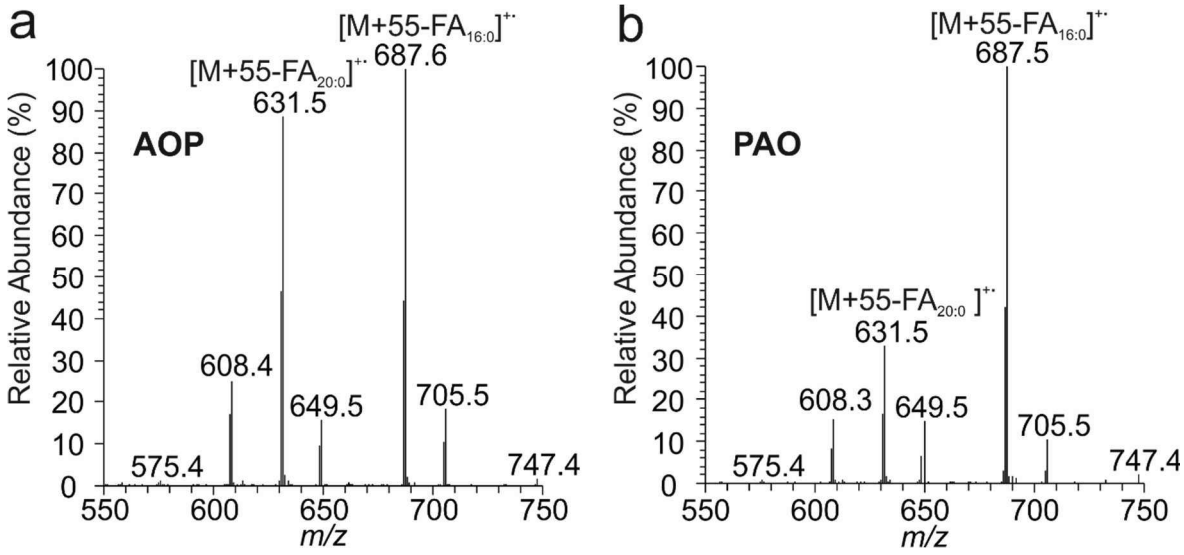

Figure 33. The zoomed regions of the APCI CID MS^2 spectra of the $[M + 55]^{+\bullet}$ adduct of AOP (**a**) and PAO (**b**).

In the olive oil sample, the DB position was assigned for 20 TGs. The chromatographic separation of TGs from vernix caseosa confirmed that the vernix consists of an exceptionally large number of molecular species. Unfortunately, data could be interpreted only partially because of molecular species co-elution. However, it was obvious that the α fragments mostly showed DBs up to *n*-12, but small peaks in some spectra also indicated DBs at more distant positions from the chain termini (*Publication III*).

5.2.2. Double bonds in 1,2-diol diesters

The positions of DBs in the unsaturated chains of 1,2-DDEs in vernix caseosa was determined by MS^2. The separation was performed on Nova-Pak C18 columns with acetonitrile/ethyl acetate gradient. Both CID and HCD fragmentation of $[M + 55]^{+\bullet}$ was employed. HCD fragmentation was chosen due to the possibility of fragmentation in the full mass range. The DBs were located mostly in *n*-7, *n*-9, and *n*-5. The reconstructed chromatograms for each DBs from HCD MS/MS data are in **Figure 34** (*Publication II*).

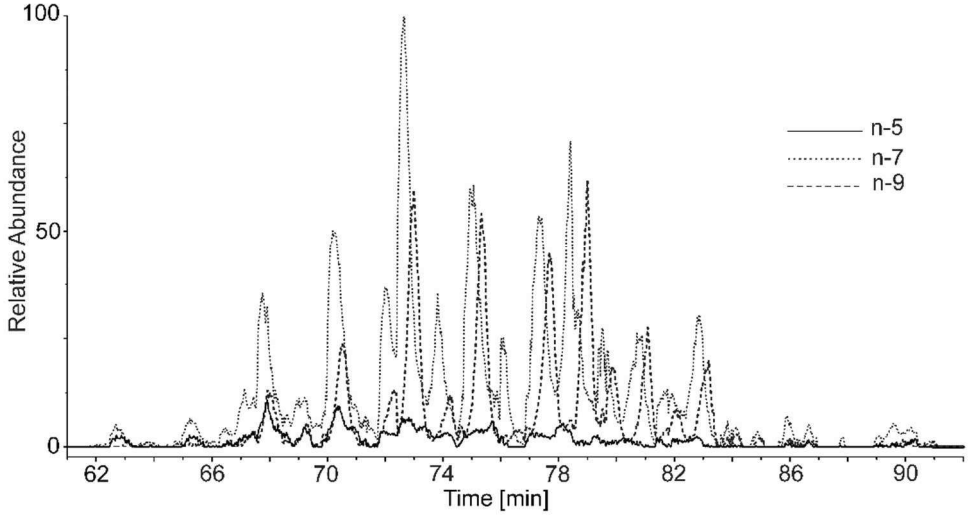

Figure 34. The overlay plot of chromatograms of vernix caseosa 1,2-DDE reconstructed for molecular species with DB in the position *n*-5, *n*-7 and *n*-9 [65].

5.3. Localization of methyl branching in hydrocarbon chains

The fraction of TGs was hydrolyzed according to Hsu et al. [78] and the AMPP derivatization was subsequently performed [80]. Full-MS spectra from TriVersa NanoMate-orbitrap showed branching in *iso*-, *anteiso*- and other positions. These results correlated well with the published data [73-75] (*Publication VI*).

- Publication I -

OPEN ACCESS Freely available online

PLOS ONE

Newborn Boys and Girls Differ in the Lipid Composition of Vernix Caseosa

Radka Míková[1,2,3], Vladimír Vrkoslav[1], Robert Hanus[1], Eva Háková[1,2], Zuzana Hábová[4], Antonín Doležal[4], Richard Plavka[4], Pavel Coufal[2], Josef Cvačka[1]*

1 Institute of Organic Chemistry and Biochemistry, Academy of Sciences of the Czech Republic, Prague, Czech Republic, **2** Department of Analytical Chemistry, Faculty of Science, Charles University in Prague, Prague, Czech Republic, **3** 3rd Internal Department, General Faculty Hospital and 1st Faculty of Medicine, Charles University in Prague, Prague, Czech Republic, **4** Department of Obstetrics and Gynaecology, General Faculty Hospital and 1st Faculty of Medicine, Charles University in Prague, Prague, Czech Republic

Abstract

Vernix caseosa protects the skin of a human fetus during the last trimester of pregnancy and of a newborn after the delivery. Besides its cellular and proteinaceous components, an important constituent and functional agent is a complex lipid fraction, implicated in a multitude of salubrious effects of vernix caseosa. Little is known about how the chemical composition of vernix caseosa lipids is affected by various biological characteristics of the baby, such as the gestational age, birth weight, and, last but not least, the gender of the newborn. This study reports on the chemical variability of lipids contained in the vernix caseosa of twenty newborn girls and boys and shows that the quantitative patterns of the lipids are sex-specific. The specificity of lipids was investigated at the level of fatty acids in the total lipid extracts and intact lipids of several neutral lipid classes. Hydrocarbons, wax esters, cholesteryl esters, diol diesters and triacylglycerols were isolated using optimized semipreparative thin-layer chromatography, and the molecular species within each class were characterized using matrix-assisted laser desorption/ionization mass spectrometry. Statistical evaluation revealed significant quantitative sex-related differences in the lipid composition of vernix caseosa among the newborns, pronounced in the two lipid classes associated with the activity of sebaceous glands. Higher proportions of wax esters and triacylglycerols with longer hydrocarbon chains were observed in newborn girls.

Citation: Míková R, Vrkoslav V, Hanus R, Háková E, Hábová Z, et al. (2014) Newborn Boys and Girls Differ in the Lipid Composition of Vernix Caseosa. PLoS ONE 9(6): e99173. doi:10.1371/journal.pone.0099173

Editor: Claude Wicker-Thomas, Cnrs France

Received November 4, 2013; **Accepted** May 12, 2014; **Published** June 9, 2014

Funding: Funding for this project was provided by Czech Science Foundation (Project No. 206/12/0750), Academy of Sciences of the Czech Republic (Project RVO 61388963), Charles University in Prague (Project SVV), research projects MSM 0021620857 and 5302-28002PVK. The funders had no role in study design, data collection and analysis, decision to publish, or preparation of the manuscript.

Competing Interests: The authors have declared that no competing interests exist.

* E-mail: cvacka@uochb.cas.cz

Introduction

Vernix caseosa (VC) is a white creamy substance which coats the skin of a human fetus and of a newborn [1] and which is produced during the third trimester of gestation [2]. In utero, it serves as a waterproofing film and modulator of transepidermal water flux [3], facilitates the final stages of the skin and gastrointestinal system development and protects the skin from some of the agents present in amniotic fluid [4]. After the birth, it acts as an antibacterial shield [5,6] and helps the neonate to adapt to the dry environment [7]. Very low birth-weight preterm infants lack VC and are susceptible to invasive infections because of insufficient formation of the stratum corneum [8,9]. The skin of prematurely born babies suffers from excessive water loss, resulting in dangerous dehydration and heat loss [10,11]. VC also shows a remarkable ability to enhance wound healing, which promises new therapies for patients with altered skin integrity after burn injuries or skin diseases. Because a therapeutic use of native VC from mature newborns is impossible, clinically relevant artificial substitutes of VC are to be developed [12,13].

VC is a complex biofilm composed of water in hydrated corneocytes (80%), surrounded by a matrix of lipids (10%) and proteins (10%) [1,2]. The lipid fraction is extremely rich and not yet fully characterized despite the efforts of numerous researchers [14–19]. The most abundant lipid classes (wax esters – WE, cholesteryl esters – CE, diol diesters – DD and triacylglycerols – TG) are known, but they are characterized typically only with respect to their fatty acids (FA) composition, investigated from hydrolyzed lipid fractions.

Virtually nothing is known about the chemical variability of VC lipids depending on the gestational age and health conditions, the changes in the chemical composition during fetal development or the possible diagnostic value of VC components. All this information is of importance for current neonatology and medicine in general. Sex-related aspects of the early skin development are not well understood either. Certain differences between VC lipids of newborn boys and girls were reported in early eighties [15,20] using analytical methodology available at that time and a limited number of samples. The data relied either on semi-quantitation of lipid classes separated by thin layer chromatography (TLC) or lipid hydrolysis followed by analysis of fatty acid methyl esters (FAME). The structures of intact lipids involved in sex-related differences have not been disclosed. Recent advances in analytical instrumentation, namely in mass spectrom-

etry, allow us to have a closer look at the chemistry of vernix caseosa and the human skin ontogeny from a different perspective.

Matrix-assisted laser desorption/ionization mass spectrometry (MALDI MS) is a powerful tool in protein and peptide analytics, increasingly utilized also in lipidomics [21–24]. The method allows intact lipids to be detected without previous modification and may yield quantitative results [25]. Modern MALDI MS setups also make it possible to fragment selected peaks, e.g., by tandem time-of-flight (TOF/TOF) instrumentation and thus to obtain more detailed structural information [22–26].

In this paper, we investigate sex-related differences in the lipid composition of VC in twenty newborn boys and girls at the level of FAME and intact, non-hydrolyzed lipids using MALDI MS. Since the cutaneous barrier formation and sebaceous gland activity are controlled by sex hormones [27–29], we test a hypothesis that the composition of VC lipids is gender-related. For this purpose, we have developed a method for a detailed characterization of intact lipids in VC. The lipids were isolated, separated into neutral lipid classes and the molecular species within the lipid classes were analyzed using MALDI-TOF MS and MALDI-TOF/TOF MS. The resulting data were statistically evaluated with respect to the sex specificity.

Materials and Methods

Chemicals

Analytical-grade hexane, chloroform, diethyl ether, acetone and ethanol were purchased from Merck (Darmstadt, Germany) or Penta (Chrudim, Czech Republic) and distilled in glass before use. Chloroform was stabilized with 1% of ethanol. Gradient-grade methanol was bought from LachNer (Neratovice, Czech Republic). 2,6-Di-terc-butyl-4-methylphenol (BHT), Florisil® for TLC and acetyl chloride were obtained from Fluka (Buchs, Switzerland). Magnesium sulfate (p.a.), polyethylene glycols (PEG, reagent-grade), primuline and rhodamine 6G were purchased from Sigma-Aldrich (St. Louis, MO, USA). Silica gel 60 G with gypsum (12%) was obtained from Merck and silver carbonate was from Lachema (Brno, Czech Republic). Deionized water was manufactured by the Milli Q system (Millipore, Milford, MA, USA). Lipid standards (99% purity) were bought from Sigma-Aldrich (squalene - SQ, stearyl behenate), Larodan (Malmö, Sweden; cholesterol – Chol, tristearin, distearin and palmitolein), Nu-Chek Prep (Elysian, MN, USA; stearic acid) and Matreya LLC (Pleasant Gap, PA, USA; phosphatidylcholine). MALDI-TOF MS matrices were supplied by Fluka (2,5-dihydroxybenzoic acid – DHB; 2-mercaptobenzothiazole – MBT; 7,7,8,8-tetracyanoquinodimethane – TCNQ; 4-nitroaniline – 4NA; picolinic acid – PA) and Sigma-Aldrich (2,4,6-trihydroxyacetophenone – THAP). The sodium salt of 2,5-dihydroxybenzoic acid (NaDHB) and the lithium salt of 2,5-dihydroxybenzoic acid (LiDHB) were synthesized and prepared as described previously [26].

Sample collecting

Healthy male (10) and female (10) subjects (Table S1) delivered at full term were included in this study. VC samples (1–2 g) were collected immediately after the delivery into glass vials and stored at −25°C. The exact location of sampling (back, buttocks, groins, legs, arms) varied depending on the VC layer thickness. Blood-contaminated samples were discarded. The samples were collected with written informed parental consent and the work was approved by the Ethics Committee of the General University Hospital, Prague (910/09 S-IV); the study was performed according to the Declaration of Helsinki.

Isolation of lipids and their TLC separation

The VC samples were suspended in 50 ml of chloroform:-methanol 2:1 (V/V) with 0.05% BHT. The suspension was cleared of epithelial cells by filtration through a column containing purified cotton-wool and silica gel (60–120 μm, ca 0.2 g). Anhydrous $MgSO_4$ (ca 5 g) was added to absorb water, and the suspension was filtered again. The solvents were removed by a rotary evaporator (35°C, 170 mbar) and a stream of argon. The isolated lipids were stored in glass vials at −25°C.

The lipids (ca 20 mg) were separated on 9×12 cm glass TLC plates coated with silica gel using hexane:diethyl ether (93:7, V/V) as a mobile phase. Each plate was developed twice to focus the zones (in the first step to 3/4 of the plate height and then, after air-drying, to the top). The zones were visualized under UV light after being sprayed with rhodamine 6G (0.05% in ethanol); an example of the thin layer chromatogram is shown in Figure S1. The zones corresponding to particular lipid fractions (classes) were identified using standards and published data [19] as follows: SQ (R_f 0.89–0.94), WE + CE in one zone (R_f 0.66–0.74), DD (R_f 0.46–0.52), TG (R_f 0.19–0.27), free fatty acids - FA (R_f 0.10–0.13), Chol (R_f 0.06–0.08) and highly polar lipids (R_f 0.00–0.01). Only neutral lipids (SQ, WE, CE, DD and TG) were further isolated and analyzed in this study. Each zone was scratched off into a column with purified cotton-wool and silica gel; neutral lipids were eluted using diethyl ether. The solvent was evaporated under a stream of argon; the separated lipids were dissolved in chloroform:methanol 2:1 (V/V, 1 mg/ml) and stored at −25°C.

Due to their similar polarities, WE did not separate from CE on silica gel sorbents; their separation required magnesium-based materials to be used [30,31]. Therefore, we separated WE (R_f 0.54–0.68) from CE (R_f 0.32–0.48) using 20×10 cm glass TLC plates coated with Florisil (activated magnesium silicate) with a hexane:diethyl ether (90:10, V/V) mobile phase [32]. The plates were activated at 120°C for 1 h before the separation. The zones were visualized using primuline in methanol:water 1:1 (V/V) under UV radiation (366 nm). WE and CE were extracted from the plates as described above.

Transesterification and GC/MS of FAME

Total lipid extracts of VC were transesterified using a method described by Stránský and Jursík [33]. Briefly, lipids were dissolved in chloroform:methanol (2:3, v/v) in a small glass ampoule. After adding acetyl chloride, the ampoule was sealed and placed in a water bath at 70°C. After 60 min the ampoule was opened, the reaction mixture was neutralized with silver carbonate and injected onto GC column. FAME were analyzed using a 7890N gas chromatograph (Agilent, Santa Clara, CA, USA) coupled to a 5975C quadrupole mass spectrometer and equipped with a fused silica capillary column DB-wax (30 m×0.25 mm, 0.25 μm, J&W 122-7032). The carrier gas was helium at 1.5 mL/min. The injector was held at 250°C and operated with a split ratio of 1:20; 2 μL of sample solution (chloroform:methanol (2:3, v/v)) was injected. The temperature program: 140°C (0 min), then 5°C/min to 250°C (50 min); total run time was 72 min. 70 eV EI mass spectra were recorded in the mass range of 25–600 u; 3 min solvent delay was used. Temperatures of the transfer line, ion source and quadrupole were 250°C, 230°C and 150°C, respectively. The chromatographic peaks representing FAME were identified based on the presence of m/z 74 and m/z 87 in their mass spectra. FAME were relatively quantified from their peak areas integrated in the total ion current chromatograms.

MALDI MS

MALDI-TOF MS measurements were performed on a Reflex IV (Bruker Daltonik GmbH, Bremen, Germany) operated in the reflectron mode with an acceleration voltage of 20 kV and an extraction pulse of 200 ns. A nitrogen UV laser (337.1 nm, a 4 ns pulse of 300 μJ, a maximum frequency of 20 Hz) was utilized for desorption and ionization. Matrix ions were suppressed below m/z 200. The mass spectra were externally calibrated using PEG oligomers. The MS spectra were averaged from 1,000 laser shots collected at various places across the spot. Fragmentation was performed using ultrafleXtreme equipped with smartbeam laser (Bruker Daltonik GmbH, Bremen, Germany). A MS/MS LIFT method for small molecules mode with an ion source and LIFT acceleration voltage set to 7.5 kV and 19 kV, respectively was utilized for the fragmentation. Precursor ions were selected by ion selector mass window ±1 Da. The spectra were averaged from at least 20,000 shots. The data were collected and processed using FlexAnalysis 3.0 or 3.3 (Bruker Daltonik GmbH).

The choice of the matrix is crucial for successful MALDI MS. Therefore, a study was undertaken to select suitable matrices for lipid classes studied in this work. Because of the neutral character of the analytes lacking easily ionizable groups, matrices permitting ionization via metal-ion attachment were needed. The matrices were selected based on 1/their ability to ionize the analytes at low laser fluencies, 2/the absence of analyte-fragment ions in the spectra, 3/the simplicity of the isotope clusters, and 4/the low interference of the matrix background ions with analyte signals. The investigated matrices were prepared as saturated solutions in the solvents specified in Table S2 and co-deposited with the samples on the MALDI plate (MTP 387-position ground steel target; Bruker Daltonik GmbH) by mixing the sample with the matrix before application (CE, DD, TG) or by covering the matrix with the sample (WE).

In agreement with previous findings [26], LiDHB, providing $[M+Li]^+$ adducts, proved to be the most suitable matrix for SQ and WE. The same matrix appeared to work well also for CE and DD; LiDHB was found to be more suitable for CE than the previously suggested DHB [22,34,35]. To the best of our knowledge, DD have not been previously analyzed by MALDI MS. NaDHB ionized easily TG giving $[M+Na]^+$ molecular adducts, similarly like DHB, MBT and THAP, suggested by other authors [36–38]. The overview of performance of the matrices is given in Table S2.

For further data processing, the intensities of the MALDI MS peaks corresponding to molecular adduct were converted into relative percentages. As only lipids of the same lipid class were ionized during the MALDI MS analysis, the signal suppression by other components was considered negligible. The peak intensities were not corrected by any response factors.

Data treatment

The chemical diversity and sex-specificity of the VC samples were evaluated using principal component analysis (PCA) and redundancy analysis (RDA) performed in the Canoco 4.5 package (Biometrics, Plant Research). The intensities of the MALDI-TOF MS responses for particular lipids within each lipid class were converted into relative percentages and the diversity of their quantitative patterns visualized using PCA. Subsequently, RDA analyses of standardized variables with sex as a categorical predictor and a Monte Carlo permutation test (unrestricted permutations, $n = 999$) were performed in order to test the significance of the differences between the relative patterns in the two sexes. Six selected TG and six selected WE with an important contribution to the differences between the two sexes were further fragmented and the relative intensities of their dominant fragments treated using the same approach. The relative proportions of 167 FAME obtained from the hydrolyzed VC lipids were arcsine transformed and subjected to PCA and RDA as described above. The differences corresponding to a p-value below 0.05 are reported as significant for the RDA and Monte Carlo permutation tests.

Results and Discussion

GC/MS of VC fatty acids

Using a set of samples of 20 newborn subjects we investigated variability of VC lipids at the fatty acids level. We detected 167 distinct FAME species, mostly with saturated and branched chains, which is in agreement with recent report [39] showing 133 FAME in VC. FAME contained 11–31 carbons and exceptionally up to 4 double bonds (Table S3). Representative chromatograms are shown in Figure 1. When carefully inspecting chromatograms and peak lists, minor differences between boy and girl data were noticed. Visualization by means of PCA (Figure 2) using the first two principal components clearly showed that the samples were separated into two groups according to the sex of newborns. A redundancy analysis confirmed that the patterns of the relative abundances of FAME were significantly different between the male and female samples ($F = 3.2$; $p = 0.002$). The contributions of individual FAME to the observed overall differences are listed in the Table S3 as percent fits of each compound with the predicted RDA model with sex as categorical predictor. The sex specificity of the FAME composition consisted in both qualitative and quantitative differences in relative abundances. Among the FAME fitting the best the RDA model, monoenic or saturated species with typically more than 20 carbons occurred, but some middle-chain FAME with 14–19 carbons were also involved in sex differentiation (Figure 3 and Table S3). The most important species in this respect were FAME 21:1 (peak No. 116) and FAME 22:1 (peak No. 123) detected in non-negligible quantities only in the girl and boy samples, respectively. Nevertheless, the sex-related differences could not have been reduced to a list of only a few important species, the differences in quantitative patterns being complex. Encouraging results with hydrolyzed total lipid extracts showing differences between male and female subjects prompted us to study the chemical composition of intact lipids in boy and girl samples.

MALDI MS of intact VC lipids

All lipid fractions obtained from VC samples provided rich MALDI spectra with series of peaks. The spectra of the SQ zone were an exception, as only a single signal of squalene was present. It is important to note that in general the peaks in the spectra could represent mixtures of lipid species having the same elemental composition. Like in all direct MS approaches (without chromatographic separation), the isomeric species cannot be distinguished by mass. Therefore, each peak was characterized by the total number of carbons and double bonds in the chains. An inspection of the mass spectra did not reveal any qualitative gender-related differences in the lipid composition of the studied fractions.

In the WE fraction (Figure 4 and Table S4), we observed wax esters with 26–46 carbons and up to three unsaturations; the most prominent peaks corresponded to molecules with one double bond in the chains. The CE fraction contained a series of cholesteryl esters with 14–32 carbons in the FA chain and between zero and two double bonds. In the DD fraction, we detected diol diesters with 46–64 carbon atoms, containing up to three unsaturations.

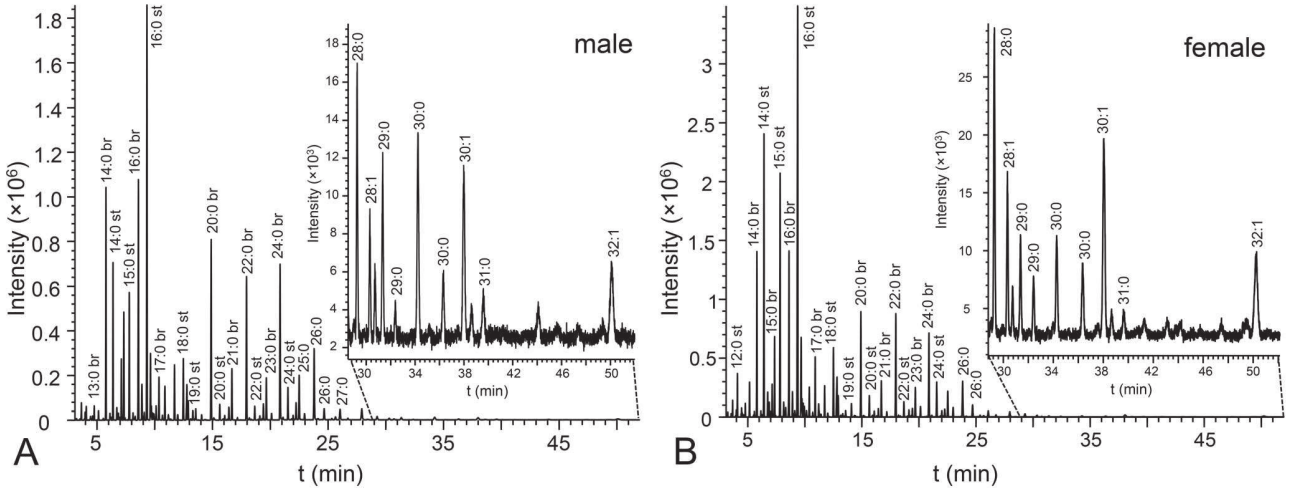

Figure 1. Chromatograms of the total lipid FAME. Characteristic reconstructed chromatogram (*m/z* 74) of FAME obtained by transesterification of vernix caseosa total lipid extract of a newborn boy (A) and girl (B).
doi:10.1371/journal.pone.0099173.g001

TG with 39–69 carbons in the FA chains and with up to four double bonds were detected in the TG fraction (Figure 5 and Table S5). Dominant peaks represented molecules with either one or two unsaturations.

Sex-related differences in intact lipids

Quantitative patterns of the relative intensities of particular compounds in each studied class (except for SQ) were compared using PCA and RDA with sex as a categorical predictor. The quantitative diversities within the DD and CE fractions were broadly overlapping in the two sexes and no significant gender-related differences could have been proved using RDA and Monte Carlo permutation tests.

On the contrary, even a simple visual inspection of the mass spectra of WE and TG fractions made it possible to discriminate between the spectra of boys and girls (Figures 4 and 5). In both classes, the compounds with a higher carbon number seemed to be over-represented in female samples while shorter carbon chains were relatively more abundant in the spectra of males. When visualized by means of PCA, depicted in Figure 6 as the first two principal components of the WE and TG samples, the two sexes were separated into two slightly overlapping groups. A redundancy analysis confirmed that the pattern of the relative abundances of WE was significantly different between the male and female

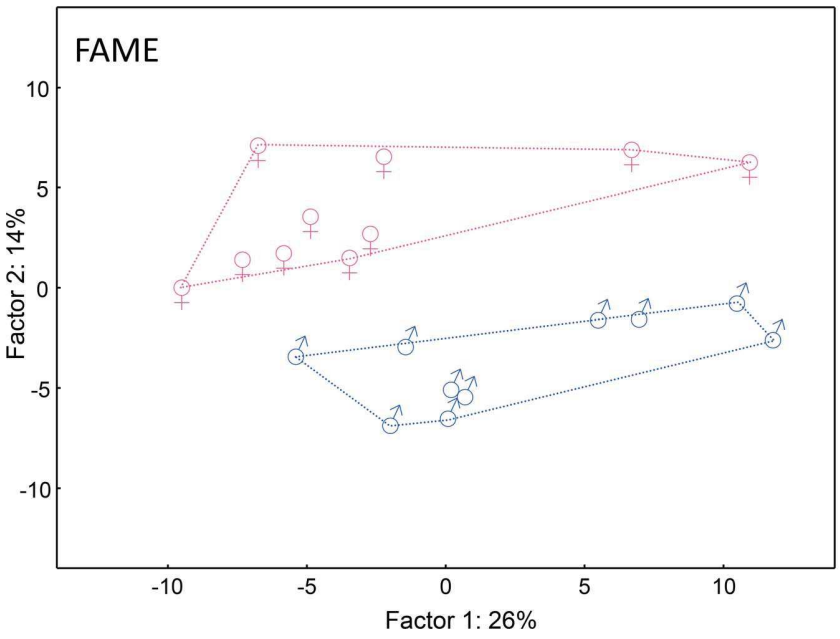

Figure 2. Quantitative pattern of vernix caseosa fatty acids in newborn boys (♂) and girls (♀). Graphic representation of the first two components of PCA calculated from the relative intensities of fatty acid methyl esters obtained from hydrolyzed vernix caseosa lipids.
doi:10.1371/journal.pone.0099173.g002

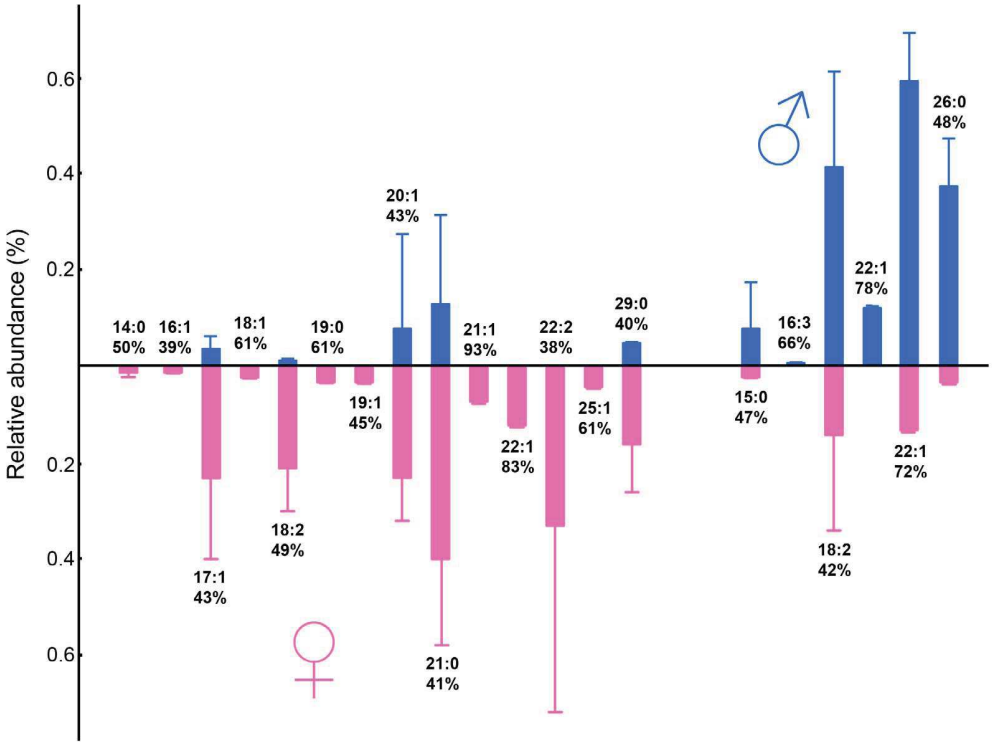

Figure 3. Comparison of relative abundances of fatty acid methyl esters from hydrolyzed vernix caseosa lipids obtained from newborn boys and girls. Relative abundances were calculated from peak areas in gas chromatograms (mean ± SD). Twenty compounds contributing the most to the sex-related differences are shown. The percentages below the peak assignments indicate the percent fit of individual variables with the model predictions of RDA with sex standing as categorical predictor.
doi:10.1371/journal.pone.0099173.g003

samples ($F = 6.9$; $p = 0.008$). The contributions of individual WE to the observed overall differences are listed in the Table S4 as percent fits of each compound with the predicted RDA model with sex as categorical predictor. The WE with higher chain lengths proved to be relatively over-represented in females, and vice versa, the short-chain WE were relatively more abundant in males. Similar conclusions were drawn for TG. The overall pattern of relative intensities differed significantly between males and females ($F = 8.8$; $p = 0.002$). Higher chain lengths were relatively more abundant in females while the relative proportions of TG were shifted towards shorter chain lengths in males, as shown in the Table S5.

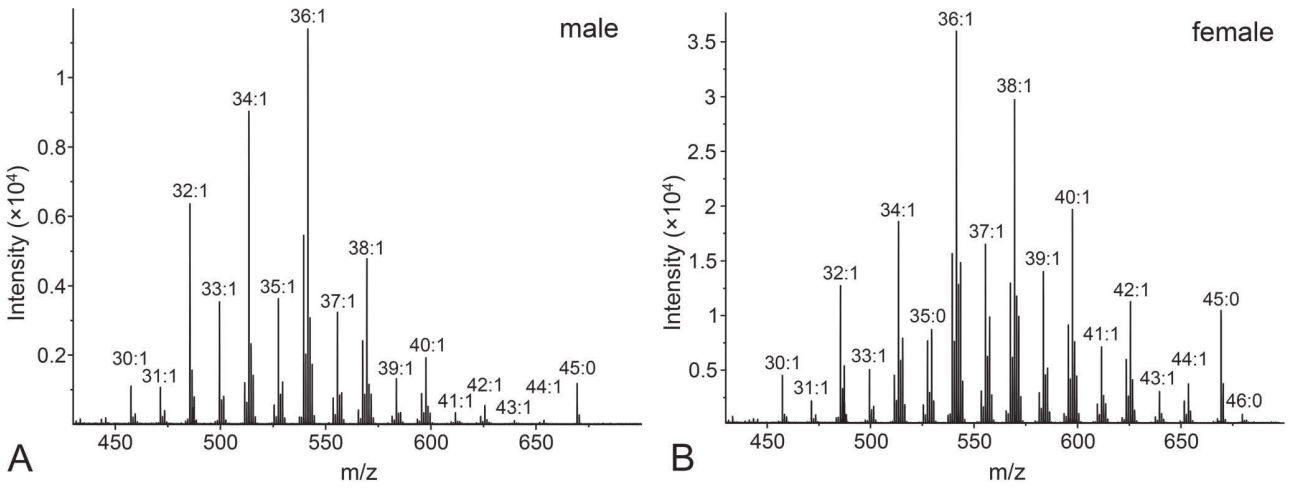

Figure 4. Mass spectra of the wax esters. Characteristic MALDI spectrum of the wax esters isolated from the vernix caseosa of a newborn boy (A) and girl (B). A LiDHB matrix was used and the signals correspond to molecular adducts with lithium ions $[M+Li]^+$.
doi:10.1371/journal.pone.0099173.g004

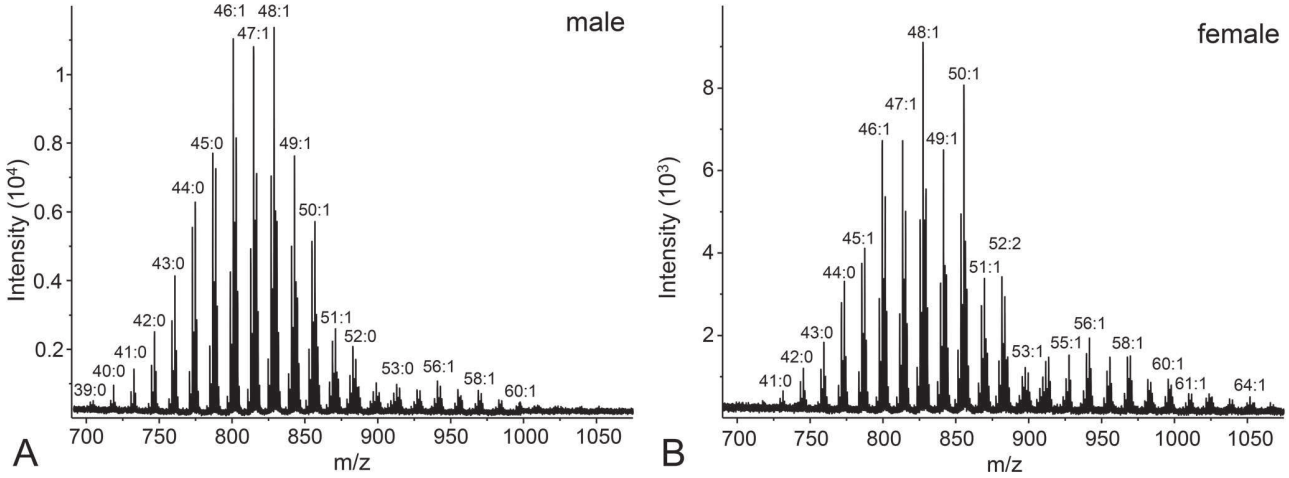

Figure 5. Mass spectra of the triacylglycerols. Characteristic MALDI spectrum of the triacylglycerols isolated from the vernix caseosa of a newborn boy (A) and girl (B). A NaDHB matrix was used and the signals correspond to molecular adducts with sodium ions $[M+Na]^+$.
doi:10.1371/journal.pone.0099173.g005

Fragmentation spectra of WE and TG

In light of these results, as several isomers can be found at the same m/z values, a question has arisen as to whether the observed differences in the WE and TG relative intensities reflect qualitative differences in the constituents of these WE and TG in boys and girls or rather quantitative differences in their production or selective sex-dependent incorporation of particular FA. To answer this question, we further fragmented twelve peaks from those most significantly contributing to the sex-specificity of TG and WE profiles and studied their identity and relative intensities of fragments in all samples using MALDI-TOF/TOF MS. Subsequently, the sex-specificity in the relative proportions of particular fragments in each fragmented compound was once again tested by means of RDA.

In the case of WE, the fragmentation spectra showed lithiated fatty acids originating from the acid parts of esters [26]. The spectra were qualitatively identical in all of the six peaks (WE 32:1, WE 34:1, WE 36:2, WE 40:1, WE 41:1, WE 42:1) and both sexes; the spectra were dominated by five signals representing over 95% of the total intensity, i.e. $[FA\ 14:1+Li]^+$, $[FA\ 15:0+Li]^+$, $[FA\ 16:1+Li]^+$, $[FA\ 17:1+Li]^+$ and $[FA\ 18:1+Li]^+$. On the other hand, a RDA revealed significant gender-related differences in the relative intensities of these five fragments in all six fragmented peaks. Among the fatty acids contributing the most to the sex-related differences, the relative intensities of the fragments $[FA\ 16:1+Li]^+$ and $[FA\ 18:1+Li]^+$ were systematically over-represented in male and female subjects, respectively, with 37–75% fit with the predicted model for $[FA\ 16:1+Li]^+$ and 36–74% fit for $[FA\ 18:1+Li]^+$.

The fragmentation spectra of the six TG peaks (sodium adducts of TG 45:0, TG 45:1, TG 46:1, TG 52:1, TG 62:1, TG 64:1) showed signals consistent with neutral loss of fatty acids and fatty acid sodium salts. The fragments appeared in clusters differing from each other by the number of carbons. The most intense peak of each cluster corresponding to neutral loss of fatty acid sodium salt (Table 1) has been chosen for further study. There were no qualitative differences in the dominant fragments between the two sexes. However, like for WE, we detected significant differences

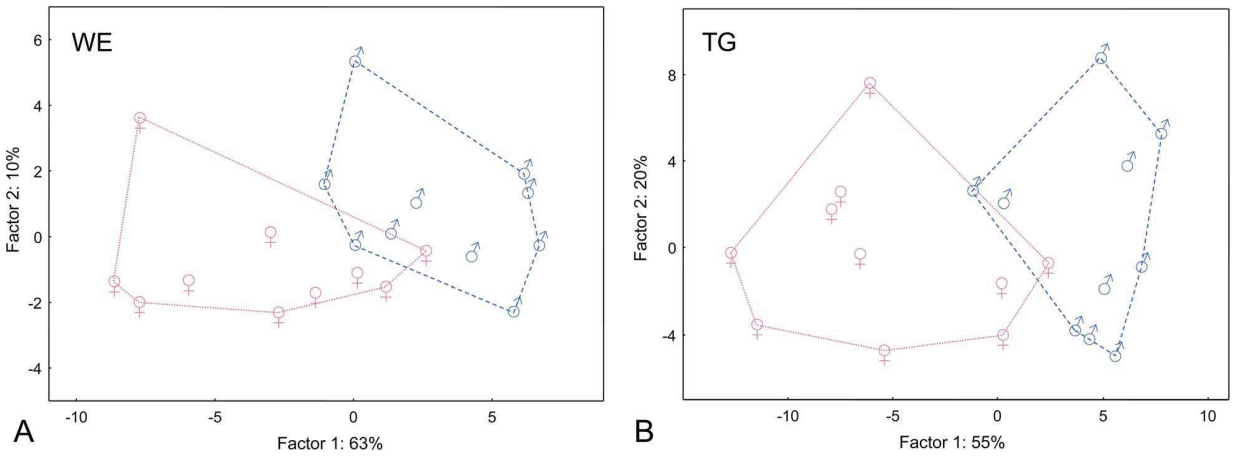

Figure 6. Quantitative pattern of vernix caseosa lipids in newborn boys and girls. Graphic representation of the first two components of PCA calculated from the relative intensities of the wax esters (A) and triacylglycerols (B) isolated from the vernix caseosa of newborn boys (♂) and girls (♀).
doi:10.1371/journal.pone.0099173.g006

Table 1. MALDI-TOF/TOF data for VC triacylglycerols.

Precursor $[M+Na]^+$	Main fragments (*m/z*)	Neutral loss (RCOONa)
TG 45:1 (*m/z* 785.7)	481, 495, 509, 521, 535, 549, 563	FA 18:1, FA 17:1, FA 16:1, FA 15:0, FA 14:0, FA 13:0, FA 12:0
TG 45:0 (*m/z* 787.7)	481, 495, 509, 523, 537, 551, 565	FA 18:0, FA 17:0, FA 16:0, FA 15:0, FA 14:0, FA 13:0, FA 12:0
TG 46:1 (*m/z* 799.7)	495, 509, 523, 535, 549, 563, 577	FA 18:1, FA 17:1, FA 16:1, FA 15:0, FA 14:0, FA 13:0, FA 12:0
TG 52:1 (*m/z* 883.8)	495, 509, 523, 535, 549, 563, 577	FA 24:1, FA 23:1, FA 22:1, FA 21:0, FA 20:0, FA 19:0, FA 18:0
TG 62:1 (*m/z* 1023.9)	523, 549, 577, 605, 717, 745, 773	FA 32:1, FA 30:0, FA 28:0, FA 26:0, FA 18:0, FA 16:0, FA 14:0
TG 64:1 (*m/z* 1051.8)	523, 551, 577, 605, 745, 773, 801	FA 34:1, FA 32:1, FA 30:0, FA 28:0, FA 18:0, FA 16:0, FA 14:0

doi:10.1371/journal.pone.0099173.t001

between males and females in the relative proportions of the dominant fragments of the six fragmented TG.

Sex-specificity of VC lipid composition

Our results strongly support the hypothesis that the composition of VC lipids is gender-related. We showed statistically significant differences between male and female samples both at the level of fatty acids in the total lipid extracts and at the level of intact lipids in two lipid classes. At the current stage of our knowledge, we can only hypothesize the biological aspects underlying these differences. First, the differences in VC chemistry may result from differential temporal dynamics in the skin development in boys and girls controlled by steroid hormones; previous studies in rats have documented that the formation of the cutaneous barrier is accelerated by estrogen and delayed by testosterone [40]. VC of human male fetuses was previously shown to contain more sebum than that of female fetuses, which has a higher proportion of epidermal lipids [15]. We found the differences in WE and TG, i.e., lipid classes that are of sebaceous origin [1]. Therefore, the observed sex-related differences are likely associated with the activities of sebaceous glands in the skin of the fetus. Interestingly, when we analyzed VC obtained from a girl prematurely born in the 35^{th} week, the lipid profiles greatly differed from those of full-term girls and were rather similar to that of full-term boys. This accidental observation further supports the hypothesis of differential dynamics in VC production between the two sexes. Alternatively, permanent and fixed differences in the chemistry of the storage pool of FA, shifted towards longer carbon chains in some lipid classes in females, can account for the observed sex specificity of VC lipids.

The quest for an unambiguous verification of these hypotheses prompts further studies aiming at dynamics in VC production and composition involving newborn males and females of varied gestational age. Because of extreme complexity of VC lipids, lipidomics approaches based on cutting edge analytical chemistry are desirable.

Conclusions

In the present study, we show that the quantitative pattern of lipids contained in the vernix caseosa of full-term newborns is sex-specific, namely because of the higher proportions of wax esters and triacylglycerols with longer hydrocarbon chains in newborn girls. These results pave the way to further investigations of the vernix caseosa, aiming at both structural and dynamic patterns of the lipid constituents and biological determinants underlying these patterns.

Supporting Information

Figure S1 Image of semipreparative thin layer silica gel plate with separated zones of vernix caseosa lipids.
(PDF)

Table S1 List of subjects, their basic biological characteristics and sampled body parts.
(PDF)

Table S2 Suitability of the MALDI matrices for neutral lipids of vernix caseosa.
(PDF)

Table S3 Relative peak areas of fatty acid methyl esters.
(PDF)

Table S4 Relative intensities of wax esters in vernix caseosa of newborn boys and girls.
(PDF)

Table S5 Relative intensities of triacylglycerols in vernix caseosa of newborn boys and girls calculated from MALDI spectra (mean ± SD).
(PDF)

Author Contributions

Conceived and designed the experiments: RM VV RH AD JC. Performed the experiments: RM EH VV. Analyzed the data: RM EH VV RH PC. Contributed reagents/materials/analysis tools: ZH RP AD. Wrote the paper: RM VV RH PC ZH RP JC.

References

1. Hoath SB, Pickens WL, Visscher MO (2006) The biology of vernix caseosa. Int J Cosmetic Sci 28:319–333.
2. Singh G, Archana G (2008) Unraveling the mystery of vernix caseosa. Indian J Dermatol 53:54–60.
3. Youssef W, Wickett RR, Hoath SB (2001) Surface free energy characterization of vernix caseosa. Potential role in waterproofing the newborn infant. Skin Res Technol 7:10–17.
4. Tansirikongkol A, Wickett RR, Visscher MO, Hoath SB (2007) Effect of Vernix Caseosa on the Penetration of Chymotryptic Enzyme: Potential Role in Epidermal Barrier Development. Pediatr Res 62:49–53.
5. Yoshio H, Tollin M, Gudmundsson GH, Lagercrantz H, Jornvall H, et al. (2003) Antimicrobial Polypeptides of Human Vernix Caseosa and Amniotic Fluid: Implications for Newborn Innate Defense. Pediatr Res 53:211–216.
6. Tollin M, Bergsson G, Kai-Larsen Y, Lengqvist J, Sjövall J, et al. (2005) Vernix caseosa as a multi-component defence system based on polypeptides, lipids and their interactions. Cell Mol Life Sci 62:2390–2399.
7. Visscher MO, Narendran V, Pickens WL, LaRuffa AA, Meinzen-Derr J, et al. (2005) Vernix caseosa in neonatal adaptation. J Perinatol 25:440–446.
8. Bautista MI, Wickett RR, Visscher MO, Pickens WL, Hoath SB (2000) Characterisation of Vernix Caseosa as a Natural Biofilm: Comparison to Standard Oil-Based Ointments. Pediatr Dermatol 17:253–260.

9. Nopper AJ, Horii KA, Sookdeo-Drost S, Wang TH, Mancini AJ, et al. (1996) Topical ointment therapy benefits premature infants. J Pediatr 128:660–669.
10. Tansirikongkol A, Visscher MO, Wickett RR (2007) Water-handling properties of vernix caseosa and a synthetic analogue. J Cosmet Sci 58:651–662.
11. Ågren J, Zelenin S, Håkansson M, Eklöf AC, Aperia A, et al. (2003) Transepidermal Water Loss in Developing Rats: Role of Aquaporins in the Immature Skin. Pediatr Res 53:558–565.
12. Rissmann R, Oudshoorn MH, Kocks E, Hennink WE, Ponec M, et al. (2008) Lanolin-derived lipid mixtures mimic closely the lipid composition and organization of vernix caseosa lipids. Biochim Biophys Acta 1778:2350–2360.
13. Rissmann R, Oudshoorn MH, Zwier R, Ponec M, Bouwstra JA, et al. (2009) Mimicking vernix caseosa–Preparation and characterization of synthetic biofilms. Int J Pharm 372:59–65.
14. Kärkkäinen J, Nikkari T, Ruponen S, Haahti E (1965) Lipids of vernix caseosa. J Invest Dermatol 44:333–338.
15. Nazzaro-Porro M, Passi S, Boniforti L, Belsito F (1979) Effects of aging on fatty acids in skin surface lipids. J Invest Dermatol 73:112–117.
16. Rissmann R, Gooris G, Ponec M, Bouwstra J (2009) Long periodicity phase in extracted lipids of vernix caseosa obtained with equilibration at physiological temperature. Chem Phys Lipids 158:32–38.
17. Ansari MN, Fu HC, Nicolaides N (1970) Fatty acids of the alkane diol diesters of vernix caseosa. Lipids 5:279–282.
18. Nicolaides N, Apon JM, Wong DH (1976) Further studies of the saturated methyl branched fatty acids of vernix caseosa lipid. Lipids 11:781–790.
19. Rissmann R, Groenink HW, Weerheim AM, Hoath SB, Ponec M, et al. (2006) New Insights into Ultrastructure, Lipid Composition and Organization of Vernix caseosa. J Invest Dermatol 126:1823–1833.
20. Stewart ME, Quinn MA, Downing DT (1982) Variability in the fatty-acid composition of wax esters from vernix-caseosa and its possible relation to sebaceous gland activity. J Invest Dermatol 78:291–295.
21. Schiller J, Süss R, Fuchs B, Muller M, Zschornig O, et al. (2007) MALDI-TOF MS in lipidomics. Front Biosci 12:2568–2579.
22. Fuchs B, Schiller J (2009) Application of MALDI-TOF mass spectrometry in lipidomics. European Journal of Lipid Science and Technology 111:83–98.
23. Schiller J, Süss R, Arnhold J, Fuchs B, Lessig J, et al. (2004) Matrix-assisted laser desorption and ionization time-of flight (MALDI-TOF) mass spectrometry in lipid and phospholipid research. Prog Lipid Res 43:449–488.
24. Murphy RC, Fiedler J, Hevko J (2001) Analysis of nonvolatile lipids by mass spectrometry. Chem Rev 101:479–526.
25. Asbury GR, Al-Saad K, Siems WF, Hannan RM, Hill HH (1999) Analysis of triacylglycerols and whole oils by matrix assisted laser desorption/ionization time of flight mass spectrometry. J Am Soc Mass Spectrom 10:983–991.
26. Vrkoslav V, Míková R, Cvačka J (2009) Characterization of natural wax esters by MALDI-TOF mass spectrometry. J Mass Spectrom 44:101–110.
27. Zouboulis CC, Baron JM, Böhm M, Kippenberger S, Kurzen H, et al. (2008) Frontiers in sebaceous gland biology and pathology. Exp Dermatol 17:542–551.
28. Pochi PE, Strauss JS (1974) Endocrinologic control of the development and activity of the human sebaceous gland. J Invest Dermatol 62:191–201.
29. Smith KR, Thiboutot DM (2008) Sebaceous gland lipids: friend or foe? J Lipid Res 49:271–281.
30. Stewart ME, Downing DT (1981) Separation of Wax Esters from Steryl Esters by Chromatography on Magnesium Hydroxide. Lipids 16:355–359.
31. Nicolaides N (1970) Magnesium Oxide as an Adsorbent for the Chromatographic Separation of Molecules According to their Degree of Flatness, e.g. the Separation of Wax Esters from Sterol Esters. J Chromatogr Sci 8:717–720.
32. Carrol KK (1961) Separation of lipid classes by chromatography on florisil. J Lipid Res 2:135–141.
33. Stránský K, Jursík T (1996) Simple Quantitative Transesterification of Lipids. Introduction. Fett/Lipid 98:65–71.
34. Hidaka H, Hanyu N, Sugano M, Kawasaki K, Yamauchi K, et al. (2007) Analysis of Human Serum Lipoprotein Lipid Composition Using MALDI-TOF Mass Spectrometry. Ann Clin Lab Sci 37:213–221.
35. Zschörnig O, Pietsch M, Süss R, Schiller J, Gütschow M (2005) Cholesterol esterase action on human high density lipoproteins and inhibition studies: detection by MALDI-TOF MS. J Lipid Res 46:803–811.
36. Astigarraga E, Barreda-Gómez G, Lombardero L, Fresnedo O, Castaño F, et al. (2008) Profiling and Imaging of Lipids on Brain and Liver Tissue by Matrix-Assisted Laser Desorption/Ionization Mass Spectrometry Using 2-Mercaptobenzothiazole as a Matrix. Anal Chem 80:9105–9114.
37. Fuchs B, Süss R, Schiller J (2010) An update of MALDI-TOF mass spectrometry in lipid research. Prog Lipid Res 49:450–475.
38. Stübiger G, Belgacem O (2007) Analysis of Lipids Using 2,4,6-Trihydroxyacetophenone as a Matrix for MALDI Mass Spectrometry. Anal Chem 79:3206–3213.
39. Hauff S, Vetter W (2010) Exploring the fatty acids of vernix caseosa in form of their methyl esters by off-line coupling of non-aqueous reversed phase high performance liquid chromatography and gas chromatography coupled to mass spectrometry. J Chromatogr A 1217: 8270–8278.
40. Hanley K, Rassner U, Jiang Y, Vansomphone D, Crumrine D, et al. (1996) Hormonal Basis for the Gender Difference in Epidermal Barrier Formation in the Fetal Rat. J Clin Invest 97:2576–2584.

- Publication II -

Journal of Chromatography A, 1378 (2015) 8–18

Contents lists available at ScienceDirect

Journal of Chromatography A

journal homepage: www.elsevier.com/locate/chroma

Analysis of 1,2-diol diesters in vernix caseosa by high-performance liquid chromatography – atmospheric pressure chemical ionization mass spectrometry

Lenka Šubčíková[a], Michal Hoskovec[b], Vladimír Vrkoslav[b], Tereza Čmelíková[c], Eva Háková[a,b], Radka Míková[a,b], Pavel Coufal[a], Antonín Doležal[d], Richard Plavka[d], Josef Cvačka[b,*]

[a] Department of Analytical Chemistry, Faculty of Science, Charles University in Prague, Hlavova 2030/8, CZ-128 43 Prague 2, Czech Republic
[b] Institute of Organic Chemistry and Biochemistry v.v.i., Academy of Sciences of the Czech Republic, Flemingovo nám. 2, CZ-166 10 Prague 6, Czech Republic
[c] Joachim Barrande Grammar School, Talichova 824, CZ-266 01 Beroun, Czech Republic
[d] Department of Obstetrics and Gynaecology, General Faculty Hospital and 1st Faculty of Medicine, Charles University in Prague, Apolinářská 18, CZ-128 00 Prague 2, Czech Republic

ARTICLE INFO

Article history:
Received 9 September 2014
Received in revised form 4 November 2014
Accepted 27 November 2014
Available online 4 December 2014

Keywords:
Skin lipids
Neutral lipids
Lipidomics
Mass spectrometry
Double-bond position

ABSTRACT

Fatty acid diesters of long-chain 1,2-diols (1,2-DDE), or type II wax diesters, were analyzed in the vernix caseosa of a newborn girl. 1,2-DDE were isolated from the total lipid extract by the semipreparative TLC using plates coated with silica gel. Chromatographic separation of the 1,2-DDE molecular species was achieved on the non-aqueous reversed-phase HPLC with two Nova-Pak C18 columns connected in series (a total length of 45 cm) and using an acetonitrile–ethyl acetate gradient. 1,2-DDE eluted from the column in the order of their equivalent chain number. The analytes were detected as ammonium adducts by an ion-trap mass spectrometer equipped with an atmospheric pressure chemical ionization source. Their structures were elucidated using tandem mass spectrometry with MS, MS^2 and MS^3 steps in a data-dependent mode. More than two thousand molecular species of 1,2-DDE were identified in 141 chromatographic peaks. The most abundant 1,2-DDE were monounsaturated lipids consisting of a C22 diol and a C18:1 fatty acid together with C16:0, C14:0 or C15:0 fatty acids. The positions of double bonds were characterized by the fragmentation of $[M+C_3H_5N]^{+\bullet}$ formed in the ion source.

1. Introduction

Fatty acid diesters of long-chain 1,2-diols (1,2-DDE), or type II wax diesters, are condensation products of two fatty acid molecules with a long-chain 1,2-diol. These lipids are widely associated with the skin of mammals; they are frequently found in sebum, a species-specific mixture of relatively neutral lipids synthesized de novo by sebaceous glands [1]. The first reports on 1,2-DDE appeared in the literature in the 1960s [2–5], about a decade after the structural characterization of 1,2-diols in wool wax [6,7]. Since then, 1,2-DDE have been identified in the skin surface lipids of many mammalian species. 1,2-DDE have been detected in the skin of rodents such as the mouse, rat, guinea pig, golden Syrian hamster or gerbil [2,5,8–10], as an abundant lipid class forming 14–61% of the total lipids. The ventral gland secretion of a male dwarf hamster was found to contain 1,2-diols and their monopentanoates [11]. An analysis of the rat 1,2-DDE has shown that 1,2-diols (having the chiral center on carbon 2) exist in the D form [12]. Further experiments with the lipase hydrolysis of 1,2-DDE from the golden Syrian hamster and the mouse have revealed that fatty acids in the positions 1 and 2 are not distributed randomly [13]. Canine skin lipids were reported to comprise 32% of the 1,2-DDE constituting branched diols esterified with long-chain fatty acid and isovaleric acid [14]. The skin of cows was found to produce 8% of diol diesters [15]. In primates, 1,2-DDE formed 21% of the skin lipids of the baboon [8]. Two types of 1,2-DDE were found in the skin lipids of the macaque: the less abundant type (17%) with two long-chain fatty acids and the second type (40%) with short branched-chain acids (mostly isovaleric acid) in the position 1 of the diol [16]. Concerning the human species, 1,2-DDE are almost missing in the adult skin [17], but they are produced in the early stages of skin development. 1,2-DDE are present in vernix caseosa,

* Corresponding author. Tel.: +420 220183303; fax: +420 220183583.
E-mail address: cvacka@uochb.cas.cz (J. Cvačka).

http://dx.doi.org/10.1016/j.chroma.2014.11.075
0021-9673/

a uniquely human proteolipid film coating the skin of the fetus in the last trimester of pregnancy and protecting the embryonic skin from amniotic water. Vernix caseosa has remarkable hydration, waterproofing, anti-infective, antioxidant and wound-healing properties [18]. 1,2-DDE constitute 3–9% of the total lipids in vernix caseosa [3,19]. Although vernix caseosa diols have been found to be mostly methyl-branched (*iso*, *anteiso*) and saturated straight-chain 1,2-diols with 20–25 carbons [3,4], shorter chains (C14–C19) have been detected as well [5]. Fatty acyls have been identified as saturated straight-chain or methyl-branched (*iso*, *anteiso*) and unsaturated straight-chain, mostly monoenic. The most abundant saturated chains appeared to contain 16 carbons (both straight and *iso*-methyl branched chains) and the predominant unsaturated acids were C18:1*n*-7 and C18:1*n*-9 [19]. The biosynthesis of human 1,2-DDE was found to involve catalysis by acyl CoA:diacylglycerol acyltansferase DGAT1, an enzyme highly expressed in the skin [20]. 1,2-DDE are rare in other biotas. They have been reported in uropygial (preen) gland secretions of some birds [21–23], where isomeric 2,3-DDE are usually found. In the plant kingdom, long-chain 1,2-diols have been discovered in the skin wax of apples [24] and, together with their monoacetates, in the cuticular wax of Mexican aster petals [25]. Alkane-1,2-diol-based glycolipids have been found in hot spring microbial mats [26,27].

1,2-Diols and 1,2-DDE are utilized in cosmetic and pharmaceutical products. Non-esterified 1,2-diols are frequently used as skin and hair conditioning agents, viscosity- and foam-increasing agents [28–30]. They have bacteriostatic activities against a broad range of strains, which makes them useful as a treatment of skin diseases caused by bacteria, such as acne [31–33], and they are also suggested as a prophylaxis and/or treatment of fungal skin infections [34]. Recently, 1,2-diols have been patented as antispasmodics to relieve the spasms associated with pain [35], and they can also serve for controlling underarm and foot odor [31]. Esters of 1,2-diols are used less frequently. Monoesters of 1,2-diols can be used for the treatment of acne or seborrheic dermatitis [36]. 1,2-DDE have been suggested as edible fat with substantially fewer calories than commonly used triacylglycerols [37]. Mixtures of mono- and diesters of propane-1,2-diol are utilized as emulsifiers and aerating agents for bakery products (food additive E477).

Taking into account the large variability of the fatty acids biosynthesized by the mammal skin, the total number of 1,2-DDE might be enormous. The theoretical number of the 1,2-DDE that can be formed from N diols and n fatty acids equals $N \times n^2$. We have reported previously that vernix caseosa lipids contain at least 167 different fatty acids [38], which, even for a low number of diols, gives 10^4–10^5 possible combinations. The complexity of 1,2-DDE thus compares with extremely rich mixtures of triacylglycerols (where the number of theoretically formed species equals n^3). Not surprisingly, a comprehensive characterization of 1,2-DDE mixtures at the level of intact molecular species has not been published so far. 1,2-DDE with very short-chain diols were earlier analyzed by electron ionization MS [39], but the method is not applicable for mixtures and lipids with long-chain diols. Previously published methods for skin 1,2-DDE mostly relied on saponification or transesterification, i.e. procedures that release fatty acids and alcohols. Fatty acids and diols released from 1,2-DDE were investigated using GC, often preceded by various chemical derivatizations including the formation of trimethylsilyl, acetyl, isopropylidene or acetonide derivatives, hydrogenation or oxidation [4,19,40]. Although these approaches have enabled the structural characterization of fatty-acid and diol building blocks, the structures of intact 1,2-DDE have not been disclosed yet.

In this work, we analyzed the 1,2-DDE of vernix caseosa using non-aqueous reversed-phase HPLC/APCI-tandem MS. The method was carefully optimized to achieve good chromatographic resolution and obtain reliable information on the molecular species structure. More than 2000 molecular species have been identified and their retention behavior has been studied.

2. Experimental

2.1. Sample collection

The vernix caseosa sample (1.0 g) was collected from the skin of a full-term healthy female neonate immediately after spontaneous vaginal delivery and stored at −25 °C in an amber glass vial. The sample was collected with informed parental consent and the work was approved by the Ethics Committee of the General University Hospital, Prague (910/09 S-IV); the study was performed according to the Declaration of Helsinki.

2.2. The isolation of 1,2-DDE

The sample was suspended in 50 mL of chloroform:methanol (2:1, v/v) with 0.05% of butylated hydroxytoluene (2,6-bis(1,1-dimethylethyl)-4-methylphenol; an antioxidant). The suspension was cleared of epithelial cells by filtration through a column containing purified cotton wool and silica gel (60–120 μm, ca 0.2 g). Anhydrous magnesium sulfate (ca 5 g) was added to absorb water, and the suspension was filtered again. The solvents were removed by a rotary evaporator (35 °C, 170 mbar) and a stream of argon, yielding 78 mg of the total lipid extract. The extract (ca 20 mg) was separated on 9 cm × 12 cm glass TLC plates coated with silica gel using hexane:diethyl ether (93:7, v/v) as a mobile phase. Each plate was developed twice to focus the zones (in the first step to 3/4 of the plate height and then, after air-drying, to the top). The zones were visualized under UV light after being sprayed with rhodamine 6G (0.05% in ethanol). The zone corresponding to 1,2-DDE (R_F = 0.46–0.52) was scraped off the plate into a small glass column with purified cotton wool and silica gel; lipids were eluted with diethyl ether. The solvent was evaporated under a stream of argon; the residues were dissolved in chloroform:methanol (2:1, v/v; 10 mg/mL) and stored at −25 °C in the dark. Prior to HPLC analysis, the sample was diluted by acetonitrile:chloroform (10:9, v/v) to a concentration of 1 mg/mL (compound identification) or concentrated to a concentration of 25 mg/mL (the localization of double bonds).

2.3. Chemical synthesis of standards

Fatty acid chloride (or an equimolar mixture of fatty acid chlorides) was added dropwise to a stirred solution of alkane-1,2-diol in 10 mL of anhydrous pyridine at 0 °C. After stirring for 72 h at ambient temperature, the mixture was diluted with diethyl ether (100 mL), washed with 10% hydrochloric acid (2× 100 mL), a saturated solution of sodium hydrogen carbonate (2× 100 mL), brine (100 mL), and dried over sodium sulfate. The solvent was evaporated in vacuo and the oily residue was purified by flash chromatography (150 g of Merck Kiesegel 60; the mobile phase hexane:ethyl acetate (95:5, v/v)) to give 1,2-DDE. The reactant weights and the reaction yields are specified in the Supplementary Information.

2.4. Chemicals

Acetonitrile, ethyl acetate and methanol (purity: for MS, Sigma–Aldrich, St. Louis, MO, USA) were used as received; the other solvents (chloroform, hexane, dichloromethane; all from Penta, Czech Republic) were distilled in glass from analytical-grade solvents. Ammonium formate (Fluka, Buchs, Switzerland), magnesium sulfate (Sigma–Aldrich), rhodamine 6G (Sigma–Aldrich) and

butylated hydroxytoluene (Fluka) were of reagent grade and used as purchased.

2.5. HPLC/APCI–MS

The liquid chromatograph consisted of a Rheos 2200 quaternary gradient pump (Flux Instruments, Reinach, Switzerland), a PAL HTS autosampler (CTC Analytics, Zwingen, Switzerland), a DeltaChrom CTC 100 column oven (Watrex, Prague, Czech Republic) and an LTQ Orbitrap XL hybrid FT mass spectrometer equipped with an Ion Max source with an APCI probe installed (Thermo Fisher Scientific, San Jose, CA, USA); the system was controlled by Xcalibur software (Thermo Fisher Scientific). Two Nova-Pak C18 stainless-steel columns connected in series (150 and 300 mm × 3.9 mm, particle size: 4 μm; Waters, Milford, MA, USA) were used at a column temperature of 30 °C. The mobile phase flow rate was 0.7 mL/min. The autosampler injected 10 μL of the sample and the injection system was washed with chloroform/acetonitrile (1:1, v/v). The mobile phase was mixed from acetonitrile (A) and ethyl acetate (B). The linear gradient program was as follows: 0 min: 70% of A and 30% of B; 100 min: 100% of B; 130 min: 100% of B. Ammonium formate (50 mM solution in 2-propanol/water 9:1, v/v; 9 μl/min) was added to the effluent. The APCI vaporizer and heated capillary temperatures were set to 270 °C and 170 °C, respectively; the corona discharge current was 7 μA. Nitrogen served both as the sheath and auxiliary gas at a flow rate of 32 and 17 arbitrary units, respectively. The MS method encompassed eight scan events for a linear ion trap: (1) the full scan in the 400–1500 *m/z* range; (2) CID MS/MS of the *N*th most intense ion from the parent mass list with a normalized collision energy of 28–30% and isolation with 2 Da; (3–8) CID MS^3 from the first to sixth most abundant fragments recorded in the previous event using a normalized collision energy of 32% and isolation with 2 Da. The same sample was analyzed six times; the *N* in the second scan event was gradually increased from *N* = 1 (the MS/MS of the most intense ion from the parent mass list in the MS spectrum) to *N* = 6 (the MS/MS of the sixth most intense ion from the parent mass list in the MS spectrum). The parent mass list was calculated for $[M+NH_4]^+$ ions of all possible 1,2-DDE with the total number of carbons and double bonds in the range of 49–91 and 0–4, respectively. Two additional HPLC runs were used to localize the positions of double bonds using $[M+C_3H_5N]^{+\bullet}$ formed in the APCI source [41] under the same separation conditions as described above. In both runs, the MS method consisted of two scan events; the first scan event was the full scan in the 400–1500 *m/z* range and the second scan was either ion-trap CID of the most intense $[M+C_3H_5N]^{+\bullet}$ ion from the parent mass list with the normalized collision energy of 29–33% and isolation with 2 Da or quadrupole HCD of the most intense $[M+C_3H_5N]^{+\bullet}$ ion from the parent mass list with the normalized collision energy of 18–21% and isolation with 2 Da. The isolation width of 2 Da used throughout this work enabled us to achieve high signal intensity while maintaining monoisotopic precursor selection. The parent mass list was built for mono- and diunsaturated 1,2-DDE. 1,2-DDE standards dissolved in the mobile phase were also directly infused into the mobile phase flow via a T-piece using a syringe pump of the instrument. The exact masses were recorded by the Orbitrap at a resolution of 100,000. The HPLC/MS^3 data were interpreted manually.

2.6. The 1,2-DDE abbreviations and nomenclature

An abbreviated nomenclature for 1,2-DDE was used in this work. The aliphatic chains were expressed by the number of carbons and the number of double bonds. The position of the double bond (or a group of m ethylene-interrupted double bonds) was indicated as *n-x*, where *x* is the distance from the terminal end of the hydrocarbon chain. Unless stated otherwise, the *cis* double-bond geometry was assumed. The abbreviation first specifies 1,2-diol and then fatty acid chains. For instance, the abbreviation 10:0//18:1*n*-9/16:0 is used for 2-(palmitoyloxy)decyl oleate or 2-(hexadecanoyloxy)decyl (*Z*)-octadec-9-enoate. The underscore character between fatty acids (10:0//18:1*n*-9_16:0) indicates that the positions of the fatty acids are not known [42]. The ECN stands for the equivalent carbon number (ECN = CN − 2DB, where CN and DB are the total numbers of the carbon atoms and double bonds, respectively). The diagnostic fragments indicating the position of a double bond in the MS/MS spectra were labeled either α (for the fragments containing a diester moiety) or ω (for the fragments carrying the terminal-carbon end).

3. Results and discussion

3.1. The mass spectra of 1,2-DDE

The APCI mass spectra of 1,2-DDE were studied using standards prepared synthetically. The full-scan APCI mass spectra showed signals of protonated molecules, partially overlapping with radical cations $[M]^{+\bullet}$. The addition of ammonium formate promoted the creation of ammonium adducts. A full-scan mass spectrum of 16:0//18:1*n*-9/18:1*n*-9 (Fig. 1A) showed mostly $[M+NH_4]^+$ at *m/z* 804.6 (the spectrum base peak) and less abundant signals of $[M+H]^+$ at *m/z* 787.1, $[M+C_3H_5N]^{+\bullet}$ [41,43] at *m/z* 841.8 and an $[M+H-FA]^+$ fragment at *m/z* 505.5. Collision-induced dissociation of the ammonium adducts in the ion trap (MS/MS) provided signals consistent with a neutral loss of ammonia ($[M+NH_4-NH_3]^+$, i.e. $[M+H]^+$) and fatty acids ($[M+H-FA_1]^+$, $[M+H-FA_2]^+$). In the case of monoacid 16:0//18:1*n*-9/18:1*n*-9, these ions appeared at *m/z* 804.4 ($[M+NH_4]^+$), *m/z* 787.7 ($[M+H]^+$) and *m/z* 505.5 ($[M+H-FA_{18:1}]^+$), see Fig. 1B. In the case of diacid 10:0//16:0_18:1*n*-9, two signals corresponding to a neutral loss of fatty acids were detected at *m/z* 395.4 and *m/z* 421.4 (Fig. 2A). Further fragmentation of $[M+H-FA]^+$ ions (i.e. MS^3) allowed us to detect fragments related to the second fatty acids and thus complete the information on the number of carbons and double bonds in diol and fatty acid chains. MS^3 spectra showed a loss of a doubly dehydrated diol, i.e. alkadiene in the case of 1,2-DDE with a saturated diol chain. The second fatty acid appeared as a protonated molecule $[FA+H]^+$ accompanied by its dehydration products $[FA+H-H_2O]^+$ and $[FA+H-2H_2O]^+$. These ions for 16:0//18:1*n*-9/18:1*n*-9 were detected at *m/z* 283.2, *m/z* 265.3 and *m/z* 247.3, respectively (Fig. 1C). The MS^3 spectrum base peaks were $[FA+H]^+$ for saturated FA (Fig. 2B), whereas, in the case of monounsaturated FA, the most abundant ions were typically $[FA+H-H_2O]^+$ (Fig. 2C). For a general fragmentation scheme of 1,2-DDE, see Fig. 3. The MS^2 of $[M+C_3H_5N]^{+\bullet}$ made it possible to the establish the position of the double bond based on two fragments corresponding to the cleavage of the C—C bonds next to the site of the double bond. The covalent adducts $[M+C_3H_5N]^{+\bullet}$ can be generated by gas-phase reactions in the APCI sources in the presence of acetonitrile, and we have shown that these ions are useful for the localization of double bonds in various lipids [41,43]. The CID fragmentation of *m/z* 841.8 ($[M+C_3H_5N]^{+\bullet}$ of 16:0//18:1*n*-9/18:1*n*-9) in the ion trap gave a prominent fragment *m/z* 728.7 (α-ion), which can be rationalized by the loss of octane radical, and indicated the *n*-9 position of the double bond (Fig. 4A). The CID spectra also contained satellite fragments resulting from the cleavages of the C—C bonds more distant from the site of the double bond (mostly ±14 Da, *m/z* 714.6 and *m/z* 742.7) [41,43]. A cleavage from the opposite side of the double bond (the ω-ion at *m/z* 194, the elimination of $C_{42}H_{79}O_4^{\bullet}$) was not observed due to a low mass cutoff of the ion trap. The CID spectrum showed also fragments not related to the double-bond position, e.g. the relatively abundant neutral loss of fatty acid ($[M+C_3H_5N-FA]^{+\bullet}$) at *m/z* 559.5. In contrast, the quadrupole HCD

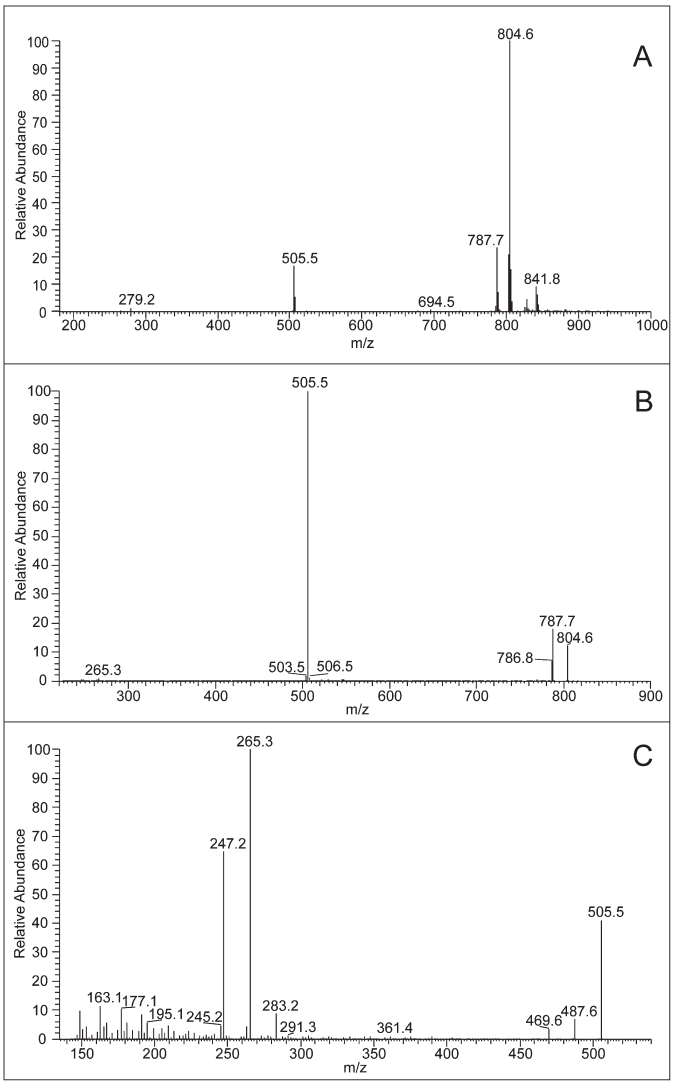

Fig. 1. The APCI mass spectra of 16:0//18:1*n*-9/18:1*n*-9; the full-scan MS (A), the ion-trap CID MS^2 of *m*/*z* 804.6 (the fragmentation of $[M+NH_4]^+$) (B), and the ion-trap CID MS^3 of *m*/*z* 505.5 (the fragmentation of $[M+H-FA_{18:1}]^+$) (C).

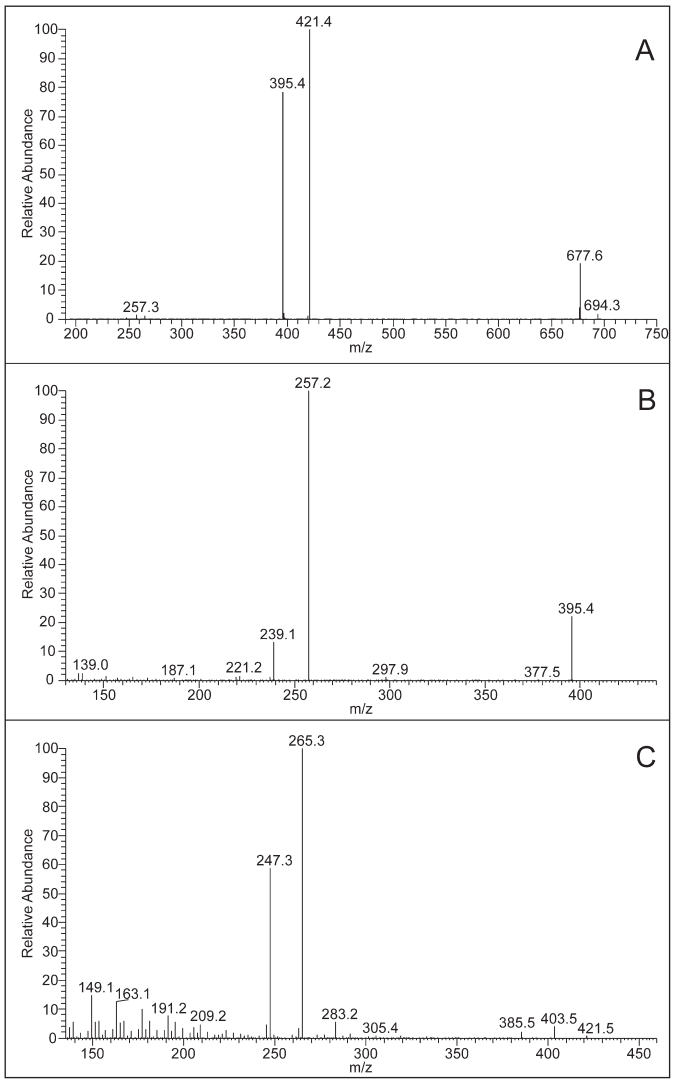

Fig. 2. The APCI mass spectra of 10:0//16:0_18:1*n*-9; the ion-trap CID MS^2 of *m*/*z* 694.3 (the fragmentation of $[M+NH_4]^+$) (A), the ion-trap CID MS^3 of *m*/*z* 395.4 (the fragmentation of $[M+H-FA_{18:1}]^+$) (B), and the-ion trap CID MS^3 of *m*/*z* 421.5 (the fragmentation of $[M+H-FA_{16:0}]^+$) (C).

spectra were less complicated, showing only ω and α diagnostic fragments accompanied by small satellite ions at +14 Da (Fig. 4B). The difference between the appearance of the CID and HCD spectra was presumably caused by different collision energies and the activation time scales. Whereas HCD is a beam-type collision dissociation imparting one or two higher-energy collisions, the ion trap CID slowly heats the precursor with many low-energy collisions, which causes extensive isomerization of the precursor. The lack of 1,2-DDE standards with a double bond in the diol chain did not make it possible to investigate whether MS^3 spectra are useful for distinguishing between isomers whose double bond is located either in diol or fatty acid chains. The elemental composition of all ions discussed in this chapter was confirmed by an exact mass measurement on an Orbitrap mass analyzer (Table S1 in the Supplementary Information).

3.2. The optimization of chromatographic separation

In order to achieve a good separation of the extremely rich mixture of 1,2-DDE, a thoroughly optimized HPLC method was required. The unavailability of 1,2-diols with appropriate chain lengths made it impossible to synthesize standards with the same chain length as in the sample. Therefore, the separation conditions were optimized directly with the 1,2-DDE isolated from vernix caseosa. Based on experience with other neutral lipids such as triacylglycerols, wax esters or fatty acid methyl esters [43–45], a non-aqueous reversed-phase system with a NovaPak C18 column with a total column length of 45 cm was selected. The quality of separation in terms of peak-to-peak resolution and peak shape was investigated in binary solvent systems containing methanol, acetonitrile, propan-2-ol, ethyl acetate or toluene. Good peak-to-peak resolutions were achieved in systems combining acetonitrile and either 2-propanol or ethyl acetate. The use of 2-propanol was limited because of its high viscosity causing excessive column back pressure. Similar chromatographic systems with acetonitrile replaced with methanol provided a notably lower chromatographic resolution. Acetonitrile/toluene appeared to be an inappropriate solvent system for the separation of 1,2-DDE because of poor chromatographic resolution and significant signal suppression. The highest separation efficiency was achieved using a linear increase of ethyl acetate in acetonitrile for 100 min (Fig. 5A). The molecular species of 1,2-DDE eluted between 62 and 101 min. The peak width at its half maximum measured in the chromatograms reconstructed for $[M+NH_4]^+$ was typically 0.4 min.

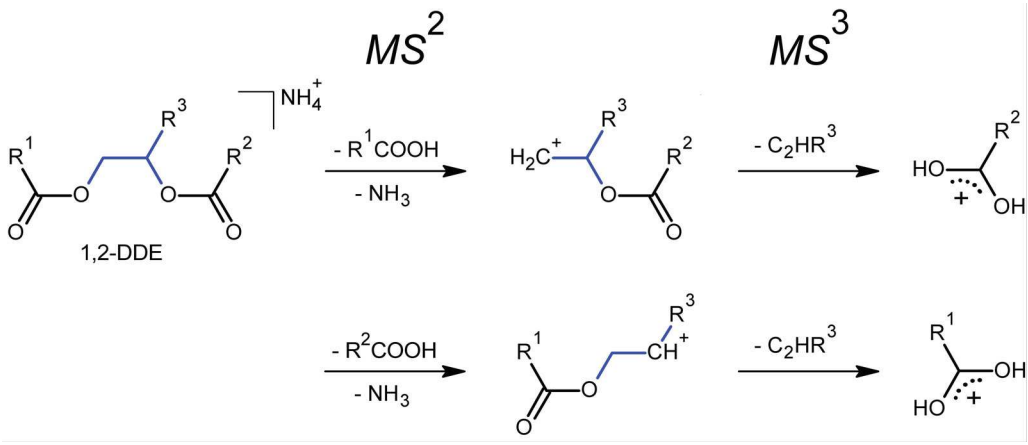

Fig. 3. The general scheme of 1,2-DDE fragmentation. Collision activation of the ammonium adduct (MS^2) promotes a neutral loss of ammonia and fatty acid from the position 1 or 2 of the diol. In the next step (MS^3), the neutral molecule of hydrocarbon (a former aliphatic chain of 1,2-diol) is cleaved, yielding protonated fatty acid. The R^1, R^2, R^3 are aliphatic chains.

This separation method was also tested with a mixture of 1,2-DDE standards with shorter chains (Fig. 5B). The chromatogram showed good separation of 1,2-DDE differing by ECN and a variable degree of separation of the molecular species with the same ECN. In the group of standards with ECN = 42, the isomers differing just by the position of double bonds (10:0//18:1*n*-7/18:1*n*-7, 10:0//18:1*n*-9/18:1*n*-9 and 10:0//18:1*n*-12/18:1*n*-12) were separated from each other (peaks no.1, 2 and 3). Saturated 10:0//16:0/16:0 eluted with the highest and distinct retention time (peak no. 5), whereas 10:0//18:1*n*-9_16:0 (peak no. 4) co-eluted with 10:0//18:1*n*-12/18:1*n*-12. Baseline separation was reached for the 1,2-DDE differing by ECN values, i.e. for 10:0//18:0/18:0 (peak no. 6, ECN = 46) and 16:0//18:1*n*-9/18:1*n*-9 (peak no. 7, ECN = 48).

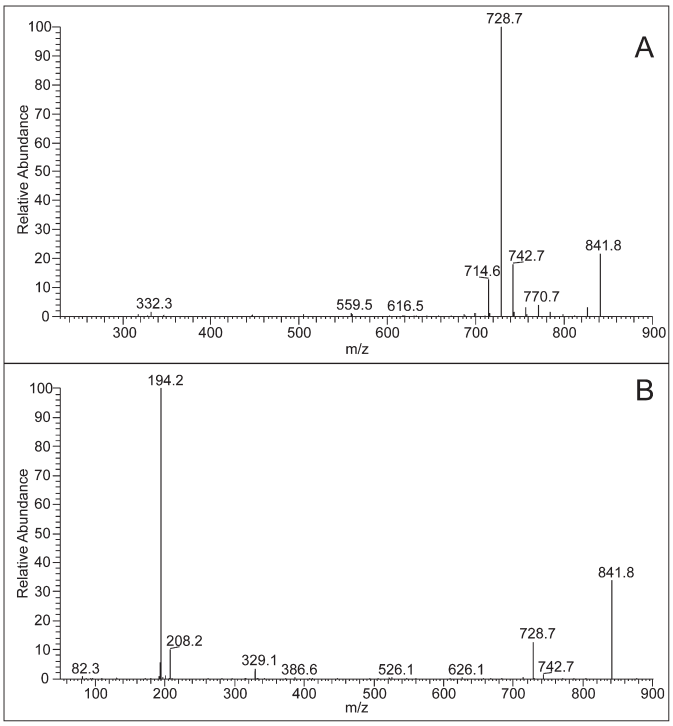

Fig. 4. The APCI MS^2 of the C_3H_5N adduct of 16:0//18:1*n*-9/18:1*n*-9 (the fragmentation of $[M+C_3H_5N]^{+\bullet}$ at *m/z* 841.8); the ion-trap CID spectrum (A) and the quadrupole HCD spectrum (B).

3.3. Analysis of 1,2-DDE from vernix caseosa

As vernix caseosa contains many lipid classes, we first verified the structure of isolated lipids using high-resolution mass spectrometry and tandem mass spectrometry. Within the above-mentioned elution range, the masses were consistent with the ammonium adducts of 1,2-DDE (of the elemental compositions $C_nH_{(2n+x)}O_4N$, where $x = 2$, 0, −2 or −4 depending on the number

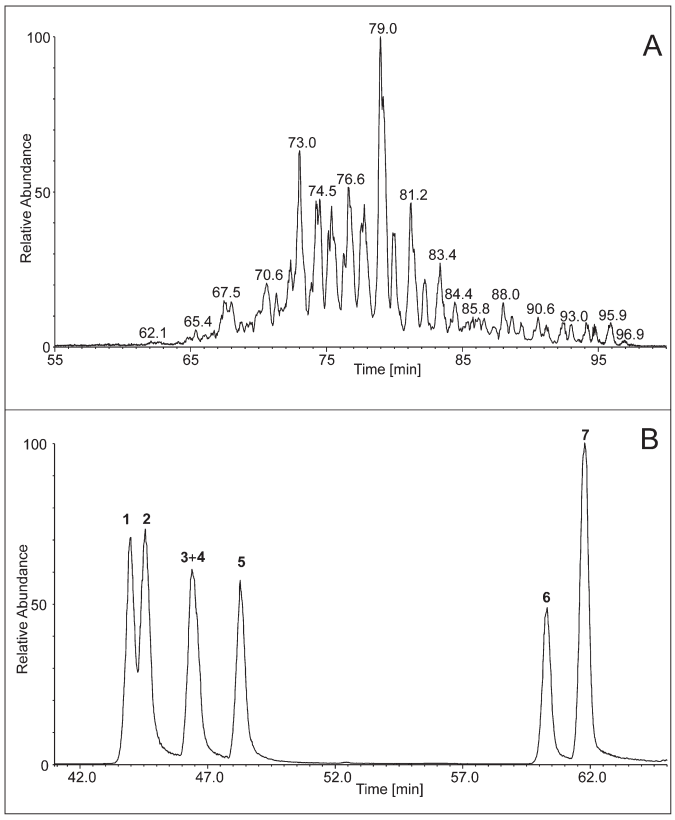

Fig. 5. The base-peak chromatograms (*m/z* 400–1500) of 1,2-DDE isolated from vernix caseosa (1 mg/mL; A) and 1,2-DDE standards (ca 0.1 mg/mL each; B). The mobile-phase gradient:0 min:70% of acetonitrile and 30% of ethyl acetate; 100 min:100% of ethyl acetate; 130 min:100% of ethyl acetate. The peak identity: 10:0//18:1*n*-7/18:1*n*-7 (**1**), 10:0//18:1*n*-9/18:1*n*-9 (**2**) 10:0//18:1*n*-12/18:1*n*-12 (**3**), 10:0//18:1*n*-9_16:0 (**4**), 10:0//16:0/16:0 (**5**), 10:0//18:0/18:0 (**6**), 16:0//18:1*n*-9/18:1*n*-9 (**7**).

of double bonds). The MS/MS spectra were analogous to those of synthetically prepared standards. They showed the elimination of ammonia and fatty acids (of the elemental compositions $C_nH_{(2n-y)}O_2$, where $y = 1$, 3, 5 or 7 depending on the number of double bonds). The typical mass errors were in the range of 0.5–1.5 ppm. These data together with the fact that the R_F on silica TLC matched the R_F of the synthetic standards of 1,2-DDE strongly indicated that the lipids were indeed 1,2-DDE. Although the isolation procedure (two-step TLC) was carefully optimized, the method selectivity appeared to be insufficient for the complete removal of unwanted lipids. The sample was found to be contaminated by an unknown lipid class exhibiting polarity very similar to 1,2-DDE. In our reversed-phase chromatographic system, these lipids eluted mostly at higher retention times and did not interfere with the analysis of 1,2-DDE (Supplementary Fig. S1). High-resolution mass spectra showed that the molecular species of this unknown lipid class contained four oxygen atoms and a sterol part. The molecular weights were considerably larger than those of 1,2-DDE and exhibited the maximum signals around m/z 1100. These lipids were not further explored.

As regards 1,2-DDE, the chromatographic data showed a high number of peaks partially overlapping in the base peak trace (Fig. 5A). The chromatograms reconstructed for m/z values of particular ammonium adducts typically showed several peaks. The compounds represented by these peaks had the same total number of carbons and double bonds, i.e. the ECN value. Saturated 1,2-DDE provided three or four peaks (Fig. 6A), with the second peak in the distribution being the most abundant and the fourth one of very low intensity. The separated peaks likely represented groups of molecular species differing in the number of methyl branches. Based on the analogy with wax esters [45], we speculate that the most retained species contained straight chains and each additional methyl branch shortened the retention time. Unfortunately, no standards of methyl-branched 1,2-DDE were available to prove this hypothesis. The MS^2 spectra taken across the peaks differed by the intensity of the fragments, which indicated different distributions of the chain lengths (Fig. S2). Monounsaturated 1,2-DDE showed up to three peaks in their reconstructed chromatograms (Fig. 6B). When compared to saturated 1,2-DDE, the peaks tended to be broader and less resolved. The explanation might be a combined effect of various positions of the double bond, *cis–trans* isomerism and chain branching. We hypothesize that the peak broadening was caused by retention time variations of the species with a different double-bond position. The observed separation of the peaks was likely caused by methyl branching or *cis–trans* isomerism rather than by the double-bond position, as the MS data showed a similar distribution of double-bond positions in the separated peaks (Table 1). Note that the double bond might be present either in a diol chain or fatty acyls. Since the number of separated peaks of monounsaturated 1,2-DDE was lower (by one) than in the case of saturated species, we speculate that the monounsaturated chains were not branched, whereas the remaining saturated chains were branched like the chains in fully saturated 1,2-DDE. The chromatographic resolution of the peaks representing doubly unsaturated 1,2-DDE (Fig. 6C) was even worse than in previous cases. The peak broadening was likely caused by an increased number of variations of double-bond positions. Double bonds could be located either in the diol chain and one fatty acyl, or in both fatty acyls, or all the double bonds could be present in a single chain, either diol or acyl. Moreover, the double bonds could be found in various positions within the chains. Like in less unsaturated 1,2-DDE, the MS^2 spectra revealed differences in the intensities of the fragments (Fig. S2) indicating variabilities in chain distribution. 1,2-DDE with three double bonds were detected only in trace concentrations. In general, 1,2-DDE eluted from the column in the order of increasing chain length as shown in Fig. S3. When recalculated to ECN values

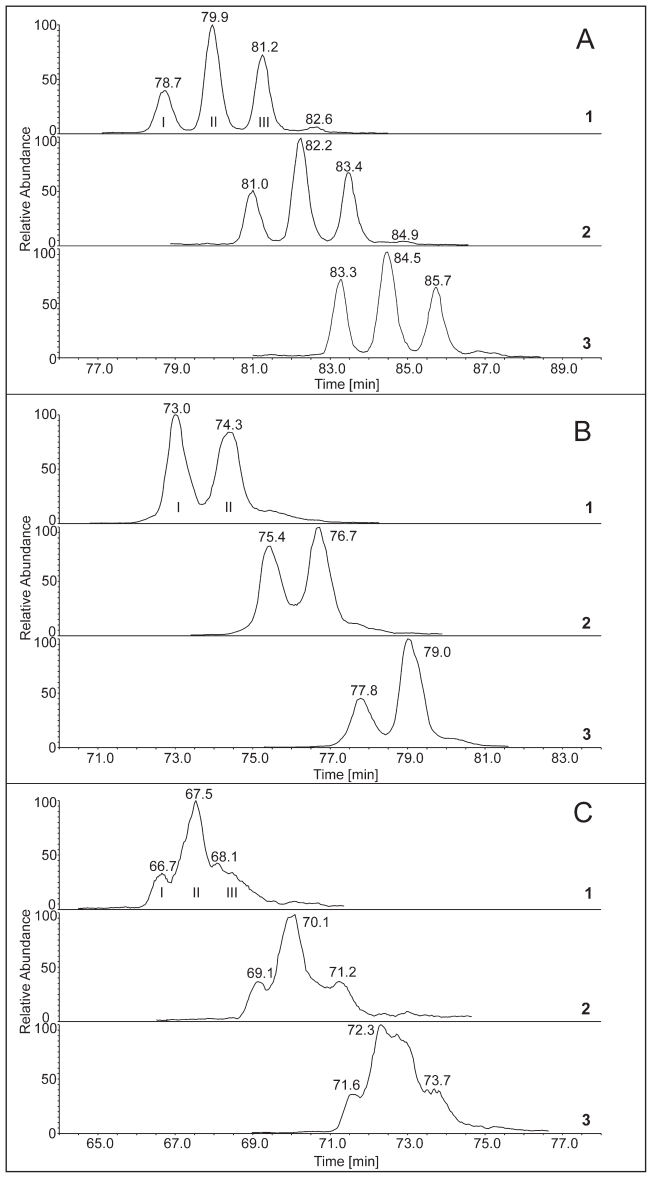

Fig. 6. The chromatograms of vernix caseosa 1,2-DDE reconstructed for selected saturated (A), monounsaturated (B) and diunsaturated (C) species: C56:0 (A1); C57:0 (A2); C58:0 (A3); C56:1 (B1); C57:1 (B2); C58:1 (B3); C56:2 (C1); C57:2 (C2); C58:2 (C3). The experimental conditions were the same as in Fig. 5.

and plotted against retention time, all molecular species appeared on a band almost linearly rising with the retention time (Fig. 7). Such behavior indicates the validity of the ECN concept assuming the same effect of a double bond as that of the shortening of the chain by two methylene groups. The ECN concept is valid for reversed-phase separations of many lipid classes including triacylglycerols, wax esters, fatty acid methyl esters or glyceroglycolipids [45–47] and used as an independent criterion for the validation of the structures assigned from LC/MS data.

The APCI-tandem MS detection with data-dependent scanning was used to identify the molecular species of 1,2-DDE. Because of the finite speed of the MS analyzer, the sample had to be re-measured several times to obtain good-quality spectra also for minor components. The total number of carbons and double bonds was deduced from the full-scan spectra showing the $[M+NH_4]^+$ of 1,2-DDE. The ammonium adducts were fragmented in the MS^2 step. The first fatty acid (attached either to the carbon 1 or 2 of the diol) was cleaved off (neutral loss) and the fragment was subjected to

Table 1
The 1,2-DDE identified in vernix caseosa.*

t_R (min)	m/z of $[M+NH_4]^+$	Peak area %	CN:DB	ECN	Identification[a]	Double-bond position[b]
61.73	804.4	0.04	52:2	48	–	*n*-7, *n*-5
62.52	778.4	0.02	50:1	48	–	–
62.59	804.4	0.22	52:2	48	20:0//16:1_16:1 [+6]	*n*-7, *n*-5
63.15	778.4	0.18	50:1	48	20:0//16:1_14:0 [+12]	*n*-7, *n*-5
63.54	804.4	0.10	52:2	48	22:1//16:1_14:0 [+4]	*n*-7, *n*-6, *n*-5, *n*-9, *n*-10
63.76	752.4	0.06	48:0	48	–	N/A
63.98	844.5	0.07	55:3	49	–	–
64.53	778.4	0.06	50:1	48	20:0//16:1_14:0 [+4]	*n*-7, *n*-5, *n*-10, *n*-9
64.57	818.4	0.10	53:2	49	17:0//16:1_20:1 22:1//16:1_15:0 [+9]	*n*-7, *n*-6, *n*-5
64.57	844.5	0.12	55:3	49	27:0//18:2_10:1 [+1]	–
64.98	752.4	0.05	48:0	48	–	N/A
65.13	792.4	0.05	51:1	49	22:1//14:0_15:0 [+9]	–
65.22	818.4	0.30	53:2	49	21:0//16:1_16:1 [+15]	*n*-7, *n*-6, *n*-5
65.85	792.4	0.24	51:1	49	20:0//16:1_15:0 21:0//16:1_14:0 [+19]	*n*-7, *n*-5
66.40	752.4	0.02	48:0	48	–	N/A
66.41	792.4	0.11	51:1	49	21:0//16:1_14:0 [+13]	–
66.43	766.4	0.20	49:0	49	20:0//14:0_15:0 [+10]	N/A
66.45	818.4	0.11	53:2	49	20:0//18:2_15:0 [+8]	–
66.45	858.6	0.35	56:3	50	24:1//16:1_16:1 [+8]	–
66.99	832.5	0.35	54:2	50	22:1//14:0_18:1 [+10]	*n*-7, *n*-5, *n*-9
67.11	792.4	0.15	51:1	49	20:0//16:1_15:0 21:0//16:1_14:0 [+10]	–
67.24	858.6	0.30	56:3	50	22:1//18:2_16:0 [+8]	–
67.70	858.6	0.11	56:3	50	21:3//16:0_19:0 [+6]	–
67.72	832.5	1.35	54:2	50	22:0//16:1_16:1 [+39]	*n*-7, *n*-5, *n*-9, *n*-10
67.75	766.4	0.17	49:0	49	20:0//14:0_15:0 [+10]	N/A
67.77	806.5	0.08	52:1	50	–	–
68.41	806.5	1.38	52:1	50	20:0//14:0_18:1 [+41]	*n*-7, *n*-9, *n*-5
68.59	832.5	0.55	54:2	50	20:0//18:2_16:0 [+22]	–
68.95	872.6	0.16	57:3	51	23:0//16:1_18:2 [+5]	–
69.08	766.4	0.05	49:0	49	–	N/A
69.15	780.5	0.56	50:0	50	22:0//14:0_14:0 [+12]	N/A
69.65	846.5	0.37	55:2	51	24:1//15:0_16:1 [+20]	–
69.71	872.6	0.20	57:3	51	29:0//10:1_18:2	–
69.82	806.5	1.13	52:1	50	20:0//14:0_18:1 20:0//16:1_16:0 [+31]	*n*-7, *n*-9, *n*-5
70.28	846.5	1.43	55:2	51	21:0//18:1_16:1 [+40]	*n*-7, *n*-9, *n*-6, *n*-10
70.29	820.5	0.13	53:1	51	–	–
70.42	780.5	0.58	50:0	50	20:0//14:0_16:0 [+18]	N/A
70.43	766.4	0.01	49:0	49	–	N/A
70.96	820.5	2.24	53:1	51	21:0//14:0_18:1 [+57]	*n*-7, *n*-9, *n*-10, *n*-5, *n*-8, *n*-6
71.07	806.5	0.15	52:1	50	20:0//16:1_16:0 [+7]	–
71.07	846.5	0.54	55:2	51	21:0//18:2_16:0 [+17]	–
71.33	886.6	0.63	58:3	52	24:1//16:1_18:1 [+23]	–
71.70	794.4	1.03	51:0	51	22:0//14:0_15:0 [+19]	N/A
71.80	780.5	0.21	50:0	50	20:0//14:0_16:0 [+6]	N/A
71.88	886.6	0.43	58:3	52	28:3//16:0_14:0 [+7]	–
71.98	860.6	0.71	56:2	52	24:1//18:1_14:0 [+15]	*n*-7, *n*-5
72.13	806.5	0.04	52:1	50	–	–
72.24	820.5	1.36	53:1	51	21:0//14:0_18:1 [+42]	*n*-7, *n*-9, *n*-5, *n*-6, *n*-10
72.69	860.6	2.49	56:2	52	22:0//16:1_18:1 [+51]	*n*-7, *n*-9, *n*-5
72.94	820.5	0.24	53:1	51	21:0//16:1_16:0 [+15]	–
72.97	834.5	0.20	54:1	52	22:0//18:1_14:0 [+12]	–
73.09	794.4	1.16	51:0	51	22:0//15:0_14:0 [+21]	N/A
73.23	780.5	0.04	50:0	50	–	N/A
73.24	860.6	1.62	56:2	52	22:1//18:1_16:0 [+23]	–
73.42	834.5	4.62	54:1	52	22:0//14:0_18:1 [+45]	*n*-7, *n*-9, *n*-8, *n*-5, *n*-6, *n*-10
74.02	860.6	0.64	56:2	52	22:0//18:2_16:0 [+34]	–
74.26	808.5	1.11	52:0	52	22:0//14:0_16:0 [+20]	N/A
74.31	794.4	0.24	51:0	51	21:0//14:0_16:0 [+9]	N/A
74.31	874.6	0.34	57:2	53	24:1//18:1_15:0 [+7]	–
74.86	834.5	2.72	54:1	52	20:0//16:0_18:1 [+57]	*n*-7, *n*-9, *n*-5, *n*-10, *n*-8, *n*-6, *n*-11
75.14	874.6	1.58	57:2	53	23:0//16:1_18:1 [+24]	*n*-7, *n*-9, *n*-8, *n*-11
75.60	808.5	2.01	52:0	52	22:0//16:0_14:0 [+20]	N/A
75.79	848.5	4.36	55:1	53	22:0//18:1_15:0 [+60]	*n*-7, *n*-9, *n*-8, *n*-10, *n*-5, *n*-6
75.80	794.4	0.04	51:0	51	–	N/A
75.87	834.5	0.60	54:1	52	22:0//16:0_16:1 [+26]	–
76.43	874.6	0.42	57:2	53	23:1//18:1_16:0 [+18]	–
76.66	888.6	0.37	58:2	54	24:1//18:1_16:0 [+2]	–
76.69	822.5	1.21	53:0	53	22:0//16:0_15:0 [+25]	N/A
76.89	808.5	0.82	52:0	52	20:0//16:0_16:0 [+13]	N/A
77.11	848.5	4.33	55:1	53	21:0//16:0_18:1 [+52]	*n*-7, *n*-9, *n*-8, *n*-10, *n*-5, *n*-6
77.34	888.6	0.95	58:2	54	22:0//18:1_18:1 [+12]	–
77.89	888.6	1.79	58:2	54	24:1//18:1_16:0 [+60]	*n*-7, *n*-9, *n*-5, *n*-10
77.96	822.5	2.44	53:0	53	22:0//16:0_15:0 [+28]	N/A
78.03	848.5	0.24	55:1	53	21:0//16:0_18:1 [+15]	–
78.09	862.6	3.43	56:1	54	22:0//16:0_18:1 [+50]	*n*-7, *n*-9, *n*-8, *n*-5, *n*-10
78.19	808.5	0.11	52:0	52	–	N/A

Table 1 (*Continued*)

79.07	836.5	0.93	54:0	54	22:0//16:0_16:0 [+22]	N/A
79.29	822.5	0.91	53:0	53	21:0//16:0_16:0 [+20]	N/A
79.38	862.6	7.36	56:1	54	22:0//16:0_18:1 [+38]	*n*-7, *n*-9, *n*-10, *n*-8, *n*-5, *n*-6
79.48	902.7	1.06	59:2	55	23:0//18:1_18:1 [+29]	–
80.32	876.6	2.12	57:1	55	23:0//16:0_18:1 [+37]	*n*-7, *n*-9, *n*-8, *n*-10, *n*-5
80.33	836.5	2.25	54:0	54	22:0//16:0_16:0 [+28]	N/A
80.49	822.5	0.03	53:0	53	–	N/A
80.54	862.6	0.37	56:1	54	22:0//16:0_18:1 [+22]	–
81.28	916.5	0.11	60:2	56	24:0//18:1_18:1 [+15]	–
81.32	850.6	0.68	55:0	55	23:0//16:0_16:0 [+23]	N/A
81.54	876.6	3.99	57:1	55	23:0//16:0_18:1 [+31]	*n*-7, *n*-9, *n*-8, *n*-10, *n*-5, *n*-6
81.60	836.5	1.43	54:0	54	22:0//16:0_16:0 [+16]	N/A
82.58	890.6	1.48	58:1	56	22:0//16:0_20:1 [+38]	*n*-7, *n*-9, *n*-5, *n*-11
82.59	850.6	1.43	55:0	55	23:0//16:0_16:0 [+26]	N/A
82.71	876.6	0.15	57:1	55	23:0//16:0_18:1 [+11]	–
82.89	836.5	0.11	54:0	54	22:0//16:0_16:0	N/A
83.39	930.7	0.17	61:2	57	19:0//18:1_24:1 [+1]	–
83.55	864.6	0.30	56:0	56	24:0//16:0_16:0 [+17]	N/A
83.57	890.6	1.46	58:1	56	22:0//16:0_20:1 [+34]	*n*-7, *n*-9, *n*-10, *n*-5
83.77	850.6	0.56	55:0	55	23:0//16:0_16:0 [+14]	N/A
84.00	930.7	0.10	61:2	57	–	–
84.66	904.7	0.77	59:1	57	23:0//16:0_20:1 [+29]	*n*-7, *n*-9
84.79	864.6	0.86	56:0	56	23:0//16:0_17:0 24:0//16:0_16:0 [+25]	N/A
84.81	890.6	0.28	58:1	56	24:0//16:0_18:1 [+7]	–
85.06	850.6	0.05	55:0	55	–	N/A
85.29	944.7	0.38	62:2	58	24:1//18:1_20:0 [+2]	–
85.55	904.7	0.67	59:1	57	23:0//20:1_16:0 [+11]	*n*-7, *n*-9
85.68	878.6	0.49	57:0	57	22:0//14:0_21:0 [+23]	N/A
85.99	864.6	0.54	56:0	56	22:0//16:0_18:0 24:0//16:0_16:0 [+16]	N/A
86.31	918.7	0.21	60:1	58	24:1//20:0_16:0 [+2]	–
86.71	918.7	0.45	60:1	58	22:0//16:1_22:0 [+19]	*n*-7, *n*-9, *n*-10, *n*-5
86.86	878.6	0.56	57:0	57	24:0//16:0_17:0 [+20]	N/A
87.22	864.6	0.05	56:0	56	–	N/A
87.44	918.7	0.42	60:1	58	24:1//20:0_16:0 [+11]	*n*-7, *n*-5, *n*-9
87.62	892.7	0.50	58:0	58	22:0//14:0_22:0 [+14]	N/A
88.07	932.6	0.10	61:1	59	–	–
88.15	878.6	0.22	57:0	57	23:0//16:0_18:0 [+12]	N/A
88.70	932.6	0.32	61:1	59	23:0//16:1_22:0 [+14]	*n*-7, *n*-5, *n*-9
88.99	892.7	0.65	58:0	58	22:0//16:0_20:0 [+25]	N/A
89.27	932.6	0.16	61:1	59	24:1//16:0_21:0 [+2]	*n*-7, *n*-5, *n*-6, *n*-9, *n*-10
89.55	906.7	0.43	59:0	59	21:0//14:0_24:0 [+17]	N/A
89.97	946.7	0.13	62:1	60	24:1//14:0_24:0 [+4]	*n*-7, *n*-5
90.17	892.7	0.18	58:0	58	22:0//16:0_20:0 [+6]	N/A
90.60	946.7	0.41	62:1	60	22:0//16:1_24:0 [+25]	*n*-7, *n*-5, *n*-9
90.78	906.7	0.55	59:0	59	23:0//16:0_20:0 [+17]	N/A
91.15	946.7	0.19	62:1	60	23:1//16:0_23:0 [+3]	*n*-7, *n*-5, *n*-9
91.40	920.7	0.46	60:0	60	22:0//14:0_24:0 [+15]	N/A
91.80	906.7	0.04	59:0	59	20:0//16:0_23:0 [+1]	N/A
92.83	920.7	0.39	60:0	60	22:0//16:0_22:0 [+17]	N/A
93.26	934.6	0.41	61:0	61	22:0//14:0_25:0 [+16]	N/A
93.86	920.7	0.09	60:0	60	22:0//16:0_22:0	N/A
94.37	934.6	0.52	61:0	61	22:0//16:0_23:0 [+17]	N/A
94.96	948.7	0.37	62:0	62	22:0//15:0_25:0 23:0//15:0_24:0 [+11]	N/A
95.45	934.6	0.08	61:0	61	–	N/A
96.10	948.7	0.50	62:0	62	22:0//16:0_24:0 [+16]	N/A
96.67	962.7	0.25	63:0	63	22:0//15:0_26:0 [+10]	N/A
97.21	948.7	0.08	62:0	62	–	N/A
97.80	962.7	0.40	63:0	63	22:0//16:0_25:0 [+9]	N/A
98.19	976.7	0.20	64:0	64	–	N/A
98.77	962.7	0.06	63:0	63	–	N/A
99.30	976.7	0.30	64:0	64	22:0//16:0_26:0 [+8]	N/A
99.78	990.7	0.12	65:0	65	–	N/A
100.30	976.7	0.05	64:0	64	–	N/A
100.86	990.7	0.09	65:0	65	–	N/A
101.70	990.7	0.03	65:0	65	–	N/A

[*] A full version of this table can be found in the Supplementary Information (Table S2).

[a] The numbers in brackets indicate the number of additional identified 1,2-DDE; see the Supplementary Information (Table S2) for their structures.

[b] Based on the MS/MS of $[M+C_3H_5N]^{+\bullet}$; the double-bond positions are listed in the order of the corresponding peak intensities. The double bond positions identified from the ion trap CID spectra (based on the α-ions) are given as unformatted text and the double-bond positions identified from the quadrupole HCD spectra (based on the ω-ions) are displayed in italics; the double-bond positions identified in both types of spectra are bolded.

another fragmentation reaction. The MS^3 spectra showed the elimination of diols (a neutral loss of diene) and the resulting fragments were protonated second fatty acids accompanied by their dehydration products ($[FA+H-H_2O]^+$ and $[FA+H-2H_2O]^+$) in the case of unsaturated species. By manual interpretation of the data, we identified 2250 molecular species of 1,2-DDE in 141 chromatographic peaks. Although the separation conditions were optimized very carefully, the chromatographic peaks still represented mixtures with up to 61 identified molecular species of 1,2-DDE (with the same number of carbon atoms and double bonds, but differently

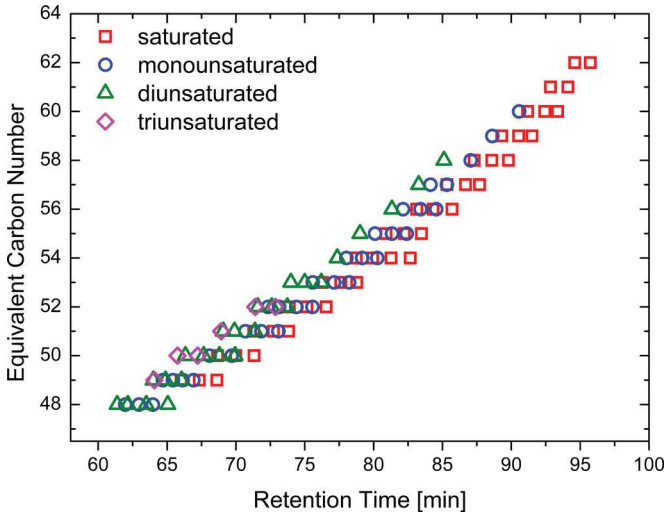

Fig. 7. The plot of calculated ECN values vs. retention times for 1,2-DDE identified in the vernix caseosa sample.

distributed among the chains). A short summary of the identified lipids is given in Table 1; for the full version with all 2250 species, please refer to the Supplementary Information (Table S2).

The molecular species of 1,2-DDE could not be quantified because of extensive co-elution and unavailability of standards. As lipid response factors depend on the number of double bonds and chain length [48], it was possible to make only a rough estimate of the real proportions based on relative peak areas. The peak areas used for the calculations were integrated in the full-scan chromatograms reconstructed for $[M+NH_4]^+$. In this way, we found that the peak area of all saturated 1,2-DDE corresponded to 30% of the total integrated signal. Monounsaturated, diunsaturated and triunsaturated lipids accounted for 49%, 18% and 3%, respectively. As the direct quantitative evaluation of the distribution of diol and acid chains among the identified 1,2-DDE species was not possible because of coelutions, we used a different approach based on counting their relative frequency of occurrence. Obviously, this way of counting systematically underestimated the most abundant chains and overestimated the least abundant ones. Nevertheless, it allowed us to identify the most abundant chains occurring in 1,2-DDE. The plots of the relative frequency of occurrence are shown in

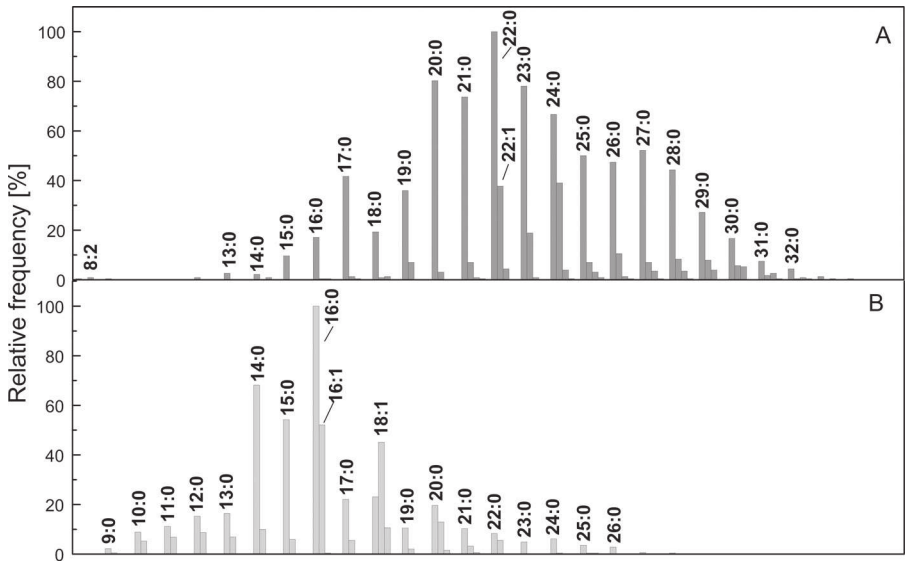

Fig. 8. The relative frequencies of occurrence for 1,2-diols (A) and fatty acids (B) in 1,2-DDE identified in the vernix caseosa sample.

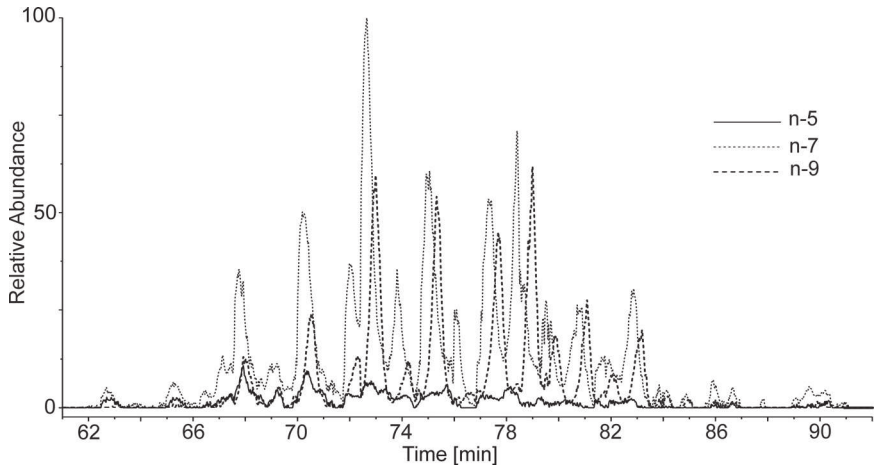

Fig. 9. The overlay plot of the chromatograms of vernix caseosa 1,2-DDE reconstructed for molecular species with the double bond in the positions *n*-5 (*m*/*z* 138.13; solid line), *n*-7 (*m*/*z* 166.16; dotted line) and *n*-9 (*m*/*z* 194.19; dashed line). Based on quadrupole HCD MS/MS data, the experimental conditions were the same as in Fig. 5 (the sample concentration was 50 mg/mL).

Fig. 8A (diols) and Fig. 8B (fatty acids). Diol chains appeared to be mostly saturated with 8–34 carbons and the distribution of their chain length had a maximum around C22:0 (Fig. 8A). Monounsaturated diols were also present, particularly C24:1, C22:1 and C23:1; diunsaturated diols were infrequent. The results were in agreement with literature data. In the total lipids of vernix caseosa, Nikkari [5] reported mostly saturated and branched C14–C26 diols; almost 95% of them contained 20–24 carbons, with C22 being by far the most abundant. These diols were also identified four years earlier by Kärkkäinen et al. [3]. Fu and Nicolaides [4] analyzed the diol diester fraction and found C20–C25 1,2-diols, mostly *iso*- and *anteiso*-branched. Our results confirmed these observations and additionally showed the presence of both shorter-chain (C8–C13) and longer-chain (C27–C34) 1,2-diols. As regards fatty acyls, we detected chains with 8–32 carbons, roughly in the same range as in the case of 1,2-diols. However, the most frequently occurring fatty acyl chains were noticeably shorter than those of 1,2-diols (Fig. 8B). The most frequently occurring acyls were saturated C14–C16 together with monounsaturated C16:1 and C18:1. The most significant doubly unsaturated acyl was C18:2. These results were in agreement with the report of Ansari et al. [19], who found straight-chain, *iso*- and *anteiso*-branched saturated acids and straight-chain monoenic acids with 12–36 carbons. The most abundant acyls appeared to be C16:0 and C18*n*-7, C18*n*-9. Similar results were obtained earlier by Kärkkäinen et al. [3], who also showed the presence of C18:2 and C18:3. As regards the molecular species of 1,2-DDE in the vernix caseosa sample, their ECN values ranged between 48 and 65 with the maximum around 54–56 (Fig. S4). The most abundant 1,2-DDE were monounsaturated species combining a C22 diol and a C18:1 fatty acid together with a C16:0, C14:0 or C15:0 fatty acid (Table 1 and Table S2). The position of double bonds in the unsaturated chains was deduced from the MS^2 spectra of the $[M+C_3H_5N]^{+\bullet}$ formed in the APCI source. Both ion-trap CID and quadrupole HCD data revealed double bonds in several positions within the chain in the chromatographically separated peaks. It is important to note that, without the separation of the molecular species, the double bond could not be assigned to individual 1,2-DDE. Neither was it possible to distinguish between the double bond in the acid and the diol chain. Ion-trap CID appeared to provide good-quality spectra even for low abundant compounds, but the interpretation was complicated by the presence of satellite fragments formed by cleavages of other neighboring bonds. Therefore, strict rules regarding ion abundances were applied to distinguish between signals of diagnostic fragments (α-ions) and their satellites to avoid false positive results. Consequently, the less frequently occurring double-bond positions were possibly undetected. The interpretation of the quadrupole HCD spectra was much more straightforward, as the formation of satellites was significantly lower. Unfortunately, very low abundant 1,2-DDE provided spectra of poor quality, likely because of ion-beam losses during the transfer of the precursors to the HCD cell and the products to the Orbitrap via C-trap. Nevertheless, both fragmentation techniques allowed for the localization of double bonds in moderately and highly abundant peaks of 1,2-DDE. The data showed that double bonds were located mostly in *n*-7 and *n*-9, less frequently in *n*-5 and other positions (Table 1 and Table S2). The quadrupole HCD data allowed us to make reconstructed chromatograms for each double-bond position. The overlay plot (Fig. 9) shows that the peak maxima were shifted, i.e. the retention times depended on the position the of double bond. The retention times of *n*-9 peaks were typically higher than those of *n*-7, which was also consistent with the relative retention of 10:0//18:1*n*-7/18:1*n*-7 and 10:0//18:1*n*-9/18:1*n*-9 (see Fig. 5). The observed variations in the retention times caused by the double-bond positions also explain the broadening of the chromatographic peaks of unsaturated 1,2-DDE. Based on the integration of the peak area in the reconstructed chromatograms, the relative proportions of the chains with different double-bond positions appeared to be as follows: *n*-7 (61%), *n*-9 (30%), *n*-5 (8%) and *n*-11 (2%). The double-bond positions determined here were in agreement with the structure of the 1,2-DDE fatty acyls reported previously. The most abundant unsaturated fatty acyls in the 1,2-DDE fraction identified by Ansari et al. [19] appeared to be C18:1*n*-7, C18:1*n*-9, C16:1 *n*-7, C18:1*n*-10, C16:1*n*-5, C16:1*n*-10 and C20:1*n*-7; fatty acyls unsaturated in other positions were detected as well. As regards 1,2-diols, to the best of our knowledge no information about the positions of double bonds in their chains has been published so far.

4. Conclusions

Using HPLC/APCI–tandem MS, we detected more than 2000 molecular species of 1,2-DDE. The actual number of distinct 1,2-DDE in vernix caseosa is probably much higher taking into account chains with various positions of double bonds and/or methyl branching as well as regioisomers not distinguished by our method. 1,2-DDE detected in this work contained 72 diols and 62 fatty acids differing in the number of carbons and double bonds. Theoretically, one could combine them into 276,768 different 1,2-DDE. As the number of detected lipids was about two orders of magnitude lower than it could theoretically be, we assume that the human skin in its early stages of development synthesizes 1,2-DDE non-randomly, preferring only certain combinations. The number of detected 1,2-DDE is still astonishing, especially when considering that 1,2-DDE constitute only a small part of vernix caseosa lipids and many other classes, likely with a similar degree of complexity, are biosynthesized as well. This work also points out the limitations of the current separation technology. Nowadays, one can hardly imagine a separation system, even multidimensional, capable of separating thousands of structurally similar molecular species, particularly lipids associated with the skin of mammals. A comprehensive characterization of the molecular species in the skin lipidome is a challenging task for scientists.

Acknowledgements

Financial support from the Czech Science Foundation (Project No P206/12/0750), the Academy of Sciences of the Czech Republic (RVO 61388963) and Charles University in Prague (Project SVV) is hereby acknowledged with appreciation.

Appendix A. Supplementary data

Supplementary data associated with this article can be found, in the online version, at http://dx.doi.org/10.1016/j.chroma.2014.11.075.

References

[1] C.C. Zouboulis, J.M. Baron, M. Bohm, S. Kippenberger, H. Kurzen, J. Reichrath, A. Thielitz, Frontiers in sebaceous gland biology and pathology, Exp. Dermatol. 17 (2008) 542–551.
[2] T. Nikkari, Composition and secretion of the skin surface lipids of the rat; effects of dietary lipids and hormones, Scand. J. Clin. Lab. Invest. 17 (1965) 1–140.
[3] J. Kärkkäinen, T. Nikkari, S. Ruponen, E. Haahti, Lipids of vernix caseosa, J. Invest. Dermatol. 44 (1965) 333–338.
[4] H.C. Fu, N. Nicolaides, The structure of alkane diols of diesters in vernix caseosa lipids, Lipids 4 (1969) 170–175.
[5] T. Nikkari, The occurrence of diester waxes in human vernix caseosa and in hair lipids of common laboratory animals, Comp. Biochem. Physiol. 29 (1969) 795–803.
[6] D.H.S. Horn, F.W. Hougen, Wool wax. 4. The constitution of the aliphatic diols, J. Chem. Soc. (1953) 3533–3538.
[7] L.F. Fieser, W.-Y. Huang, B.K. Bhattacharyya, Cholesterol and companions. X. The diol fraction, J. Org. Chem. 22 (1957) 1380–1384.
[8] N. Nicolaides, H.C. Fu, M.N.A. Ansari, Diester waxes in surface lipids of animal skin, Lipids 5 (1970) 299–307.

[9] P.C. Schmid, Y. Wedmid, H.H.O. Schmid, 15-Methyl-1,2-hexadecanediol, a major constituent of hamster surface wax, Lipids 13 (1978) 825–827.
[10] D. Yeung, S. Nacht, R.E. Cover, The composition of the skin surface lipids of the gerbil, Biochim. Biophys. Acta 663 (1981) 524–535.
[11] B.V. Burger, D. Smit, H.S.C. Spies, C. Schmidt, U. Schmidt, A.Y. Telitsina, G.R. Grierson, Mammalian exocrine secretions XV. Constituents of secretion of ventral gland of male dwarf hamster, *Phodopus sungorus sungorus*, J. Chem. Ecol. 27 (2001) 1259–1276.
[12] P.C. Bandi, H.H.O. Schmid, Configurational analysis of long-chain alkanediols, Chem. Phys. Lipids 17 (1976) 267–274.
[13] P.C. Schmid, H.H.O. Schmid, Lipase hydrolysis of mammalian long-chain 1,2-alkanediol diesters. Nonrandom distribution of fatty acids, J. Lipid Res. 19 (1978) 894–898.
[14] D.M. Sharaf, S.J. Clark, D.T. Downing, Skin surface lipids of the dog, Lipids 12 (1977) 786–790.
[15] D.T. Downing, J.S. Lindholm, Skin surface lipids of the cow, Comp. Biochem. Physiol. B 73 (1982) 327–330.
[16] T. Nishimaki-Mogami, K. Minegishi, A. Takahashi, Y. Kawasaki, Y. Kurokawa, M. Uchiyama, Characterization of skin-surface lipids from the monkey (*Macaca fascicularis*), Lipids 23 (1988) 869–877.
[17] T. Nikkari, Comparative chemistry of sebum, J. Invest. Dermatol. 62 (1974) 257–267.
[18] K.A. Haubrich, Role of vernix caseosa in the neonate: potential application in the adult population, AACN Clin. Issues 14 (2003) 457–464.
[19] M.N.A. Ansari, H.C. Fu, N. Nicolaides, Fatty acids of the alkane diol diesters of vernix-caseosa, Lipids 5 (1970) 279–282.
[20] C.-L.E. Yen, M. Monetti, B.J. Burri, R.V. Farese Jr., The triacylglycerol synthesis enzyme DGAT1 also catalyzes the synthesis of diacylglycerols, waxes, and retinyl esters, J. Lipid Res. 46 (2005) 1502–1511.
[21] K. Saito, M. Gamo, Distribution of diol waxes in preen glands of some birds. 3. The occurrence of 1,2-diols, Comp. Biochem. Physiol. 45 (1973) 603–611.
[22] P.E. Kolattukudy, Structure and cell-free synthesis of alkane-1,2-diols of the uropygial gland of white crowned sparrow *Zonotrichia leucophrys*, Biochem. Biophys. Res. Commun. 49 (1972) 1376–1383.
[23] J.S.S. Damsté, M. Dekker, B.E. van Dongen, S. Schouten, T. Piersma, Structural identification of the diester preen-gland waxes of the red knot (*Calidris canutus*), J. Nat. Prod. 63 (2000) 381–384.
[24] M.S. Dodova-Anghelova, C.P. Ivanov, On the composition and structure of diols from the skin wax of some apple varieties, Dokl. Bolg. Akad. Nauk 22 (1969) 1039–1042.
[25] C. Buschhaus, C. Peng, R. Jetter, Very-long-chain 1,2- and 1,3-bifunctional compounds from the cuticular wax of Cosmos bipinnatus petals, Phytochemistry 91 (2013) 249–256.
[26] R. Wait, L. Carreto, M.F. Nobre, A.M. Ferreira, M.S. DaCosta, Characterization of novel long-chain 1,2-diols in *Thermus* species and demonstration that *Thermus* strains contain both glycerol-linked and diol-linked glycolipids, J. Bacteriol. 179 (1997) 6154–6162.
[27] M.T.J. van der Meer, S. Schouten, S. Hanada, E.C. Hopmans, D.J.S. Sinninghe, D.M. Ward, Alkane-1,2-diol-based glycosides and fatty glycosides and wax esters in *Roseiflexus castenholzii* and hot spring microbial mats, Arch. Microbiol. 178 (2002) 229–237.
[28] W. Johnson Jr., W.F. Bergfeld, D.V. Belsito, R.A. Hill, C.D. Klaassen, D. Liebler, J.G. Marks Jr., R.C. Shank, T.J. Slaga, P.W. Snyder, F.A. Andersen, Safety assessment of 1,2-glycols as used in cosmetics, Int. J. Toxicol. 31 (2012) 147S–168S.
[29] S. Behrens, A. Bleckmann, R. Kroepke, U. Meiring, J. Nielsen, Cosmetic O/W emulsion comprising 1,2-hexanediol, Patent US8084507 B2 (December 27, 2011).
[30] J. Nielsen, A. Bleckmann, H. Argembeaux, M. Detert, S. Ruppert, H. Albrecht, J. Küther, A. Aechtner, S. Thompson, M. Köhler, Cosmetic preparation in the form of an oil-in-water emulsion containing 1,2-alkanediol(s)), Patent EP1942864 A1 (July 16, 2008).
[31] G. Schmaus, S. Lange, H. Joppe, Synergistic mixtures of 1,2-alkane diols, U.S. Patent US20050222276 A1 (October 6, 2005).
[32] D. Greff, Cosmetic, dermopharmaceutical or veterinary compositions for disinfecting human or animal skin, US patent 6123953 A (September 26, 2000).
[33] A. Kobayashi, F. Okada, H. Okamoto, Antiseptic bactericides and cosmetics, drugs and foods containing the antiseptic bactericides, Patent WO2004028520 A1 (April 8, 2004).
[34] S. Lange, G. Schmaus, Use of c10-c14-alkane-1,2-diols in the preparation of a composition for the prophylaxis and/or treatment of dermatophyte infections, Patent WO2008046796 A3 (June 12, 2008).
[35] P.S. Shah, Antispasmodic 1,2-diols and 1,2,3-triols, Patent WO2013181084 A1 (December 5, 2013).
[36] D. Redoules, S. Daunes-Marion, M.-F. Aries, Polyunsaturated fatty acid and diol ester as an anti-acne agent, U.S. Patent US8623916 B2 (January 7, 2014).
[37] J.W. Finley, L.P. Klemann, A. Scimone, Long chain diol diesters as low calorie fat mimetics, U.S. Patent US5008126 A (April 16, 1991).
[38] R. Míková, V. Vrkoslav, R. Hanus, E. Háková, Z. Hábová, A. Doležal, R. Plavka, P. Coufal, J. Cvačka, Newborn Boys, Girls differ in the lipid composition of vernix caseosa, PLOS ONE 9 (2014) e99173.
[39] W.J. Baumann, J. Seufert, H.W. Hayes, R.T. Holman, Mass spectrometric analysis of long-chain esters of diols, J. Lipid Res. 10 (1969) 703–709.
[40] D.T. Downing, Fatty acid composition of vernix caseosa, Aust. J. Chem. 16 (1963) 679–682.
[41] V. Vrkoslav, M. Háková, K. Pecková, K. Urbanová, J. Cvačka, Localization of double bonds in wax esters by high-performance liquid chromatography/atmospheric pressure chemical ionization mass spectrometry utilizing the fragmentation of acetonitrile-related adducts, Anal. Chem. 83 (2011) 2978–2980.
[42] G. Liebisch, J.A. Vizcaino, H. Kofeler, M. Trotzmuller, W.J. Griffiths, G. Schmitz, F. Spener, M.J.O. Wakelam, Shorthand notation for lipid structures derived from mass spectrometry, J. Lipid Res. 54 (2013) 1523–1530.
[43] V. Vrkoslav, J. Cvačka, Identification of the double-bond position in fatty acid methyl esters by liquid chromatography/atmospheric pressure chemical ionisation mass spectrometry, J. Chromatogr. A 1259 (2012) 244–250.
[44] E. Kofroňová, J. Cvačka, V. Vrkoslav, R. Hanus, P. Jiroš, J. Kindl, O. Hovorka, I. Valterová, A comparison of HPLC/APCI–MS and MALDI–MS for characterising triacylglycerols in insects: species-specific composition of lipids in the fat bodies of bumblebee males, J. Chromatogr. B 877 (2009) 3878–3884.
[45] V. Vrkoslav, K. Urbanová, J. Cvačka, Analysis of wax ester molecular species by high performance liquid chromatography/atmospheric pressure chemical ionisation mass spectrometry, J. Chromatogr. A 1217 (2010) 4184–4194.
[46] B. Nikolova-Damyanova, Reversed phase HPLC: general principles and application to fatty acids and triacylglycerols, in: W.W. Christie (Ed.), Advances in Lipid Methodology – Four, The Oily Press, Ayr, Scotland, 1997, pp. 193–251.
[47] M. Zábranská, V. Vrkoslav, J. Sobotníková, J. Cvačka, Analysis of plant galactolipids by reversed-phase high-performance liquid chromatography/mass spectrometry with accurate mass measurement, Chem. Phys. Lipids 165 (2012) 601–607.
[48] M. Holčapek, M. Lísa, P. Jandera, N. Kabátová, Quantitation of triacylglycerols in plant oils using HPLC with APCI–MS, evaporative light-scattering, and UV detection, J. Sep. Sci. 28 (2005) 1315–1333.

- Publication III -

Anal Bioanal Chem
DOI 10.1007/s00216-015-8537-1

RESEARCH PAPER

Localization of double bonds in triacylglycerols using high-performance liquid chromatography/atmospheric pressure chemical ionization ion-trap mass spectrometry

Eva Háková · Vladimír Vrkoslav · Radka Míková · Karolina Schwarzová-Pecková · Zuzana Bosáková · Josef Cvačka

Received: 12 December 2014 / Revised: 28 January 2015 / Accepted: 5 February 2015

Abstract A method for localizing double bonds in triacylglycerols using high-performance liquid chromatography–tandem mass spectrometry with atmospheric pressure chemical ionization (APCI) was developed. The technique was based on collision-induced dissociation or pulsed Q collision-induced dissociation of the $C_3H_5N^{+\bullet}$ adducts ($[M + 55]^{+\bullet}$) formed in the presence of acetonitrile in the APCI source. The spectra were investigated using a large series of standards obtained from commercial sources and prepared by randomization. The fragmentation spectra made it possible to determine (i) the total number of carbons and double bonds in the molecule, (ii) the number of carbons and double bonds in acyls, (iii) the acyl in the *sn*-2 position on the glycerol backbone, and (iv) the double-bond positions in acyls. The double-bond positions were determined based on two types of fragments (alpha and omega ions) formed by cleavages of C–C bonds vinylic to the original double bond. The composition of the acyls and their positions on glycerol were established from the masses and intensities of the ions formed by the elimination of fatty acids from the $[M + 55]^{+\bullet}$ precursor. The method was applied for the analysis of triacylglycerols in olive oil and vernix caseosa.

Keywords Double bond · Gas-phase chemistry · Lipidomics · Olive oil · Vernix caseosa

Introduction

Triacylglycerols (TGs) are the main storage lipids in animal and plant tissues and consequently they are the major fat in the human diet [1]. The TG molecules contain a glycerol backbone, to which three fatty acids are esterified; the variety of fatty acids distributed among the *sn*-1, *sn*-2, and *sn*-3 positions of glycerol often makes TG mixtures very rich. The structure of TGs affects their physico-chemical properties and metabolic fates. Therefore, analytical tools which make it possible to elucidate their molecular structures are of great importance for various branches of life science and industry.

A complete structural characterization of TGs in their mixtures is not an easy task. The molecular species of TGs typically need to be separated from each other before elucidating their structures. Chromatographic separations are mostly carried out in various systems based on (U)HPLC in reversed-phase [2–5], silver-ion [4, 6, 7], and chiral [8] modes. Because of entirely different separation mechanisms, they can be combined in 2D systems [9, 10]. Retention parameters are useful for TG characterization, especially when standards are available for comparison [11]. However, the structures of TGs are usually deduced from their mass spectra. Various methods are

Published in the topical collection *Lipidomics* with guest editor Michal Holčapek.

Electronic supplementary material The online version of this article (doi:10.1007/s00216-015-8537-1) contains supplementary material, which is available to authorized users.

E. Háková · R. Míková · K. Schwarzová-Pecková · Z. Bosáková
Department of Analytical Chemistry, Faculty of Science, Charles University in Prague, Hlavova 2030/8, 128 43 Prague 2, Czech Republic

E. Háková · V. Vrkoslav · R. Míková · J. Cvačka (✉)
Institute of Organic Chemistry and Biochemistry v.v.i, Academy of Sciences of the Czech Republic, Flemingovo nám. 2, 166 10 Prague 6, Czech Republic
e-mail: Cvacka@uochb.cas.cz

Published online: 21 February 2015

used for ionizing TGs, including electrospray ionization (ESI) [5, 12–14], atmospheric pressure chemical ionization (APCI) [2–4, 6, 7, 15], atmospheric pressure photoionization (APPI) [16], matrix-assisted laser desorption/ionization (MALDI) [17–19], desorption electrospray ionization (DESI) or desorption atmospheric pressure photoionization (DAPPI) [20], fast atom bombardment (FAB) [21], electron ionization (EI) [22], chemical ionization (CI), and field desorption (FD) [23]. Ionization methods permitting on-line coupling with liquid chromatography are more convenient and often indispensable for complex TG mixtures. The first-stage mass spectra usually provide information on molecular weight, i.e.. the total number of carbons and double bonds in TG molecules. Depending on the ionization used, the spectra may already contain fragments useful for the structure elucidation, for instance ions formed by a neutral loss of fatty acids. In other cases, collision-induced dissociation (CID) of the molecular adducts or ions is used for the structure elucidation.

To date, several mass spectrometry-based strategies have been demonstrated for the localization of double bonds in TGs [12, 18, 21, 24–30]. In principle, a double bond can be localized either by direct fragmentation of unsaturated chains utilizing charge-remote fragmentation (CRF) channels, or by charge- or radical-driven fragmentations of specific products formed by reactions at the site of a double bond. The CRF of TGs can be achieved using high-energy CID on double-focusing or four-sector mass spectrometers and tandem time-of-flight instruments [18, 21]. Molecular adducts with ammonium ions or sodium ions generated by ESI, FAB, or MALDI and activated at several keV provide a series of CRF ions by the elimination of C_nH_{2n+1} and C_nH_{2n+2} from the precursor ions. The double bond in the chain becomes evident from the irregularities of the CRF-ion intensities. The CRF can also be achieved using low-energy CID in triple quads and ion traps utilizing lithium adducts of TGs [12, 27]. In the fundamentally different approaches, TGs are chemically derivatized on the double bond to create products that provide fragments indicating the original position of the double bond. Such reactions are preferably performed in the gas phase. A reaction with ozone introduced into an electrospray ion source (OzESI-MS) has been used for an on-line analysis of unsaturated TGs [24]. Ozone-induced fragments bearing an aldehyde and an α-methoxyhydroperoxide group enabled the localization of a double bond. The method was later modified and the reaction was carried out in an ion-trap analyzer with mass-selected precursors (OzID) [26], which was also effective for the identification of double-bond positions in polyunsaturated TGs [28]. Radical-driven fragmentations promote intrachain cleavages, which can also be used for localizing double bonds in TGs. This approach has recently been demonstrated using bifunctional reagents containing a lipid-adducting group and a photocaged radical initiator such as 4-iodoaniline [30]. The reagent is noncovalently attached to a TG molecule; the adduct is isolated in an ion trap and irradiated by a UV laser. The nascent radical unmasked by photodissociation presumably adds to the double bond of TG. Subsequent CID of the product gives rise to radical-directed dissociation of the unsaturated acyl chains.

The double bonds in lipids can also be localized using gas-phase chemistry of acetonitrile. These approaches are potentially advantageous and convenient for TGs, because acetonitrile is commonly used in mobile phases for HPLC separations and the reactions can be performed directly in the APCI sources. Common mass spectrometers without any modification can be used for this purpose. The acetonitrile gas-phase reactions were initially utilized for the localization of double bonds in CI mass spectrometry [31–43]. The lipids reacted with (1-methylenimino)-1-ethenylium ($C_3H_4N^+$) generated by an ion-molecule reaction between $C_2H_2N^+$ and neutral acetonitrile [32, 44]. The $[M + C_3H_4N]^+$ covalent adduct formed by a [2+2]cycloaddition reaction provided fragments indicative for the position of a double bond [35]. The method was mostly applied for fatty acid methyl esters (FAMEs), including methylene-interrupted and non-methylene-interrupted polyunsaturated FAMEs [35–43]. This approach has also been adapted for APCI and applied for monoene- and diene-containing TGs [25]. Similarly to CI, the $C_3H_4N^+$ ions reacted with unsaturated TGs, yielding $[M + 54]^+$ covalent adducts. The CID of $[M + 54]^+$ in a triple-quadrupole linear ion trap provided ions corresponding to cleavage either vinylic or allylic to the site of the double bond. Other acetonitrile-related adducts, namely $[M + 40]^+$, $[M + 81]^+$, and $[M + 95]^+$, were formed as well, and these ions were also useful for the localization of double bonds. We have previously demonstrated the use of APCI and acetonitrile gas-phase chemistry for the localization of double bonds in various unsaturated neutral lipids [29, 45, 46]. For the investigated lipids, we have observed the formation of radical cations $[M + 55]^{+\bullet}$ ($[M + C_3H_5N]^{+\bullet}$) rather than $[M + 54]^+$ ($[M + C_3H_4N]^+$), described for TGs [25]. When fragmented by CID, the $[M + 55]^{+\bullet}$ provided useful diagnostic fragments for the localization of double bonds [29, 45, 46]. Moreover, the ion-source conditions were fully compatible with the high flow rates of solvents typically used for HPLC/APCI-MS.

Here, we discuss the advantages and limitations of the localization of double bonds in TGs using ion-trap CID and pulsed Q collision-induced dissociation (PQD) of $[M + 55]^{+\bullet}$ formed in the presence of acetonitrile. The CID and PQD fragmentation spectra were measured for a large series of TG standards differing by the number, position, and geometry of double bonds to investigate the usefulness of this approach. The spectra obtained in this way were compiled into an annotated library with 125 entries. The existing methods for the analysis of TGs based on HPLC/APCI-MS have been modified by adding a fragmentation step to obtain additional information on the double-bond position. The practicability of

these methods was demonstrated for olive oil and unsaturated TGs from vernix caseosa.

Material and methods

Chemicals and reagents

MS grade acetonitrile and propan-2-ol (Sigma Aldrich, St. Louis, MO, USA) were used as received. The other solvents (chloroform, hexane, diethyl ether; all from Penta, Czech Republic) were distilled in glass from analytical-grade solvents. Sodium methoxide and Rhodamine 6G were from Sigma Aldrich; 4′,5′-dichlorofluorescein was purchased from Fluka (Buchs, Switzerland). The TG standards (purity: 99 %) were obtained from Nu-Chek-Prep (Elysian, MN, USA) and their standard solutions were prepared in chloroform (20 μg/mL).

Synthesis of TGs by randomization

The randomization (interesterification) procedure [7] was downscaled as follows: two standards of TGs (5 mg of each) and sodium methoxide (5 mg) were weighed into a dry glass ampoule. Hexane (200 μL) dried over molecular sieves (4 Å, pellets 3.2 mm, Sigma Aldrich, USA) was added, the ampoule was sealed and heated in a water bath at 80 °C for 30 min. Randomized TGs were isolated by semi-preparative thin-layer chromatography (TLC) on glass plates (36 mm×76 mm) coated with 0.2 mm of Adsorbosil-Plus (Applied Science Labs; with gypsum (12 %)) using hexane/diethyl ether (80:20, *v*/*v*) mobile phase. TLC zones were made visible by spraying Rhodamine 6G solution (0.05 % in ethanol). A zone corresponding to TGs (R_f=0.45–0.55) was scraped off the plate and extracted with freshly distilled diethyl ether. The solvent was evaporated to dryness under nitrogen stream. The randomized TGs were reconstituted in chloroform (300–500 μg/mL).

Samples of natural TGs

Olive oil (extra virgin, Frantoio Larocca, Italy) was dissolved in acetonitrile/propan-2-ol/hexane (1:1:1, *v*/*v*/*v*) at a concentration of 10 mg/mL and used without any further purification. Vernix caseosa was obtained from a healthy female subject delivered at full term. The sample was collected with a written informed parental consent and the work was approved by the Ethics Committee of the General University Hospital, Prague (910/09S-IV). Vernix caseosa (1 g) was suspended in 50 mL of chloroform:methanol (2:1, *v*/*v*) with 0.05 % of 2,6-di-*tert*-butyl-4-methylphenol. The suspension was filtered, treated with anhydrous $MgSO_4$ to eliminate water, and filtered again. The solvents were removed by a rotary evaporator and the total lipid extract (20 mg) was separated on 90 mm× 120 mm glass TLC plates coated with a 0.2 mm layer of silica gel 60 G (Merck, Darmstadt, Germany) using hexane:diethyl ether (93:7, *v*/*v*) as a mobile phase. The plate was developed twice to focus the zones (in the first step to 3/4 of the plate height and then, after air-drying, to the top). The zone corresponding to TGs (R_f=0.19–0.27; identical with R_f of triolein) was scraped off into a column with purified cotton-wool. Lipids were eluted with diethyl ether and the solvent was evaporated under a stream of argon. Vernix caseosa TGs were further separated using argentation TLC to obtain a fraction of unsaturated TGs. Argentation TLC was performed on glass plates (36 mm×76 mm) coated with a 0.2 mm layer of silica gel with 10 % of silver nitrate (Sigma) and 12 % of gypsum. The mobile phase consisted of chloroform:methanol (99:1, *v*/*v*). The zone of unsaturated TGs (R_f=0.35–0.83) visualized under UV light after the plates were sprayed with 4′,5′-dichlorofluorescein (0.1 % in methanol) was scraped off the plates and extracted with chloroform. The solvent was evaporated and TGs were reconstituted in chloroform at a concentration of 3.0 mg/mL.

APCI-MS and HPLC/APCI-MS

The experiments were performed using a system consisting of a Rheos Allegro UHPLC pump, an Accela autosampler with an integrated column oven and a LCQ Fleet ion-trap mass spectrometer equipped with an APCI source; the system was controlled by Xcalibur software (all provided by Thermo Fisher Scientific, San Jose, CA, USA). For direct infusion experiments, TGs dissolved in chloroform (20 μg/mL for commercial standards; 300–500 μg/mL for randomized TGs) were delivered by a syringe pump (a flow rate of 20 μL/min) to a low-dead-volume T-piece, where they were mixed with the mobile phase (acetonitrile, 0.5 mL/min). The APCI vaporizer and heated capillary temperatures were set to 250 and 180 °C, respectively. Nitrogen served both as the sheath and auxiliary gas at a flow rate of 60 and 45 arbitrary units, respectively. The MS spectra of the positively charged ions were recorded from 250 to 1050 *m*/*z*. The precursors were selected with an isolation width of 0.4–2.4 Da and fragmented using CID or PQD; the mass spectra were averaged from 2–10-min records. The TG mixtures were separated using Nova-Pak C18 columns (300+150 mm×3.9 mm, particle size: 4 μm; Waters, Milford, MA, USA) with a C18 pre-column (4 mm×2 mm, Phenomenex, USA) at 30 °C. The gradient program for olive oil: 0 min: 100 % acetonitrile; 106 min: 31 % acetonitrile/69 % propan-2-ol; 109 min: 100 % acetonitrile [47]; the mobile-phase flow rate was 0.8 mL/min and the injected volume of the sample was 10 μL. The gradient program for vernix caseosa TGs: 0 min: 100 % acetonitrile, 0.8 mL/min; 99 min: 34 % acetonitrile/66 % propan-2-ol, 0.8 mL/min; 114.5 min: 24 % acetonitrile/76 % propan-2-ol, 0.55 mL/min; 142 min: 5 % acetonitrile/95 % propan-2-ol, 0.3 mL/

min; 165 min: 5 % acetonitrile/95 % propan-2-ol, 0.3 mL/min; the injected volume of the sample was 25 μL. The flow rate of the mobile phase had to be lowered in the course of the analysis to avoid excessive column back pressure at high concentrations of propan-2-ol. The CID MS^2 spectra of $[M + 55]^{+\bullet}$ were collected using data-dependent analysis with an isolation width of 2 Da and a normalized collision energy of 33–34 %. The masses of the acetonitrile adducts for fragmentation were calculated as higher partners of the base peaks (*m/z* of $[M + H]^+ + 54$ Da).

The nomenclature and notation of fragment ions

The TGs in this work are abbreviated as "TG" followed by three fatty acyls expressed as the number of carbon atoms:the number of double bonds. The fatty acyls are separated either by an underscore character (when their positions are not known or when they are distributed randomly) or by a slash (when the positions are proven) [48]. The positions of the double bonds are given in the *n*–*x* nomenclature. Unless stated otherwise, *cis* double-bond geometry and methylene-interrupted double bonds in polyunsaturated chains are assumed. Thus, for instance, "TG 18:1(*n*−9)/16:0/16:0" indicates 1-oleoyl-2,3-dipalmitoyl-glycerol or 1-olein-2,3-dipalmitin. The fragments of $[M + 55]^{+\bullet}$ originated by the cleavages of the C–C bonds next to the double bond are labeled as "α" if they contain ester moieties, or "ω" if they carry the terminal-carbon end and do not include an ester group. If needed, "α" and "ω" fragments have been specified with a subscript indicating a double bond within a chain and/or by a superscript indicating the chain within a TG. For instance, $\alpha_{n-6}^{18:2}$ refers to an α fragment corresponding to an *n*−6 double bond on an 18:2 acyl in a TG. The ECN stands for the equivalent carbon number (ECN=CN-2DB, where CN and DB are the total numbers of the carbon atoms and double bonds, respectively).

Results and discussion

The preparation of TGs with randomized acyls

The offer of commercially available TG standards is limited mostly to monoacid TGs having the same acyls in all three glycerol positions. In order to study the mass spectra of structurally diverse TGs occurring in nature, we prepared a set of standards using chemical interesterification, also called randomization [49]. This process causes fatty-acid redistribution within and among TG molecules according to the laws of probability. The randomization reactions were performed with two monoacid TGs (AAA, BBB) having up to six double bonds in acyls. This made it possible to obtain mixtures of TGs combining two fatty acyls. Besides the reactants (AAA, BBB), two new signals appeared in the APCI spectra of the randomized samples: the first one for regioisomers with one "A" chain and two "B" chains (ABB, BBA, BAB) and the second representing regioisomers with two "A" chains and one "B" chain (BAA, AAB, ABA). The randomized TGs were used for MS^2 experiments directly, without their chromatographic separation. In compliance with the nomenclature used in this work, the randomized standards were abbreviated with underscore separators (i.e., TG A_B_B or TG B_A_A).

The formation of $[M + 55]^{+\bullet}$ ions

As already discussed in our previous work [29], direct infusion of unsaturated TGs into the APCI source in the presence of acetonitrile promoted the formation of acetonitrile-related adducts. For instance, 1,2-palmitin-3-olein (TG 16:0/16:0/18:1(*n*−9)) provided a spectrum shown in Fig. 1a. The acetonitrile-related adducts were observed at *m/z* 871.6 ($[M + 39]^+$), *m/z* 874.0 ($[M + 41]^{+\bullet}$; likely with a contribution of $[M + 42]^+$, as the mass was slightly shifted), *m/z* 887.4 ($[M + 55]^{+\bullet}$), *m/z* 913.5 ($[M + 81]^+$) and *m/z* 927.4 ($[M + 95]^+$). The relative intensity of the acetonitrile-related adducts varied depending on the TG structure as well as the settings of the ion source. For instance, the $[M + 41]^{+\bullet}$ ion (not useful for the localization of double bonds in TGs) was highly abundant in the spectra of TGs with monounsaturated chains and low for polyunsaturated TGs. Lowering the acetonitrile flow rate significantly decreased the formation of this ion. Concerning the $[M + 55]^{+\bullet}$, monounsaturated TGs provided somewhat more abundant signals than the polyunsaturated species and the ion intensity was not significantly dependent on the acetonitrile flow rate. The intensities of $[M + 55]^{+\bullet}$ were rather low, typically 1–5 % with regard to $[M + H]^+$. Our attempts to increase the signal intensity by changing the ion-source parameters were successful only partially; higher $[M + 55]^{+\bullet}$ signals were achieved at lower vaporizer temperature with the optimum around 250 °C. Despite the relatively low abundance of $[M + 55]^{+\bullet}$, the quality of the MS/MS spectra was generally good.

The other peaks in the spectrum shown in Fig. 1a corresponded to a protonated molecule (*m/z* 833.4) and diacylglycerol fragments originated after the loss of oleic acid (*m/z* 551.4) and palmitic acid (*m/z* 577.4).

MS^2 of $[M + 55]^{+\bullet}$: TGs with monounsaturated chains

The MS^2 spectra of the $[M + 55]^{+\bullet}$ ions were investigated for a large series of TGs obtained from commercial sources or prepared by randomization reactions. The resonance excitation CID mass spectrum of 1,2-palmitin-3-olein is shown in Fig. 1b. The spectrum basepeak at *m/z* 774.4 was an α fragment formed by the cleavage of the C–C bond vinylic to the original double bond. A neutral loss of palmitic acid from the precursor yielded *m/z* 631.5 ($[M + 55\text{-}FA_{16:0}]^{+\bullet}$). Note that a

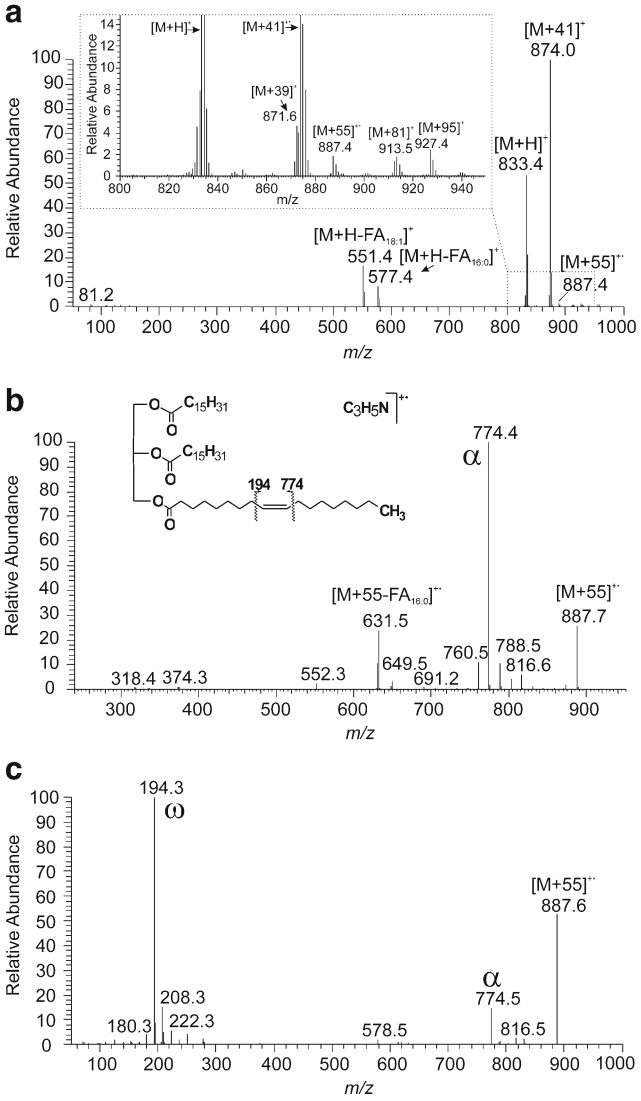

Fig. 1 The full-scan APCI mass spectrum (**a**), the APCI CID MS^2 spectrum of the $[M + 55]^{+\bullet}$ adduct (**b**) and the APCI PQD MS^2 spectrum of the $[M + 55]^{+\bullet}$ adduct (**c**) of TG 16:0/16:0/18:1(*n*−9) (1,2-palmitin-3-olein). The standard solution (20 μg/mL in chloroform) delivered by a syringe pump (20 μL/min) was mixed in a T-piece with acetonitrile (0.5 mL/min) and infused into the ion source (the spectra averaged from 0.5-, 2.0-, and 4.0-min records, respectively)

neutral loss of oleic acid was not observed, obviously because oleyl was covalently modified with $C_3H_5N^{+\bullet}$. The diagnostic fragment formed by a cleavage of the C–C bond on the opposite side of the original double bond (ω fragment) was not detected because of the low-mass cut-off of the ion trap. This problem can be circumvented with PQD, which activates ions at high Q values and collects fragments at low *Q* values, resulting in spectra similar to CID containing also low *m/z* fragments. PQD also helps to access higher-energy dissociation channels. The main drawback of PQD is less effective ion fragmentation relative to CID, which results in spectra of lower overall intensities. A PQD spectrum of 1,2-palmitin-3-olein is shown in Fig. 1c; both diagnostic fragments were detected (α at *m/z* 774.5 and ω at *m/z* 194.3). The spectra also showed smaller peaks accompanying the α and ω fragments (14 Da difference; $\pm(CH_2)_n$) created by less probable cleavages of the more distant C–C bonds with regard to the double bond. Although PQD provided both diagnostic fragments and the CID only one, both types of activation afforded spectra allowing for an unambiguous assignment of the double bond to the *n*−9 position on the 18:1 chain. A regioisomer 1,3-dipalmitin-2-olein (TG 16:0/18:1(*n*−9)/16:0) provided very similar spectra, with slightly modified ion abundances (Spectrum S7). The spectra of other TGs with one monounsaturated acyl (see more examples in the Electronic Supplementary Material (ESM)) provided analogous spectra, facilitating straightforward localization of the double bond.

The MS^2 spectra of TGs with two or three identical monounsaturated chains were found to be analogous to the previously discussed ones. The covalent attachment of $C_3H_5N^{+\bullet}$ occurred randomly on one of the unsaturated chains and the remaining chains stayed unmodified. For instance, CID of 1,3-olein-2-palmitin (TG 18:1(*n*−9)/16:0/18:1(*n*−9)), see Fig. 2a, provided mainly an α ion at *m/z* 800.5 and fragments consistent with the neutral loss of palmitic acid (*m/z* 657.2; $[M + 55\text{-}FA_{16:0}]^{+\bullet}$) and oleic acid (*m/z* 631.5; $[M + 55\text{-}FA_{18:1}]^{+\bullet}$). The CID of triolein (TG 18:1(*n*−9)/18:1(*n*−9)/18:1(*n*−9)) provided an α fragment at *m/z* 826.5 and $[M + 55\text{-}FA18:1]^{+\bullet}$ at *m/z* 657.6 (Fig. 2b). The PQD MS^2 spectrum of triolein (Fig. 2c) showed also an ω fragment at *m/z* 194.3 and relatively high abundant ions at *m/z* 318.4 and *m/z* 332.5. These fragments, which are not straightforward to rationalize, were also present as small peaks in the CID spectrum (Fig. 2b). We speculate that these fragments did not originate from a precursor with just one double bond modified with $C_3H_5N^{+\bullet}$ but rather from a cross-linked precursor, where $C_3H_5N^{+\bullet}$ bridges two double bonds on neighboring chains. The fragments might be rationalized by C–C bond cleavages at the positions which are vinylic to the site of the former double bonds on both chains (*m/z* 332.5) and cleavages yielding a product that is one methylene group shorter (*m/z* 318.4). Hence, the masses of these even electron products containing a nitrogen atom but no oxygen must depend on the positions of double bonds. This was indeed observed in the spectra of other monoacid TGs containing C18:1 acyls with different double-bond positions. The above-mentioned fragments were shifted by 56 Da (4 methylene units) towards lower *m/z* values in trivaccenin (TG 18:1(*n*−7)/18:1(*n*−7)/18:1(*n*−7)), see Spectrum S32, and by 84 Da (6 methylene units) towards higher *m/z* values in tripetroselinin (TG 18:1(*n*−12)/18:1(*n*−12)/18:1(*n*−12)), see Spectrum S28. No shifts of the fragment masses were observed in the spectrum of trielaidin (TG 18:1(*n*−9 t)/18:1(*n*−9 t)/18:1(*n*−9 t)), see Spectrum S31, which has double bonds at the same positions as triolein, but their geometry is *trans*. Unfortunately, we were not able to record MS^3 spectra

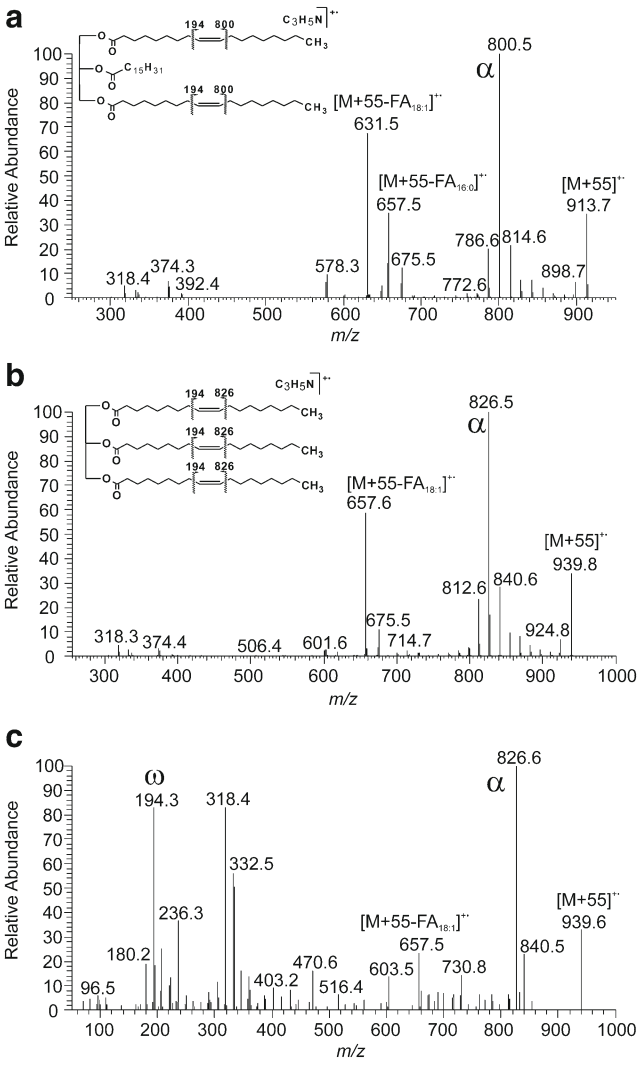

Fig. 2 The APCI CID MS^2 spectrum of the $[M + 55]^{+\bullet}$ adduct of TG 18:1(*n*−9)/16:0/18:1(*n*−9) (1,3-olein-2-palmitin) (**a**) and 18:1(*n*−9)/18:1(*n*−9)/18:1(*n*−9) (triolein) (**b**). The APCI PQD MS^2 spectrum of the $[M + 55]^{+\bullet}$ adduct of TG 18:1(*n*−9)/18:1(*n*−9)/18:1(*n*−9) (triolein) (**c**). The standard solution (20 μg/mL in chloroform) delivered by a syringe pump (20 μL/min) was mixed in a T-piece with acetonitrile (0.5 mL/min) and infused into the ion source (the spectra averaged from a 2-min record)

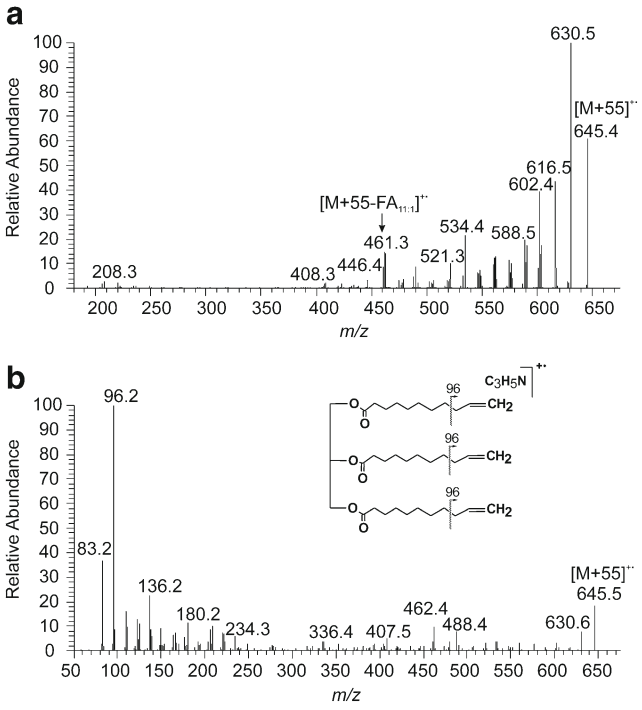

Fig. 3 The APCI CID (**a**) and PQD (**b**) MS^2 spectra of the $[M + 55]^{+\bullet}$ adduct of TG 11:1(*n*−1)/11:1(*n*−1)/11:1(*n*−1) (triundecenoin). The standard solution (20 μg/mL in chloroform) delivered by a syringe pump (20 μL/min) was mixed in a T-piece with acetonitrile (0.5 mL/min) and infused into the ion source (the spectra averaged from 3- and 5-min records, respectively)

and reliably measure the exact masses to confirm our hypothesis further.

The fragmentation spectra were noticeably different for TGs with the double bond located at the chain terminus (*n*−1 position). In the CID spectrum of triundecenoin (TG 11:1(*n*−1)/11:1(*n*−1)/11:1(*n*−1)) (Fig. 3a), the most abundant fragment at *m/z* 630.5 corresponded to the loss of methyl radical. The PQD spectrum (Fig. 3b) showed *m/z* 96.2 as a basepeak, indicating C–C bond cleavage at a position that is allylic to the site of the former double bond. Analogous diagnostic fragments ($[M + 55\text{-}CH_3]^+$ and *m/z* 96) were also found in the randomized TGs with one or two 10*Z*-undecenoyls (Spectra S1, S11, S107, and S111).

As regards the double-bond geometry, no significant differences between fragmentation spectra were observed. The ion abundances were similar for the *cis* and *trans* isomers, see Spectra S2/S3 and S4/S5.

In all TGs with one or more identical monounsaturated chains, the diagnostic fragments reliably and unambiguously indicated the position of double bond(s). However, TGs can consist of two or three monounsaturated chains with different positions of the double bond. For such TGs, the MS^2 spectra did not allow the assignment of the double-bond position to a particular chain. In principle, MS^3 spectra can be used in these cases. In dioleinpalmitolein (TG 18:1(*n*−9)_18:1(*n*−9)_16:1(*n*−7)), for instance, two α ions were recorded: α_{n-7} at *m/z* 826.4 and α_{n-9} at *m/z* 798.6 (Fig. 4a). We, of course, know that the palmitoleyl has an *n*−7 double bond and the oleyl an *n*−9 double bond, but one cannot say that from the spectrum. Supposedly, MS^3 of the α ions should show a neutral loss of 18:1 acid (if we fragment an ion derivatized on the 16:1 chain) or a loss of both 16:1 and 18:1 acids (if we fragment an ion derivatized on the 18:1 chain). This is indeed true; the fragmentation of α_{n-9} gives $[\alpha_{n-9}\text{-}FA_{18:1}]^+$ (*m/z* 516.5) and $[\alpha_{n-9}\text{-}FA_{16:1}]^+$ (*m/z* 544.5) (Fig. 4b), whereas the fragmentation of α_{n-7} gives mostly $[\alpha_{n-7}\text{-}FA_{18:1}]^+$ (*m/z* 544.5) (Fig. 4c). Therefore, an *n*−7 double bond must be in a 16:1 chain, whereas an *n*−9 double bond in an 18:1 chain. However, this approach was found to be somewhat limited by low specificity. In the MS^3 spectrum of α_{n-7}, we also detected a small but

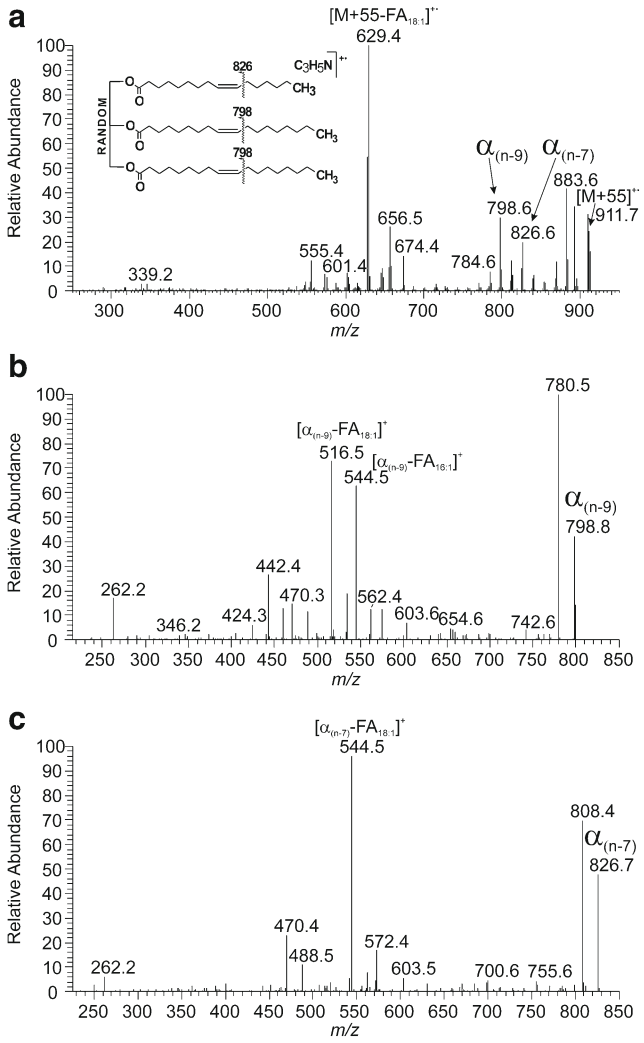

Fig. 4 The APCI CID MS^2 spectrum of the $[M + 55]^{+\bullet}$ adduct of TG 18:1(*n*−9)_18:1(*n*−9)_16:1(*n*−7) (**a**),the MS^3 spectrum of α ions corresponding to the *n*−9 double bond (911.9 → 798.6) (**b**) and the MS^3 spectrum of α ions corresponding to the *n*−7 double bond (911.9 → 826.5) (**c**). The standard solution (20 μg/mL in chloroform) delivered by a syringe pump (20 μL/min) was mixed in a T-piece with acetonitrile (0.5 mL/min) and infused into the ion source (the spectra averaged from a 2-min record)

significant peak $[\alpha_{n-7}\text{-}FA_{16:1}]^+$ (*m*/*z* 572.4), which in theory should not be formed. The presence of this peak can be explained by (i) the co-isolation of an α-like ion derivatized on the 18:1 chain but cleaved in a propenylic C–C bond or (ii) the scrambling or migration of the $C_3H_5N^{+\bullet}$ modification. The MS^3 spectra of $[M + 55\text{-}FA]^{+\bullet}$ also provided fragments indicating the double-bond positions (analogous to α fragments; the loss of hydrocarbon radical), but at unusably low intensities.

MS^2 of $[M + 55]^{+\bullet}$: TGs with di- and polyunsaturated chains

With the increasing number of double bonds in acyls, the fragmentation spectra of $[M + 55]^{+\bullet}$ become more complex. The covalent adduct formation took place on each double bond of the chains, which increased the structural variability of the $[M + 55]^{+\bullet}$ precursors. Upon fragmentation, each double bond-site provided specific fragments (cleavages vinylic (or allylic) to the site of the double bond), together with unspecific fragments (cleavages on more distant C–C bonds from the site of the double bond). Consequently, the diagnostic ions became less pronounced and somewhat hidden among other fragments. We have noticed that the efficiency of adduct formation (or cleavage) depends on the double-bond position. Thus, for instance, the spectrum of distearin-linolein (TG 18:0_18:0_18:2(*n*−6)) showed a significantly more abundant α-ion corresponding to the *n*−6 double bond (α_{n-6} at *m*/*z* 866.5) when compared to the α-ion corresponding to the *n*−9 double bond (α_{n-9} at *m*/*z* 826.6) (Fig. 5a). It can be explained by the easier accessibility of the double bonds closer to the chain termini and/or by electronic effects. The same trend was also observed for other TGs with polyunsaturated chains, see for instance distearin-α-linolenin (TG 18:0_18:0_18:3(*n*−3)), Spectrum S21. For all three identical polyunsaturated acyl chains, the diagnostic fragments were easier to distinguish among other ions, like in the case of trilinolein (TG 18:2(*n*−6)/18:2(*n*−6)/18:2(*n*−6)), see Fig. 5b. Although the intensities of α and ω ions generally decreased with the distance of the double bond from the unsaturated chain terminus, some TGs showed enhanced intensities of α ions corresponding to the second (or third) double bond counting from the chain terminus (see for instance tri-α-linolenin, Spectrum S87). The most polyunsaturated TG investigated in this work was tridocosahexaenoin (TG 22:6(*n*−3)/22:6(*n*−3)/22:6(*n*−3)), Fig. 5c. Even in this compound, the α-ions corresponding to all double bonds were relatively easily recognizable. We can conclude that the localization of double bonds in TGs with one or more identical di- and polyunsaturated chains can be achieved. At least, the double bonds close to chain termini provided signals reliably indicating their positions.

The spectra of TGs with all the acyls unsaturated and/or polyunsaturated in various positions were challenging to interpret. The intensities of diagnostic ions indicating double bonds closer to glycerol in polyunsaturated chains were significantly suppressed. The spectra usually clearly showed only diagnostic ions corresponding to a double bond in the monounsaturated chain(s) and the outermost double bond in polyunsaturated chain(s). For instance, in the CID spectrum of dipetroselinin-linolelaidin (TG 18:1(*n*−12)_18:1(*n*−12)_18:2(*n*−6 t)), Fig. 6a, the double bond on the monounsaturated petroselinyl chain provided easily distinguishable $\alpha_{n-12}{}^{18:1}$ at *m*/*z* 782.6, similarly to the *n*−6 double bond in the diunsaturated linolelaidinyl chain ($\alpha_{n-6}{}^{18:2}$ at *m*/*z* 866.7). The $\alpha_{n-9}{}^{18:2}$ ion reflecting the *n*−9 double bond in the linolelaidinyl chain was detected at *m*/*z* 826.6, but its intensity did not exceed the surrounding ions. The polyunsaturated chains frequently contain double bonds on the same positions counting from the chain termini ("*n*−3" or "*n*−6" fatty chains). In these cases, the diagnostic fragments had the same mass and their intensities were enhanced. For

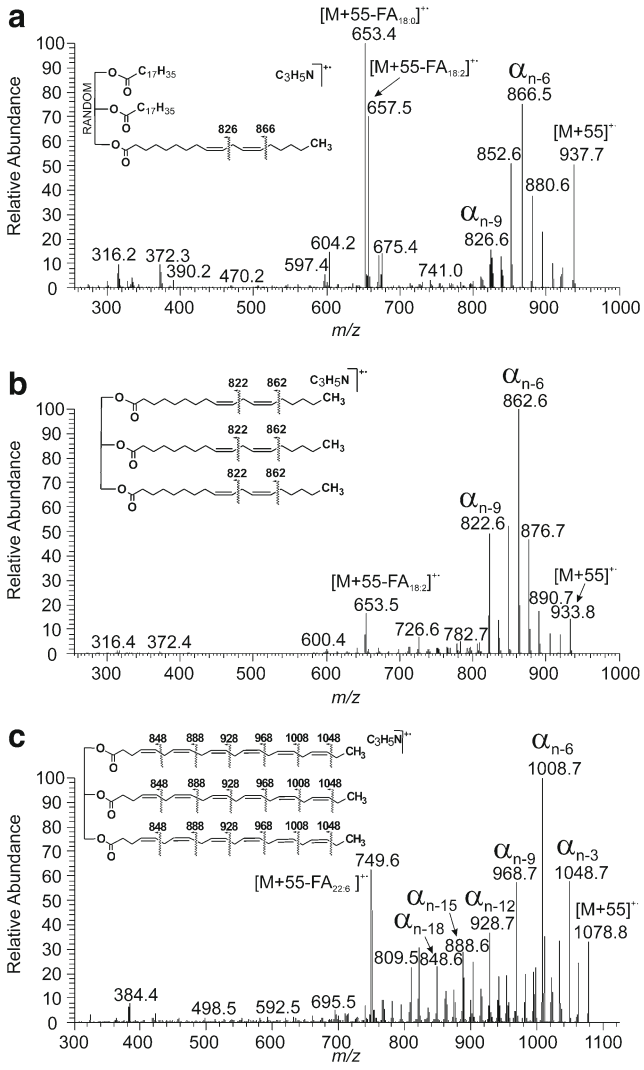

Fig. 5 The APCI CID MS^2 spectra of the $[M + 55]^{+\bullet}$ adduct of distearin-linolein (TG 18:0_18:0_18:2(*n*−6)) (**a**), trilinolein (TG 18:2(*n*−6)/18:2(*n*−6) 18:2(*n*−6)) (**b**) and tridocosahexaenoin (TG 22:6(*n*−3)/22:6(*n*−3)/22:6(*n*−3)) (**c**). The standard solution (20 μg/mL in chloroform) delivered by a syringe pump (20 μL/min) was mixed in a T-piece with acetonitrile (0.5 mL/min) and infused into the ion source (the spectra averaged from 4-, 2-, and 2-min records, respectively)

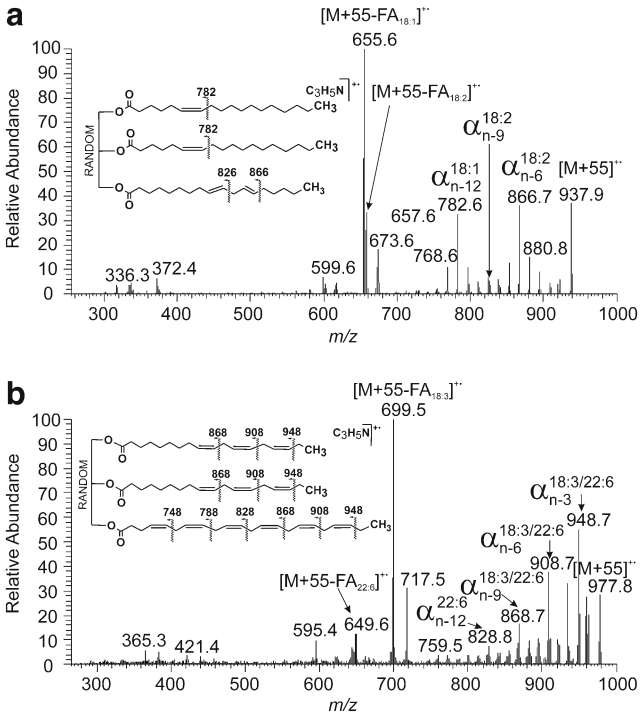

Fig. 6 The APCI CID MS^2 spectra of the $[M + 55]^{+\bullet}$ adduct of dipetroselinin-linolelaidin (TG 18:1(*n*−12)_18:1(*n*−12)_18:2(*n*−6 t)) (**a**) and di-α-linolenin-docosahexaenoin (TG 18:3(*n*−3)_18:3(*n*−3)_22:6(*n*−3)) (**b**). The standard solution (20 μg/mL in chloroform) delivered by a syringe pump (20 μL/min) was mixed in a T-piece with acetonitrile (0.5 mL/min) and infused into the ion source (the spectrum averaged from a 5-min record)

instance, the α fragments in di-α-linolenin-docosahexaenoin (TG 18:3(*n*−3)_18:3(*n*−3)_22:6(*n*−3)) were for all chains at the same *m/z* values ($\alpha_{n-3}^{22:6}$ and $\alpha_{n-3}^{18:3}$ at *m/z* 948.7; $\alpha_{n-6}^{22:6}$ and $\alpha_{n-6}^{18:3}$ at *m/z* 908.7; $\alpha_{n-9}^{22:6}$ and $\alpha_{n-9}^{18:3}$ at *m/z* 868.7), see Fig. 6b. The remaining (inner) double bonds on docosahexaenoyls provided small α fragments almost indistinguishable from the background.

Fragment intensity ratio in regioisomers

The intensities of the diacylglycerol fragments in the APCI mass spectra of TGs ($[M + H\text{-}RCOOH]^+$) are known to indicate acyl positions on the glycerol [50]. The elimination of fatty acids from the *sn*-1 and *sn*-3 positions is more likely and equally favored, whereas the fatty acid in the *sn*-2 position is less probable to cleave (the corresponding fragment is the least intense). Therefore, one can distinguish the acyl in the *sn*-2 position from those attached to the *sn*-1/*sn*-3 positions by comparing the fragment intensities. It is important to note that the fragment intensities are also affected by the chain-length and the degree of unsaturation of the cleaving fatty acid, which can lead to an incorrect assignment of the chain positions in some cases [51, 52]. Our results have indicated that the elimination of fatty acid in *sn*-2 position is less probable also in the case of the CID of $[M + 55]^{+\bullet}$. Hence, the intensities of the $[M + 55\text{-}FA]^{+\bullet}$ fragments could be useful for the acyl-position assignment like the intensities of the $[M + H\text{-}FA]^+$ ions in the APCI full-scan mass spectra. However, the intensities of $[M + 55\text{-}FA]^{+\bullet}$ cannot be used exactly in the same way as the intensities of $[M + H\text{-}FA]^+$, because the acyl with the double bond modification is not cleaved. To test the hypothesis, the MS^2 spectra of $[M + 55]^{+\bullet}$ were repeatedly measured for TG regioisomers and the ratios of the fragments were calculated (Table 1). Figure 7 shows zoomed spectral regions with fragments of 1-arachidin-2-olein-3-palmitin (TG 20:0/18:1(*n*−9)/16:0; AOP) and 1-palmitin-2-arachidin-3-olein (TG 16:0/20:0/18:1(*n*−9); PAO) regioisomers. The oleyl chain

Table 1 The ratio of the $[M + 55\text{-}FA]^{+\bullet}$-fragment intensities in the CID MS^2 spectra of isomeric TGs

TG	Fragment no. 1	Fragment no. 2	Fragment intensity ratio Frg. 1/Frg. 2[a]
TG 18:1(*n*−9)/16:0/18:1(*n*−9)	$[M + 55\text{-}FA_{18:1}]^{+\bullet}$	$[M + 55\text{-}FA_{16:0}]^{+\bullet}$	1.7±0.1
TG 18:1(*n*−9)/18:1(*n*−9)/16:0			0.4±0.0
TG 20:0/18:1(*n*−9)/16:0	$[M + 55\text{-}FA_{20:0}]^{+\bullet}$	$[M + 55\text{-}FA_{16:0}]^{+\bullet}$	0.8±0.0
TG 16:0/20:0/18:1(*n*−9)			0.3±0.0
TG 18:1(*n*−9)/18:2(*n*−6)/18:1(*n*−9)	$[M + 55\text{-}FA_{18:2}]^{+\bullet}$	$[M + 55\text{-}FA_{18:1}]^{+\bullet}$	0.2±0.0
TG 18:1(*n*−9)/18:1(*n*−9)/18:2(*n*−6)			0.4±0.0

[a] The values have been averaged from five measurements (2-min records)

was modified with $C_3H_5N^{+\bullet}$. Therefore, only the two saturated acyls were cleaved off as neutral fatty acids (or ketenes as minor peaks). In the case of the regioisomer with both saturated chains in the outer positions (AOP), the intensity of $[M + 55\text{-}FA_{20:0}]^{+\bullet}$ and $[M + 55\text{-}FA_{16:0}]^{+\bullet}$ was roughly the same (Fig. 7a), whereas the isomer with arachidyl in the middle (PAO) eliminated arachidic acid less efficiently (Fig. 7b). In the full-scan APCI spectra of these regioisomers, the fragment intensities reflected the acyl positions as expected; the fragments corresponding to the acyl in the *sn*-2 position provided peaks of the lowest intensities (Fig. 7c, d). Interestingly, the peak intensity ratio $[M + 55\text{-}FA_{20:0}]^{+\bullet}/[M + 55\text{-}FA_{16:0}]^{+\bullet}$ (Table 1) was exactly the same as the $[M + H\text{-}FA_{20:0}]^{+}/[M + H\text{-}FA_{16:0}]^{+}$ ratio calculated from the full-scan APCI spectrum (the intensity ratio $[M + H\text{-}FA_{20:0}]^{+}/[M + H\text{-}FA_{16:0}]^{+}$ was 0.8 for AOP and 0.3 for PAO). In a regioisomeric pair 1,3-diolein-2-palmitin (TG 18:1(*n*−9)/16:0/18:1(*n*−9); OPO) and 1,2-diolein-3-palmitin (TG 18:1(*n*−9)/18:1(*n*−9)/16:0; OOP), Spectra S17 and S18, one of two oleyls was modified with $C_3H_5N^{+\bullet}$, likely with similar probability. Again, the neutral loss from the *sn*-2 position was less efficient as the ratio $[M + 55\text{-}FA_{18:1}]^{+\bullet}/[M + 55\text{-}FA_{16:0}]^{+\bullet}$ was significantly higher for OPO with both oleyls in the outer positions on glycerol (Table 1). Not surprisingly, the corresponding fragment intensity ratio was also significantly higher for OPO in the full-scan APCI spectra (the intensity ratio $[M+H\text{-}FA_{18:1}]^{+}/[M+H\text{-}FA_{16:0}]^{+}$ was 7.7 for OPO and 1.7 for OOP). The position of acyls on the glycerol backbone was also possible to follow in

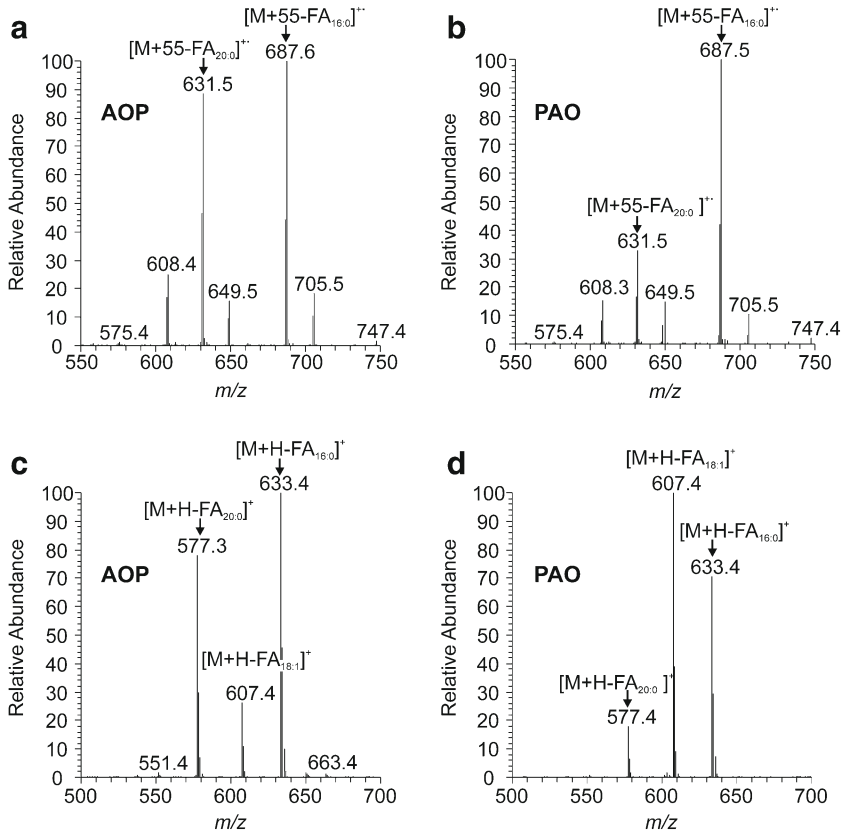

Fig. 7 The zoomed regions of the APCI CID MS^2 spectra of the $[M + 55]^{+\bullet}$ adduct of 1-arachidin-2-olein-3-palmitin (TG 20:0/18:1(*n*−9)/16:0) (**a**) and 1-palmitin-2-arachidin-3-olein (TG 16:0/20:0/18:1(*n*−9)) (**b**). The zoomed regions of the APCI full-scan spectra of 1-arachidin-2-olein-3-palmitin (TG 20:0/18:1(*n*−9)/16:0) (**c**) and 1-palmitin-2-arachidin-3-olein (TG 16:0/20:0/18:1(*n*−9)) (**d**). The standard solution (20 μg/mL in chloroform) delivered by a syringe pump (20 μL/min) was mixed in a T-piece with acetonitrile (0.5 mL/min) and infused into the ion source (the spectrum averaged from a 2-min record)

the CID spectra of polyunsaturated TGs like in 1,2-olein-3-linolein (TG 18:1(*n*−9)/18:1(*n*−9)/18:2(*n*−6); OOL) and 1,3-olein-2-linolein (TG 18:1(*n*−9)/18:2(*n*−6)/18:1(*n*−9); OLO) (Spectra S42 and S43). However, as the probability of the $C_3H_5N^{+\bullet}$ adduct formation might be different for individual double bonds in various (poly)unsaturated chains, the fragment-ion ratios should be interpreted with caution. In this particular example, the neutral loss of linoleic acid was more efficient in the case of OOL (Table 1), which is again in agreement with the less efficient neutral loss from the *sn*-2 position.

Applications

The applicability of HPLC/APCI-MS^2 with $[M + 55]^{+\bullet}$ fragmentation in the ion trap for the comprehensive structural characterization of TGs in mixtures was assessed using olive oil and unsaturated TGs isolated from vernix caseosa. The TG molecular species were resolved using a proven method based on Nova-Pak C18 columns and an acetonitrile/propan-2-ol gradient [47, 19, 53]. There was no need to modify the separation conditions as acetonitrile in the mobile phase afforded the formation of the $[M + 55]^{+\bullet}$ adducts. The full-scan spectra provided molecular adducts and fragments useful for deducing the total number of carbons and double bonds in TG acyls [54]. The same information was possible to extract also from the CID spectra of $[M + 55]^{+\bullet}$. The masses of the precursors determined the total number of carbons and double bonds. The fatty-acid neutral loss ions ($[M + 55\text{-FA}]^{+\bullet}$) were used for the determination of the number of carbon atoms and double bonds in acyls and the relative proportions of these ions reflected the positions of acyl on the glycerol backbone, like in case of $[M + H\text{-FA}]^+$ in the full-scan spectra. Moreover, the CID MS/MS spectra provided information on the double-bond positions.

Table 2 shows the results on the olive oil sample obtained by the interpretation of the CID spectra of $[M + 55]^{+\bullet}$ only; the full-scan data were not used. For comparison purposes, the data were also interpreted in a classical way using the full-scan APCI spectra; the results summarized in the ESM (Table S1; Fig. S1) were in excellent agreement with a previously published report [47]. The interpretation of the CID spectra of $[M + 55]^{+\bullet}$ allowed us to gain information on double-bond positions in 20 TGs. Those were the most abundant TGs in the sample (93 % of the sample based on the peak areas); the spectra were interpretable even for TGs with the relative peak areas as low as 0.1 % in some cases. In the interpretation procedure, we focused on α ions labeled relative to the precursor ($[M + 55]^{+\bullet}$) mass. The α ions thus appeared at −29 Da, −43 Da, −57 Da, −71 Da, −85 Da, −99 Da, −113 Da etc., and indicated double bonds in the positions

Table 2 The unsaturated TGs identified in olive oil using CID of $[M + 55]^+$

R_t [min]	$[M + 55]^{+\bullet}$	Fatty acid (neutral loss)	Double-bond position	TG[a]	ECN
65.0	933.5	18:2	*n*−6, *n*−9	18:2(*n*−6,9)/18:2(*n*−6,9)/18:2(*n*−6,9)[b]	42
65.8	933.5		*n*−9, *n*−6, *n*−3	18:1(*n*−9)_18:3(*n*−3,6,9)_18:2(*n*−6,9)[c]	42
71.2	935.8	18:1, 18:2	*n*−9, *n*−6	18:1(*n*−9)_18:2(*n*−6,9)_18:2(*n*−6,9)[b]	44
71.7	909.8	16:1, 18:1, 18:2	*n*−9, *n*−7, *n*−6	16:1(*n*−9)_18:1(*n*−9)_18:2(*n*−6,9)	44
71.9	935.6	18:1, 18:3	*n*−9, *n*−3	18:1(*n*−9)_18:1(*n*−9)_18:3(*n*−3,6,9)	44
72.6	909.5	16:0, 18:2	*n*−9, *n*−6	16:0_18:2(*n*−6, 9)_18:2(*n*−6, 9)[b]	44
73.4	909.6	16:0, 18:1, 18:3	*n*−9, *n*−3	16:0_18:1(*n*−9)_18:3(*n*−3,6,9)	44
77.0	937.7	18:1, 18:2	*n*−9, *n*−6	18:1(*n*−9) _18:1(*n*−9)_18:2(*n*−6,9)	46
77.6	911.6	16:1, 18:1	*n*−9, *n*−7	16:1(*n*−7)_18:1(*n*−9)_18:1(*n*−9)	46
78.5	911.6	16:0, 18:1, 18:2	*n*−9, *n*−7	16:0_18:1(*n*−9)_18:2(*n*−6, 9)	46
80.3	925.8	17:1, 18:1	*n*−9, *n*−8	17:1(*n*−8)_18:1(*n*−9)_18:1(*n*−9)	47
81.8	899.9	17:1	*n*−9, *n*−8	16:0_17:1(*n*−8)_18:1(*n*−9)	47
82.7	939.6	18:1	*n*−9	18:1(*n*−9)/18:1(*n*−9)/18:1(*n*−9)[b]	48
83.9	939.9		*n*−9, *n*−6	18:0_18:1(*n*−9)_18:2(*n*−6, 9)[c]	48
84.3	913.5	16:0, 18:1	*n*−9	16:0_18:1(*n*−9)_18:1(*n*−9)[b]	48
87.9	967.7	18:1, 20:1	*n*−9	18:1(*n*−9)_18:1(*n*−9)_20:1(*n*−9)[b]	50
89.1	967.7	18:1, 20:0	*n*−9	18:1(*n*−9)_18:2(*n*−6,9)_20:0	50
89.7	941.7		*n*−9	18:0_18:1(*n*−9)_18:1(*n*−9)[c]	50
94.6	969.7	18:1, 20:0	*n*−9	18:1(*n*−9)_18:1(*n*−9)_20:0[b]	52

[a] The most likely structures of TGs identified from the spectra

[b] Unambiguously identified

[c] The missing information on acyl composition has been taken from the full-scan spectrum

n−3, *n*−4, *n*−5, *n*−6, *n*−7, *n*−8, *n*−9, respectively. When the neutral radical already carried one double bond (i.e., another double bond existed closer to the chain terminus), the values were 2 mass units shifted. In the case of methylene-interrupted double bonds, the distances between α ions in the spectra were 40 Da. We clearly detected α ions corresponding to double bonds in monounsaturated acyls. In the case of polyunsaturated chains, we frequently observed only α ions indicating the outermost double bonds. If methylene-interrupted acyls were expected, this information was sufficient. However, an unequivocal interpretation of the spectra was not always possible even for a complete set of α ions. It is important to realize that the MS^2 spectra afforded cumulative information on double bonds in all three chains, without direct information on which chain the double bond existed. The double-bond assignment to a particular chain would be possible using MS^3 performed with α ions or $[M + 55\text{-}FA]^{+\bullet}$ ions. Unfortunately, the MS^3-spectra intensities were low, which makes their practical use hard to imagine. Nevertheless, the MS^2 alone might be sufficient for unambiguous double-bond localization in some cases. For instance, the peak in 71.2 min represented TG with one 18:1 and two 18:2 acyls (based on the$[M + 55]^{+\bullet}$ and $[M + 55\text{-}FA]^{+\bullet}$ masses) with the 18:2 chain in the *sn*-2 position (based on the $[M + 55\text{-}FA]^{+\bullet}$ fragment intensity ratio), see Fig. 8a. The α ions appeared at *m/z* 864.7 (−71 Da, *n*−6), *m/z* 822.6 (−113 Da, *n*−9), and *m/z* 824.6 (−111 Da, *n*−9 in an acyl with one additional double bond closer to the chain terminus). In this case, the interpretation was unequivocal: the double bonds *n*−6 and *n*−9 were in the doubly unsaturated acyls and *n*−9 is in the monounsaturated acyl. Therefore, the spectrum represented oleindilinolein with linoleic acid in the *sn*-2 position (*cis* double bonds assumed). The spectral interpretation was also straightforward in the case of TGs with identical unsaturated acyls (e.g., the most abundant peak at the 82.2nd min with all double bonds in *n*−9, identified as trioloein, or the peak at the 84.3rd min with one C16:0 and two *n*−9 C18:1 chains, interpreted as palmitin-diolein). In several minor TGs, we were not able to detect the $[M + 55\text{-}FA]^{+\bullet}$ fragments reliably, but we clearly saw α ions, enabling us to localize the positions of double bonds.

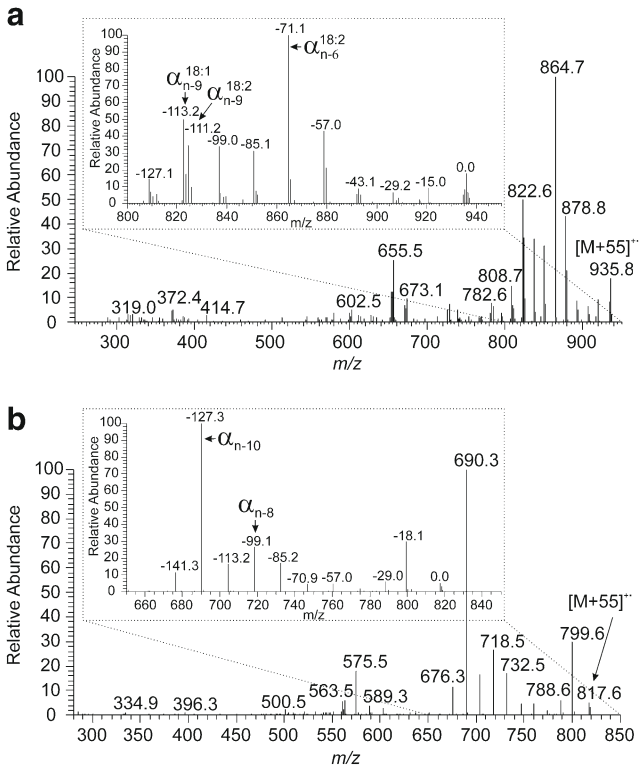

Fig. 8 The APCI CID MS^2 spectra of the TG $[M + 55]^{+\bullet}$ adduct taken across the chromatographic peak (t_R=71.2 min) in the olive oil sample and interpreted as 18:1(*n*−9)_18:2(*n*−6,9)_18:2(*n*−6,9) (**a**) and the chromatographic peak (t_R=70.0 min) in the vernix caseosa sample (**b**). For experimental conditions, see the "Material and methods" section

Vernix caseosa lipids are known as an extremely complex mixture of various lipids with branched and unsaturated chains [55]. TGs of vernix caseosa consist of an exceptionally large number of molecular species, which makes their analysis particularly challenging. A comprehensive analysis of all TGs in vernix caseosa was not attempted in this work and the data were interpreted only partially. The α fragments mostly showed a double bond up to *n*−12, but small peaks in some spectra also indicated double bonds at more distant positions from the chain termini. Figure 8b shows a spectrum for a peak at the 70.0th min (see the basepeak chromatogram in ESM Fig. S2). The spectrum represents a mixture of TGs with two saturated fatty acyls (14:0, 15:0, or 16:0) and one monounsaturated acyl (14:1, 15:1, 16:1, or 17:1) with double bonds mainly in *n*−10 and *n*−8. The results indicated the feasibility of the localization of double bonds in the TGs of vernix caseosa; however, a reliable and comprehensive analysis cannot be achieved without substantial improvement of the separation method. As the concentration of acetonitrile in the mobile phase gradually decreased in the course of the analysis, TGs with high ECN values were ionized at low concentrations of acetonitrile. Consequently, the efficiency of the $[M + 55]^{+\bullet}$ formation was reduced and the MS^2 spectra were of rather poor quality at higher retention times. The concentration of acetonitrile during ionization might be increased by a post-column addition of acetonitrile, but this approach was not tested in this work.

Conclusions

The results in this work have proven that acetonitrile-related $[M + 55]^{+\bullet}$ ions formed in APCI source are useful for the structure elucidation of TGs. The fragmentation spectra of these ions provided information on (i) the total number of carbons and double bonds in the whole molecule (the mass of the $[M + 55]^{+\bullet}$ precursor), (ii) the number of carbons and

double bonds in acyls (masses of the $[M + 55\text{-}FA]^{+\bullet}$ fragments), (iii) the acyl in the *sn*-2 position on the glycerol backbone (the intensity ratios of the $[M + 55\text{-}FA]^{+\bullet}$ fragments), and (iv) the double-bond positions in acyls (the masses of the α and ω ions). The $[M + 55]^{+\bullet}$ ions were generated under the common conditions used for the separation of TGs on classical HPLC columns, i.e., in the mobile phases containing acetonitrile and submilliliter per minute flow rates. Therefore, it is not difficult to adapt the existing HPLC/APCI-MS methods for the localization of double bonds. The fragmentation of $[M + 55]^{+\bullet}$ was achieved in the ion trap using either CID or PQD. Although PQD afforded for each double bond two diagnostic ions and CID only one, the CID was preferred because of its higher sensitivity. Although the fragmentation spectra of $[M + 55]^{+\bullet}$ usually provide all information for characterizing TG structures, such spectra are better to be used for double-bond localization only; all the other information is more easily accessible from the full-scan spectra. The MS^2 spectra of $[M + 55]^{+\bullet}$ generally contained diagnostic peaks for all (or most) of the double bonds in the molecule. Yet in the case of unknowns, the interpretation was not always straightforward. The MS^2 spectra contained cumulative information on all double bonds in all three acyls, which complicated or even hindered a correct assignment of particular signals. This limitation would likely have been solved by the use of MS^3, but the sensitivity was an issue. Despite the limitations discussed above, the method is an easy way of determining double bonds in TGs, which has been demonstrated with a large set of standards and also for natural samples.

Acknowledgments This work was financially supported by the Czech Science Foundation (Project No. P206/12/0750), the Academy of Sciences of the Czech Republic (RVO 61388963) and Charles University in Prague (Project SVV). The authors thank Dr. Miroslav Lísa for advices with the randomization synthesis.

References

1. Gunstone FD, Harwood JL, Dijkstra AJ (2007) The lipid handbook 3 edn. CRC, Boca Raton
2. Holčapek M, Jandera P, Fischer J, Prokeš B (1999) Analytical monitoring of the production of biodiesel by high-performance liquid chromatography with various detection methods. J Chromatogr A 858(1):13–31
3. Fauconnot L, Hau J, Aeschlimann JM, Fay LB, Dionisi F (2004) Quantitative analysis of triacylglycerol regioisomers in fats and oils using reversed-phase high-performance liquid chromatography and atmospheric pressure chemical ionization mass spectrometry. Rapid Commun Mass Spectrom 18(2):218–224. doi:10.1002/rcm.1317
4. Cvačka J, Hovorka O, Jiroš P, Kindl J, Stránský K, Valterová I (2006) Analysis of triacylglycerols in fat body of bumblebees by chromatographic methods. J Chromatogr A 1101(1–2):226–237. doi:10.1016/j.chroma.2005.10.001
5. Sandra K, Pereira AD, Vanhoenacker G, David F, Sandra P (2010) Comprehensive blood plasma lipidomics by liquid chromatography/quadrupole time-of-flight mass spectrometry. J Chromatogr A 1217(25):4087–4099. doi:10.1016/j.chroma.2010.02.039
6. Laakso P, Voutilainen P (1996) Analysis of triacylglycerols by silver-ion high-performance liquid chromatography—atmospheric pressure chemical ionization mass spectrometry. Lipids 31(12):1311–1322. doi:10.1007/bf02587918
7. Lísa M, Velínská H, Holčapek M (2009) Regioisomeric characterization of triacylglycerols using silver-ion HPLC/MS and randomization synthesis of standards. Anal Chem 81(10):3903–3910. doi:10.1021/ac900150j
8. Lísa M, Holčapek M (2013) Characterization of triacylglycerol enantiomers using chiral HPLC/APCI-MS and synthesis of enantiomeric triacylglycerols. Anal Chem 85(3):1852–1859. doi:10.1021/ac303237a
9. Dugo P, Kumm T, Crupi ML, Cotroneo A, Mondello L (2006) Comprehensive two-dimensional liquid chromatography combined with mass spectrometric detection in the analyses of triacylglycerols in natural lipidic matrixes. J Chromatogr A 1112(1–2):269–275. doi:10.1016/j.chroma.2005.10.070
10. van der Klift EJC, Vivo-Truyols G, Claassen FW, van Holthoon FL, van Beek TA (2008) Comprehensive two-dimensional liquid chromatography with ultraviolet, evaporative light scattering and mass spectrometric detection of triacylglycerols in corn oil. J Chromatogr A 1178(1–2):43–55. doi:10.1016/j.chroma.2007.11.039
11. Perrin JL, Naudet M (1983) Identification and determination of triglycerides in natural fats by high-performance liquid-chromatography. Revue Francaise Des Corps Gras 30(7–8):279–285
12. Hsu FF, Turk J (1999) Structural characterization of triacylglycerols as lithiated adducts by electrospray ionization mass spectrometry using low-energy collisionally activated dissociation on a triple stage quadrupole instrument. J Am Soc Mass Spectrom 10(7):587–599. doi:10.1016/s1044-0305(99)00035-5
13. Holčapek M, Jandera P, Zderadička P, Hrubá L (2003) Characterization of triacylglycerol and diacylglycerol composition of plant oils using high-performance liquid chromatography-atmospheric pressure chemical ionization mass spectrometry. J Chromatogr A 1010(2):195–215. doi:10.1016/s0021-9673(03)01030-6
14. Han XL, Gross RW (2003) Global analyses of cellular lipidomes directly from crude extracts of biological samples by ESI mass spectrometry: a bridge to lipidomics. J Lipid Res 44(6):1071–1079. doi:10.1194/jlr. R300004-JLR200
15. Byrdwell WC (2001) Atmospheric pressure chemical ionization mass spectrometry for analysis of lipids. Lipids 36(4):327–346. doi:10.1007/s11745-001-0725-5
16. Cai SS, Syage JA (2006) Comparison of atmospheric pressure photoionization, atmospheric pressure chemical ionization, and electrospray ionization mass spectrometry for analysis of lipids. Anal Chem 78(4):1191–1199. doi:10.1021/ac0515834
17. Asbury GR, Al-Saad K, Siems WF, Hannan RM, Hill HH (1999) Analysis of triacylglycerols and whole oils by matrix-assisted laser desorption/ionization time of flight mass spectrometry. J Am Soc Mass Spectrom 10(10):983–991. doi:10.1016/s1044-0305(99)00063-x
18. Pittenauer E, Allmaier G (2009) The renaissance of high-energy CID for structural elucidation of complex lipids: MALDI-TOF/RTOF-MS of alkali cationized triacylglycerols. J Am Soc Mass Spectrom 20(6):1037–1047. doi:10.1016/j.jasms.2009.01.009
19. Kofroňová E, Cvačka J, Vrkoslav V, Hanus R, Jiroš P, Kindl J, Hovorka O, Valterová I (2009) A comparison of HPLC/APCI-MS and MALDI-MS for characterising triacylglycerols in insects: species-specific composition of lipids in the fat bodies of bumblebee males. J Chromatogr B-Anal Technol Biomed Life Sci 877(30):3878–3884. doi:10.1016/j.jchromb.2009.09.040
20. Suni NM, Aalto H, Kauppila TJ, Kotiaho T, Kostiainen R (2012) Analysis of lipids with desorption atmospheric pressure

photoionization-mass spectrometry (DAPPI-MS) and desorption electrospray ionization-mass spectrometry (DESI-MS). J Mass Spectrom 47(5):611–619. doi:10.1002/jms.2992
21. Cheng CF, Gross ML (1998) Complete structural elucidation of triacylglycerols by tandem sector mass spectrometry. Anal Chem 70(20):4417–4426. doi:10.1021/ac9805192
22. Lauer WM, Aasen AJ, Graff G, Holman RT (1970) Mass spectrometry of lipids. 5. Mass spectrometry of triglycerides. 1. Structural effects. Lipids 5(11):861–868. doi:10.1007/bf02531117
23. Games DE (1978) Soft ionization mass-spectral methods for lipid analysis. Chem Phys Lipids 21(4):389–402. doi:10.1016/0009-3084(78)90048-8
24. Thomas MC, Mitchell TW, Harman DG, Deeley JM, Murphy RC, Blanksby SJ (2007) Elucidation of double bond position in unsaturated lipids by ozone electrospray ionization mass spectrometry. Anal Chem 79(13):5013–5022. doi:10.1021/ac0702185
25. Xu Y, Brenna JT (2007) Atmospheric pressure covalent adduct chemical ionization tandem mass spectrometry for double bond localization in monoene- and diene-containing triacylglycerols. Anal Chem 79(6):2525–2536. doi:10.1021/ac062055a
26. Thomas MC, Mitchell TW, Harman DG, Deeley JM, Nealon JR, Blanksby SJ (2008) Ozone-induced dissociation: elucidation of double bond position within mass-selected lipid ions. Anal Chem 80(1): 303–311. doi:10.1021/ac7017684
27. Hsu F-F, Turk J (2010) Electrospray ionization multiple-stage linear ion-trap mass spectrometry for structural elucidation of triacylglycerols: assignment of fatty acyl groups on the glycerol backbone and location of double bonds. J Am Soc Mass Spectrom 21(4):657–669. doi:10.1016/j.jasms.2010.01.007
28. Brown SHJ, Mitchell TW, Blanksby SJ (2011) Analysis of unsaturated lipids by ozone-induced dissociation. Biochimt Biophys Acta-Mol Cell Biol Lipids 1811(11):807–817. doi:10.1016/j.bbalip.2011.04.015
29. Vrkoslav V, Háková M, Pecková K, Urbanová K, Cvačka J (2011) Localization of double bonds in wax esters by high-performance liquid chromatography/atmospheric pressure chemical ionization mass spectrometry utilizing the fragmentation of acetonitrile-related adducts. Anal Chem 83(8):2978–2986. doi:10.1021/ac1030682
30. Pham HT, Ly T, Trevitt AJ, Mitchell TW, Blanksby SJ (2012) Differentiation of complex lipid isomers by radical-directed dissociation mass spectrometry. Anal Chem 84(17):7525–7532. doi:10.1021/ac301652a
31. Moneti G, Pieraccini G, Dani F, Turillazzi S, Favretto D, Traldi P (1997) Ion-molecule reactions of ionic species from acetonitrile with unsaturated hydrocarbons for the identification of the double-bond position using an ion trap. J Mass Spectrom 32(12):1371–1373. doi:10.1002/(sici)1096-9888(199712)32:12<1371::aid-jms588>3.0.co;2-e
32. Moneti G, Pieraccini G, Favretto D, Traldi P (1998) Acetonitrile in chemical ionization of monounsaturated hydrocarbons: a C-13 and H-2 labeling study. J Mass Spectrom 33(11):1148–1149. doi:10.1002/(sici)1096-9888(1998110)33:11<1148::aid-jms707>3.0.co;2-y
33. Moneti G, Pieraccini G, Favretto D, Traldi P (1999) Reactions of ionic species from acetonitrile with long-chain saturated and unsaturated alcohols. J Mass Spectrom 34(12):1354–1360. doi:10.1002/(sici)1096-9888(199912)34:12<1354::aid-jms894>3.0.co;2-1
34. Oldham NJ, Svatoš A (1999) Determination of the double bond position in functionalized monoenes by chemical ionization ion-trap mass spectrometry using acetonitrile as a reagent gas. Rapid Commun Mass Spectrom 13(5):331–336. doi:10.1002/(sici)1097-0231(19990315)13:5<331::aid-rcm487>3.3.co;2-1
35. Van Pelt CK, Carpenter BK, Brenna JT (1999) Studies of structure and mechanism in acetonitrile chemical ionization tandem mass spectrometry of polyunsaturated fatty acid methyl esters. J Am Soc Mass Spectrom 10(12):1253–1262
36. Van Pelt CK, Brenna JT (1999) Acetonitrile chemical ionization tandem mass spectrometry to locate double bonds in polyunsaturated fatty acid methyl esters. Anal Chem 71(10):1981–1989. doi:10.1021/ac981387f
37. Van Pelt CK, Huang MC, Tschanz CL, Brenna JT (1999) An octaene fatty acid, 4,7,10,13,16,19,22,25-octacosaoctaenoic acid (28: 8*n*−3), found in marine oils. J Lipid Res 40(8):1501–1505
38. Michaud AL, Diau GY, Abril R, Brenna JT (2002) Double bond localization in minor homoallylic fatty acid methyl esters using acetonitrile chemical ionization tandem mass spectrometry. Anal Biochem 307(2):348–360. doi:10.1016/s0003-2697(02)00037-4
39. Michaud AL, Yurawecz MP, Delmonte P, Corl BA, Bauman DE, Brenna JT (2003) Identification and characterization of conjugated fatty acid methyl esters of mixed double bond geometry by acetonitrile chemical ionization tandem mass spectrometry. Anal Chem 75(18):4925–4930. doi:10.1021/ac034221+
40. Michaud AL, Lawrence P, Adlof R, Brenna JT (2005) On the formation of conjugated linoleic acid diagnostic ions with acetonitrile chemical ionization tandem mass spectrometry. Rapid Commun Mass Spectrom 19(3):363–368. doi:10.1002/rcm.1797
41. Lawrence P, Brenna JT (2006) Acetonitrile covalent adduct chemical ionization mass spectrometry for double bond localization in non-methylene-interrupted polyene fatty acid methyl esters. Anal Chem 78(4):1312–1317. doi:10.1021/ac0516584
42. Gomez-Cortes P, Tyburczy C, Brenna JT, Juarez M, Angel de la Fuente M (2009) Characterization of *cis*-9 trans-11 *trans*-15 C18:3 in milk fat by GC and covalent adduct chemical ionization tandem MS. J Lipid Res 50(12):2412–2420. doi:10.1194/jlr. M800662-JLR200
43. Alves SP, Tyburczy C, Lawrence P, Bessa RJB, Brenna JT (2011) Acetonitrile covalent adduct chemical ionization tandem mass spectrometry of non-methylene-interrupted pentaene fatty acid methyl esters. Rapid Commun Mass Spectrom 25(14):1933–1941. doi:10.1002/rcm.5065
44. Oldham NJ (1999) Ion/molecule reactions provide new evidence for the structure and origin of C3H4N (+) from acetonitrile chemical ionization plasma. Rapid Commun Mass Spectrom 13(16):1694–1698. doi:10.1002/(sici)1097-0231(19990830)13:16<1694::aid-rcm702>3.0.co;2-1
45. Vrkoslav V, Cvačka J (2012) Identification of the double-bond position in fatty acid methyl esters by liquid chromatography/atmospheric pressure chemical ionisation mass spectrometry. J Chromatogr A 1259:244–250. doi:10.1016/j.chroma.2012.04.055
46. Šubčíková L, Hoskovec M, Vrkoslav V, Čmelíková T, Háková E, Míková R, Coufal P, Doležal A, Plavka R, Cvačka J (2015) Analysis of 1,2-diol diesters in vernix caseosa by high-performance liquid chromatography—atmospheric pressure chemical ionization mass spectrometry. J Chromatogr A 1378:8–18. doi:10.1016/j.chroma.2014.11.075
47. Lísa M, Holčapek M, Boháč M (2009) Statistical evaluation of triacylglycerol composition in plant oils based on high-performance liquid chromatography-atmospheric pressure chemical ionization mass spectrometry data. J Agric Food Chem 57(15):6888–6898. doi:10.1021/jf901189u
48. Liebisch G, Vizcaino JA, Koefeler H, Troetzmueller M, Griffiths WJ, Schmitz G, Spener F, Wakelam MJO (2013) Shorthand notation for lipid structures derived from mass spectrometry. J Lipid Res 54(6): 1523–1530. doi:10.1194/jlr.M033506
49. Rousseau D, Marangoni AG (2002) In: Akoh CC, Min DB (eds) Food lipids: chemistry, nutrition, and biotechnology, 2nd edn. CRC, New York

50. Mottram HR, Evershed RP (1996) Structure analysis of triacylglycerol positional isomers using atmospheric pressure chemical ionisation mass spectrometry. Tetrahedron Lett 37(47):8593–8596. doi:10.1016/0040-4039(96)01964-8
51. Laakso P (2002) Mass spectrometry of triacylglycerols. Eur J Lipid Sci Technol 104(1):43–49. doi:10.1002/1438-9312(200201)104:1<43::AID-EJLT43>3.0.CO;2-J
52. Baiocchi C, Medana C, Dal Bello F, Giancotti V, Aigotti R, Gastaldi D (2015) Analysis of regioisomers of polyunsaturated triacylglycerols in marine matrices by HPLC/HRMS. Food Chem 166:551–560. doi:10.1016/j.foodchem.2014.06.067
53. Kofroňová E, Cvačka J, Jiroš P, Sýkora D, Valterová I (2009) Analysis of insect triacylglycerols using liquid chromatography-atmospheric pressure chemical ionization-mass spectrometry. Eur J Lipid Sci Technol 111:519–525. doi:10.1002/ejlt.200800228
54. Cvačka J, Krafková E, Jiroš P, Valterová I (2006) Computer-assisted interpretation of atmospheric pressure chemical ionization mass spectra of triacylglycerols. Rapid Commun Mass Spectrom 20(23):3586–3594. doi:10.1002/rcm.2770
55. Rissmann R, Groenink HWW, Weerheim AM, Hoath SB, Ponec M, Bouwstra JA (2006) New insights into ultrastructure, lipid composition and organization of vernix caseosa. J Invest Dermatol 126(8):1823–1833. doi:10.1038/sj.jid.5700305

- Publication IV -

Cholesteryl esters of ω-(*O*-acyl)-hydroxy fatty acids in vernix caseosa

Aneta Kalužíková[a,b], Vladimír Vrkoslav[b], Eva Harazim[a,b], Michal Hoskovec[b], Richard Plavka[c], Miloš Buděšínský[b], Zuzana Bosáková[a], Josef Cvačka[a,b *]

[a] Department of Analytical Chemistry, Faculty of Science, Charles University in Prague, Hlavova 2030/8, CZ-128 43 Prague 2, Czech Republic

[b] The Institute of Organic Chemistry and Biochemistry of the Czech Academy of Sciences, Flemingovo nám. 2, CZ-166 10 Prague 6, Czech Republic

[c] Department of Obstetrics and Gynaecology, General Faculty Hospital and 1st Faculty of Medicine, Charles University in Prague, Apolinářská 18, CZ-128 00 Prague 2, Czech Republic

* To whom correspondence should be addressed: Josef Cvačka, The Institute of Organic Chemistry and Biochemistry of the Czech Academy of Sciences, Flemingovo náměstí 2, CZ-166 10, Prague 6, Czech Republic, Tel.: +420 220 183 303, E-mail: josef.cvacka@uochb.cas.cz.

Running Title: Cholesteryl esters of ωOAHFAs in vernix caseosa

Abbreviations: 1,2-DDE, 1,2-diol diester; APCI, atmospheric pressure chemical ionization; αHFA, α-hydroxy fatty acid; Chl-ωOAHFA, cholesteryl ester of ω-(*O*-acyl)-hydroxy fatty acid; CID, collision-induced dissociation; FA, fatty acid; FAME, fatty acid methyl ester; HFA, hydroxy fatty acid; HFAME, hydroxy fatty acid methyl ester; RP-HPLC, reversed-phase HPLC; ωOAHFA, ω-(*O*-acyl)-hydroxy fatty acid; ωHFA, ω-hydroxy fatty acid.

ABSTRACT

Cholesteryl esters of *ω*-(*O*-acyl)-hydroxy fatty acids (Chl-*ω*OAHFAs) were identified for the first time in vernix caseosa and characterized using chromatography and mass spectrometry. Chl-*ω*OAHFAs were isolated using adsorption chromatography on silica gel and magnesium hydroxide. Their general structure was established using high-resolution and tandem mass spectrometry of intact lipids, and products of their transesterification and derivatizations. Individual molecular species were characterized using non-aqueous reversed-phase HPLC coupled to atmospheric pressure chemical ionization. The analytes were detected as protonated molecules, and their structures were elucidated in the negative ion mode using controlled thermal decomposition and data-dependent fragmentation. About three hundred molecular species of Chl-*ω*OAHFAs were identified in this way. The most abundant Chl-*ω*OAHFAs contained 32:1 *ω*-hydroxy fatty acid and 14:0, 15:0, 16:0, 16:1 and 18:1 fatty acids. The double bond in the 32:1 *ω*-hydroxy fatty acid was in the *n*-7 and *n*-9 positions. Chl-*ω*OAHFAs are estimated to account for ca 1 - 2 % of vernix caseosa lipids.

Key words:

Vernix caseosa, skin lipids, neutral lipids, cholesterol, lipidomics, mass spectrometry

INTRODUCTION

Vernix caseosa is a white, cheese-like, naturally occurring biofilm that coats the skin of the fetus during the last trimester of gestation and usually remains present on the skin during delivery. It is a highly cellular material consisting of hydrophilic desquamated corneocytes embedded in a lipid matrix. Vernix caseosa is essential for skin development *in utero* as well as post-birth adaptation providing multiple functions (1-3).

Vernix caseosa consists of water (80 %), proteins (10 %), and a complex mixture of lipids (10 %). Although the investigations of lipid composition have started more than seventy years ago (4), the entire lipidome of vernix caseosa has not been described comprehensively yet. Lipids exist in intercellular space as free (extractable) components, or they are covalently bound to the cornified envelope. About 90 % of the free lipids are nonpolar species like squalene, sterol esters, wax esters, diesters, and triacylglycerols, and the remaining 10 % are barrier lipids, mostly cholesterol, free fatty acids (FAs), and ceramides. The lipids covalently linked to the cornified envelope consist of ω-hydroxy fatty acids (ωHFAs) and ω-hydroxyceramides (5).

Nonpolar diesters form 3 - 9 % of the total vernix caseosa lipids (6, 7). The first report (6) characterized them as esters of an alkane 1,2-diol with two FAs (later described as Type II diesters or 1,2-DDE) with a small amount of esters of an HFA with a fatty alcohol and an FA (Type I diesters). Four years later, Type II diesters were confirmed as the main constituents of the diester fraction (8, 9). The analyses of hydrolysis products also disclosed α-hydroxy fatty acids (αHFAs), sterols and fatty alcohols, which prompted the authors to hypothesize on the existence of additional types of diesters, Type I diesters and Type I diesters with the fatty alcohol having replaced by a sterol (9). However, the existence of the additional type of diesters in vernix caseosa has never been substantiated. No diester lipids have been detected in adult human sebum or epidermal surface, where triacylglycerols and their breakdown products

(monoacylglycerols, diacylglycerols, and free fatty acids) are found instead (10, 11). On the contrary, the skin surface lipids of many animals are rich in diesters. Mammals like rabbit, cat or cow biosynthesize Type I diesters, whereas mouse, hamster, guinea-pig or gerbil produce mostly Type II diesters (1,2-DDE) (8, 12-14). A special sort of Type II, with one FA replaced by isovaleric acid, has been found in the dog (15) and macaque (16). Uropygial (preen) glands of birds mostly produce 2,3-DDE (17). The existence of various types of esters in sebum of man and animals has been discussed in terms of physicochemical properties of the lipids and their likely roles in the skin protection and control of microbiome (10, 11).

Recently we reported on the analysis of molecular species of 1,2-DDE (18) from vernix caseosa. Diesters were isolated from a total lipid extract using thin-layer chromatography (TLC) and separated by non-aqueous reversed-phase high-performance liquid chromatography (HPLC). 1,2-DDE molecular species were identified using tandem mass spectrometry with atmospheric pressure chemical ionization (APCI). In addition to 1,2-DDE, molecular species of an unknown lipid class appeared in the chromatogram at higher retention times. In this work, we isolated the unknown lipids from a fresh material using multistep chromatography and identified them as cholesteryl esters of ω-(*O*-acyl)-hydroxy fatty acids (Chl-ωOAHFAs). To the best of our knowledge, these diesters represent a new lipid class for vernix caseosa. An HPLC/APCI-MS^2 method was developed and applied for comprehensive characterization of Chl-ωOAHFA molecular species in vernix caseosa.

MATERIALS AND METHODS

Material

Vernix caseosa (1 - 2 g) was collected from healthy newborn subjects delivered at full term (gestation week 39 - 42) immediately after the delivery. The samples were stored in amber glass vials at −80 °C. The study was approved by the Ethics Committee of the General University Hospital, Prague (910/09 S-IV) and the samples were collected with a written informed parental consent.

Chemicals

LC-MS grade acetonitrile, ethyl acetate, methanol and propan-2-ol (Sigma-Aldrich, United States) were used as received. Chloroform, hexane, and dichloromethane (Penta, Czech Republic) were distilled in glass from analytical-grade solvents. Rhodamine 6G, silica gel (both Merck & Co., United States), *N,N*-dimethylformamide (Acros Organics, part of Thermo Fisher Scientific, United States), anhydrous magnesium sulfate, magnesium hydroxide, primuline, (*Z*)-octadec-9-enoyl chloride, 16-hydroxyhexadecanoic acid, hydrochloric acid, sodium bicarbonate, pyridine, *N,N′*-dicyclohexylcarbodiimide, *N*,*O*-bis(trimethylsilyl)acetamide, dichloromethane, 4-(dimethylamino)pyridine, cholesterol, pyridinium dichloroformate, acetyl chloride, silver carbonate (all from Sigma-Aldrich, United States) were of reagent grade and used as purchased.

Standard synthesis

Cholesteryl ester of 16-{[(9Z)-octadec-9-enoyl]oxy}hexadecanoic acid was synthesized by stirring (*Z*)-octadec-9-enoyl chloride and 16-hydroxyhexadecanoic acid in anhydrous pyridine. The oily product was purified by flash chromatography and treated with cholesterol in dichloromethane in the presence of *N,N′*-dicyclohexylcarbodiimide and 4-(dimethylamino)pyridine (19). The final purified product was obtained in 39% overall yield and its structure was verified by NMR. The details on the synthetic procedure and NMR data are given in the Supplemental data (Section 1).

Isolation of total lipids

Lipids were extracted from 20 samples equally representing gender of newborns (10 boys, 10 girls). Each sample was processed separately as follows: The sample (300 mg) was suspended in methanol:chloroform (2:1, by vol.; 3 ml) in a conical-bottom glass centrifuge tube, and homogenized using a vortex shaker followed by a 2-minute treatment in an ultrasonic bath. Then, chloroform (1 ml) and water (1.8 ml) were added and the suspension was shaken for 1 hour. The mixture was centrifuged at 400 g for 5 minutes. The chloroform layer was transferred into a new glass tube, vortexed with 1.8 ml of water and collected after centrifugation. The water layer was re-extracted with 1 ml of chloroform. The chloroform extracts were combined, treated with anhydrous magnesium sulfate to remove the water residues, and filtered through pre-cleaned cotton wool. The lipid extracts from all 20 samples were combined and concentrated on a rotary evaporator (37 °C, 170 mbar) to approximately one-third of the original volume. The rest of the solvent was evaporated under a stream of nitrogen. In total, 6.000 g of vernix caseosa yielded 561.1 mg of total lipids. The lipids were reconstituted in chloroform:methanol (19:1 by vol.) at the concentration of 30 mg/ml and stored at −20 °C.

Fractionation of lipids

Approximately half of the total lipid extract was fractionated in two steps using semi-preparative TLC. In the first step, lipids were separated on glass plates coated with silica gel using hexane:diethyl ether (93:7, by vol.) mobile phase. The zones were visualized under ultraviolet light after spraying with rhodamine 6G (0.05% in ethanol). Silica gel with diesters (R_f = 0.35 - 0.48) was scraped off the plates and the lipids were extracted with freshly distilled diethyl ether. The solvent was evaporated under a nitrogen stream. The procedure was used repeatedly (ca 3 mg of lipids separated in each step) and yielded 27.6 mg of diesters (F-1).

In the second step, F-1 was reconstituted in chloroform:methanol (2:1, by vol.) at a concentration of 30 mg/ml and separated on glass plates coated with magnesium hydroxide (for details on the TLC plates

preparation see Supplemental data, Section 2). Hexane:ethyl acetate (99.95:0.05, by vol.) was used as a mobile phase. Prior to the separation, a filter paper was inserted into the developing chamber. After the filter paper was fully soaked with the solvent, each plate was developed twice to focus the zones; in the first step to ¾ of the plate height and then, after air-drying, to the top. After air-drying, the zones were sprayed with 0.05% primuline in ethanol and then visualized under ultraviolet light. A synthesized standard (18:1(n-9)/16:0-Chl) was used to verify the R_f of Chl-ωOAHFAs. The sorbent layer corresponding to R_f = 0.66 - 0.76 was collected and extracted with diethyl ether. The procedure was used repeatedly to process the whole F-1 (ca 3 mg separated in each step), and yielded 5.8 mg of Chl-ωOAHFAs (F-2). The lipids were dissolved in chloroform:methanol (9:1, by vol.) at a concentration of 5 mg/ml and stored at −20 °C. The whole isolation and fractionation procedure is depicted in Figure 1.

Transesterification

Chl-ωOAHFAs were transesterified using an acid catalyst (20). Briefly, F-2 was dissolved in chloroform:methanol (2:3, by vol.) in a small glass ampoule. After adding acetyl chloride, the ampoule was sealed and heated at 70 °C for 60 minutes. The reaction mixture was neutralized with silver carbonate and the organic layer was used for further analyses.

Trimethylsilylation

Trimethyl silyl (TMS) derivatives of HFA were prepared according to a published procedure (21). FAMEs were dissolved in dried acetonitrile (0.4 mg/ml) and treated with excess of *N*,*O*-bis(trimethylsilyl)acetamide at 40 °C for 10 minutes. The solvent was evaporated under a stream of nitrogen, the residues were dissolved in chloroform (250 µl) and the sample was injected onto the GC column.

Oxidation with pyridinium dichromate in DMF

HFAs were oxidized with pyridinium dichromate (PDC) in *N,N*-dimethylformamide (DMF) (22). The

solution of FAMEs in chloroform:methanol, 2:3, by vol. (100 µl) was shaken with 5 mg of PDC and 50 µl of DMF for 24 hours at laboratory temperature. The reaction mixture was transferred into a small glass column with silica gel, and the reaction products were eluted with chloroform (2 × 200 µl). The sample volume was reduced to 30 µl under a stream of nitrogen.

GC/EI-MS

The analyses were performed on a 7890N gas chromatograph coupled to a 5975C mass spectrometer, equipped with electron ionization (EI) and quadrupole analyzer (Agilent Technologies, Santa Clara, CA, United States). The sample (2 µl) was injected in the split mode with a split ratio of 5:1. The injector and transfer line temperatures were set to 350 °C and 340 °C, respectively. A DB-5HT fused silica capillary column (15 m × 250 µm; a film thickness 0.10 µm) from Agilent Technologies was used. The carrier gas was helium at a constant flow rate of 1.5 ml/min. The temperature program was set as follows: 100 °C (2 min), then 6 °C/min to 370 °C (3 min). The ion source and quadrupole temperatures were 230 °C and 150 °C, respectively. EI spectra (70 eV) were recorded from *m/z* 20 to *m/z* 700.

Direct infusion MS and HPLC/APCI-MS

Direct infusion and HPLC/MS experiments were performed using an LTQ Orbitrap XL hybrid FT mass spectrometer equipped with an Ion Max source and controlled by Xcalibur (all Thermo Fisher Scientific, San Jose, CA, United States). The mass spectrometer was coupled to an HPLC system consisting of a Rheos 2200 quarternary gradient pump (Flux Instruments, Reinach, Switzerland), a PAL HTS autosampler (CTC Analytics, Zwingen, Switzerland), and a DeltaChrom CTC 100 column oven (Watrex, Prague, Czech Republic). Molecular species of Chl-ωOAHFAs were separated in non-aqueous reversed-phase HPLC and detected by APCI-MS^2 using the conditions as follows: The temperature of the sample tray was set at 10 °C. The autosampler injected 5 µl of the sample and the injection system was washed with chloroform/acetonitrile (1:1, by vol.). Two Nova-Pak C18 stainless-steel columns connected in series (150 and 300 mm × 3.9 mm, particle size 4 µm; Waters, Milford, MA, United States) were placed in a

column oven set at 40 °C. The mobile phase was prepared from acetonitrile (A) and ethyl acetate (B) using the following linear gradient program: 0 min: 30 % of A and 70 % of B; 74.5 min: 67.25 % of B; 75 min: 67.5 % of B; 140 min: 100 % of B; 140.5 min: 100 % of B; 154 min: 100 % of B. The mobile phase flow rate was set as follows: 0-74.5 min 0.6 µl/min, 75-140 0.15 µl/min and 140.5-154 min 0.6 µl/min. The APCI corona discharge current, vaporizer, and heated capillary temperatures were 5 µA, 500 °C and 170 °C, respectively. The sheath and auxiliary gas (nitrogen) were set at the flow rate of 52 and 22 arbitrary units, respectively. The MS method encompassed three scan events: (1) the Orbitrap full MS scan event in the 300 - 1600 *m/z* range, in the positive ion mode at a resolution of 30,000, (2) the linear ion trap full MS scan event in the 200 -1600 *m/z* range in the negative ion mode and (3) the CID MS^2 scan event of the first most intense ion from the parent mass list with a normalized collision energy of 21.5 % and isolation window 2 Da in the negative ion mode. The CID MS^2 parent mass list was calculated for $[M - H - Chl + H_2O]^-$ (i.e. $[OAHFA]^-$) ions of all possible Chl-*ω*OAHFAs with the total number of carbons and double bonds in the range 37 - 60 and 0 - 3, respectively. The HPLC/MS^2 data were interpreted manually, with the help of an in-house developed Excel macro.

Shorthand nomenclature

Considering previous literature (23, 24), sterol esters of *ω*-(*O*-acyl)-hydroxy fatty acids are abbreviated St-*ω*OAHFAs. In the case of cholesterol, Chl-*ω*OAHFAs is used. Molecular species within this class are abbreviated using a FA/*ω*HFA-Chl format, which is consistent with the established shorthand nomenclature for *ω*OAHFAs (25) and reflects the chemical structure of Chl-*ω*OAHFAs. Thus, for instance, a molecular species identified in this work as 16:0/32:1-Chl corresponds to cholesteryl ester of *ω*HFA with 32 carbons and 1 double bond, with the hydroxyl esterified to a saturated FA with 16 carbons. In the ion description, "Chl" is considered as neutral cholesterol molecule. Thus, for instance, protonated *ω*OAHFA, which is an ion resulting by neutral loss of dehydrated cholesterol from Chl-*ω*OAHFA (M), is $[M - Chl + H_2O]^+$.

RESULTS

General structure elucidation

As shown in our previous paper (18), the unknown lipids eluted in the reversed-phase HPLC at higher retention times than aliphatic 1,2-DDEs. High-resolution APCI mass spectra revealed for protonated molecules elemental compositions $C_nH_{2n-x}O_4$, where x = 11, 13, 15 or 17. The existence of four oxygen atoms and similar retention on silica gel as 1,2-DDE pointed out to diester lipids. The formulas corresponded to ring plus double bond equivalents (RDBE) of 6.5-9.5, showing an unusually high degree of unsaturation and/or presence of rings (the RDBE values for 1,2-DDEs ranged from 1.5 to 3.5). Protonated molecules of unknown lipids were found at higher *m/z* values (*m/z* 1000 - 1250) than 1,2-DDE (*m/z* 800 - 1000). The APCI spectra of all molecular species showed neutral loss of 368 Da typical for sterol-containing compounds. The occurrence of a sterol corresponded well with the high RDBE values. The presence of a sterol in the unknown diesters and its absence in 1,2-DDE made it possible to separate these two diester lipid classes from each other using TLC on magnesium-based sorbents (26, 27). Commercial production of such sorbents was mostly discontinued, which forced us to use common reagent-grade chemicals. Nevertheless, a fraction of unknown, sterol-containing diesters with satisfactory purity was obtained. In the next step, the unknown lipids were transesterified and analyzed by high-temperature GC/EI-MS and high-resolution MS. The GC/EI-MS data showed cholesterol and a rich mixture of FAMEs (Supplemental Figure S4). A group of FAMEs at unusually high retention times was identified as methyl esters of HFAs (HFAMEs). Their TMS derivatives (Figure 2) provided spectra consistent with a hydroxy group at the terminal carbon (28, 29), and revealed saturated and monounsaturated ωHFA with 29 - 34 carbons. Interestingly, saturated ωHFA eluted in two chromatographically separated peaks, obviously differing by chain branching. The mass spectra of earlier eluting isomers of 30:0 and 32:0 showed significantly more abundant *m/z* 103, which could indicate methyl branching in the iso position. The chromatographic peaks of TMS derivatives of monounsaturated ωHFAMEs were distorted, likely because of double bond positional isomers. The original transesterified

JOURNAL OF LIPID RESEARCH ASBMB

mixture was also analyzed by high-resolution APCI-MS (Supplemental Figure S5a). The positive ion spectra displayed abundant *m/z* 369.3510 (cholesterol; $[Chl + H - H_2O]^+$) and showed ions consistent with protonated molecules of saturated and monounsaturated hydroxy FAMEs (exact masses within 2 ppm error). To confirm the position of the hydroxy group in an independent experiment, oxidation with PDC in DMF was performed. As known from the literature (22), the oxidation of primary alcohol gives carboxyl, whereas the reaction of secondary alcohol provides carbonyl group. High-resolution electrospray mass spectrum of negative ions showed reaction products with one extra oxygen, i.e., carboxyl derivatives (Supplemental Figure S5b). Therefore, hydroxy group on the terminal carbons of HFAs was confirmed. Double bond position in unsaturated *ω*HFAs was investigated using our previously developed method based on gas phase reactions of acetonitrile (30-32). Collision-induced dissociation MS/MS spectra of the $[M + 55]^{+\bullet}$ adduct of *ω*HFAME (32:1) revealed double bond in two positions, *n*-7 (more abundant) and *n*-9 (less abundant), see Supplemental Figure S5c. The existence of two isomers corresponded well with the distorted peaks in GC chromatogram discussed above. The entire analytical strategy used for the lipid class identification is summarized on a flowchart in Supplemental Figure S6.

All the results directed us to a hypothesis of diesters composed of *ω*HFAs having cholesterol attached to the carboxyl and common FA to the hydroxyl. The unknown diester lipids in vernix caseosa were identified as cholesteryl esters of *ω*-(*O*-acyl)-hydroxy fatty acids (Chl-*ω*OAHFAs) with the general structure shown in Figure 3.

Optimization of HPLC/APCI-MS

The mass spectra of a synthetic standard were studied with the aim to develop an HPLC/MS method for comprehensive characterization of Chl-*ω*OAHFA molecular species. The APCI spectrum of 18:1(*n*-9)/16:0-Chl in the positive ion mode (Figure 4a) showed protonated molecule (*m/z* 905.6), protonated and dehydrated cholesterol $[Chl + H - H_2O]^+$ (*m/z* 369.5), and fragments consistent with a neutral loss of dehydrated cholesterol (*m/z* 537.5) and cholesterol (*m/z* 519.7). The CID MS/MS spectrum

of protonated molecule (Figure 4b) resembled the full scan spectrum, providing identical fragments. Structural information on the FAs and/or HFAs was searched in the MS^3 spectra of $[M + H - Chl + H_2O]^+$ (Figure 4c) and $[M + H - Chl]^+$ (Figure 4d). Unluckily, the fragmentation channels proceeded almost exclusively via elimination of water. Thus, positive ion mode turned out to be useless for structure elucidation of Chl-*ω*OAHFAs. The standard did not provide $[M - H]^-$ in the negative ion mode because of the absence of groups prone to deprotonation. Fortunately, elevated temperature in the ion source induced thermal degradation to OAHFA that easily deprotonated in the corona discharge (Figure 5a). The process was not very efficient under the conditions used and required optimization of the ion source parameters. The ion source temperature and the mobile phase flow rate, as well as ion optics voltages, were tuned to maximize signal of deprotonated OAHFA (Supplemental data, Section 6). Fragmentation of deprotonated *ω*OAHFAs is known to give structural information on FAs and HFAs; the MS/MS spectrum of 18:1(*n*-9)/16:0 (Figure 5b) showed the same fragments as in previously published work (33).

The chromatography was optimized using the lipid sample from vernix caseosa, with the aim to achieve highest possible resolution for molecular species in a reasonable time. Based on our previous experience with 1,2-DDEs (18), a non-aqueous reversed-phase system with the two Nova-Pak C_{18} columns connected in series with a total length of 45 cm was developed. Various binary mobile phases containing methanol, propan-2-ol, acetonitrile, ethyl acetate, and acetone were studied. Finally, we ended up with separation conditions similar to those used for 1,2-DDE (18), i.e., a linear increase of ethyl acetate in acetonitrile in 140 min. The flow rate of the mobile phase in the elution window of Chl-*ω*OAHFAs was reduced from 0.6 ml/min to 0.15 ml/min to increase detection sensitivity.

Chl-*ω*OAHFAs in vernix caseosa

The base peak chromatogram of Chl-*ω*OAHFAs showed many overlapping peaks (Figure 6a). The extracted chromatograms displayed up to several peaks for each *m/z* value, obviously representing isomers. The elution order followed the equivalent carbon number (ECN) concept (34); retention

increased with the length of the chain and decreased with the number of double bonds. As shown in Figure 7, the molecular species appeared on a band rising almost linearly with the retention time (at higher retention times the curve rises exponentially as the flow rate increased from 150 µl/min back to 600 µl/min).

The molecular species of Chl-ωOAHFAs were detected and identified using APCI-tandem MS with data-dependent scanning. The high-resolution full-scan mass spectra of positively charged ions (Figure 6b) were used for determining the total number of carbons and double bonds in fatty chains and served for confirmation of the expected elemental composition. The typical mass errors were in the range of 0.5-1.5 ppm. The ion-trap full-scan mass spectra in the negative ion mode (showing deprotonated ωOAHFAs, Figure 6c) further confirmed the total number of carbons and double bonds in fatty chains and served for data-dependent selection of precursors for MS/MS. The ion-trap MS^2 spectra in the negative ion mode (Figure 6d) revealed FAs and ωHFAs. The deprotonated ωHFA ions ($[HFA - H]^-$) were always accompanied by less abundant water loss peaks ($[HFA - H - H_2O]^-$), which made it possible to distinguish them from deprotonated FA ions. In total, 295 molecular species of Chl-ωOAHFAs was fully characterized in 59 chromatographic peaks, and Chl-ωOAHFAs in additional 11 peaks were characterized by the total number of carbons and double bonds. The list of 50 most abundant species is given in Table 1 (for all identified Chl-ωOAHFAs see Supplemental Table S1). The relative proportions of identified molecular species were estimated from peak areas integrated in the chromatograms reconstructed for $[M + H]^+$ and relative intensities of deprotonated FA ions in MS^2 spectra. It is important to note that response factors of lipids depend on the number of double bonds and carbon chain length (35, 36). As neither standards nor response factors were available for quantification, the relative proportions must be considered merely as an estimate.

The most abundant molecular species were composed of cholesterol, ωHFA 32:1 and FAs commonly found in skin lipids, namely FA 15:0, FA 14:0, FA 18:1, FA 16:1, and FA 16:0 (15:0/32:1-Chl, 14:0/32:1-

Chl, 18:1/32:1-Chl, 16:1/32:1-Chl, and 16:0/32:1-Chl). Relative proportions of FAs and HFAs in Chl-ωOAHFAs calculated from HPLC/APCI-MS^2 are shown in Figure 8. Chl-ωOAHFAs detected in vernix caseosa appeared to contain 34 FAs with 12-28 carbons (up to 2 double bonds) and 32 ωHFAs with 24 - 38 carbons (up to 3 double bonds). All saturated Chl-ωOAHFAs corresponded to 11 % of the total integrated signal, whereas monounsaturated, diunsaturated and triunsaturated species accounted for 55 %, 30 %, and 4 %, respectively.

DISCUSSION

Indirect evidence of cholesterol-containing diesters in vernix caseosa appeared in 1969 when a subclass of Type I diesters (also called "Type III diester waxes" (11), composed of αHFAs esterified on the hydroxyl group with an unsubstituted FA and on the carboxyl group with a sterol, was proposed (9). However, a diester lipid class with a sterol moiety has never been substantiated in vernix caseosa. Our work brings evidence that the sterol-containing diesters are in fact Chl-ωOAHFAs comprised of long-chain ωHFAs.

ωHFAs form 2-3 % of free (unesterified) FAs in vernix caseosa (5). Although they have been identified in hydrolysates of sterol esters, wax esters, diol diesters and triacylglycerols (5), intact neutral lipids containing ωHFAs have not been reported yet. The detection of ωHFAs in diol diester fraction (5) was very likely because of Chl-ωOAHFAs co-isolated with diol diesters. As regards more polar lipids, ωHFAs are found in three ceramide subclasses, EOS (Cer 1), EOH (Cer 4) and EOP (Cer 9), which together form about 1/4 of all vernix caseosa ceramides (5, 37, 38). These ceramides are composed of long-chain ωHFAs linked by amide bond with a sphingoid base (sphingosine in EOS, 6-hydroxy-sphingosine in EOH and dihydrosphingosine in EOP), with the ω-hydroxyl group esterified with an FA. The ωHFAs in EOS have long aliphatic chains with 28-32 carbons (37). Vernix caseosa ceramides are derived from the fetal epidermis and they represent the key barrier lipids (38). As in the case of stratum corneum, ωHFAs and ceramides with ωHFAs are also covalently linked (esterified through the ω-hydroxyl group) to the cornified cell envelope (39). Whereas covalently bound ω-hydroxyceramides in stratum corneum mostly contain 30:0, 32:1 and 34:1 chains (40, 41), in vernix caseosa predominates ω-hydroxyeicosanoic acid; C30-C34 ωHFAs are present as minor components (5).

Ester lipids containing ωHFAs are important constituents of meibum, which is a secretion of holocrine meibomian glands in the eyelids of humans and most animals. Meibum lipids form the outermost layer of the tear film that protects the ocular surface from desiccating and bacterial infection (42). The existence of

long-chain ωHFAs in meibum is known from the early eighties when they were found in steer and human samples (43, 44). Mostly monounsaturated, straight-chain ωHFAs with 30-36 carbons formed ca. 10 % of the total acids. Soon after, St-ωOAHFAs (ωType I-St) have been isolated and identified in steer and human meibum. It was the first report on these diesters in animal samples (45). In addition to the ωHFAs, meibomian St-ωOAHFAs appeared to contain predominantly FAs with 18:1 and 16:1 chains and cholesterol (60 %) or lathosterol (35 %). St-ωOAHFAs formed ca 5 % of steer meibomian lipids. The interest in St-OAHFAs increased again after discovering ωOAHFAs in meibum (33). The ωOAHFAs are likely either precursors or degradation products of St-ωOAHFAs, and they are considered one of the amphiphilic compounds that separate and stabilize interfacial layer between very hydrophobic lipids of meibum and the aqueous layer of the tear film (46). They are linked to dry eye disease and might represent biomarkers of the disease progression (47). The complex mixture of ωOAHFAs in human meibum contains molecular species composed mostly of monounsaturated FA with 18 and 16 carbons and 28:1 - 34:1 ωHFAs (46, 48). Recently, 61 ωOAHFAs with 34 - 56 carbon atoms and 1 - 7 double bonds in human meibum has been reported (25). The occurrence of St-ωOAHFAs in meibum was reconfirmed by the analysis of their intact molecules (49). The ωOAHFA moieties of St-ωOAHFAs and ωOAHFAs in meibum are closely related (50). Their abundances are also similar, with each lipid class accounting for 3 - 5 % of meibomian lipids (24, 47). St-ωOAHFAs have also been found in meibum of several animal species including dog, mice or rabbit (23). Very recently, ωOAHFAs similar to meibomian ones have been detected in equine sperm and the essential role of these amphiphilic lipids in sperm function was hypothesized (51). It is worth noting that mammals also biosynthesize isomeric OAHFAs derived from HFAs with non-terminal hydroxyl. These recently discovered endogenous lipids (also known as fatty acyl esters of hydroxy fatty acids - FAHFAs) exhibit anti-inflammatory and anti-diabetic effects (52, 53).

In this work, Chl-ωOAHFAs comprised ca 20 % of the nonpolar diester fraction. As diesters form 3 - 9 % of the total lipids (6, 7), Chl-ωOAHFAs are estimated to account for ca 1 - 2 % of vernix caseosa lipids, which is less than in human meibum (3 - 5 %) (24, 45, 47). Chl-ωOAHFAs were detected and

comprehensively characterized from a pooled sample representing 10 male and 10 female full-term babies. Moreover, some experiments were also performed with samples from individual subjects (data not shown). Chl-ωOAHFAs were detected in all samples at a similar level, suggesting that these esters are commonly present in vernix caseosa and they are not related to fetus gender. Our experiments showed that the sterol moiety in Chl-*ω*OAHFAs is represented by cholesterol; lathosterol, reported in addition to cholesterol in meibomian St-*ω*OAHFAs (45), has been detected in this work only in traces. *ω*HFAs in Chl-*ω*OAHFAs from vernix caseosa resembled those existing in meibomian St-*ω*OAHFAs and *ω*OAHFAs. The most abundant *ω*HFAs in vernix caseosa (32:1, 34:1 and 30:1) were also the most abundant in St-*ω*OAHFAs (44, 45) and *ω*OAHFAs (25) from meibum. High proportions of these *ω*HFAs have also been reported for equine sperm (51). Saturated *ω*HFAs of meibum are both straight chain and methyl branched (44), which is also in agreement with our findings. The level of similarity can be illustrated by *i*-30:0 and *i*-32:0 *ω*HFAs identified in vernix caseosa based on the mass spectra of their TMS derivatives (Figure 2). The earlier work showed that meibomian even-carbon *ω*HFAs are *iso*-methyl branched, whereas odd-carbon *ω*HFAs are predominantly of *anteiso* type (44). As regards double bond position in unsaturated *ω*HFAs in meibum, the available data are scarce. The action of Δ9-desaturases was proposed (44) and *n*-9 and *n*-7 double bonds were assumed (46). We clearly demonstrated that the double bonds in 32:1 *ω*HFAs in vernix caseosa is in both positions, *n*-7 (more abundant) and *n*-9 (less abundant). As regards FAs, the largest signals provided Chl-*ω*OAHFAs with 14:0, 15:0, 16:0, 16:1 and 18:1 chains, which is not surprising for a sample of vernix caseosa origin (54, 55). The distribution of FAs in Chl-*ω*OAHFAs (Figure 8a) was similar to the overall representation of FAs in vernix caseosa lipidome reported earlier (56), cf. Supplemental Figure S8. The higher levels of 16:1 and 18:1 observed for Chl-*ω*OAHFAs has to be interpreted with caution because, as discussed above, APCI-MS is somewhat more sensitive to unsaturated lipids (35, 36). Nevertheless, the results indicate that Chl-ωOAHFAs are biosynthesized from a pool of all FAs, likely with a certain preference for 16:1 and 18:1 chains. The meibomian St-*ω*OAHFAs and *ω*OAHFAs tend to incorporate more exclusively fatty acyls with 16 and 18 carbons (24, 25, 45, 47). Meibomian *ω*OAHFAs have been reported to comprise a relatively large

proportion of FA 18:2 (24), which is not the case of vernix caseosa Chl-ωOAHFAs. Nevertheless, 18:2 was the most abundant diunsaturated FA in Chl-ωOAHFAs from vernix caseosa. Considering the intact molecules, this study showed the ratio of unsaturated and saturated Chl-ωOAHFAs 89 % : 10 %, which is in a good agreement with meibum (91 ± 3 % : 9 ± 1 %) (57). The main species in vernix caseosa are represented by 15:0/32:1-Chl, 14:0/32:1-Chl, 18:1/32:1-Chl, 16:1/32:1-Chl, and 16:0/32:1-Chl, which reflects the higher incorporation of saturated, shorter chain FAs than in meibum.

The biological role of Chl-ωOAHFAs in vernix caseosa remains to be clarified. The diesters are structurally related to cholesteryl esters, important constituents of neutral lipids in vernix caseosa (6). Chl-ωOAHFAs might be a storage or inactivated form of ωOAHFAs, similarly to cholesteryl esters of very long chain FAs and ωOAHFAs in meibum (46, 58). However, nothing is known if non-esterified ωOAHFAs exist in vernix caseosa (or eventually in amniotic fluid) or not. One can imagine that amphiphilic properties of ωOAHFAs might be important for proper functions and/or cohesion of vernix caseosa. It seems reasonable to assume that Chl-ωOAHFAs are products of the sebaceous gland, taking into account that they are produced by meibomian gland (a type of sebaceous gland). Sebaceous glands in the developing skin are presumed source of structurally related cholesteryl esters in vernix caseosa (2). On the other hand, OAHFA structural motives in certain ceramides (5, 37, 38) cannot be overlooked, and epidermal origin of Chl-ωOAHFAs should be considered as well.

We finally wish to briefly comment analytical methodology used in this work. Although positive ion mode of APCI-MS provided intense signals of protonated Chl-ωOAHFAs, it has turned out unusable for detailed structural elucidation because of virtually missing fragments related to FA and HFAs. Negative ion mode is unlikely to be efficient for diester-type structures lacking easily deprotonable groups. Although deprotonated molecules of St-OAHFAs have been reported (49), we found negative ion mode insensitive. On-line thermal degradation of Chl-ωOAHFAs to ωOAHFAs in the APCI source worked well and made it possible to detect about 300 molecular species of Chl-ωOAHFAs, by far the highest number

of reported Chl-ωOAHFAs to date.

ACKNOWLEDGEMENTS

Financial support from the Czech Science Foundation (Project No P206/12/0750) and Charles University in Prague (Project SVV260440) is hereby acknowledged with appreciation.

REFERENCES

[1] Haubrich, K. A. 2003. Role of vernix caseosa in the neonate: potential application in the adult population. *AACN Clin. Issues*. **14**: 457-464.

[2] Hoath, S. B., W. L. Pickens, and M. O. Visscher. 2006. The biology of vernix caseosa. *Int. J. Cosmet. Sci.* **28**: 319-333.

[3] Singh, G., and G. Archana. 2008. Unraveling the mystery of vernix caseosa. *Indian J. Dermatol.* **53**: 54-60.

[4] Schmid, R. 1939. Notizen zur Kenntnis der Vernix caseosa. *Arch. Gynakol.* **168**: 445-450.

[5] Rissmann, R., H. W. W. Groenink, A. M. Weerheim, S. B. Hoath, M. Ponec, and J. A. Bouwstra. 2006. New insights into ultrastructure, lipid composition and organization of vernix caseosa. *J. Invest. Dermatol*. **126**: 1823-1833.

[6] Kaerkkaeinen, J., T. Nikkari, S. Ruponen, and E. Haahti. 1965. Lipids of vernix caseosa. *J. Invest. Dermatol.* **44**: 333-338.

[7] Ansari, M. N., H. C. Fu, and N. Nicolaides. 1970. Fatty acids of the alkane diol diesters of vernix caseosa. *Lipids*. **5**: 279-282.

[8] Nikkari, T. 1969. The occurrence of diester waxes in human vernix caseosa and in hair

lipids of common laboratory animals. *Comp. Biochem. Physiol.* **29**: 795-803.

[9] Fu, H. C., and N. Nicolaides. 1969. The structure of alkane diols of diesters in vernix caseosa lipids. *Lipids*. **4**: 170-175.

[10] Nicolaides, N., H. C. Fu, and G. R. Rice. 1968. The skin surface lipids of man compared with those of eighteen species of animals. *J. Invest. Dermatol*. **51**: 83-89.

[11] Nikkari, T. 1974. Comparative chemistry of sebum. *J. Invest. Dermatol.* **62**: 257-267.

[12] Nicolaides, N., H. C. Fu, and M. N. Ansari. 1970. Diester waxes in surface lipids of animal skin. *Lipids*. **5**: 299-307.

[13] Yeung, D., S. Nacht, and R. E. Cover. 1981. The composition of the skin surface lipids of the gerbil. *Biochim. Biophys. Acta.* **663**: 524-535.

[14] Schmid, P. C., Y. Wedmid, and H. O. Schmid. 1978. 15-Methyl-1,2-hexadecanediol, a major constituent of hamster surface wax. *Lipids*. **13**: 825-827.

[15] Sharaf, D. M., S. J. Clark, and D. T. Downing. 1977. Skin surface lipids of the dog. *Lipids*. **12**: 786-790.

[16] Nishimaki-Mogami, T., K. Minegishi, A. Takahashi, Y. Kawasaki, Y. Kurokawa, and M. Uchiyama. 1988. Characterization of skin-surface lipids from the monkey (*Macaca fascicularis*).

Lipids. **23**: 869-877.

[17] Haahti, E. O. A., and H. M. Fales. 1967. The uropygiols: identification of the unsaponifiable constituent of a diester wax from chicken preen glands. *J. Lipid Res.* **8**: 131-137.

[18] Šubčíková, L., M. Hoskovec, V. Vrkoslav, T. Čmelíková, E. Háková, R. Míková, P. Coufal, A. Doležal, R. Plavka, and J. Cvačka. 2015. Analysis of 1,2-diol diesters in vernix caseosa by high-performance liquid chromatography - atmospheric pressure chemical ionization mass spectrometry. *J. Chromatogr. A*. **1378**: 8-18.

[19] Neises B., and W. Steglich. (1978) Simple method for the esterification of carboxylic acids. *Angew. Chem. Int. Ed. Engl*. **17**: 522-524.

[20] Stránský, K., and T. Jursík. 1996. Simple quantitative transesterification of lipids, 1. Introduction. *Fett/Lipid*. **98**: 65-71.

[21] Carvalho, F., L. T. Gauthie, D. J. Hodgson, B. Dawson, and P. H. Buist. 2005. Quantitation of hydroxylated byproduct formation in a Saccharomyces cerevisiae Δ9 desaturating system. *Org. Biomol. Chem.* **3**: 3979-3983.

[22] Corey, E. J.; and G. Schmidt. 1979. Useful procedures for the oxidation of alcohols involving pyridinium dichromate in approtic media. *Tetrahedron Lett.* **20**: 399-402.

[23] Butovich, I. A., H. Lu, A. McMahon, and J. C. Eule. 2012. Toward an animal model of

the human tear film: biochemical comparison of the mouse, canine, rabbit, and human meibomian lipidomes. *Invest. Ophthalmol. Vis. Sci*. **53**: 6881-6895.

[24] Butovich, I. A. 2013. Tear film lipids. *Exp. Eye Res.* **117**: 4-27.

[25] Mori, N., Y. Fukano, R. Arita, R. Shirakawa, K. Kawazu, M. Nakamura, and S. Amano. 2014 Rapid identification of fatty acids and (O-acyl)-ω-hydroxy fatty acids in human meibum by liquid chromatography/high-resolution mass spectrometry. *J. Chromatogr. A*. **1347**: 129-136.

[26] Nicolaides, N. 1970. Magnesium oxide as an adsorbent for the chromatographic separation of molecules according to their degree of flatness, e.g. the separation of wax esters from sterol esters. *J. Chromatogr. Sci*. **8**: 717-720.

[27] Stewart, M. E., and D. T. Downing. 1981. Separation of wax esters from steryl esters by chromatography on magnesium hydroxide. *Lipids*. **16**: 355-359.

[28] Nicolaides, N., V. G. Soukup, and E. C. Ruth. 1983. Mass spectrometric fragmentation patterns of the acetoxy and trimethylsilyl derivatives of all the positional isomers of the methyl hydroxypalmitates. *Biol. Mass Spectrom.* **10**: 441-449.

[29] Christie, W. W. Mass spectrometry of methyl esters, hydroxy fatty acids – trimethylsilyl derivatives. The Lipid Web [Internet]. 2016 [cited 2017 Jan 5]. Available from: http://www.lipidhome.co.uk/ms/methesters/me-hydroxy-2/index.htm

[30] Vrkoslav, V., E. Háková, K. Pecková, K. Urbanová, and J. Cvačka. 2011. Localization of double bonds in wax esters by high-performance liquid chromatography/atmospheric pressure chemical ionization mass spectrometry utilizing the fragmentation of acetonitrile-related adducts. *Anal. Chem*. **83**: 2978-2986.

[31] Vrkoslav, V., and J. Cvačka. 2012. Identification of the double-bond position in fatty acid methyl esters by liquid chromatography/atmospheric pressure chemical ionisation mass spectrometry. *J. Chromatog. A*. **1259**: 244-250.

[32] Háková, E., V. Vrkoslav, R. Míková, K. Schwarzová-Pecková, Z. Bosáková, and J. Cvačka. 2015. Localization of double bonds in triacylglycerols using high-performance liquid chromatography/atmospheric pressure chemical ionization ion-trap mass spectrometry. *Anal. Bioanal. Chem.* **407**: 5175-5188.

[33] Butovich, I. A., J. C. Wojtowitz, and M. Molai. 2009. Human tear film and meibum. Very long chain wax esters and (O-acyl)-omega-hydroxy fatty acids of meibum. *J. Lipid Res.* **50**: 2471-2485.

[34] Christie, W. W. 1987. The separation of molecular species of glycerolipids. *In* High-performance liquid chromatography and lipids, A practical guide. Christie, W. W., editor. Pergamon Press, Oxford. 169-210.

[35] Holčapek, M., M. Lísa, P. Jandera, and N. Kabátová. 2005. Quantitation of triacylglycerols in plant oils using HPLC with APCI-MS, evaporative light-scattering, and UV

detection. *J. Sep. Sci*. **28**: 1315-1333.

[36] Vrkoslav, V., K. Urbanová, and J. Cvačka. 2010. Analysis of wax ester molecular species by high performance liquid chromatography/atmospheric pressure chemical ionisation mass spectrometry. *J. Chromatogr. A*. **1217**: 4184-4194.

[37] Oku, H., K. Mimura, Y. Tokitsu, K. Onaga, H. Iwasaki, and I. Chinen. 2000. Biased distribution of the branched-chain fatty acids in ceramides of vernix caseosa. *Lipids*. **35**: 373-381.

[38] Hoeger, P. H., V. Schreiner, I. A. Klaassen, C. C. Enzmann, K. Friedrichs, and O. Bleck. 2002. Epidermal barrier lipids in human vernix caseosa: corresponding ceramide pattern in vernix and fetal skin. *Br. J. Dermatol*. **146**: 194-201.

[39] Stewart, M. E., and D. T. Downing. 2001. The omega-hydroxyceramides of pig epidermis are attached to corneocytes solely through omega-hydroxyl groups. *J. Lipid Res.* **42**: 1105-1110.

[40] Swartzendruber, D. C., P. W. Wertz, K. C. Madison, and D. T. Downing. 1987. Evidence that the corneocyte has a chemically bound lipid envelope. *J. Invest. Dermatol*. **88**: 709-713.

[41] Wertz, P. W., K. C. Madison, and D. T. Downing. 1989. Covalently Bound Lipids of Human Stratum Corneum. *J. Invest. Dermatol.* **92**: 109-111.

[42] Davidson, H. J., and V. J. Kuonen. 2004. The tear film and ocular mucins. *Vet. Ophthalmol.* **7**: 71-77.

[43] Nicolaides, N., and E. C. Ruth. 1982. Unusual fatty acids in the lipids of steer and human meibomian gland excreta. *Curr. Eye Res.* **2**: 93-98.

[44] Nicolaides, N., E. C. Santos, and K. Papadakis. 1984. Double-bond patterns of fatty acids and alcohols in steer and human meibomian gland lipids. *Lipids*. **19**: 264-277.

[45] Nicolaides, N., and E. C. Santos. 1985. The di- and triesters of the lipids of steer and human meibomian glands. *Lipids*. **20**: 454-467.

[46] Butovich, I. A. 2011. Lipidomics of human meibomian gland secretions: Chemistry, biophysics, and physiological role of meibomian lipids. *Prog. Lipid Res.* **50**: 278-301.

[47] Lam, S. M., L. Tong, S. S. Yong, B. Li, S. S. Chaurasia, G. Shui, and M. R. Wenk. 2011. Meibum lipid composition in Asians with dry eye disease. *PLoS One*. **6**: e24339.

[48] Chen, J. Z., K. B. Green-Church, and K. K. Nichols. 2010. Shotgun lipidomic analysis of human meibomian gland secretions with electrospray ionization tandem mass spectrometry. *Invest. Ophthalmol. Vis. Sci.* **51**: 6220-6231.

[49] Butovich, I. A., A. M. Borowiak, and J. C. Eule. 2011. Comparative HPLC-MS analysis of canine and human meibomian lipidomes: Many similarities, a few differences. *Sci. Rep.* **1**: 24.

[50] Butovich, I. A. 2011. On the presence of (O-acyl)-omega-hydroxy fatty acids and of their

esters in human meibomian gland secretions. *Invest. Ophthalmol. Vis. Sci.* **52**: 639-641.

[51] Wood, P. L., K. Scoggin, B. A. Ball, M. H. Troedsson, and E. L. Squires. 2016. Lipidomics of equine sperm and seminal plasma: Identification of amphiphilic (O-acyl)-ω-hydroxy-fatty acids. *Theriogenology*. **86**: 1212-1221.

[52] Yore, M. M., I. Syed, P. M. Moraes-Vieira, T. Zhang, M. A. Herman, E. A. Homan, R. T. Patel,, J. Lee, S. Chen, O. D. Peroni, A. S. Dhaneshwar, A. Hammarstedt, U. Smith, T. E. McGraw, A. Saghatelian, and B. B. Kahn. 2014. Discovery of a class of endogenous mammalian lipids with anti-diabetic and anti-inflammatory effects. *Cell*. **159**: 318-332.

[53] Kuda, O., M. Brezinova, M. Rombaldova, B. Slavikova, M. Posta, P. Beier, P. Janovska, J. Veleba, J. Jr. Kopecky, E. Kudova, T. Pelikanova, and J. Kopecky. 2016. Docosahexaenoic Acid-Derived Fatty Acid Esters of Hydroxy Fatty Acids (FAHFAs) With Anti-inflammatory Properties. *Diabetes*. **65**: 2580-2590.

[54] Haahti, E., T. Nikkari, A. M. Salmi, and A. L. Laaksonen. 1961. Fatty acids of vernix caseosa. *Scand. J. Clin. Lab. Inv.* **13**: 70-73.

[55] Míková, R., V. Vrkoslav, R. Hanus, E. Háková, Z. Habová, A. Doležal, R. Plavka, P. Coufal, and J. Cvačka. 2014. Newborn Boys and Girls Differ in the Lipid Composition of Vernix Caseosa. *PLoS One*. **9**: 1-8.

[56] Hauff, S., and W. Vetter. 2010. Exploring the fatty acids of vernix caseosa in form of

their methyl esters by off-line coupling of non-aqueous reversed phase high performance liquid chromatography and gas chromatography coupled to mass spectrometry. *J. Chromatogr. A*. **1217**: 8270-8278.

[57] Chen, J., K. B. Green, and K. K. Nichols. 2013. Quantitative profiling of major neutral lipid classes in human meibum by direct infusion electrospray ionization mass spectrometry. *Invest. Ophthalmol. Vis. Sci.* **54**: 5730-5753.

[58] Butovich, I. A. 2009. Cholesteryl esters as a depot for very long chain fatty acids in human meibum. *J. Lipid Res.* **50**: 501-513.

TABLES

Table 1. List of 50 abundant Chl-ωOAHFAs identified in vernix caseosa.[1]

t_R [min]	*m/z* of $[M + H]^+$	*m/z* of [ωOAHFA]$^-$	Relative peak area[2] [%]	Identification[3]
112.64	1098.02	727.66	0.53	16:1/32:2-Chl
114.50	1072.01	701.65	1.45	16:1/30:1-Chl
114.50	1072.01	701.65	0.57	14:1/32:1-Chl
116.18	1045.99	675.63	1.46	14:0/30:1-Chl
118.04	1086.02	715.66	0.68	16:1/31:1-Chl
118.04	1086.02	715.66	0.49	15:0/32:2-Chl
119.60	1126.05	755.69	0.75	18:2/32:1-Chl
119.74	1060.01	689.65	2.53	**15:0/30:1-Chl**
119.74	1060.01	689.65	1.41	13:0/32:1-Chl
119.74	1060.01	689.65	1.29	14:0/31:1-Chl
121.51	1100.04	729.68	5.33	**16:1/32:1-Chl**
121.51	1100.04	729.68	1.76	**18:1/30:1-Chl**
121.51	1100.04	729.68	0.53	14:0/34:2-Chl
122.78	1074.02	703.66	5.85	**14:0/32:1-Chl**
122.78	1074.02	703.66	0.94	16:0/30:1-Chl
122.78	1074.02	703.66	0.62	15:0/31:1-Chl
122.78	1074.02	703.66	0.50	16:1/30:0-Chl
123.97	1114.05	743.69	1.27	17:1/32:1-Chl
123.97	1114.05	743.69	0.72	16:1/33:1-Chl
123.97	1114.05	743.69	0.64	15:0/34:2-Chl
123.97	1114.05	743.69	0.60	18:1/31:1-Chl
124.24	1074.02	703.66	1.17	14:0/32:1-Chl
125.33	1048.01	677.65	0.81	14:0/30:0-Chl
125.58	1088.04	717.68	6.14	**15:0/32:1-Chl**
125.58	1088.04	717.68	0.81	14:0/33:1-Chl
126.41	1088.04	717.68	0.90	15:0/32:1-Chl
126.89	1128.07	757.71	5.70	**18:1/32:1-Chl**
126.89	1128.07	757.71	1.97	**16:1/34:1-Chl**
127.77	1062.02	691.66	0.80	15:0/30:0-Chl
128.06	1102.05	731.69	4.33	**16:0/32:1-Chl**
128.06	1102.05	731.69	2.38	**14:0/34:1-Chl**
128.06	1102.05	731.69	0.78	15:0/33:1-Chl
128.06	1102.05	731.69	0.74	18:1/30:0-Chl
128.94	1102.05	731.69	1.71	**16:0/32:1-Chl**
128.94	1102.05	731.69	0.62	18:1/30:0-Chl
128.94	1102.05	731.69	0.52	14:0/34:1-Chl
128.94	1142.08	771.72	0.67	18:1/33:1-Chl
128.94	1142.08	771.72	0.56	17:1/34:1-Chl
130.10	1076.04	705.68	1.02	14:0/32:0-Chl
130.10	1076.04	705.68	0.58	16:0/30:0-Chl
130.30	1116.07	745.71	0.48	18:1/31:0-Chl
130.30	1116.07	745.71	2.36	**15:0/34:1-Chl**
130.30	1116.07	745.71	1.74	**17:0/32:1-Chl**

131.14	1156.10	785.74	2.37	**18:1/34:1-Chl**
132.32	1090.05	719.69	0.96	15:0/32:0-Chl
132.44	1130.08	759.72	1.77	**16:0/34:1-Chl**
132.44	1130.08	759.72	0.77	18:1/32:0-Chl
133.34	1130.08	759.72	0.52	16:0/34:1-Chl
134.38	1144.10	773.74	0.70	17:0/34:1-Chl
134.38	1104.07	733.71	0.75	16:0/32:0-Chl

[1] A full list of all 306 Chl-ωOAHFAs can be found in the Supplemental Table S1.

[2] The values of relative peak area were calculated in two steps. In the first step, full scan trace in the positive ion mode was used to create reconstructed ion chromatograms for individual *m/z* values ($[M + H]^+$). The peak areas were integrated and put in relative values. In the second step, relative proportions of the isomers within each peak were established from relative intensities of the deprotonated fatty acid ions in the negative ion MS/MS spectra.

[3] Molecular species with the relative peak area higher than 1.5 % are bolded.

JOURNAL OF LIPID RESEARCH

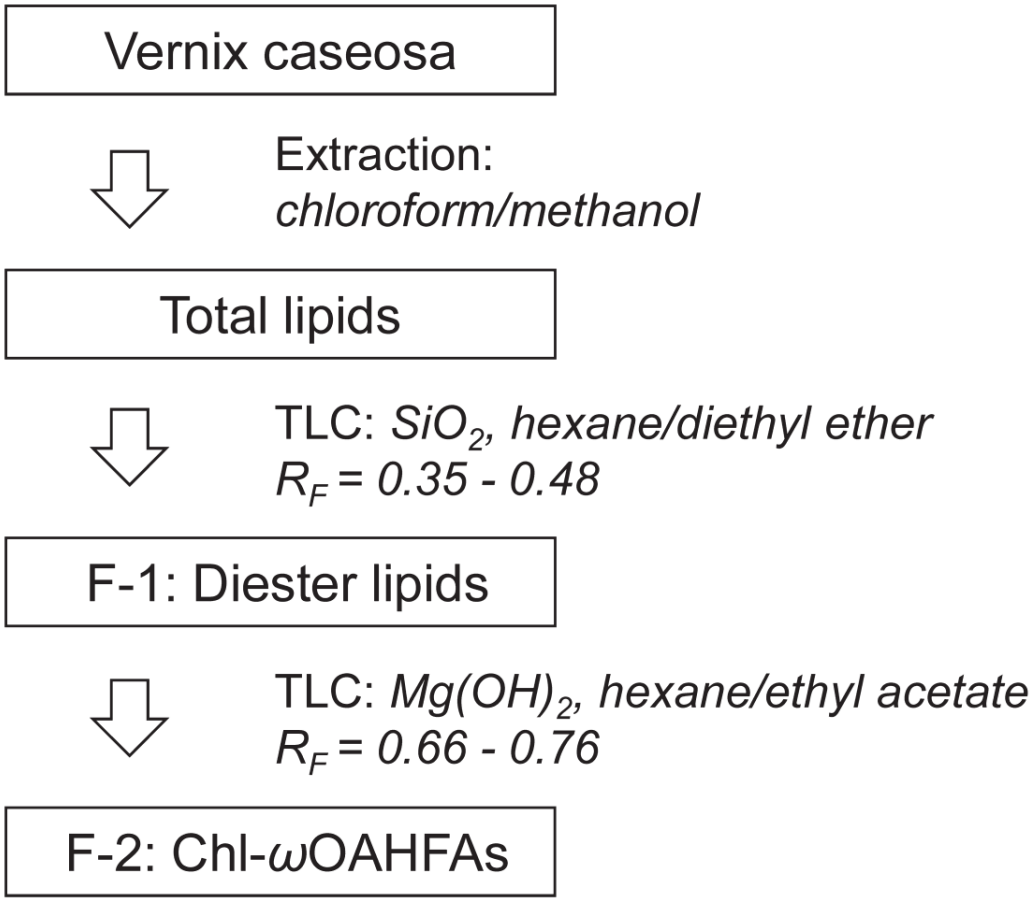

Figure 1. Scheme of the isolation and fractionation procedure.

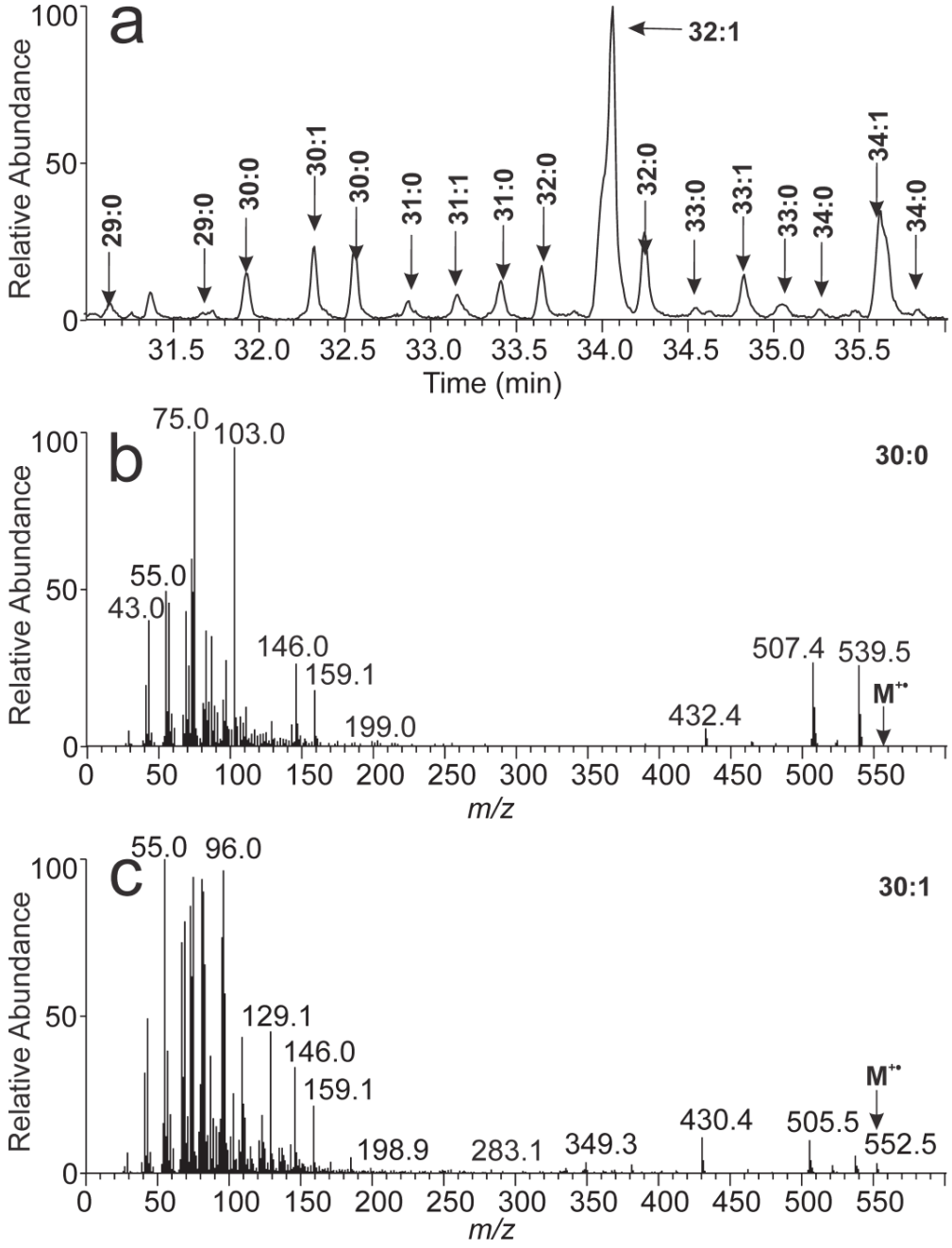

Figure 2. A section of GC/MS chromatogram reconstructed for *m/z* 75 showing TMS derivatives of HFAMEs from Chl-*ω*OAHFAs (a). The EI-MS (70 eV) spectrum of TMS derivative of HFAME 30:0 (t_R = 31.9 min) (b). The EI-MS (70 eV) spectrum of TMS derivative of HFAME 30:1 (t_R = 32.3 min) (c).

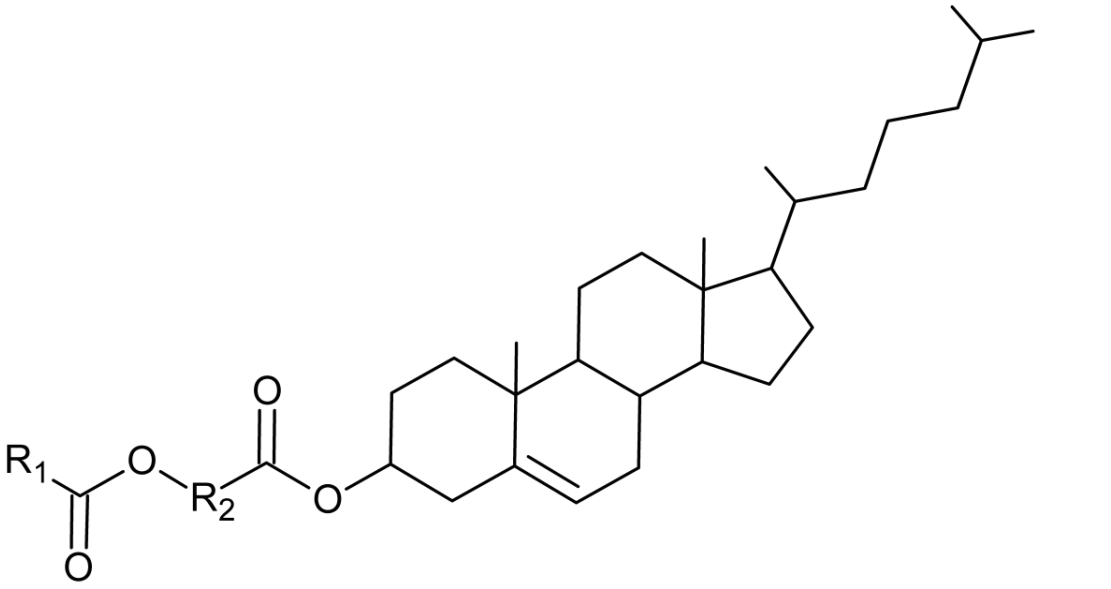

Figure 3. The general structure of Chl-ωOAHFAs. (R_1: aliphatic chain of FA, R_2: aliphatic chain of HFA).

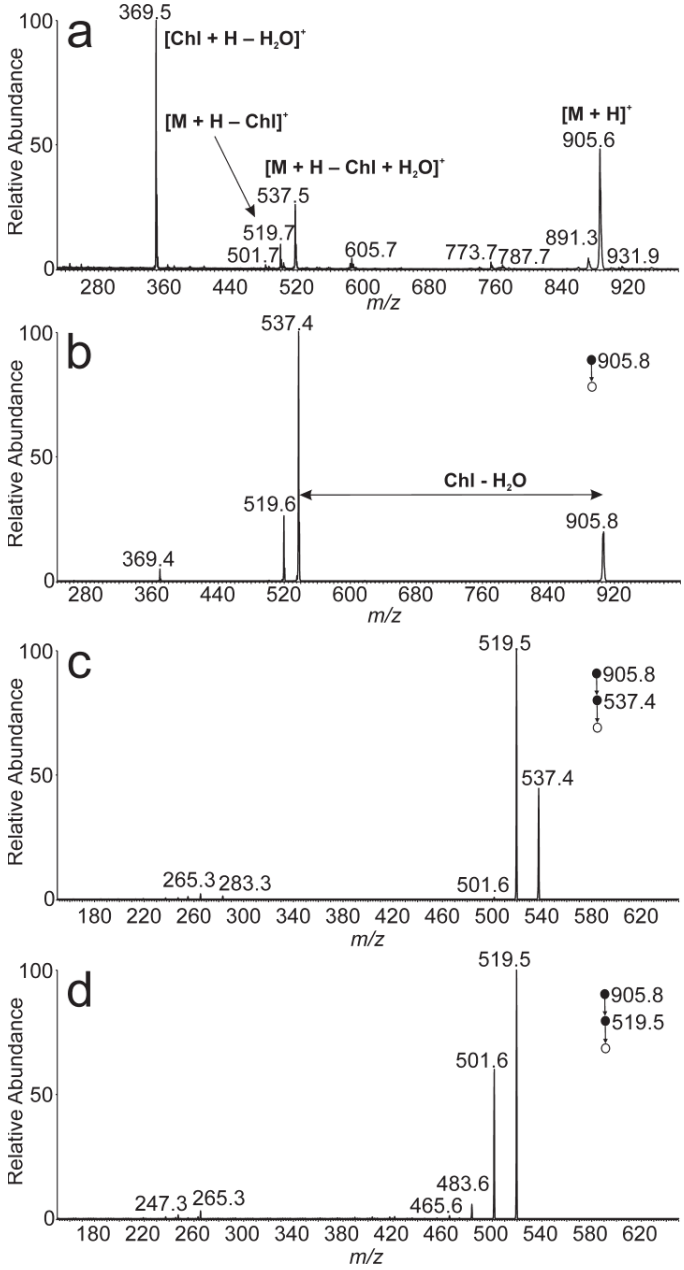

Figure 4. APCI mass spectra of 18:1(*n*-9)/16:0-Chl in the positive ion mode. Full scan spectrum (a). CID MS^2 spectrum of the protonated molecule (*m/z* 905.8; normalized collision energy 15 %) (b). CID MS^3 spectrum of $[M + H – Chl + H_2O]^+$ (*m/z* 537.4; normalized collision energy 16 %) (c). CID MS^3 spectrum of $[M + H – Chl]^+$ (*m/z* 519.5; normalized collision energy 16 %) (d). The chloroform solution (1 mg/ml) delivered by a syringe pump (5 µl/min) was mixed with acetonitrile:ethyl acetate (45:55, by vol.) flowing at 150 µl/min. The mixture was directly infused into the ion source.

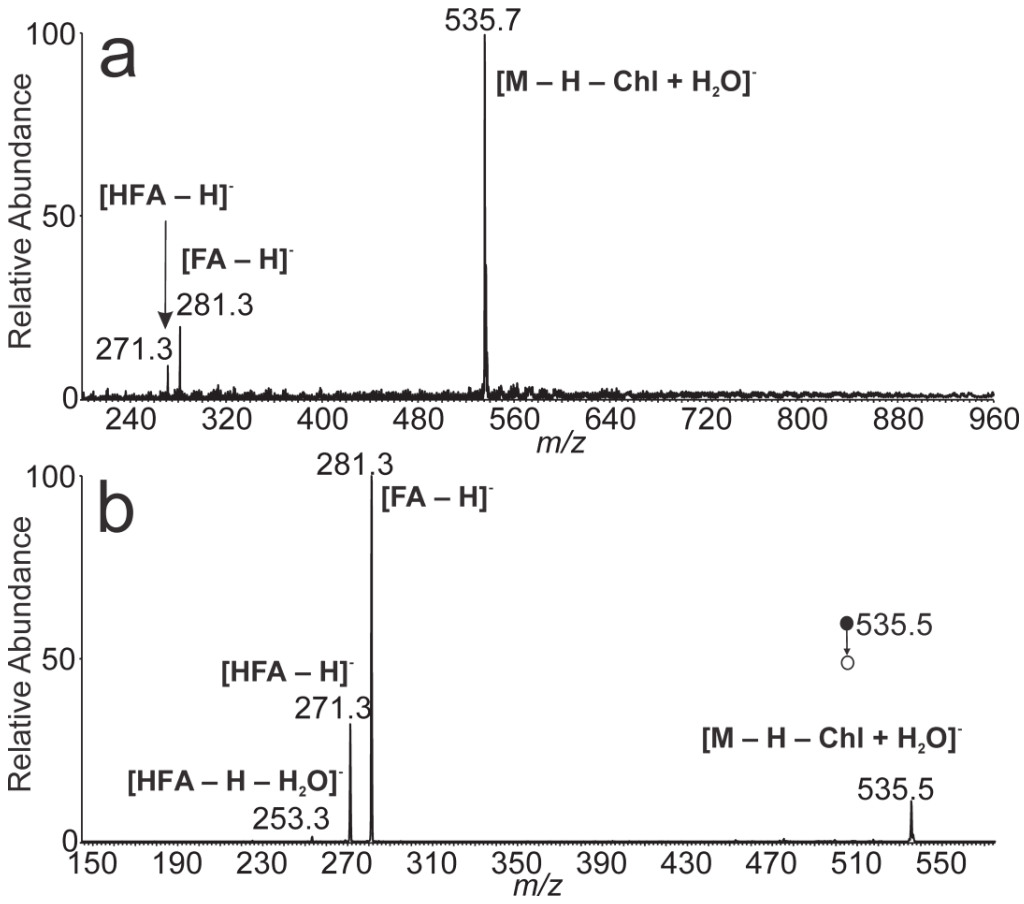

Figure 5. APCI mass spectra of 18:1(*n*-9)/16:0-Chl in the negative ion mode. Full scan spectrum (a). CID MS^2 spectrum of $[M - H - Chl + H_2O]^-$ (*m/z* 535.5; normalized collision energy 15 %) (b). The chloroform solution (1 mg/ml) delivered by a syringe pump (5 µl/min) was mixed with acetonitrile:ethyl acetate (45:55, by vol.) flowing at 150 µl/min. The mixture was directly infused into the ion source.

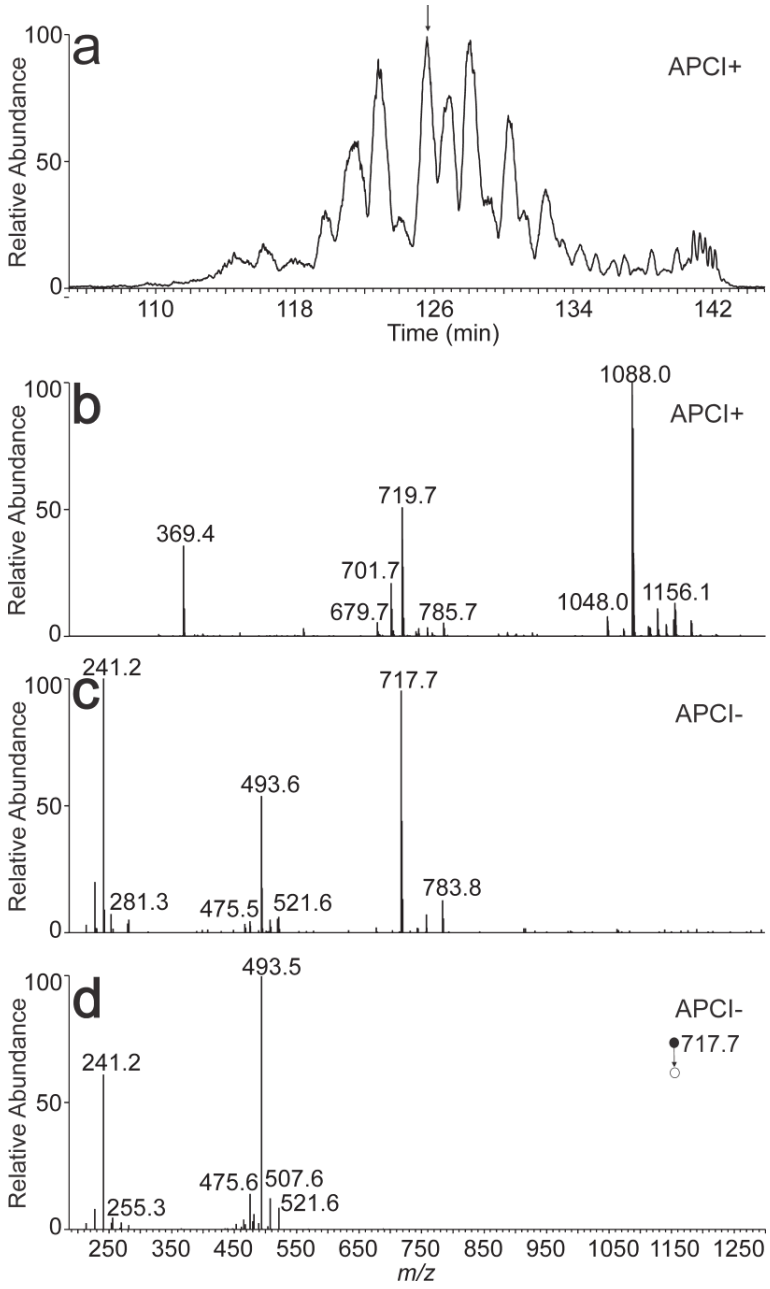

Figure 6. Positive ion base-peak chromatogram (*m/z* 1000 – 1300) of Chl-*ω*OAHFAs isolated from vernix caseosa (a) and the APCI mass spectra used for the structure elucidation of a species with t_R= 126.0 min (b-d). Full scan spectrum in the positive ion mode (b). Full scan spectrum in the negative ion mode (c). CID MS^2 spectrum of *m/z* 717.7 in the negative ion mode (normalized collision energy 21.5 %) (d).

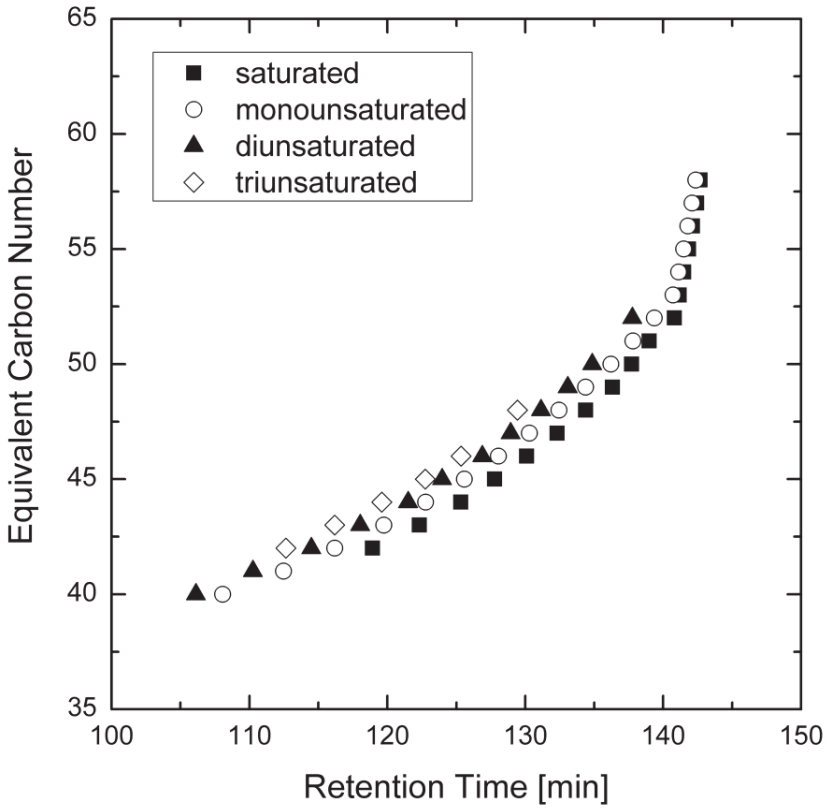

Figure 7. Plot of calculated equivalent carbon number (ECN) values vs. retention times for the Chl-ωOAHFAs identified in vernix caseosa (ECN=CN-2DB where CN is the total number of carbons and DB is the total number of double bonds in the ωOAHFA part of the molecules).

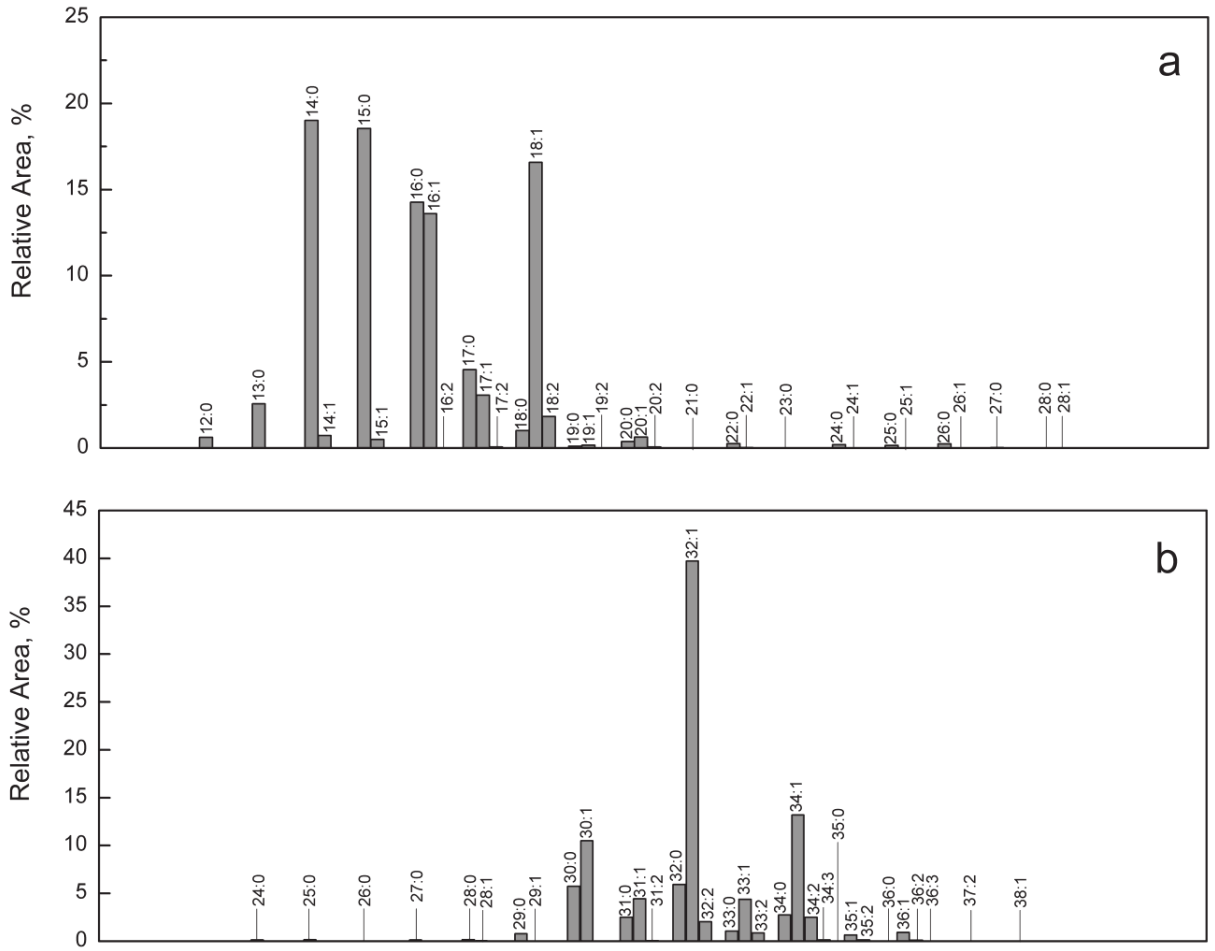

Figure 8. Histogram showing relative proportions of FAs (a) and ωHFAs (b) in Chl-ωOAHFAs from vernix caseosa. The proportions were calculated using HPLC/MS data given in Supplemental Table S1 (extended version of Table 1).

- Proceeding I -

P34 SEPARATION OF NONPOLAR LIPIDS FROM VERNIX CASEOSA

Eva Háková[1,2], Radka Míková[1,2], Vladimír Vrkoslav[2], Antonín Doležal[3], Richard Plavka[3], Josef Cvačka[2]

[1]Department of Analytical Chemistry, Faculty of Science, Charles University in Prague, Prague, Czech Republic
[2]Institute of Organic Chemistry and Biochemistry v.v.i., Academy of Sciences of the Czech Republic, Prague, Czech Republic
[3]Department of Obstetrics and Gynaecology, General Faculty Hospital and 1[th]Faculty of Medicine, Charles University in Prague, Prague, Czech Republic

Summary
The aim of this work is to develop a separation method for characterization of unknown nonpolar lipids in vernix caseosa. Here we optimized adsorption chromatography coupled to mass spectrometry detection with exact mass measurement. A long silica gel column (250 + 250 x 4.6 mm, particle size: 5μm) provided the best separation of nonpolar lipids present in vernix caseosa.

1 Introduction

Vernix caseosa is a multicomponent mixture, which is consisted of water (80 %) and proteins and lipids roughly in the same proportion (10 % each). This uniquely human material starts to be formed in the third trimester of pregnancy and is present on the skin of newborns after delivery [1, 2]. The lipids of vernix caseosa are classified as barrier lipids (cholesterol, free fatty acids, phospholipids, ceramides) and lipids originated from fetal sebaceous glands. Nonpolar lipids such as sterol esters, wax esters and triacylglycerols are dominant components of vernix caseosa [2, 3].

2 Experimental

2.1 Preparation of samples

Lipids from vernix caseosa were extracted by chloroform:methanol (2:1, v/v). A large-scale separation of lipids was carried out using classical low pressure column chromatography with 4.7 grams of lipids isolated from vernix caseosa. A silica gel column (length of glass column 41 cm, diam. 4.48 cm; particle size: 60-120 μm) with mobile phase hexane/diethyl ether gradient (from 1:99 to 50:50, v/v) was used to separate total lipid extract into fractions.

2.2 HPLC/APCI- MS/MS

The experiments were performed using LTQ Orbitrap XL hybrid FT mass spectrometer equipped with Ion Max source with APCI probe installed (Thermo Fisher Scientific, San Jose, CA, USA) and coupled to HPLC, which was consisted of a Rheos 2200 quaternary gradient pump (Flux Instruments, Reinach, Schwitzerland), PAL HTS autosampler (CTC Analytics, Zwingen, Schwitzerland); the system was controlled by Xcalibur software (Thermo Fisher Scientific). Samples were separated

using Acquity HILIC column (50 x 2.1 mm, particle size: 1.7 µm; Waters, Milford, MA, USA) or Spherisorb column (250 + 250 x 4.6 mm, particle size: 5 µm; Waters, Milford, MA, USA) at 30 °C. The gradient program for Acquity HILIC column, phase A (hexane), B (hexane/propan-2-ol, 96:4, v/v): 0 min: 99% A/1% B; 20 min: 85% A/15% B and 0 min: 99% A/1% B; 20 min: 66% A/34% B. The gradient program for Spherisorb column, phase A (hexane), B (hexane/propan-2-ol, 96:4, v/v): 0 min: 96% A/4% B; 60 min: 53% A/47% B. The mobile phase flow rate was 1.0 mL/min and the injected volume of samples was 10 µl in each chromatography. The APCI vaporiser and heated capillary temperatures were set to 270 °C and 170 °C, respectively. Nitrogen served both as the sheath and auxiliary gas at a flow rate of 15 and 17 arbitrary units, respectively. The MS spectra of the positively charged ions were recorded from 250 to 2000 *m/z*.

3 Results and Discussion

The total lipid extract was separated into 30 fractions. In this work we focused on fractions no. 12 and no. 13, i.e., those containing lipids of low or moderate polarities.

We compared two silica-based analytical columns for their ability to separate neutral lipids in vernix caseosa fractions. For each column the mobile phase gradient was optimized to provide optimum chromatographic resolution. The Acquity HILIC column allowed for short analysis time, but the column was not able to sufficiently separate lipid components of the sample (Fig. 1). Significantly better results were achieved with two Spherisorb columns connected in series (Fig. 2). The chromatographic peaks corresponded to various lipid classes. They were characterized using high resolution/accurate mass measurement mass spectrometry. General elemental formulas for lipid classes were obtained in this way. Fraction no. 12 was found to contain lipids with four oxygens, mostly diol diesters, and other lipid classes. This fraction also contained 2,3-oxosqualne (confirmed by GC/MS) and unknown lipids with five oxygens. In the fraction no. 13 we identified 2,3-oxosqualne, diol diesters and lipids with four and five oxygens too, but these lipids exhibited different retention times. Therefore, we hypothesize that these lipids have different structure than those in the fraction no. 12.

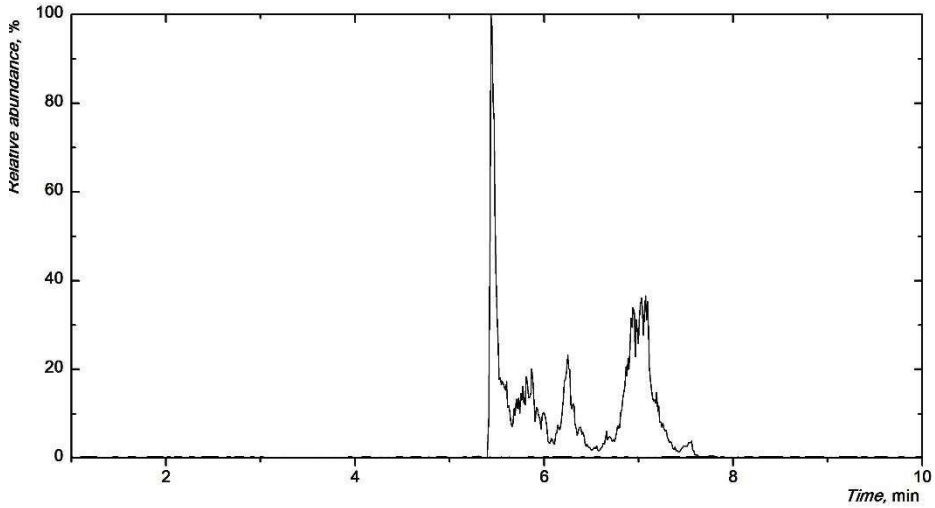

Fig. 1. Base peak chromatogram of the fraction no. 12 obtained using Acquity HILIC column (50 x 2.1 mm, particle size 1.7 μm).

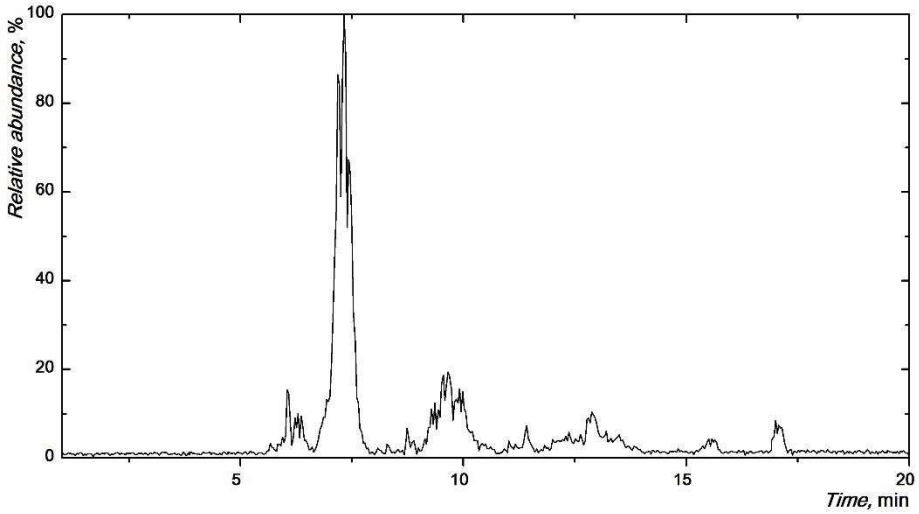

Fig. 2. Base peak chromatogram of the fraction no. 12 obtained using Spherisorb column (250 + 250 x 4.6 mm, particle size 5 μm).

4 Conclusions

Good separation of lipid classes of similar polarities and structures in complex lipid matrix of vernix caseosa was achieved using a 500 mm long silica gel column with a conventional diameter of 4.6 mm packed with 5 μm-particles. Attempts to use short column with small diameter particles were not successful. The lipids were characterized by their elemental formulas. The next experiments based on tandem mass spectrometry will be focused on disclosing their chemical structures.

Acknowledgement

This work was financial supported by the Czech Science Foundation (Project No. P206/12/0750) and Charles University in Prague (Project SVV).

References
[1] Hoat, S.B., Maibach, H. I., *Neonatal Skin, Structure and Function*. 2nd ed. Marcel Dekker, New York 2003.
[2] Rissmann, R., Groenink, H. W. W., Weerheim, A. M. et al., *J. Invest. Dermatol.* 2006, 126, 1823-1833.
[3] Kärkakäinen, J., Nikkari, T., Ruponen, S., Haahti, E., *J. Invest. Dermatol.* 1965, 44, 333-338.

P35 PREPARATION OF LOW-COST MICROFLUIDIC DEVICES BASED ON FILTER AND BAKERY PAPERS BY USING AN OFFICE LAMINATOR

Lenka Hárendarčíková, Jan Petr

Regional Centre of Advanced Technologies and Materials, Department of Analytical Chemistry, Palacký University in Olomouc, Olomouc, Czech Republic
harendarcikova.lenka@gmail.com

Summary
In our work, we developed a new paper-based microfluidic device for determination of active content of common drugs. The device represents a fast, cheap and portable alternative for common analytical techniques used in forensic analysis. The main problem of injection into four parallel channels was overcame using a bakery paper integrated into the device.

1 Introduction

Miniaturization of analytical techniques is recently common and significant topic in analytical chemistry. The main aim is in enabling fast and cheap determination of water and food quality, medical diagnostics etc. without using instrumental devices. This could be very profitable not only for developed countries but also for the third world countries where the needs for low-cost analysis increase year by year. Martinez et al. [1] and Carillo et al. [2] described "paper-tape-based microfluidic devices" (μPADs), which can be easily produced for many purposes using filtration papers or nitrocellulose membranes.

In our work, we want to design microfluidic "paper-foil-based device" by using an office laminator, which will be able to determine active content of some mostly used drugs in medicine (for forensic screening purposes). Similar approach was presented recently by Cassano et al. [3] who called this device as "laminated paper-based analytical devices" (LPADs) and also by our group [4].

- Proceeding II -

Analysis of low abundant lipids in vernix caseosa using chromatographic methods and mass spectrometry

Eva Háková[a, b, *], Radka Míková[a], Vladimír Vrkoslav[b], Richard Plavka[c], Josef Cvačka[b]

[a] *Charles University in Prague, Faculty of Science, Department of Analytical Chemistry, Hlavova 2030/8, 128 43 Prague 2, Czech Republic* ✉ *hakova@uochb.cas.cz*
[b] *Institute of Organic Chemistry and Biochemistry AS CR, v.v.i., Team of Mass Spectrometry, Flemingovo nám. 2, 166 10 Prague 6, Czech Republic*
[c] *Charles University in Prague, Department of Obstetrics and Gynaecology, General Faculty Hospital and 1th Faculty of Medicine, Apolinářská 18, 128 51 Prague 2, Czech Republic*

Keywords
gas chromatography
high performance liquid chromatography
mass spectrometry
vernix caseosa

Abstract
The aim of this work is to develop a separation method for characterization of unknown lipids in vernix caseosa. We focused on very low abundant lipids which have not been previously described in vernix caseosa. The total lipid extract was fractionated using low pressure normal phase liquid chromatography to obtain sub-fractions. The sub-fractions were further separated in high performance liquid chromatography mode to isolate classes of lipids. This procedure enabled us to characterise lipid classes by mass spectrometry and identify one of the lipid class as acyl-ceramides with non-hydroxylated fatty acids.

1. Introduction

Vernix caseosa is a multicomponent mixture, which is consisted of water (80 %) and proteins and lipids roughly in the same proportion (10 % each). This unique human material starts to be formed in the third trimester of a pregnancy and is present on the skin of newborns after a delivery [1, 2]. Vernix caseosa has a number of not fully understood functions. It works mainly to protect a fetus from the maceration in the amniotic fluid, protects a newborn during the birth from bacteria that populate the genital area of a woman and moisturizes the skin of the fetus [2]. It was found that vernix caseosa has a potential to be used in medicine because of its healing and antibacterial effects [3, 4].

The lipids of vernix caseosa are classified as barrier lipids (cholesterol, free fatty acids, phospholipids, ceramides) and nonpolar lipids such as sterol esters, wax esters and triacylglycerols which are originated from fetal sebaceous glands. These nonpolar lipids are also the main components of vernix caseosa lipids [5, 6].

Ceramides are the largest component of polar lipids in vernix caseosa. Nine types of ceramides have been identified so far using high performance thin layer chromatography in vernix caseosa and they were characterized by nuclear magnetic resonance and gas chromatography after their conversion to fatty acid methyl esters [7]. The molecular species of intact ceramides of vernix caseosa have not been described in detail yet. Rabionet et al. in 2003 published a presence 1-O-acylceramides with non-hydroxylated fatty acids in stratum corneum [8]. However, this type of ceramides has not been described in vernix caseosa, where other similar types of ceramides (α-OH-hydroxyacid/dihydrosphingosine ceramides) exist [7].

The present work describes a multidimensional separation of low abundant lipids. We hypothesise on the basis of the chromatographic behaviour, elemental formulae and composition of fatty acids after transesterification reaction that one of the investigated low abundant lipid sub-fraction corresponds to acyl-ceramides with non-hydroxylated fatty acids.

2. Experimental

2.1 Reagents and chemicals

Mass spectrometry grade methanol, hexane and propan-2-ol (Sigma-Aldrich) were used as received. Diethyl ether, chloroform (both from Penta, Czech Republic) and acetyl chloride (Fluka) were distilled in glass from analytical-grade solvents. Sodium methoxide was purchased from Sigma-Aldrich and silver carbonate was from Lachema (Brno, Czech Republic). Silica gel (10–100 μm, water content 10.3 %) was obtained from Merck and was activated according to Pitra et al. [9].

2.2 Sample collecting

Healthy male and female subjects delivered at full term were included in this study. Vernix caseosa samples (1–2 g) were collected immediately after the delivery into glass vials and stored at –25 °C. The exact location of sampling (back, buttocks, groins, legs, arms) varied depending on the vernix caseosa layer thickness. Blood contaminated samples were discarded. The samples were collected with written informed parental consent and the work was approved by the Ethics Committee of the General University Hospital, Prague (910/09 S-IV); the study was performed according to the Declaration of Helsinki.

2.3 Lipid extraction and separation of lipid classes

Lipids from vernix caseosa were extracted by chloroform:methanol (2:1, v/v). A large-scale separation of lipids was carried out using classical low pressure column chromatography with 4.7 grams of lipids isolated from vernix caseosa.

A silica gel column (length of glass column 41 cm, diam. 4.48 cm; particle size: 60–120 μm) with mobile phase hexane/diethyl ether gradient (from 1:99 to 50:50, v/v) was used to separate total lipid extract into fractions. The experiments were performed using LTQ Orbitrap XL hybrid FT mass spectrometer equipped with Ion Max source with ESI and APCI probe installed (Thermo Fisher Scientific) and coupled to HPLC, which was consisted of a Rheos 2200 quaternary gradient pump (Flux Instruments, Reinach, Schwitzerland), PAL HTS autosampler (CTC Analytics, Zwingen, Schwitzerland); the system was controlled by Xcalibur software (Thermo Fisher Scientific). The direct injection into ESI source was used for 30 fractions. The parameters of ESI source: the heated capillary temperature was set to 275 °C. Nitrogen served both as the sheath gas at a flow rate of 35 arbitrary units. The MS spectra of the positively charged ions were recorded from 150 to 2000 *m/z.* The sample of the fraction no. 23 was separated using Spherisorb column (250 + 250×4.6 mm, particle size: 5 μm; Waters) at 30 °C. The gradient program, phase A (hexane), B (hexane/propan-2-ol, 96:4, v/v): 0 min: 80% A/-20% B; 30 min: 71% A/29% B; 60 min: 53%A/47%B. The mobile phase flow rate was 1.0 mL/min and the injected volume of samples was 10 μl in each chromatography. The APCI vaporiser and heated capillary temperatures were set to 270 °C and 170 °C, respectively. Nitrogen served both as the sheath and auxiliary gas at a flow rate of 15 and 17 arbitrary units, respectively. The MS spectra of the positively charged ions were recorded from 250 to 2000 *m/z*.

2.4 Transesterification and GC/MS of fatty acid methyl esters

Lipids were transesterified using methods described by Stránský et al. [10] (for ester-linked fatty acids) and Oku et al. [7] (for amide-linked fatty acids). Fatty acid methyl esters were analyzed using an Agilent 6890N gas chromatograph coupled to a 5975B MSD quadrupole mass spectrometer and equipped with a fused silica capillary column Rxi-5ms (Restek). The carrier gas was helium at 1.0 mL/min. The injector was held at 230 °C and operated with a split ration 10:1; 2 μL of samples solution (hexan or chloroform:methanol (2:3, v/v)) was injected. The temperature program: 140 °C (0 min) to 330 °C (47 min); total run time was 47 min. 70 eV EI mass spectra were recorded in the mass range of 25–800 u; 4 min solvent delay was used. Temperatures of the transfer line, ion source and quadrupole were 280 °C, 230 °C and 150 °C, respectively. The chromatographic peaks representing fatty acid methyl esters were identified based on the presence of *m/z* 74 and *m/z* 87 in their mass spectra.

3. Results and discussion

The total lipid extract was separated into 30 fractions (mainly nonpolar lipids) by low pressure column chromatography. Due to the high complexity of the investigated material most of the fractions were mixtures as evident from TLC and

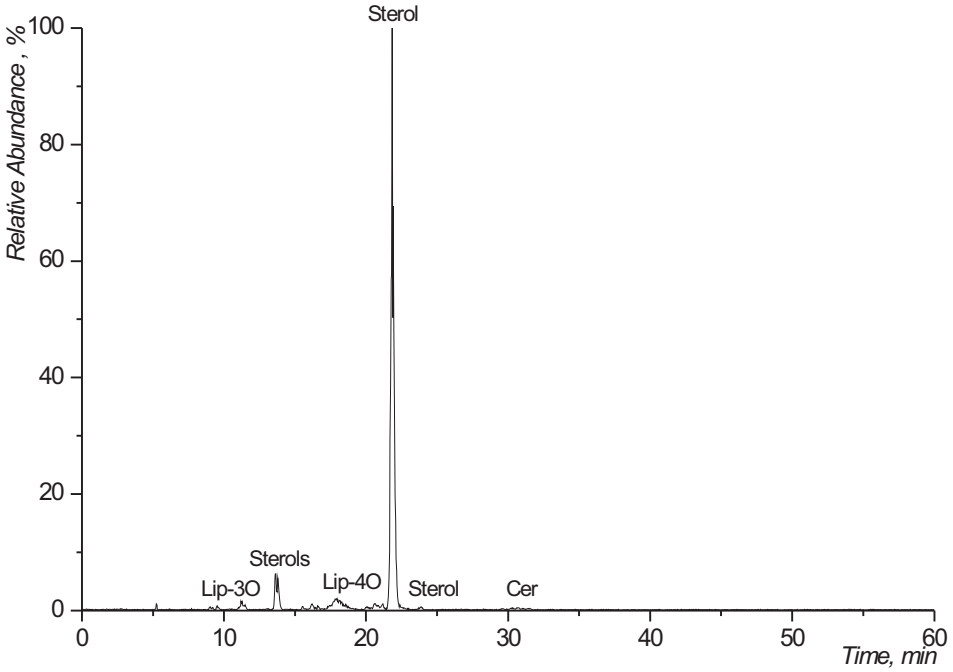

Fig. 1. NP-HPLC/MS base peak chromatogram of the fraction no. 23.

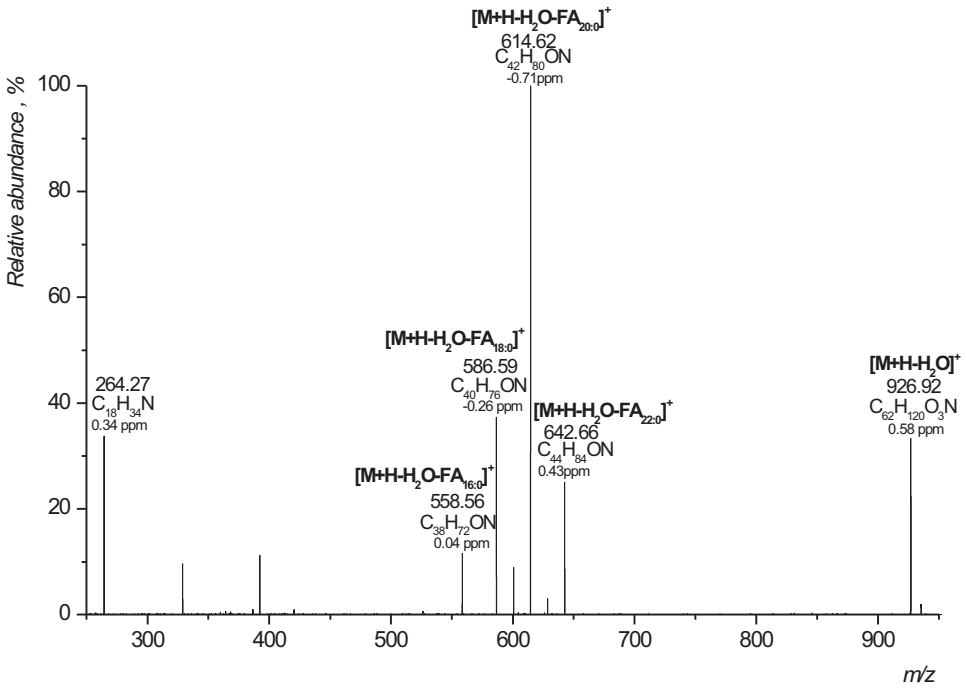

Fig. 2. APCI-MS/MS spectrum of dehydrated protonated molecule of an acyl-ceramide (M_{mi} = = 943.93 Da).

MS with direct infusion into the ESI source. In this work we focused on one particular fraction (F 23) containing several unknown lipid classes. In the next step we optimized high performance liquid chromatography method for separation of all lipid classes present in this fraction. The base peak chromatogram recorded under optimized chromatographic conditions is shown in Fig. 1; a good separation of individual lipid classes was achieved. The lipids were characterized using high resolution/accurate mass measurement mass spectrometry. General elemental formulas for lipid classes were obtained in this way. We detected lipids with three and four oxygens, sterols, and lipids with one nitrogen atom and four oxygens. We used this chromatographic system for a semi-preparative isolation of individual lipid classes and collected a sub-fraction of nitrogen-containing lipids. We hypothesized that these lipids could be structurally related to ceramides. The identification was supported by experiments based on transesterification reaction carried out in two different ways to cleave either ester-linked fatty acids or both ester and amide-linked fatty acids. Mainly saturated fatty acid methyl esters were observed in GC/MS data – for both procedures. An ESI-MS analysis of transesterifid samples made it possible to characterize remaining parts of the lipid molecules. We also employed tandem mass spectrometry and fragmented intact lipids (dehydrated protonated molecule $[M+H-H_2O]^+$, which was the spectrum base peak); the APCI-MS/MS spectrum is shown in Fig. 2. The ions at *m/z* 558.56, 586.59, 614.62 and 642.66 were rationalized as products of neutral losses of fatty acids (FA) from the parent ion, thus marked as $[M+H-H_2O-FA_{16:0}]^+$, $[M+H-H_2O-FA_{18:0}]^+$, $[M+H-H_2O-FA_{20:0}]^+$ and $[M+H-H_2O-FA_{22:0}]^+$, respectively. The other important peak *m/z* 264.27 was identified as dehydrated sphingosine. This fragmentised spectrum indicated presence of multiple isobaric species. These spectra also supported the hypothesis of acyl-ceramides with non-hydroxylated fatty acids.

4. Conclusions

Vernix caseosa is a biological material which is known for its high complexity. Therefore, the identification of new and low abundant components requires more separation steps. High resolution mass spectrometry makes it possible to determine elemental composition of the lipids in each chromatographic peak. The transesterification reaction helps to conclude the lipid structure because it brings detailed view of the composition of products of hydrolysis. The aforementioned method of analysis was used to discover and identify acyl-ceramides with non-hydroxylated fatty acids in vernix caseosa.

Acknowledgments

This work was supported by the Czech Science Foundation (Project No. P206/12/0750) and Charles University in Prague (Project No. SVV260205).

References

[1] Hoat S.B.: *Neonatal Skin, Structure and Function.* 2nd ed. New York, Marcel Dekker 2003.
[2] Pickens W.L., Warner R.R., Boissy Y.L., Boissy R.E., Hoath S.B.: *J. Invest. Dermatol.* **115** (2000), 875–881.
[3] Tollin M., Bergsson G., Kai-Larsen Y., Lengqvist J., Sjövall J., Griffiths W., Skúladóttir G.V., Haraldson Á., Jörnvall H., Gudmundsso G.H., Agerberth B.: *Cell. Mol. Life Sci.* **62** (2005), 2390–2399.
[4] Singh G.: *Indian J. Dermatol.* **53** (2008), 54–60.
[5] Kärkakäinen, J., Nikkari, T., Ruponen, S., Haahti, E.: *J. Invest. Dermatol.* **44** (1965), 333–338.
[6] Rissmann R., Groenink H.W.W., Weerheim A.M., Boath S.B., Ponec M., Bouwstra J.A.: *J. Invest. Dermatol.* **126** (2006), 1823–1833.
[7] Oku H., Mimura K., Tokitsu Y., Onaga K., Iwasaki H., Chinen I.: *Lipids* **35** (2000), 373–381.
[8] Rabionet M., Bayerle A., Marsching Ch., Jennemann R., Gröne H.J., Yildiz Y., Wachten D., Shaw W., Shayman J.A., Sandhoff R.: *J. Lipid Res.* **54** (2013), 3312–3321.
[9] Pitra J., Štěrba J.: *Chem. Listy* **56** (1962), 544.
[10] Stránský K., Jursik T.: *Eur. J. Lipid Sci. Technol.* **98** (1996), 65–71.

SUMMARY AND CONCLUSION

The aim of the research summarized in this Thesis was to contribute to the knowledge about the lipid composition of vernix caseosa. For this purpose, it was necessary to develop and optimize separation methods and couple them with mass spectrometry.

The main part of my Ph.D. project was to find, identify and characterize new lipid classes. A new multistep isolation method for low abundant lipids present in vernix caseosa has been developed. This method with TLC and NP-HPLC steps made it possible to isolate 1-*O*-acylceramides from vernix caseosa for the first time. The characterization by RP-HPLC/MS^3 uncovered more than 2,000 molecular species in this lipid subclass. Cholesteryl esters of ω-(*O*-acyl)-hydroxy fatty acids were the next lipid class which was newly identified and characterized in vernix caseosa.

The method for localization of DBs using $C_3H_5N^{+\bullet}$ adducts formed in the presence of acetonitrile in the APCI source developed in our laboratory was applied for the detailed characterization of TGs in vernix caseosa and olive oil. The data from vernix TGs analysis were interpreted only partially because of its considerable complexity. This method was also applied for characterizing 1,2-DDEs, where mostly *n*-7, *n*-9, and *n*-5 positions of DBs were detected.

AMPP derivatization reaction was used for the study of branched acyl chains in TGs. The data show methyl-branching in *iso*-, *anteiso*- and other uncommon positions.

Transesterification of the whole lipidome revealed that vernix caseosa consists of at least 167 distinct FAME species. This study also confirmed that the production of vernix caseosa lipids is affected by the gender of newborns.

This work demonstrates that the analysis of intact lipid molecule is challenging because of the presence of a large number of molecular species in each lipid class or subclass, their variety in the length, number and position of DBs and methyl-branching on acyl chains. Moreover, many low abundant lipid classes are still waiting to be discovered. Our publications focusing on the characterization of intact lipids in vernix caseosa belong to the first of their type. Therefore, future research should be focused on new lipid classes to complete our knowledge about vernix caseosa lipidome. Such knowledge is important for understanding biology of this unique biofilm and for developing new ways of treatment for very preterm babies lacking functional skin or people with serious skin injuries or diseases.

REFERENCES

1. Han, X.L. and R.W. Gross, *Global Analyses of Cellular Lipidomes Directly from Crude Extracts of Biological Samples by ESI Mass Spectrometry: A Bridge to Lipidomics*. Journal of Lipid Research, 2003. **44**(6): p. 1071-1079.

2. Han, X., *Lipids and Lipidomics*, in *Lipidomics*. 2016, John Wiley & Sons, Inc. p. 1-20.

3. Brown, H.A. and R.C. Murphy, *Working Towards an Exegesis for Lipids in Niology.* Nature Chemical Biology, 2009. **5**(9): p. 602-606.

4. van Meer, G., *Cellular Lipidomics*. Embo Journal, 2005. **24**(18): p. 3159-3165.

5. Han, X.L., *Lipidomics: Developments and Applications Preface.* Journal of Chromatography B-Analytical Technologies in the Biomedical and Life Sciences, 2009. **877**(26): p. 2663-2663.

6. Blanksby, S.J. and T.W. Mitchell, *Advances in Mass Spectrometry for Lipidomics.* Annual Review of Analytical Chemistry, Vol 3, 2010. **3**: p. 433-465.

7. Ekroos, K., *Lipidomics Perspective: From Molecular Lipidomics to Validated Clinical Diagnostics*, in *Lipidomics*. 2012, Wiley-VCH Verlag GmbH & Co. KGaA. p. 1-19.

8. Fahy, E., et al., *Lipid Classification, Structures and Tools*. Biochimica Et Biophysica Acta-Molecular and Cell Biology of Lipids, 2011. **1811**(11): p. 637-647.

9. Fahy, E., et al., *A Comprehensive Classification System for Lipids.* Journal of Lipid Research, 2005. **46**(5): p. 839-861.

10. Fahy, E., et al., *Update of the LIPID MAPS Comprehensive Classification System for Lipids.* Journal of Lipid Research, 2009. **50**: p. S9-S14.

11. Carrapiso, A.I. and C. Garcia, *Development in Lipid Analysis: Some New Extraction Techniques and in Situ Transesterification.* Lipids, 2000. **35**(11): p. 1167-1177.

12. Folch, J., M. Lees, and G.H.S. Stanley, *A Simple Method for the Isolation and Purification of Total Lipides from Animal Tissues.* Journal of Biological Chemistry, 1957. **226**(1): p. 497-509.

13. Bligh, E.G. and W.J. Dyer, *A Rapid Method of Total Lipid Extraction and Purification.* Canadian Journal of Biochemistry and Physiology, 1959. **37**(8): p. 911-917.

14. Matyash, V., et al., *Lipid Extraction by Methyl-tert-butyl Ether for High-Throughput Lipidomics.* Journal of Lipid Research, 2008. **49**(5): p. 1137-1146.

15. Cajka, T. and O. Fiehn, *Comprehensive Analysis of Lipids in Biological Systems by Liquid Chromatography-Mass Spectrometry.* TrAC Trends in Analytical Chemistry, 2014. **61**: p. 192-206.

16. Christie, W.W. and X. Han, *Lipid Analysis*. Isolation, Separation, Identification and Lipidomic Analysis, ed. F. Edition. 2006.

17. Sherma, J. and B. Fried, *Handbook of Thin-Layer Chromatography*. 2003, Marcel Dekker: New York.

18. Klein, T.R., et al., *Prion Rods Contain Small Amounts of Two Host Sphingolipids as Revealed by Thin-Layer Chromatography and Mass Spectrometry.* Biological Chemistry, 1998. **379**(6): p. 655-666.

19. Fuchs, B., et al., *Lipid Analysis by Thin-Layer Chromatography - A review of the Current State.* Journal of Chromatography A, 2011. **1218**(19): p. 2754-2774.

20. Mossoba, M.M., et al., *Lipid Analysis and Lipidomics: New Techniques and Applications*. 2006, Champaign, Illinois, USA: AOCS Publishing.

21. Han, X., *Mass Spectrometry-Based Lipidomics Approaches*, in *Lipidomics*. 2016, John Wiley & Sons, Inc. p. 53-88.

22. Wenk, M.R., *The Emerging Field of Lipidomics.* Nat Rev Drug Discov, 2005. **4**(7): p. 594-610.

23. Li, M., et al., *Recent Advances of Chromatography and Mass Spectrometry in Lipidomics.* Anal Bioanal Chem, 2011. **399**(1): p. 243-9.

24. Ding, J., et al., *Application of the Accurate Mass and Time Tag Approach in Studies of the Human Blood Lipidome.* J Chromatogr B Analyt Technol Biomed Life Sci, 2008. **871**(2): p. 243-52.

25. Sandra, K., et al., *Comprehensive Blood Plasma Lipidomics by Liquid Chromatography/Quadrupole Time-of-Flight Mass Spectrometry.* J Chromatogr A, 2010. **1217**(25): p. 4087-99.

26. Laakso, P., *Mass Spectrometry of Triacylglycerols.* European Journal of Lipid Science and Technology, 2002. **104**(1): p. 43-49.

27. Miwa, T.K., et al., *Gas Chromatographic Characterization of Fatty Acids. Identification Constants for Mono- and Dicarboxylic Methyl Esters.* Analytical Chemistry, 1960. **32**(13): p. 1739-1742.

28. Cvačka, J., et al., *Analysis of Triacylglycerols in Fat Body of Bumblebees by Chromatographic Methods.* Journal of Chromatography A, 2006. **1101**(1–2): p. 226-237.

29. Stránský, K., I. Valterová, and P. Fiedler, *Nonsaponifiable Lipid Components of the Pollen of Elder (Sambucus nigra L.).* Journal of Chromatography A, 2001. **936**(1–2): p. 173-181.

30. Stránský, K., M. Zarevúcka, and Z. Wimmer, *Gas Chromatography Analysis of Blackcurrant Oil in Relation to its Stability.* Food Chemistry, 2005. **92**(3): p. 569-573.

31. Zaikin, V. and J.M. Halket, *A handbook of Derivatives for Mass Spectrometry*. 2009, Charlton, Chichester: IM Publications.

32. Christie, W.W. *Preparation of Ester Derivatives of Fatty Acids for Chromatographic Analysis*. 2011; Available from: http://lipidlibrary.aocs.org/Analysis/content.cfm?ItemNumber=40374#D.

33. Stránský, K. and T. Jursík, *Simple Quantitative Transesterification of Lipids . 1. Introduction.* Fett-Lipid, 1996. **98**(2): p. 65-71.

34. Robb, E.W. and J.J. Westbrook, *Preparation of Methyl Esters for Gas Liquid Chromatography of Acids by Pyrolysis of Tetramethylammonium salts*. Analytical Chemistry, 1963. **35**(11): p. 1644-1647.

35. Butte, W., J. Eilers, and M. Kirsch, *Trialkylsulfonium- and Trialkylselenoniumhydroxides for the Pyrolytic Alkylation of Acidic Compounds*. Analytical Letters, 1982. **15**(10): p. 841-850.

36. Yamauchi, K., T. Tanabe, and M. Kinoshita, *Trimethylsulfonium Hydroxide: A New Methylating Agent.* The Journal of Organic Chemistry, 1979. **44**(4): p. 638-639.

37. El-Hamdy, A.H. and W.W. Christie, *Preparation of Methyl Esters of Fatty Acids with Trimethylsulphonium Hydroxide - An Appraisal.* Journal of Chromatography A, 1993. **630**(1): p. 438-441.

38. Han, X., *Mass Spectrometry for Lipidomics*, in *Lipidomics*. 2016, John Wiley & Sons, Inc. p. 21-52.

39. Yang, K. and X. Han, *Lipidomics: Techniques, Applications, and Outcomes Related to Biomedical Sciences.* Trends in Biochemical Sciences. **41**(11): p. 954-969.

40. Gross, J.H., *Mass Spectrometry*. 2004, Germany: Springer.

41. *LCQ Fleet, Hardware Manual*. 2007, Thermo Fisher Scientific.

42. Banerjee, S. and S. Mazumdar, *Electrospray Ionization Mass Spectrometry: A Technique to Access the Information beyond the Molecular Weight of the Analyte.* International Journal of Analytical Chemistry, 2012. **2012**: p. 40.

43. Ham, B.M., *Even Electron Mass Spectrometry with Biomolecule Applications*. 2008, New Jersey: John Wiley & Sons, Inc.

44. Byrdwell, W.C., *Atmospheric Pressure Chemical Ionization Mass Spectrometry for Analysis of Lipids.* Lipids, 2001. **36**(4): p. 327-346.

45. Craig Byrdwell, W., *Atmospheric Pressure Ionization Techniques in Modern Lipid Analysis*, in *Modern Methods for Lipid Analysis by Liquid Chromatography*. 2005, AOCS Publishing.

46. Hoffmann, E.D. and V. Stroobant, *Mass Spectrometry - Principles and Applications*. 3rd ed. 2007.

47. Pól, J., et al., *Molecular Mass Spectrometry Imaging in Biomedical and Life Science Research.* Histochemistry and Cell Biology, 2010. **134**(5): p. 423-443.

48. Church, D.A., *Storage-Ring Ion Trap Derived from the Liear Quadrupole Radio-Frequency Mass Filter* Journal of Applied Physics, 1969. **40**(8): p. 3127-&.

49. Deutch, B.I., et al., *Antihydrogen Production by Positronium-Antiproton Collisions in an Ion Trap.* Physica Scripta, 1988. **T22**: p. 248-255.

50. Stafford, G., *Ion Trap Mass Spectrometry: A Personal Perspective.* Journal of the American Society for Mass Spectrometry, 2002. **13**(6): p. 589-596.

51. Douglas, D.J., A.J. Frank, and D.M. Mao, *Linear Ion Traps in Mass Spectrometry.* Mass Spectrometry Reviews, 2005. **24**(1): p. 1-29.

52. March, R.E., *Quadrupole Traps.* Mass Spectrometry Reviews, 2009. **28**(6): p. 961-989.

53. Quarmby, S.T. and R.A. Yost, *Fundamental Studies of Ion Injection and Trapping of Electrosprayed Ions on a Quadrupole Ion Trap.* International Journal of Mass Spectrometry, 1999. **190–191**: p. 81-102.

54. Hu, Q.Z., et al., *The Orbitrap: A New Mass Spectrometer.* Journal of Mass Spectrometry, 2005. **40**(4): p. 430-443.

55. Mitchell, T.W., S.H.J. Brown, and S.J. Blanksby, *Structural Lipidomics*, in *Lipidomics*. 2012, Wiley-VCH Verlag GmbH & Co. KGaA. p. 99-128.

56. Vrkoslav, V. and J. Cvačka, *Identification of the Double-Bond Position in Fatty Acid Methyl Esters by Liquid Chromatography/Atmospheric Pressure Chemical Ionisation Mass Spectrometry.* Journal of Chromatography A, 2012. **1259**: p. 244-250.

57. Alves, S.P., et al., *Acetonitrile Covalent Adduct Chemical Ionization Tandem Mass Spectrometry of Non-Methylene-Interrupted Pentaene Fatty Acid Methyl Esters.* Rapid Communications in Mass Spectrometry, 2011. **25**(14): p. 1933-1941.

58. Lawrence, P. and J.T. Brenna, *Acetonitrile Covalent Adduct Chemical Ionization Mass Spectrometry for Double Bond Localization in Non-Methylene-Interrupted Polyene Fatty Acid Methyl Esters.* Analytical Chemistry, 2006. **78**(4): p. 1312-1317.

59. Michaud, A.L., et al., *Identification and Characterization of Conjugated Fatty Acid Methyl Esters of Mixed Double Bond Geometry by Acetonitrile Chemical Ionization Tandem Mass Spectrometry.* Analytical Chemistry, 2003. **75**(18): p. 4925-4930.

60. Van Pelt, C.K., B.K. Carpenter, and J.T. Brenna, *Studies of Structure and Mechanism in Acetonitrile Chemical Ionization Tandem Mass Spectrometry of Polyunsaturated Fatty Acid Methyl Esters.* Journal of the American Society for Mass Spectrometry, 1999. **10**(12): p. 1253-1262.

61. Van Pelt, C.K. and J.T. Brenna, *Acetonitrile Chemical Ionization Tandem Mass Spectrometry To Locate Double Bonds in Polyunsaturated Fatty Acid Methyl Esters*. Analytical Chemistry, 1999. **71**(10): p. 1981-1989.

62. Vrkoslav, V., et al., *Localization of Double Bonds in Wax Esters by High-Performance Liquid Chromatography/Atmospheric Pressure Chemical Ionization Mass Spectrometry Utilizing the Fragmentation of Acetonitrile-Related Adducts*. Analytical Chemistry, 2011. **83**(8): p. 2978-2986.

63. Háková, E., et al., *Localization of Double Bonds in Triacylglycerols Using High-Performance Liquid Chromatography/Atmospheric Pressure Chemical Ionization Ion-Trap Mass Spectrometry.* Analytical and Bioanalytical Chemistry, 2015. **407**(17): p. 5175-5188.

64. Xu, Y. and J.T. Brenna, *Atmospheric Pressure Covalent Adduct Chemical Ionization (APCACI) Tandem Mass Spectrometry for Double Bond Localization in Monoene and Diene-containing Triacylglycerols.* Analytical chemistry, 2007. **79**(6): p. 2525-2536.

65. Šubčíková, L., et al., *Analysis of 1,2-Diol Diesters in Vernix Caseosa by High-Performance Liquid Chromatography - Atmospheric Pressure Chemical Ionization Mass Spectrometry.* Journal of Chromatography A, 2015. **1378**: p. 8-18.

66. Marshall, D.L., et al., *Sequential Collision- and Ozone-Induced Dissociation Enables Assignment of Relative Acyl Chain Position in Triacylglycerols.* Analytical Chemistry, 2016. **88**(5): p. 2685-2692.

67. Kozlowski, R.L., et al., *Combining Liquid Chromatography with Ozone-Induced Dissociation for the Separation and Identification of Phosphatidylcholine Double Bond Isomers*. Analytical and Bioanalytical Chemistry, 2015. **407**(17): p. 5053-5064.

68. Thomas, M.C., et al., *Ozone-Induced Dissociation: Elucidation of Double Bond Position within Mass-Selected Lipid Ions*. Analytical Chemistry, 2008. **80**(1): p. 303-311.

69. Poad, B.L.J., et al., *Ozone-Induced Dissociation on a Modified Tandem Linear Ion-Trap: Observations of Different Reactivity for Isomeric Lipids*. Journal of the American Society for Mass Spectrometry, 2010. **21**(12): p. 1989-1999.

70. Mitchell, T., S. Blanksby, and R. Kozlowskia, *Separation and Identification of Phosphatidylcholine Regioisomers by Combining Liquid Chromatography with a Fusion of Collision-and Ozone-Induced Dissociation.* Eur J Mass Spectrom (Chichester), 2015. **21**(3): p. 191-200.

71. Sun, C., Y.-Y. Zhao, and J.M. Curtis, *Characterization of Phospholipids by Two-Dimensional Liquid Chromatography Coupled to In-line Ozonolysis–Mass Spectrometry.* Journal of Agricultural and Food Chemistry, 2015. **63**(5): p. 1442-1451.

72. Hancock, S.E., et al., *Advances and Unresolved Challenges in the Structural Characterization of Isomeric Lipids.* Anal Biochem, 2017. **524**: p. 45-55.

73. Ran-Ressler, R.R., et al., *Branched Chain Fatty Acids are Constituents of the Normal Healthy Newborn Gastrointestinal Tract.* Pediatr Res, 2008. **64**(6): p. 605-9.

74. Hauff, S. and W. Vetter, *Exploring the Fatty Acids of Vernix Caseosa in Form of Their Methyl Esters by Off-Line Coupling of Non-Aqueous Reversed Phase High Performance Liquid Chromatography and Gas Chromatography Coupled to Mass Spectrometry.* J Chromatogr A, 2010. **1217**(52): p. 8270-8.

75. Rissmann, R., et al., *New Insights Into Ultrastructure, Lipid Composition and Organization of Vernix Caseosa.* Journal of Investigative Dermatology, 2006. **126**(8): p. 1823-1833.

76. Andersson, B.A. and R.T. Holman, *Mass-Spectrometric Localization of Methyl Branching in Fatty-Acids Using Acylpyrrolidines.* Lipids, 1975. **10**(11): p. 716-718.

77. Harvey, D.J., *Picolinyl Esters as Derivatives for the Structural Determination of Long-Chain Branched and Unsaturated Fatty-Acids.* Biomedical Mass Spectrometry, 1982. **9**(1): p. 33-38.

78. Hsu, F.F., *Characterization of Hydroxyphthioceranoic and Phthioceranoic Acids by Charge-Switch Derivatization and CID Tandem Mass Spectrometry.* Journal of the American Society for Mass Spectrometry, 2016. **27**(4): p. 622-632.

79. Yang, K., B.G. Dilthey, and R.W. Gross, *Identification and Quantitation of Fatty Acid Double Bond Positional Isomers: A Shotgun Lipidomics Approach Using Charge-Switch Derivatization.* Analytical Chemistry, 2013. **85**(20): p. 9742-9750.

80. Wang, M., R.H. Han, and X.L. Han, *Fatty Acidomics: Global Analysis of Lipid Species Containing a Carboxyl Group with a Charge-Remote Fragmentation-Assisted Approach.* Analytical Chemistry, 2013. **85**(19): p. 9312-9320.

81. *The Oxford English Dictionary*. Second Edition ed. 1989, Oxford, England: Oxford University Press.

82. Hoath, S.B., V. Narendran, and M.O. Visscher, *The Biology and Role of Vernix.* Newborn and Infant Nursing Reviews, 2001. **1**(1): p. 53-58.

83. Lane, A.T., *Human Fetal Skin Development.* Pediatr Dermatol, 1986. **3**(6): p. 487-91.

84. Visscher, M. and V. Narendran, *Neonatal Infant Skin: Development, Structure and Function.* Newborn and Infant Nursing Reviews, 2014. **14**(4): p. 135-141.

85. Koster, M.I. and D.R. Roop, *Mechanisms Regulating Epithelial Stratification.* Annu Rev Cell Dev Biol, 2007. **23**: p. 93-113.

86. Blanpain, C. and E. Fuchs, *Epidermal Homeostasis: A Balancing Act of Stem Cells in the Skin.* Nat Rev Mol Cell Biol, 2009. **10**(3): p. 207-17.

87. Singh, G. and G. Archana, *Unraveling the Mystery of Vernix Caseosa.* Indian journal of dermatology, 2008. **53**(2): p. 54-60.

88. Holbrook, K.A. and G.F. Odland, *The Fine Structure of Developing Human Epidermis: Light, Scanning, and Transmission Electron Microscopy of the Periderm.* J Invest Dermatol, 1975. **65**(1): p. 16-38.

89. Hardman, M.J., et al., *Barrier Formation in the Human Fetus is Patterned.* J Invest Dermatol, 1999. **113**(6): p. 1106-13.

90. Visscher, M.O., et al., *Vernix Caseosa in Neonatal Adaptation.* J Perinatol, 2005. **25**(7): p. 440-6.

91. Hanley, K., et al., *Hormonal Basis for the Gender Difference in Epidermal Barrier Formation in the Fetal Rat. Acceleration by Estrogen and Delay by Testosterone.* J Clin Invest, 1996. **97**(11): p. 2576-84.

92. Hoeger, P.H., et al., *Epidermal Barrier Lipids in Human Vernix Caseosa: Corresponding Ceramide Pattern in Vernix and Fetal Skin.* British Journal of Dermatology, 2002. **146**(2): p. 194-201.

93. Haubrich, K.A., *Role of Vernix Caseosa in the Neonate: Potential application in the adult population.* 2003, Aacn Clinical Issues. p. 457-464.

94. Garcia Bartels, N., et al., *Influence of Bathing or Washing on Skin Barrier Function in Newborns During the First Four Weeks of Life.* Skin Pharmacol Physiol, 2009. **22**(5): p. 248-57.

95. Pickens, W.L., et al., *Characterization of Vernix Caseosa: Water Content, Morphology, and Elemental Analysis.* Journal of Investigative Dermatology, 2000. **115**(5): p. 875-881.

96. Rawlings, A.V., et al., *Stratum Corneum Moisturization at the Molecular Level.* Journal of Investigative Dermatology, 1994. **103**(5): p. 731-740.

97. Saijo, S. and H. Tagami, *Dry skin of newborn infants: functional analysis of the stratum corneum.* Pediatric Dermatology, 1991. **8**(2): p. 155-159.

98. Hoath, S.B., W.L. Pickens, and M.O. Visscher, *The Biology of Vernix Caseosa.* International Journal of Cosmetic Science, 2006. **28**(5): p. 319-333.

99. Yoshio, H., et al., *Antimicrobial Polypeptides of Human Vernix Caseosa and Amniotic Fluid: Implications for Newborn Innate Defense.* Pediatric Research, 2003. **53**(2): p. 211-216.

100. Marchini, G., et al., *The Newborn Infant is Protected by an Innate Antimicrobial Barrier: Peptide Antibiotics are Present in the Skin and Vernix Caseosa.* British Journal of Dermatology, 2002. **147**(6): p. 1127-1134.

101. Akinbi, H.T., et al., *Host Defense Proteins in Vernix Caseosa and Amniotic Fluid.* American Journal of Obstetrics and Gynecology, 2004. **191**(6): p. 2090-2096.

102. Tollin, M., et al., *Vernix Caseosa as a Multi-Component Defence System Based on Polypeptides, Lipids and Their Interactions.* Cellular and Molecular Life Sciences, 2005. **62**(19-20): p. 2390-2399.

103. Tollin, M., et al., *Proteome Analysis of Vernix Caseosa.* Pediatric Research, 2006. **60**(4): p. 430-434.

104. Narendran, V., et al., *Interaction Between Pulmonary Surfactant and Vernix: A Potential Mechanism for Induction of Amniotic Fluid Turbidity.* Pediatric Research, 2000. **48**(1): p. 120-124.

105. Baker, S.M., N.N. Balo, and F.T. Abdel Aziz, *Is Vernix Caseosa a Protective Material to the Newborn: A Biochemical Approach.* Indian J Pediatr, 1995. **62**(2): p. 237-9.

106. Buchman, A.L., *Glutamine: Is It a Conditionally Required Nutrient for the Human Gastrointestinal System.* J Am Coll Nutr, 1996. **15**(3): p. 199-205.

107. O'Grady, J.P., M. Prefontaine, and D.E. Hoffman, *Vernixuria: Another Sign of Uterine Rupture.* J Perinatol, 2003. **23**(4): p. 351-2.

108. Boothby, R., et al., *Vernix Caseosa Granuloma: A Rare Complication of Cesarean Section.* South Med J, 1985. **78**(11): p. 1395-6.

109. Krumerman, M.S. and G.J. Pouliot, *Maternal Vernix Caseosa Peritonitis: Rare Complication of Cesarean Section.* N Y State J Med, 1976. **76**(11): p. 1879-80.

110. Cummings, B., et al., *Vernix Caseosa Peritonitis Presenting Post Partum as Acute Cholecystitis.* Can J Surg, 2001. **44**(4): p. 298-300.

111. Nishijima, K., et al., *Management for Neonatal Aspiration Syndrome Caused by Vernix Caseosa.* Fetal Diagn Ther, 2005. **20**(3): p. 194-6.

112. Midha, R. and L.E. Becker, *Vernix Caseosa Granulomatous Meningitis (Vernicomyelia).* Can J Neurol Sci, 1991. **18**(1): p. 63-5.

113. Moraille, R., et al., *A Novel Role for Vernix Caseosa as a Skin Cleanser.* Biology of the Neonate, 2005. **87**(1): p. 8-14.

114. Rissmann, R., et al., *Mimicking Vernix Caseosa-Preparation and Characterization of Synthetic Biofilms.* International Journal of Pharmaceutics, 2009. **372**(1-2): p. 59-65.

115. Stewart, M.E., M.A. Quinn, and D.T. Downing, *Variability in the fatty acid composition of wax esters from vernix caseosa and its possible relation to sebaceous gland activity.* J Invest Dermatol, 1982. **78**(4): p. 291-5.

116. Nicolaides, N., et al., *The Fatty Acids of Wax Esters and Sterol Esters from Vernix Caseosa and from Human Skin Surface Lipid.* Lipids, 1972. **7**(8): p. 506-+.

117. Nicolaides, N., J.M.B. Apon, and D.H. Wong, *Further Studies of the Saturated Methyl Branched Fatty Acids of Vernix Caseosa Lipid.* Lipids, 1976. **11**(11): p. 781-790.

118. Nicolaides, N., *The Structures of the Branched Fatty Acids in the Wax Esters of Vernix Caseosa.* Lipids, 1971. **6**(12): p. 901-+.

119. Elias, P.M., *The Stratum Corneum Revisited.* J Dermatol, 1996. **23**(11): p. 756-8.

120. Henderson, C.A., J. Taylor, and W.J. Cunliffe, *Sebum Excretion Rates in Mothers and Neonates.* British Journal of Dermatology, 2000. **142**(1): p. 110-111.

121. Míková, R., et al., *Newborn Boys and Girls Differ in the Lipid Composition of Vernix Caseosa.* Plos One, 2014. **9**(6).

122. *The Biology of the Skin.* 2001, USA: CRC Press.

123. Williams, M.L., et al., *Ontogeny of the Epidermal Permeability Barrier.* The journal of investigative dermatology. Symposium proceedings / the Society for Investigative Dermatology, Inc. [and] European Society for Dermatological Research, 1998. **3**(2): p. 75-9.

124. Okah, F.A., et al., *Human Newborn Skin: the Effect of Isopropanol on Skin Surface Hydrophobicity.* Pediatr Res, 1994. **35**(4 Pt 1): p. 443-6.

125. Wickett, R.R., J.L. Mutschelknaus, and S.B. Hoath, *Ontogeny of Water Sorption-Desorption in the Perinatal Rat.* J Invest Dermatol, 1993. **100**(4): p. 407-11.

126. Elias, P.M., *Lipids and the Epidermal Permeability Barrier.* Arch Dermatol Res, 1981. **270**(1): p. 95-117.

127. Wysocki, S.J., et al., *Lipids in Forehead Vernix from Newborn Infants.* Biol Neonate, 1981. **39**(5-6): p. 300-4.

128. Zouboulis, C.C., et al., *Frontiers in Sebaceous Gland Biology and Pathology.* Experimental Dermatology, 2008. **17**(6): p. 542-551.

129. Rissmann, R., et al., *Lanolin-Derived Lipid Mixtures Mimic Closely the Lipid Composition and Organization of Vernix Caseosa Lipids.* Biochimica Et Biophysica Acta-Biomembranes, 2008. **1778**(10): p. 2350-2360.

130. Ansari, M.N.A., H.C. Fu, and Nicolaid.N, *Fatty Acids of the Alkane Diol Diesters of Vernix Caseosa.* Lipids, 1970. **5**(2): p. 279-&.

131. Hoath, S.B. and H.I. Maibach, *Neonatal Skin: Structure and Function.* Second edition ed. 2003, New York, NY 10016: Marcel Dekker, Inc.

132. Karkkainen, J., et al., *Lipids of Vernix Caseosa.* Journal of Investigative Dermatology, 1965. **44**(5): p. 333-+.

133. Miettinen, T.A. and T. Luukkainen, *Gas-Liquid Chromatographic and Mass Spectrometric Studies on Sterols in Vernix Caseosa, Amniotic Fluid and Meconium.* Acta Chem Scand, 1968. **22**(8): p. 2603-12.

134. Oku, H., et al., *Biased Distribution of the Branched-Chain Fatty Acids in Ceramides of Vernix Caseosa.* Lipids, 2000. **35**(4): p. 373-381.

135. Háková, E., et al., *Separation of Nonpolar Lipids from Vernix Caseosa.* Cece 2014: 11th International Interdisciplinary Meeting on Bioanalysis, 2014: p. 216-219.

136. Háková, E., et al., *Analysis of Low Abundant Lipids in Vernix Caseosa Using Chromatographic Methods and Mass Spectrometry.* Proceedings of the 11th International Students Conference "Modern Analytical Chemistry", 2015: p. 23-28.

137. Rabionet, M., et al., *1-O-acylceramides Are Natural Components of Human and Mouse Epidermis.* Journal of Lipid Research, 2013. **54**(12): p. 3312-3321.

138. Wertz, P.W. and D.T. Downing, *Ceramides of Pig Epidermis - Structure determination.* Journal of Lipid Research, 1983. **24**(6): p. 759-765.

139. Sassa, T. and A. Kihara, *Metabolism of Very Long-Chain Fatty Acids: Genes and Pathophysiology.* Biomol Ther (Seoul), 2014. **22**(2): p. 83-92.

140. Farwanah, H., et al., *Profiling of Human Stratum Corneum Ceramides by Means of Normal Phase LC/APCI-MS.* Analytical and Bioanalytical Chemistry, 2005. **383**(4): p. 632-637.

141. Kofroňová, E., et al., *A Comparison of HPLC/APCI-MS and MALDI-MS for Characterising Triacylglycerols in Insects: Species-Specific Composition of Lipids in the Fat Bodies of Bumblebee Males.* J Chromatogr B Analyt Technol Biomed Life Sci, 2009. **877**(30): p. 3878-84.

142. Kofroňová, E., et al., *Analysis of Insect Triacylglycerols Using Liquid Chromatography-Atmospheric Pressure Chemical Ionization-Mass Spectrometry.* European Journal of Lipid Science and Technology, 2009. **111**(5): p. 519-525.

143. Lísa, M., M. Holčapek, and M. Boháč, *Statistical Evaluation of Triacylglycerol Composition in Plant Oils Based on High-Performance Liquid Chromatography−Atmospheric Pressure Chemical Ionization Mass Spectrometry Data.* Journal of Agricultural and Food Chemistry, 2009. **57**(15): p. 6888-6898.

144. Cvačka, J., et al., *Computer-Assisted Interpretation of Atmospheric Pressure Chemical Ionization Mass Spectra of Triacylglycerols.* Rapid Commun Mass Spectrom, 2006. **20**(23): p. 3586-94.